



HAL
open science

Photoactivation of PSII and regulation of photosynthetic electron transport in *Marchantia polymorpha*: study of manganese homeostasis and characterization of Plastid Terminal Oxidase (PTOX) isoforms

Marine Messant

► To cite this version:

Marine Messant. Photoactivation of PSII and regulation of photosynthetic electron transport in *Marchantia polymorpha*: study of manganese homeostasis and characterization of Plastid Terminal Oxidase (PTOX) isoforms. *Biological Physics* [physics.bio-ph]. Université Paris-Saclay, 2023. English. NNT: 2023UPASF017. tel-04500391

HAL Id: tel-04500391

<https://theses.hal.science/tel-04500391>

Submitted on 12 Mar 2024

HAL is a multi-disciplinary open access archive for the deposit and dissemination of scientific research documents, whether they are published or not. The documents may come from teaching and research institutions in France or abroad, or from public or private research centers.

L'archive ouverte pluridisciplinaire **HAL**, est destinée au dépôt et à la diffusion de documents scientifiques de niveau recherche, publiés ou non, émanant des établissements d'enseignement et de recherche français ou étrangers, des laboratoires publics ou privés.

Photoactivation of PSII and Regulation of
Photosynthetic Electron Transport in

Marchantia polymorpha :

Study of Manganese homeostasis and Characterization of
Plastid Terminal Oxidase (PTOX) isoforms

*Photoactivation du PSII et régulation du transport d'électron photosynthétique
chez Marchantia polymorpha :
Etude de l'homéostasie du Manganèse et caractérisation des isoformes de la
Plastid Terminal Oxidase (PTOX)*

Thèse de doctorat de l'université Paris-Saclay

École doctorale n°571, Sciences chimiques : molécules, matériaux,
instrumentation et biosystèmes (2MIB) Spécialité de doctorat : Chimie
Graduate school : Chimie. Référent : Faculté des Sciences d'Orsay

Thèse préparée dans l'unité de recherche : **Institute for Integrative Biology of the
Cell (I2BC) (Université Paris-Saclay, CEA, CNRS)**, sous la direction de
Andrew GALL, DR, et la codirection de **Anja KIERGER-LISZKAY**, DR.

Thèse soutenue à Paris-Saclay, le 10 Mars 2023, par

Marine MESSANT

Composition du Jury

Membres du jury avec voix délibérative

Michael HODGES DR, Institut des Plantes de Paris-Saclay	Président
Xenie JOHNSON DR, CEA, Université Aix-Marseille	Rapporteuse & Examinatrice
Marion EISENHUT AP (équival. HDR), Universität Bielefeld	Rapporteuse & Examinatrice
Sylvain MERLOT CR, Université Paris-Saclay, Saclay	Examineur

Titre : Photoactivation du PSII et régulation du transport d'électron photosynthétique chez *Marchantia polymorpha* : Etude de l'homéostasie du manganèse et caractérisation des isoformes de la Plastid Terminal Oxidase (PTOX)

Mots clés : Homéostasie du Manganèse - Photoactivation - Plastid Terminal Oxidase – Photosystème II - *Marchantia polymorpha* – Résonance Paramagnétique Electronique – Microscopie Super-Résolution

Résumé : L'évolution des organismes photosynthétiques a été marquée par de grands bouleversements (colonisation terrestre, développement des racines, des vaisseaux, des graines) pour aboutir à l'apparition des angiospermes.

La photosynthèse est au cœur du métabolisme primaire des organismes photosynthétiques et elle aussi fait l'objet de certains changements au cours de l'évolution. Elle permet de produire de l'énergie sous forme d'ATP et de NAD(P)H à partir de l'énergie lumineuse. Pour cela, la réaction d'oxydation de l'eau, catalysée par le cluster de manganèse (Mn_4CaO_5) est nécessaire. Le cluster de Mn est le seul biocatalyseur sur Terre capable de catalyser la production d'oxygène à partir de H_2O . Son assemblage dépendant de la lumière, nommé photoactivation, est obligatoire pour la maturation du photosystème II (PSII). La photosynthèse est protégée et régulée par de nombreux mécanismes lui permettant de faire face aux changements environnementaux. Parmi eux, la famille des protéines PTOX (Plastid Terminal Oxidase) permet la protection du photosystème II.

Le but de cette thèse est d'étudier deux mécanismes conservés à travers l'évolution de la lignée verte en caractérisant une plante modèle émergente : *Marchantia polymorpha*. Sa place dans l'évolution, entre les algues et les angiospermes, en fait un organisme idéal puisque l'apparition des angiospermes est marquée par la perte de nombreuses protéines régulatrices, y compris au niveau de la photosynthèse.

Dans un premier temps, la photoactivation du PSII *in vivo* et *in vitro* a été étudiée. La culture de *Marchantia* dans des conditions d'excès et de carence en Mn a mis en évidence une atteinte au niveau du métabolisme pour le premier et de la photosynthèse pour la seconde. Ensuite, des PSII isolés d'épinards dépourvus de cluster ont été étudiés par Résonance Paramagnétique Électronique de Haut champs et des méthodes

dérivées pour mettre en évidence les différents intermédiaires de la photoactivation et pour déterminer les ligands du premier Mn(II) fixé au PSII.

D'autre part, la culture de *Marchantia* à l'obscurité, rendue possible grâce à une voie de biosynthèse de la chlorophylle indépendante de la lumière, a permis le suivi de la photoactivation *in vivo* en fonction du temps. La microscopie super-résolution a montré la dynamique des thylakoïdes pendant la photoactivation et la mise en place du flux d'électron.

Dans une seconde partie, la régulation du transport d'électron photosynthétique et en particulier la fonction des protéines PTOX a été abordée. Une approche phylogénétique a montré que *Marchantia* possède deux isoformes de PTOX dont le premier est similaire à l'unique PTOX des angiospermes (PTOXa) alors que le second ressemble aux deux isoformes présents chez les algues vertes (PTOXb). Un simple mutant de chaque isoforme a été obtenu et caractérisé. Puis, un double mutant a été généré pour la première fois. Leur caractérisation a montré que les PTOX protègent contre la photoinhibition du photosystème I. Enfin, une analyse *in silico* a été menée sur les séquences protéiques de nombreux organismes photosynthétiques afin de déterminer des pistes concernant leur évolution en particulier sur la partie Nter des PTOX de type algue.

Pour finir, une réflexion théorique sur la dynamique des membranes et des complexes photosynthétiques au cours de la mise en place de différents mécanismes de protection de la chaîne a été menée.

En conclusion, *Marchantia polymorpha* est une plante modèle très importante pour l'avenir. Elle est facile à analyser et sa place dans l'évolution de la lignée verte permettra d'élargir la vision de la recherche sur la photosynthèse.

Title: Photoactivation of PSII and regulation of photosynthetic electron transport in *Marchantia polymorpha*: Study of Manganese homeostasis and characterization of Plastid Terminal Oxidase (PTOX) isoforms

Key words: Manganese Homeostasis - Photoactivation - Plastid Terminal Oxidase – Photosystem II - *Marchantia polymorpha* – Electronic Paramagnetic Resonance – Super-Resolution Microscopy

Abstract: The evolution of photosynthetic organisms was marked by great upheavals (land colonisation, development of roots, vessels, seeds) to lead to the appearance of the angiosperms that we know today.

Photosynthesis is at the heart of the primary metabolism of photosynthetic organisms and was also affected by evolutionary events. Photosynthesis allows the production of energy in the form of ATP and NAD(P)H using light energy. For this, the oxidation reaction of water catalysed by the manganese (Mn) cluster (Mn_4CaO_5) is necessary. The Mn cluster is the only biocatalyst on Earth able to catalyse oxygen production from H_2O . Its light-dependent assembly, termed photoactivation, is mandatory for photosystem II (PSII) maturation. Photosynthesis is protected and regulated by many mechanisms allowing it to cope with environmental changes. Among them, the family of PTOX proteins (Plastid Terminal Oxidase) allows the protection of photosystem II by preventing the generation of reaction oxygen species (ROS).

The Aim of this thesis is to study two mechanisms conserved through the evolution of the green lineage by characterising an emerging model plant: *Marchantia polymorpha*. Its place in evolution, between algae and angiosperms, makes it an ideal organism since the appearance of angiosperms was marked by the loss of many regulatory proteins, including at the photosynthesis level.

First, the photoactivation of PSII *in vivo* and *in vitro* was studied. The culture of *Marchantia* under Mn excess and deficiency conditions revealed an attack on the level of the metabolism for the first and of the photosynthesis for the second. Then, PSII isolated from spinach devoid of clusters were studied by High-Field Electron Paramagnetic Resonance and derivative methods to highlight the different photoactivation intermediates and to determine the ligands of the first Mn(II) bound to the PSII. On the other hand, growing *Marchantia* in

the dark, enabled by a light-independent chlorophyll biosynthesis pathway, allowed *in vivo* tracking of the photoactivation as a function of time. Super-resolution microscopy follows the dynamics of thylakoids during photoactivation and the establishment of electron flow.

In a second part, the regulation of photosynthetic electron transport, in particular the function of PTOX proteins was discussed. A phylogenetic approach showed that *Marchantia* has two isoforms of PTOX, the first of which is similar to the unique PTOX of angiosperms (PTOXa) while the second resembles the two isoforms present in green algae (PTOXb). A single mutant of each isoform was obtained and characterised. Then, a double mutant was generated for the first time. Their characterisation showed that PTOX protects against photosystem I photoinhibition. Finally, an *in silico* analysis was carried out on the protein sequences of many photosynthetic organisms in order to determine leads concerning their evolution, in particular on the Nter part of the alga-type PTOX.

Finally, a theoretical reflection on the dynamics of membranes and photosynthetic complexes during the establishment of different protection mechanisms of the photosynthetic chain was carried out.

To conclude, *Marchantia polymorpha* is a powerful plant model for the future. It is easy to analyse and its place in green lineage evolution will broaden the vision of photosynthetic research.

*Dedicated to my lovely little girl,
Alana*

Résumé en Français

La photosynthèse oxygénique est une réaction du métabolisme primaire des organismes photosynthétiques leur permettant de produire de l'énergie à partir d'eau et de CO₂ en utilisant l'énergie lumineuse. La photosynthèse permet de produire de l'oxygène grâce au seul biocatalyseur sur Terre capable de catalyser l'oxydation de l'eau : le cluster de manganèse (Mn₄CaO₅). L'étude de la photosynthèse a un grand intérêt pour l'Homme car les autotrophes sont les organismes à base de toute chaîne alimentaire, leur développement a permis l'apparition de conditions favorables à notre respiration en produisant de l'oxygène et ce sont les seuls organismes capables d'utiliser des gaz à effet de serre, produits par l'activité humaine tout en utilisant une source d'énergie inépuisable : la lumière.

Néanmoins, les études sur la photosynthèse ont jusqu'à présent ciblées qu'une petite partie des organismes photosynthétiques. Majoritairement pour des raisons techniques, deux modèles principaux ont été utilisés : *Chlamydomonas reinhardtii* (algue verte) et *Arabidopsis thaliana* (Angiosperme). L'inconvénient majeur de l'utilisation intensive de ces modèles est que le premier représente le groupe ancestral de la lignée verte, alors que le second représente le groupe le plus évolué. Ainsi, on compare souvent des mécanismes observés chez des individus dont l'apparition est séparée de plusieurs millions d'années avec tous les événements charnières qui ont pu avoir lieu entre eux.

Récemment, les avancées technologiques du séquençage ont permis la mise à disposition de données sur l'ADN de nouvelles plantes modèles, en particulier : *Physcomitrium patens* (mousse) et *Marchantia polymorpha* (hépatique, mousse ancestrale). Toutes les deux font partie du groupe des Bryophytes au sens large (mousses) qui sont considérées comme les premières plantes à avoir colonisé le milieu terrestre. *Marchantia polymorpha* en particulier est considérée comme l'une des plus anciennes. Les premières études menées montrent bien qu'elle possède des caractéristiques morphologiques et moléculaires intermédiaires entre les algues vertes et les angiospermes et la réaction de photosynthèse ne fait pas exception.

Dans cette étude, j'ai choisi d'utiliser l'organisme *Marchantia polymorpha* afin d'ouvrir de nouvelles perspectives quant à l'étude de mécanismes très conservés au niveau de la photosynthèse qui sont : l'assemblage dépendant de la lumière du cluster de manganèse, la photoactivation, ainsi qu'une famille de protéine impliquée dans la protection du photosystème II, les Plastid Terminal Oxidases (PTOX).

Dans la première partie de la thèse, je me suis intéressée au cluster de Manganèse et à son assemblage dépendant de la lumière : la **photoactivation**. Le premier objectif a été d'obtenir des mutants des deux transporteurs de manganèse dans le chloroplaste connus à ce jour : CMT1 (Chloroplast Manganese Transporter 1) et PAM71 (Photosynthesis Affected Mutant 71). Tous les essais de transformations réalisées chez *Marchantia* n'ont pas fonctionné, même en supplémentant le milieu de transformation avec du manganèse. Par ailleurs, d'autres mutants ont pu être obtenus en parallèle ce qui suggère que ces mutations sont létales.

Pour tout de même essayer de caractériser l'homéostasie du manganèse chez *Marchantia*, j'ai étudié l'impact de la carence et de l'excès de manganèse sur la photosynthèse et le métabolisme de *Marchantia polymorpha*. Les conditions de culture ont été difficiles à mettre au point. J'ai mis en évidence que *Marchantia* est très tolérante à ces deux stress. L'utilisation de différentes méthodes de microscopie a montré de grands changements dans la structure des chloroplastes ainsi que dans l'arrangement des thylakoïdes. Les analyses de chromatographie gazeuse (GC-MS) ont montré une influence importante de l'excès de Mn sur le métabolisme des thalles en augmentant la teneur en certains métabolites connus pour protéger les plantes contre un stress aux métaux lourds. J'ai mis en évidence que même si les thalles ne possèdent pas autant de molécules ou de systèmes de protection que *Arabidopsis* par exemple, ils sont tout de même capables de contenir des teneurs en Mn proches de celles de certains hyperaccumulateurs. Par ailleurs, l'accumulation importante de manganèse dans les plantes a également été visible dans les chloroplastes isolés. D'un autre côté, la carence en Mn a été très difficile à générer chez *Marchantia polymorpha*. Le remplacement de l'agar, trop contaminé en manganèse, par de l'amidon a été nécessaire pour cultiver les thalles. Les résultats des mesures de fluorescence ainsi que des mesures d'absorption du PSI obtenues semblent pointer du doigt l'importance du flux cyclique d'électron pour permettre aux thalles de survivre dans ces conditions (**article 1**).

Par ailleurs, j'ai souhaité continuer l'étude sur le cluster de Manganèse en utilisant un système plus simple, c'est-à-dire des PSII isolés d'épinards déplétés en cluster de Mn. La photoactivation, qui correspond à l'assemblage dépendant de la lumière du cluster de manganèse, est difficile à étudier. Le cluster de manganèse est localisé du côté donneur du PSII. Il a une forme plutôt cubique et a une composition complexe : quatre ions manganèse reliés entre eux par des atomes d'oxygène et un ion de calcium. Dans un premier temps, j'ai réalisé des mesures à l'électrode d'oxygène. Le principe étant de déterminer les conditions permettant la photoactivation des PSII. Si les PSII sont photoactivés, alors la présence du cluster permettant l'oxydation de l'eau entraîne un dégagement d'oxygène. Ainsi, j'ai testé l'importance de certains paramètres (pH, concentration en $MnCl_2$, durée et intensité de lumière etc.) pour déterminer de bonnes conditions de photoactivation mais des expériences complémentaires pourraient permettre d'en améliorer le rendement. Ensuite, j'ai continué l'étude de la photoactivation *in vitro* de manière plus mécanistique en changeant de méthode d'analyse. En collaboration avec Sun Un, nous avons utilisé la Résonance Paramagnétique Électronique (RPE) de haut champ et des techniques dérivées dans le but d'étudier l'attachement du premier Mn(II) côté donneur du PSII. Nous avons pu mettre en évidence que le premier Mn(II) possède dans son environnement proche (dans nos conditions expérimentales) cinq molécules d'eau et au moins un atome de N. Ensuite, la mesure de la distance entre le standard interne (la tyrosine D) et le premier atome de manganèse par la méthode du Pulse Dipolar spectroscopy a permis de montrer qu'il s'agit du résidu histidine 332 de la protéine D1, ce qui est en accord avec les structures des PSII déplétés en Mn publiées dans la littérature. Enfin, nous avons complété notre étude avec d'autres expériences de photoactivation en utilisant différentes équivalences de Mn(II) par rapport aux PSII (1.5, 3, 6 Mn(II) par PSII) qui nous ont permis de

conclure que l'état d'assemblage à deux premiers Mn semble être le plus stable et que plus de quatre Mn(II) sont nécessaires pour former un cluster.

Pour terminer cette partie, j'ai voulu trouver un système *in vivo* chez les plantes permettant de suivre la photoactivation et de voir ses effets sur la dynamique des thylakoïdes. Il est connu dans la littérature que l'assemblage du cluster change la répartition des PSII au sein des thylakoïdes. Pour ce faire, j'ai utilisé le modèle *Marchantia polymorpha*. Contrairement aux angiospermes, *Marchantia* a conservé une protéine permettant la synthèse de chlorophylle à l'obscurité, comme chez les algues. Cette protéine permet donc de produire des photosystèmes correctement assemblés à l'obscurité. Ainsi, la culture de *Marchantia* dans le noir peut permettre de suivre la photoactivation *in vivo* en temps réel. Des mesures de la fluorescence des chlorophylles ont permis de montrer que je suis capable de photoactiver des thalles en utilisant des flashes de lumière successifs. Mais, la méthode la plus efficace s'est révélée être une illumination de 5 minutes. Enfin, Andrew Gall et moi avons suivi cette photoactivation en utilisant une nouvelle technique de microscopie à fluorescence : la super-résolution avec un nouveau processus de traitement d'image mis au point au CEA de Saclay, nommé SPiRi (Single Pixel Reconstruction Imaging). J'ai été capable de suivre la dynamique des membranes des thylakoïdes lors de la photoactivation de l'échantillon.

Dans une seconde partie, j'ai étudié les protéines **Plastid Terminal Oxidases** (PTOX). La première protéine PTOX à avoir été étudiée est celle d'*Arabidopsis thaliana*, dont le mutant montre un phénotype de variégation. Il a été montré que l'unique protéine PTOX des angiospermes est impliquée dans la protection du PSII contre la photoinhibition dans des conditions de stress, de manière indirecte dans la voie de biosynthèse des caroténoïdes et enfin dans la chlororespiration qui est un flux d'électron alternatif. De plus, il est connu que certains organismes photosynthétiques, dont l'algue verte *Chlamydomonas reinhardtii* possèdent deux isoformes de la PTOX. Seulement un mutant de l'isoforme PTOX2 a pu être obtenu dans cet organisme. Il semble avoir les mêmes rôles que ceux décrits chez *Arabidopsis*. Dans cette partie, j'ai caractérisé les deux protéines PTOX de *Marchantia polymorpha*.

Dans un premier temps, j'ai caractérisé les deux simples mutants $\Delta ptoxa$ et $\Delta ptoxb$ chez *Marchantia*. Une analyse phylogénétique des séquences protéiques a mis en évidence la présence de deux types de PTOXs à travers la lignée verte. Nous avons défini les PTOXs de type "algue" qui présentent une longue partie Nter comme celles de *Chlamydomonas* alors que les PTOX de type "plante" ressemblent à l'isoforme plus évolué d'*Arabidopsis*. *Marchantia polymorpha* possède un isoforme de chaque. Ensuite, chacun des simples mutants ne montrent aucun changement de phénotype et ne semblent pas dépourvu en caroténoïdes. Par ailleurs, bien que la fonction des deux protéines semble similaire, certains indices montrent qu'elles ne sont tout de même pas entièrement complémentaires. En tout cas, elles restent importantes pour la protection de la chaîne photosynthétiques en permettant l'oxydation du pool de plastoquinone (**article 2**).

Pour aller plus loin, j'ai réussi à obtenir le premier double mutant PTOX dans l'organisme *Marchantia polymorpha*. Les deux lignées double mutants obtenues ne montrent toujours pas de phénotype, suggérant

que la PTOX n'intervient pas, contrairement à ce qui a été précédemment mis en évidence chez *Arabidopsis*, dans la biosynthèse des caroténoïdes, même de manière indirecte. De manière encore plus étonnante, les mesures de fluorescence des chlorophylles montrent que l'absence de l'activité PTOX ne change pas la photoinhibition du PSII mais celle du PSI. Ainsi, il semblerait que les PTOXs chez *Marchantia polymorpha* soient importantes pour la protection du PSI en permettant de "sacrifier" le PSII qui reste tout de même moins dommageable pour la plante (**article 3**).

Pour finir, j'ai réalisé une étude *in silico* de la partie Nter des PTOXs de types "algues" à partir des séquences protéiques utilisées dans l'**article 2**. J'ai pu mettre en évidence chez ces protéines la présence de quatre hélices α conservées qui pourraient être nécessaires pour leurs activités catalytiques. Par ailleurs, la première hélice α transmembranaire du site catalytique de ces protéines est plus courte que celles des PTOX de type "plante". On suppose que l'extension de la partie Nter pourrait faciliter l'ancrage à la membrane et avoir un rôle dans la régulation de l'activité de la protéine. Cette hypothèse est d'autant plus favorisée que certains résultats de la caractérisation des mutants semblent aller dans le sens qu'une des protéines PTOXs puisse être majoritairement attachée à la membrane (PTOXb) alors que l'autre serait plus en retrait et attachée à la membrane uniquement dans des conditions de stress intense (PTOXa).

Enfin, dans la dernière partie je me suis intéressée d'un point de vue théorique aux changements dans la **dynamique des associations entre les protéines et les membranes dans la régulation du transport d'électron photosynthétique**. En effet, les membranes des thylakoïdes à l'intérieur du chloroplaste sont très mobiles en fonction des conditions physiologiques de la plante. En particulier lors d'un stress, la mise en place des systèmes de protection que ce soit des flux d'électrons alternatifs (flux d'électron cyclique ou chlororespiration), des mécanismes du quenching non-photochimique ou l'implication de protéines particulières (ex : Plastid Terminal Oxidase, PTOX), changent la conformation des membranes. Or, les complexes de la chaîne photosynthétique eux-mêmes sont capables de migrer des grana (zones condensées) aux lamelles stromales (zones lâches) et inversement en fonction des conditions (**article 4**).

Pour conclure, dans cette étude, j'ai essayé d'avoir une vision plus globale des mécanismes ultra conservés que sont la photoactivation et un des mécanismes de protection de la chaîne photosynthétique. L'utilisation de *Marchantia polymorpha* a été un point fort aussi bien d'un point de vue technique (facilité d'utilisation, présence de protéines permettant sa culture dans des conditions particulières) que scientifique puisqu'elle présente des caractéristiques morphologiques et moléculaires évolutivement intermédiaires entre les organismes principalement étudiés : les algues vertes et les angiospermes. Je pense avoir démontré que l'étude des plantes inférieures couplée à l'utilisation de nouvelles technologies est un projet de recherche d'avenir.

Acknowledgements

Un travail d'équipe...

J'aimerais remercier **Anja** qui m'a fait confiance et m'a accompagnée depuis ma L3. Anja, grâce à toi j'ai eu la chance de pouvoir exprimer ma personnalité à travers la recherche. Je te remercie d'avoir toujours respecté mes idées et de les avoir fait grandir. Merci d'avoir répondu à mes dix milliards de questions toujours avec patience et intérêt. Merci pour ton humanité et ton ouverture d'esprit qui m'ont aidé à devenir une jeune femme épanouie dans mon travail et dans ma vie en général.

I would like to thank **Andrew** for having the patience to teach me the use of the super-resolution microscope and for accompanying me in all my imaging experiments. Andrew, I thank you for your discreet but effective presence and your valuable advice for writing the thesis.

I would like to thank **Sun** for being the best physics chemistry teacher I have ever had. Thanks to you I was able to understand the fundamental mechanisms of EPR. I wish I had more time to do experiments.

J'aimerais remercier **Bruno**. Même si tu n'as été que mon directeur de thèse "administratif" je te remercie tout de même pour la bienveillance et le soutien dont tu as fait preuve durant toutes les démarches que j'ai dû entreprendre pendant ma thèse.

J'aimerais remercier **Sébastien** pour m'avoir épaulé lors de ces longues manip d'ICP-MS contenant chacune 50.000 échantillons... Merci de m'avoir aidé à construire ce projet autour du Manganèse et de toujours m'avoir donné un avis constructif.

I would like to thank **Ginga** for all these very interesting discussions and reasoned debates. Thank you for teaching me a lot and for always answering my questions with patience. As always: see you soon in France with pleasure !

I would like to thank **Umama** for continuing to bring my project to life by taking over and for continuing the culture of Marchantia, which is an organism that is dear to me.

J'aimerais remercier **l'ensemble des (anciens) chercheurs du CEA** que je n'avais fait que croiser lors de mon premier stage et que j'ai finalement pris beaucoup de plaisir à connaître au fil des années: Pierre et Diana, Klaus et Pavel, Wilfried et Anna-maria, Tania (merci pour la relecture de la partie photoactivation)...

J'aimerais remercier **Adjélé** et **Sandrine** qui m'ont offert une aide scientifique et logistique précieuse particulièrement dans mes derniers mois de grossesse.

J'aimerais remercier **Axel** pour ces longues discussions sur le milieu de la recherche, de la publication et aussi ces 6 mois de travail partagés qui ont fini par nous lier d'une certaine affection. C'est toujours un plaisir !

J'aimerais remercier **Elodie** pour son éternelle bonne humeur et sa joie de vivre ! Si tu savais comme je t'ai regretté lorsque tu es partie à Cadarache. Le labo est devenu vide sans toi et nous attendions tous tes visites intempestives et explosives.

J'aimerais remercier **Susanne Bolte** et **Catherine de Vitry** pour nos précieuses discussions et leur bienveillance lors de mes comités de thèse.

J'aimerais remercier **Thanh** pour toutes nos discussions sur le milieu scientifique et son soutien lors de ma candidature à la bourse For Women in Science. Merci de m'avoir fait prendre conscience que beaucoup de réseaux sont mis en place autour de nous, au CEA mais aussi sur le plateau de Saclay.

I would like to thank the members of the jury : **Xenie, Marion, Sylvain** and **Michael** for sharing this last step with me ! Thanks to **Marion** for an interesting manganese discussion. Merci à **Michael** pour m'avoir toujours suivi de loin depuis mon stage dans l'équipe.

A ma famille...

J'aimerais remercier mes **parents** et ma petite sœur. Merci d'avoir toujours été là pour m'encourager dans ce long parcours difficile que sont les études. Merci de nous avoir toujours donné le nécessaire pour réussir.

Nanou, toi qui viens de terminer tes études de droits, et qui comme moi referme doucement un des épais volumes qui constitueront nos vies, j'espère que tu ouvriras le prochain avec autant de plaisir que moi ! Je te souhaite de réussir au moins autant que tu le mérites !

Alexandre, ça y est, c'est fini ! Tu n'auras plus besoin de me demander où en est ma thèse. On en aura vécu des aventures pendant ces trois années... D'abord à deux, puis à trois avec Mélo et maintenant à quatre avec Bibouille... j'ai hâte de savoir ce que nous réservent les prochaines !

Table of content

Résumé en Français	1
Acknowledgements	6
Table of content	8
List of Abbreviations	10
General Introduction	12
I) Background of photosynthesis	16
A) <u>Linear Electron flow</u>	18
1) <i>Photosystem II Structure and Electron Transport</i>	19
2) <i>Oxygen-Evolving Complex</i>	23
3) <i>Photosystem I</i>	26
4) <i>Cytochrome b6f</i>	27
B) <u>Alternative Electron Transports and different protection mechanisms</u>	29
1) <i>Cyclic Electron Flow</i>	29
2) <i>Chlororespiration</i>	31
3) <i>Non-Photochemical Quenching</i>	32
4) <i>Plastid Terminal Oxidases</i>	33
II) Chloroplast membrane dynamic	37
III) Super-resolution microscopy: an <i>in vivo</i> way to study dynamic of photosynthetic complexes	39
IV) <i>Marchantia polymorpha</i> , an emerging model plant	42
A) <u>General characteristics</u>	42
B) <u>Peculiarities of photosynthesis</u>	44
C) <u>Photosynthesis study in <i>Marchantia polymorpha</i></u>	46
Aims	48
Part I : Photosynthesis regulation at PSII donor side	
Study of Manganese homeostasis and Photoactivation	50
I) Impact of Manganese excess and deficiency on Photosynthesis and metabolism of <i>Marchantia polymorpha</i>	50
Article 1: Manganese Excess and Deficiency affect chloroplast structure and photosynthesis in <i>Marchantia polymorpha</i> (accepted)	51
II) Study of Photosystem II photoactivation	79
A) <u>Measurement of Mn-catalase like activity and apo-PSII photoactivation <i>in vitro</i> using Oxygen Electrode</u>	82
1) <i>Material and methods</i>	82
2) <i>Results</i>	82
a) Characterization of oxygen evolution caused by Mn in solution: monitoring of Mn catalase-like activity	82
b) Apo-PSII photoactivation primary experiments	83
3) <i>Conclusions and perspectives</i>	83

B) <u>In vitro</u> photoactivation of isolated PSII by High-Field EPR Spectroscopy	84
1) <i>Material and Methods</i>	84
2) <i>Results</i>	86
C) <u>Photoactivation studied in dark-grown <i>Marchantia polymorpha</i> in vivo</u>	89
1) <i>Material and Methods</i>	90
2) <i>Results</i>	91
a) Dark-grown <i>Marchantia</i>	91
b) Chlorophyll fluorescence measurement: photoactivation impact on PSII reaction centre	91
c) Super-resolution fluorescence microscopy: tracking to thylakoids dynamic during photoactivation	93
D) <u>Part I Conclusions</u>	95

Part II: Regulation of Photosynthetic Electron Transport :

Characterization of Plastid Terminal Oxidases a and b in <i>Marchantia polymorpha</i>	166
I) <i>Characterization of PTOXa and PTOXb from <i>Marchantia polymorpha</i> in vivo</i>	96
Article 2 : Evolutive differentiation between alga- and plant-type plastid terminal oxidase : study of plastid terminal oxidase PTOX isoforms in <i>Marchantia polymorpha</i>	97
II) <i>Characterization of ΔptoxaΔptoxb double mutants in <i>Marchantia polymorpha</i></i>	113
Article 3: PTOX proteins are involved in PSI photoinhibition protection in <i>Marchantia polymorpha</i> : study of the first PTOX double mutant (submitted)	114
III) <i>In silico</i> comparison of the structure of Algae and Plant-type PTOX	134
A) <u>Material and Methods</u>	134
B) <u>Results</u>	135
1) <i>Characteristics of the Nter extension of Alga-type PTOX</i>	135
a) Description of the different Nter extension structures	135
b) Special cases of Nter region of Alga-type PTOX of Nannochloropsis b and Azolla	138
2) <i>Comparison of Algae and Plant-type catalytic site sequences: re-definition of iron binding motifs</i>	140
C) <u>Part II conclusions and perspectives</u>	179

Part III : Dynamic changes in protein-membrane association for regulating Photosynthetic Electron Transport

Article 4 : Dynamic changes in protein-membrane association for regulating Photosynthetic Electron Transport	145
--	-----

Discussion and Perspectives

161

References

168

List of Abbreviations

A. thaliana : *Arabidopsis thaliana*

AH : Amphipathic helices

ATP : Adenosine Triphosphate

AOX : Alternative Oxidase

CEF : Cyclic Electron Flow

Chl : Chlorophyll

CrPTOX2 : *Chlamydomonas reinhardtii* Plastid Terminal Oxidase 2

CRISPR : Clustered Regularly Interspaced Short Palindromic Repeats

Cter : C-terminus or C-terminal region

CURT1 : Curvature Thylakoid 1

Cyt *b₆f* : Cytochrome *b₆f*

C. reinhardtii : *Chlamydomonas reinhardtii*

DCMU : 3-(3,4-dichlorophenyl)-1,1-dimethylurea

DPOR : Light independent Pchl_{id} oxidoreductase

D1 : protein of the PSII core

ELDOR-detected NMR : Electron Double Resonance detected Nuclear Magnetic Resonance spectroscopy

ENDOR : Electron Nuclear Double Resonance spectroscopy

EPR : Electron Paramagnetic Resonance

Fd : Ferredoxin

FLIM : Fluorescence Life-Time Microscopy

FLV : Class C Flavodiiron protein

FNR : Ferredoxin NADP⁺ oxidoreductase

GC-MS : Gas-Chromatography Mass Spectrometry

HAS : High Affinity Site

HF-EPR : High Field Electron Paramagnetic Resonance

HPR1 : Hydroxypyruvate reductase 1

IBM : Iron Binding Motif

LEF : Linear Electron Flow

LHC : Light Harvesting Complex

LHCI : Light Harvesting Complex I

LHCII : Light Harvesting Complex II

LHCSR : Light Harvesting Complex Stress Related

LPOR : Light dependent NAD(P)H-Pchl_{id}

Mn : Manganese

M. polymorpha : *Marchantia polymorpha*

NADP⁺ : Nicotine Adenine dinucleotide (phosphate) oxidised

NAD(P)H : Nicotine Adenine dinucleotide (phosphate) reduced

NDH : NAD(P)H dehydrogenase-like complex

NPQ : Non Photochemical Quenching

Nter : N-terminus or N-terminal region

OEC : Oxygen Evolving Complex

PALM : Photoactivated Localisation Microscopy

PAM : Pulse-Amplitude Modulated fluorometer

PC : Plastocyanin
PDS : Pulse Dipolar Spectroscopy
PGR5 : Proton Gradient Regulation 5
PGRL1 : Proton Gradient Regulator Like 1
pH : Hydrogen potential
Pheo : Pheophytin
PQ : Plastoquinone
PQH₂ : Plastoquinol
PS : Photosystem
PSBS : Photosystem II subunit S
PSI : Photosystem I
PSII : Photosystem II
PTOX : Plastid Terminal Oxidase
P. patens : *Physcomitrium patens*
P680 : Chlorophyll *a* special pair of PSII reaction centre
P700 : Chlorophyll *a* special pair of PSI reaction centre
Q_A : Photosystem II primary quinone acceptor
Q_B : Photosystem II secondary quinone acceptor
qE : Energy dependent NPQ
qI : PSII photoinhibition dependent NPQ
qT : State transition dependent NPQ
qZ : Zeaxanthin dependent NPQ
ROS : Reactive Oxygen Species
SIM : Structured Illumination Microscopy
SPiRi : Single Pixel Reconstruction Imaging Method
SQDG : SulfoQuinovosylDiacylGlycérol
SRM : Super-resolution microscopy
STED : Stimulated Emission Microscopy
TbAOX : *Trypanosoma brucei* Alternative Oxidase
Tyr_D : Tyrosine D
Tyr_Z : Tyrosine Z
T. brucei : *Trypanosoma brucei*
T. elongatus : *Thermosynechococcus elongatus*
VIPP : Vesicle Inducing Protein in Plastid proteins

General Introduction

Oxygenic photosynthesis

Oxygenic photosynthesis appeared around 2.45 million years ago (Sánchez-Baracaldo and Cardona, 2020). It requires the presence of two photosystems whose purpose is to collect light through antennae and convert it into chemical energy in their reaction centres. The electron flow then generated allows photosynthetic organisms to produce the energy necessary for their metabolism using water and atmospheric carbon dioxide (Figure 1, A). Oxygenic photosynthesis produces oxygen, necessary for our respiration, thanks to the presence of the only biocatalyst able to catalyse water oxidation: the manganese cluster or Oxygen Evolving Complex (OEC). Although photosynthesis is mostly well conserved through evolution, it has nevertheless undergone significant changes during key events in the development of photosynthetic organisms such as the appearance of multicellular individuals, the specialisation of specific tissue and then land colonisation, accompanied with the appearance of a vascular system and other specific organs.

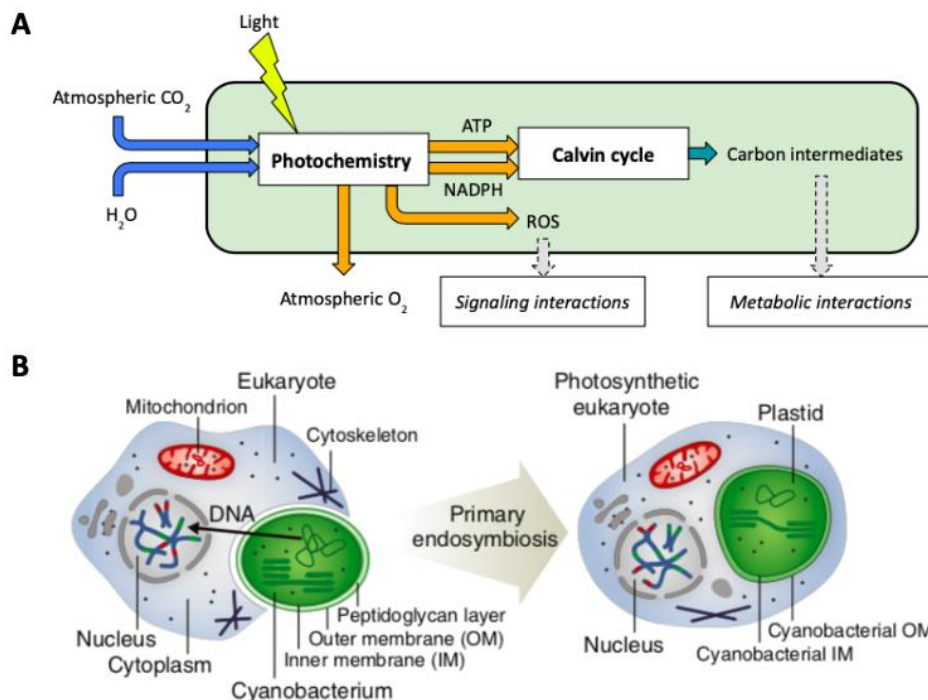


Figure 1: Energetic balance of photosynthesis and primary endosymbiosis theory

Photosynthesis energetic balance. In the chloroplast (green), photosynthesis uses light energy to oxidise water and to generate chemical energy in the form of ATP and NAD(P)H while releasing O_2 . These two sources of energy are used by the Calvin-Benson Cycle to generate carbon intermediates molecules from CO_2 . Under certain conditions, Reactive Oxygen Species (ROS) can be produced by photochemistry and electron transfer, which, at low concentrations, can act as signal molecules. Together, ROS and carbon intermediates establish interactions between the different organelles of the cell such as the nucleus or the mitochondria. **B.** Primary endosymbiosis involves the uptake of a cyanobacterium by a non-photosynthetic eukaryote. The process involves DNA transfer from the endosymbiont to the host and the evolution of a protein import apparatus into the organelle. Primary plastids are surrounded by two membranes. The peptidoglycan layer present in the cyanobacterial progenitor was lost in red and green algae. *Image and legend from Archibald, 2015.*

From the first autotroph to land colonisation

Photosynthetic organisms' origin is explained by the endosymbiosis of a cyanobacterium (McFadden, 1999; Marin *et al.*, 2005; Maréchal, 2018) by a heterotrophic protist (Figure 1, **B**), part of which evolved to form the clade of Chloroplastida, also called the green lineage. The cyanobacterium became an organelle in its own right of this cell, now called the chloroplast. The metabolism of each of these two ancestors is now regulated in relation to the other one. For example, genes encoding photosynthetic proteins are present in the nuclear genome and the proteins are then transported into the chloroplast (Martin *et al.*, 1998; Cullis *et al.*, 2009).

The green lineage is composed of chlorophytes (green algae) and land plants (streptophytes) (Figure 2). The latest evo-physio studies tend to show that the terrestrial colonisation of plant ancestors was enabled by the ability to change the environment such as the passage from salt to fresh water (Fürst-Jansen *et al.*, 2020). Thus, it is assumed that streptophytes come from an ancestral alga able to grow in freshwater.

Land colonisation by algae and first land plants make the soil a favourable environment for the development of a more complex vegetation allowing the appearance of terrestrial animals (Harrison, 2017; Ma *et al.*, 2020). The first land plants (Donoghue *et al.*, 2021; Bowles *et al.*, 2022) were members of the Bryophytes, which appeared about 480 million years ago, which includes three taxonomic groups: Marchantiophyta (liverworts), Anthocerotophyta (hornworts) and the Bryophyta (mosses). The discovery of fossils highlights that the oldest group is that of liverworts. Bryophytes in the broad sense appeared when the atmospheric CO₂ concentration was around 4500 ppm compared to the current 400 ppm (Raven and Colmer, 2016) (Figure 3). Land colonisation therefore completely changes the accessibility to resources. Indeed, CO₂ becomes more abundant, as does light, which can become excessive, and water becomes scarcer. In particular, fixed life becomes a new constraint since it does not allow evasive strategies to be carried out in changing environmental conditions as is the case for algae that can swim deeper.

Thus, early land plants had to develop essential traits such as desiccation tolerance to cope with lack of water, modifications in their light-harvesting systems, and changes in carbon absorption and utilisation and finally the use of protective polymers as a composite of the cell wall.

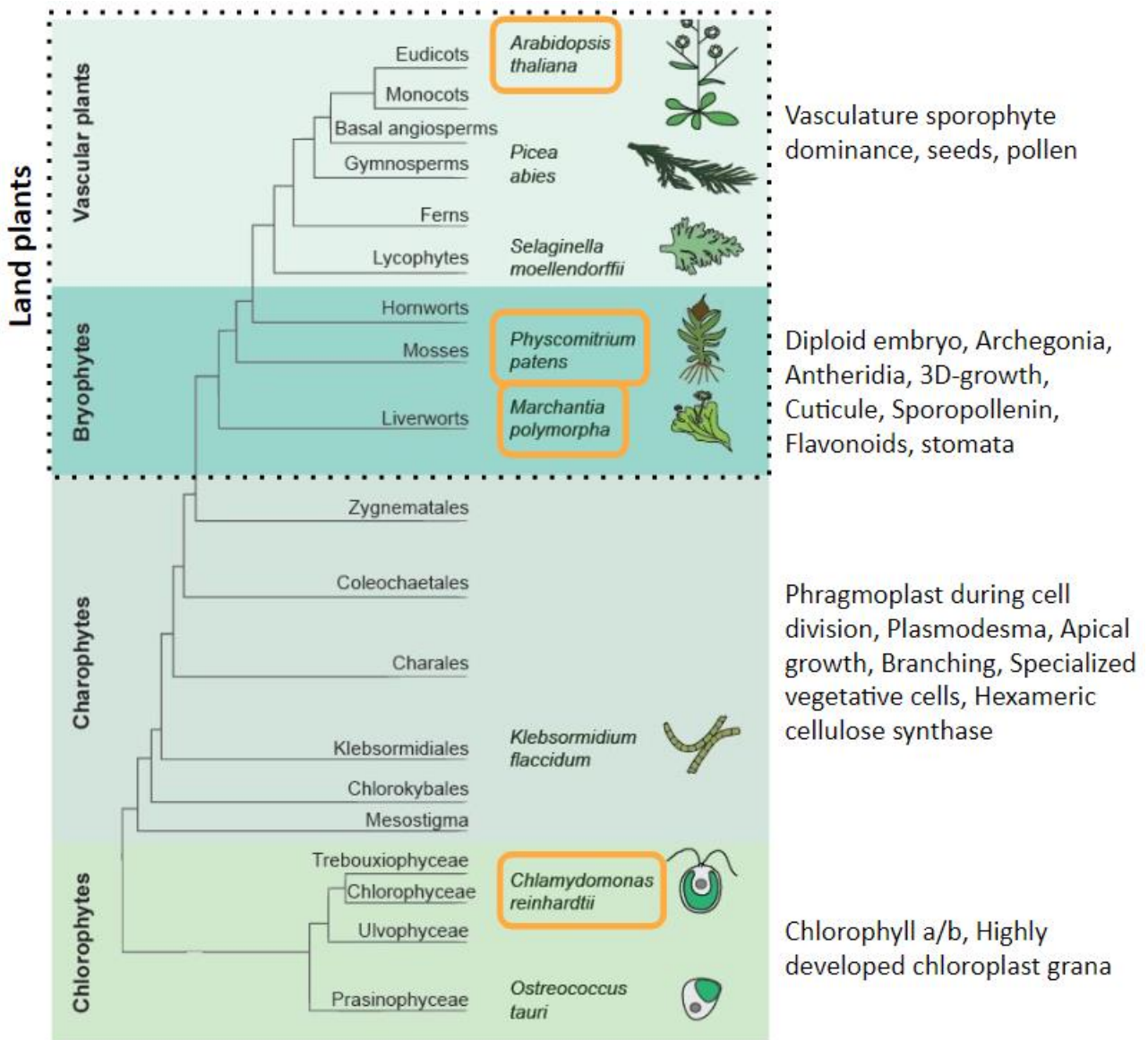


Figure 2: Phylogenetic tree of green lineage with character acquisition

Characters acquired by each of the clades during the evolution of the green lineage. Not all subclasses contain all characters. The organisms mainly cited in this thesis are circled in orange. *Image from Petersen et al., 2022 and evolutive characters from Bowman et al., 2017.*

From land colonisation to the development of the most evolved plants

Flowering and fruiting plants or angiosperms are the photosynthetic organisms considered to be the most evolved to date. They appeared about 335 million years later than Bryophytes, at a time when CO₂ atmospheric concentrations were almost 2000 ppm and O₂ concentration was almost two times higher compared to Ordovician (Figure 3). These organisms had to develop morphological adaptation strategies: vascularisation systems, leaves and specialised roots (Hetherington *et al.*, 2019), reproductive systems more independent of humidity, which were accompanied by molecular changes. In particular, the appearance of angiosperms is known to be marked by the loss of many regulatory proteins and photosynthesis is not an exception. This may make angiosperms much more efficient compared to gymnosperms and lower plants in most ecological habitats.

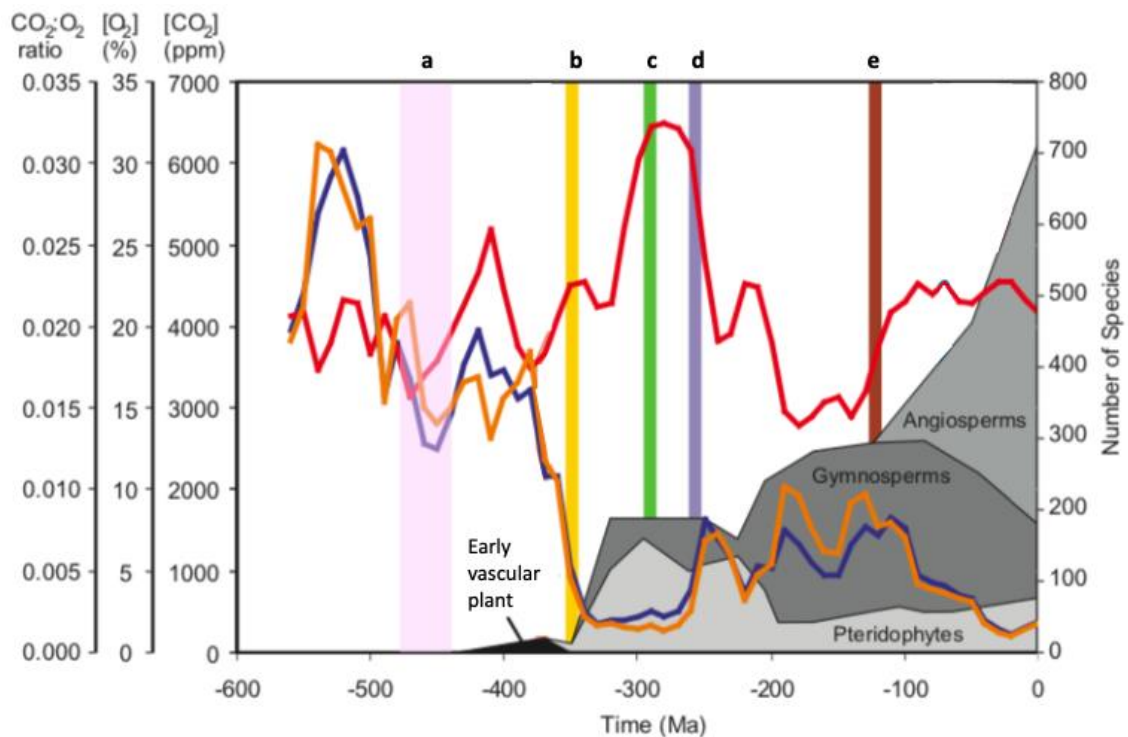


Figure 3: Atmospheric CO₂ and O₂ levels during plant evolution

Atmospheric concentrations of CO₂ (Berner *et al.*, 2006), O₂ (Berner *et al.*, 2009) and CO₂:O₂ ratio are plotted in blue, red and orange, respectively. Evolutionary periods a, b, c, d and e correspond to the development of Bryophytes (Ordovician), ferns, cycads and Ginkgoaceae, conifers and angiosperms, respectively. *Image and legend modified from Haworth et al., 2011.*

Photosynthesis research

Since the advent of sequencing in the 2000s, among the oxygenic photosynthetic organisms most studied are the green alga *Chlamydomonas reinhardtii* (Blaby *et al.*, 2014) and the angiosperm *Arabidopsis thaliana* (Arabidopsis Genom Initiative, 2000), particularly because the latter is diploid while many other angiosperms have a more complicated genomes (Figure 2). In recent years, genome sequencing of new model plants has broadened photosynthesis research and opened new perspectives in evolutionary developmental biology. This is the case for certain Bryophytes such as *Physcomitrium patens* (Lang *et al.*, 2008; Rantala *et al.*, 2008) (moss) and *Marchantia polymorpha* (Bowman *et al.*, 2017) (liverwort). The study of these new organisms provides an intermediate view of the evolutionary state of photosynthesis between the appearance of green algae and that of angiosperms. In particular, it has been shown that these organisms have intermediate characteristics: conservation of characteristics present in algae, appearance of characteristics corresponding to angiosperms or cohabitation of ancestral and evolutionary characteristics. This is particularly the case of a protein family of interest in this present work: the Plastid Terminal Oxidase (PTOX) (Messant *et al.*, 2021). On the other hand, the diversification of model organisms facilitates the study of preserved mechanisms by investigating them in simpler plants (dominating tissue haploid, easier culturing, propagation of cultivars). Here I am interested in the manganese cluster. Although studied for decades, many questions about its light-

dependent assembly (photoactivation) remain unanswered. I have chosen to use *Marchantia polymorpha* to open up new ways for studying this mechanism.

To conclude, this study aims to obtain clues on certain fundamental aspects of plant photosynthesis which are the assembly of the OEC and the Plastid Terminal Oxidase PTOX, the latter protein being involved in a protection mechanisms of the photosynthetic chain against photodamage through the panoramic vision offered by photosynthetic organisms' evolution. I will compare the results of our studies carried out in *Marchantia polymorpha* with what is already known in *Chlamydomonas reinhardtii* and *Arabidopsis thaliana*. Furthermore, *Marchantia polymorpha* being a very little studied model to date, I will compare some of my data with published data collected on the most evolutionarily close and more often studied plant: *Physcomitrium patens*, to support my findings.

In an introductory part, I will describe the main characteristics of the photosynthetic chain of plants as well as protection mechanisms. I will discuss the dynamics of photosynthetic complexes in thylakoid membranes. I will end with the presentation of super-resolution microscopy, which is an emerging tool to follow changes in the organisation of thylakoid membranes. Then, I will present the emerging model plant, *Marchantia polymorpha*, with its morphological and photosynthetic peculiarities in relation to its place in evolution and I will explain why its study was essential for my work. To summarise, this thesis addresses three main themes. The first point is a study of photosynthesis regulation at the PSII donor side. On the one hand, I characterised the impact of manganese deficiency or excess on *Marchantia polymorpha* photosynthesis and metabolism (**article 1**). Furthermore, I investigated the light-dependent mechanism of Mn cluster assembly *in vitro* and followed this process *in vivo* and compared the findings with previous works. The second point concerns the regulation of photosynthetic electron transport. It consists of a study of the PTOX (Plastid Terminal Oxidase) protein *in vivo* (**article 2, article 3**) and *in silico*. Finally, a theoretical reflection on the impact of changes in membrane dynamics leading to a modulation of photosynthetic electron flow (**article 4**) was carried out.

1) Background of photosynthesis

Oxygenic photosynthesis takes place in cellular organelles called chloroplasts. I concentrate here only on land plants, which include all clades from the appearance of Bryophytes unless otherwise specified in the text.

In land plants, chloroplasts are located in very large numbers in the photosynthetic cells. They are composed of two membranes (which is not the case for all photosynthetic organisms), an external and an internal, whose permeability is very different (Figure 4, **A**). The outer membrane is mostly unselective and allows the entry of many molecules from the cytoplasm of the cell. Conversely, the inner membrane truly serves as a selective barrier, containing transporters, allowing the selection of molecules entering the stroma (aqueous phase). Inside the chloroplast, there is a complex membrane network called thylakoids (Figure 4, **B**). The

thylakoids are either stacked, these are the grana, or bathed directly in the stroma, these are the stroma lamellae (Rumak *et al.*, 2010; Staehelin and Paolillo, 2020). Protein complexes that are part of the photosynthetic chain are located in the thylakoid membrane (Rantala *et al.*, 2020; Goss *et al.*, 2021) (Figure 4, C) while additional proteins are attached to these transmembrane protein complexes either at the luminal or stroma side of the membrane. The scheme only shows the complexes embedded in the membrane: photosystem II (PSII), the plastoquinone (PQ) pool, cytochrome *b₆f* (cyt *b₆f*) and photosystem I (PSI). The complex 3D structure of thylakoids is important for the optimization of electron transfer through the photosynthetic chain (Johnson *et al.*, 2018). The distribution of complexes on grana and stroma lamellae is also important. Finally, the complexes are oriented in the membrane. One talks about the acceptor side for the part in contact with the stroma and of the donor side for the part in contact with the lumen. Different electron flows are generated through these complexes depending on the different physiological conditions, forming the notion of Linear Electron Flow (LEF) or Cyclic Electron Flow (CEF) (Stirbet *et al.*, 2020). Finally, under stress conditions, plants have developed mechanisms to protect the photosynthetic chain. I will detail all these points in this introductory chapter.

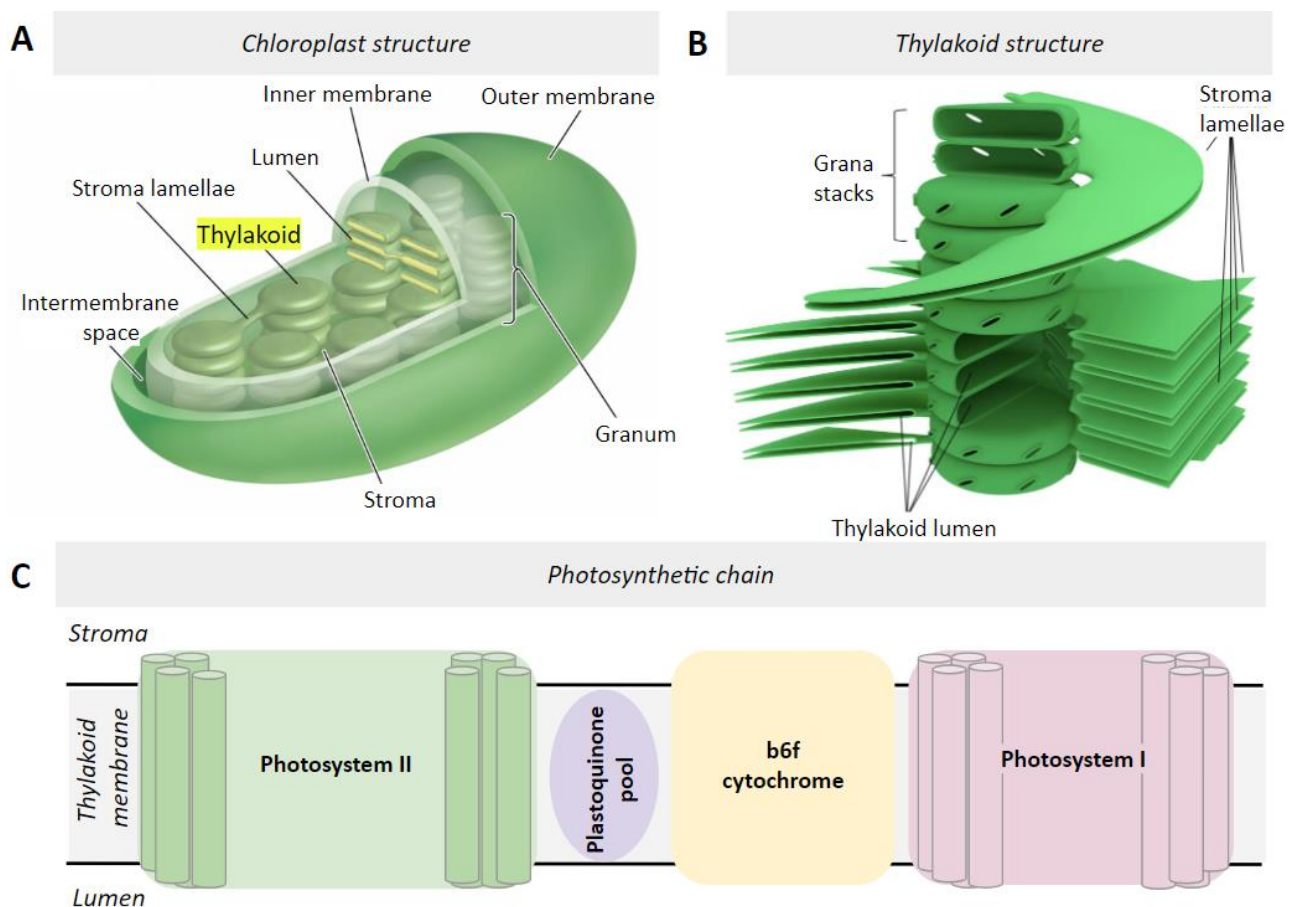


Figure 4: Chloroplast and thylakoid structure and presentation of the photosynthetic chain

A. Land plant chloroplast structure. From *encyclopaedia Britannica*, <https://www.britannica.com/science/chloroplast>. **B.** 3D thylakoid membrane structure. By *Kelvinsong*, <http://creativecommons.org/licenses/by-sa/3.0>. **C.** Scheme of the principal constituents of the photosynthetic chain: the photosystem II (green), the plastoquinone pool (purple), the cytochrome *b₆f* (yellow) and the photosystem I (red).

A) Linear Electron flow

Linear Electron Flow (LEF) from water to NADP^+ is generated through the photosynthetic electron transfer chain in order to convert the light energy from the sun into chemical potential energy. Light is collected by the antennae (Light Harvesting complexes, LHCs) of PSI and PSII thanks to chlorophyll pigments. Carotenoids are also linked to LHC proteins which are involved in photon capture but their major role is the photoprotection.

Electron transfer through the photosynthetic chain occurs as follows (Figure 5). Photon energy is converted into chemical energy through charge separation in the photosystems. Oxidation of water and reduction of PSII components result in reduction of the plastoquinone pool whose molecules are diffusible inside the thylakoid membrane. The reduced plastoquinone transmits its electrons to the cytochrome b_6/f complex, allowing, together with the proton release upon oxidation of water, the generation of a transthylakoidal proton gradient (ΔpH). This leads to the acidification of the lumen and the ΔpH together with the electrochemical gradient is the driving force (also called proton motive force) for ATP production (Höhner *et al.*, 2016; Kaur *et al.*, 2021). Then, cytochrome f reduces the plastocyanin, a diffusible molecule in the lumen which is the electron donor of PSI. On the stromal side, PSI reduces Ferredoxin (Fd) whose electrons are used by Ferredoxin-NADP⁺-Reductase (FNR) to generate reducing power in the form of NADPH.

In this part, I will detail the structures of the various complexes of the photosynthetic chain mentioned above as well as the electron flow and its regulation.

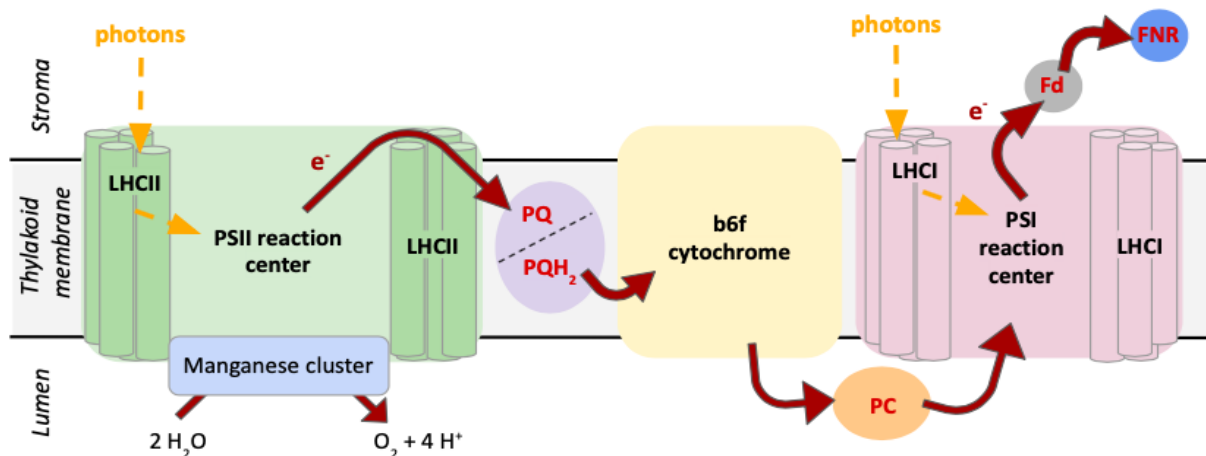


Figure 5: Simplified presentation of linear electron transfer through the protein complexes of the photosynthetic chain

Photons (broken orange arrow) excite the chlorophyll pigments present in all the antennae or Light Harvesting Complexes (LHC, cylindrical shapes) present at the level of photosystems I (red complex) and II (green complex). When the chlorophylls of the LHCIIs are excited, they transmit their energy to particular chlorophylls of the PSII reaction centre (called P680) where a charge separation takes place and electrons are transferred to a series of electron acceptors (continuous dark red arrows). A cascade of redox reactions follows which leads to the reduction of the plastoquinone (PQ) pool (purple complex). The return to the ground state of the PSII reaction centre is enabled by the manganese cluster (blue) which catalyses water oxidation. The plastoquinol (PQH_2) is reoxidized by the cytochrome b_6/f (yellow complex) which in turn will reduce the plastocyanin (PC) present in the lumen (orange complex). Within the PSI reaction centre, after excitation of chlorophylls, charge separation takes place at the special chlorophyll P700 and subsequent electron transfer steps lead to the reduction of the ferredoxin (Fd, grey) on the stromal side. It is itself oxidised by the Ferredoxin-NADP⁺-Reductase (FNR, blue), able to catalyse the reduction to NADPH, a universal energy carrier for metabolic reactions.

1) Photosystem II Structure and Electron Transport

Photosystem II is composed of the antenna proteins that harvest photons and the reaction centre which converts the resulting excitons into chemical potential energy. The ensemble of antennae and a reaction centre is called a supercomplex.

Light Harvesting Complexes in PSII (LHCII) are embedded in the membrane and surround the reaction centre (Wei *et al.*, 2016; Cao *et al.*, 2018; Sheng *et al.*, 2021). They are composed of different combinations of three LHC proteins which have the ability to non-covalently bind pigments: chlorophyll (light harvesting) and xanthophylls (light harvesting and protection). Each LHCII contains four xanthophylls: two luteins, one neoxanthin and one xanthophyll which can be violaxanthin, antheraxanthin or zeaxanthin (Liu *et al.*, 2004; Standfuss *et al.*, 2005). The latter are important for PSII protection during a mechanism called the xanthophyll cycle (see “Non-photochemical quenching”, page 32). There are three types of LHCII whose attachment to the reaction centre depends on their Lhcb protein compositions (strong, moderately or loosely bound) (Boekema *et al.*, 1999). Some of them are able to migrate under certain conditions: this is the state transition (see “Non-photochemical quenching”, page 32). LHCII are composed of three Lhcb proteins (1 to 3) combined in different ways. Once talk about homo/heterotrimers. There are also monomeric minor antennae: Lhcb4 to 6 also named CP29, CP26 and CP24, respectively. For a more detailed description, see article 4, page 165. In higher plants, the standard supercomplex for PSII-LHCII is considered to be C_2S_2 (Dekker and Boekema, 2005): a PSII core dimer attached to two strongly-associated LHCII. However, different combinations of major antennae bound to the reaction centre depending on the species can also be found (Figure 6).

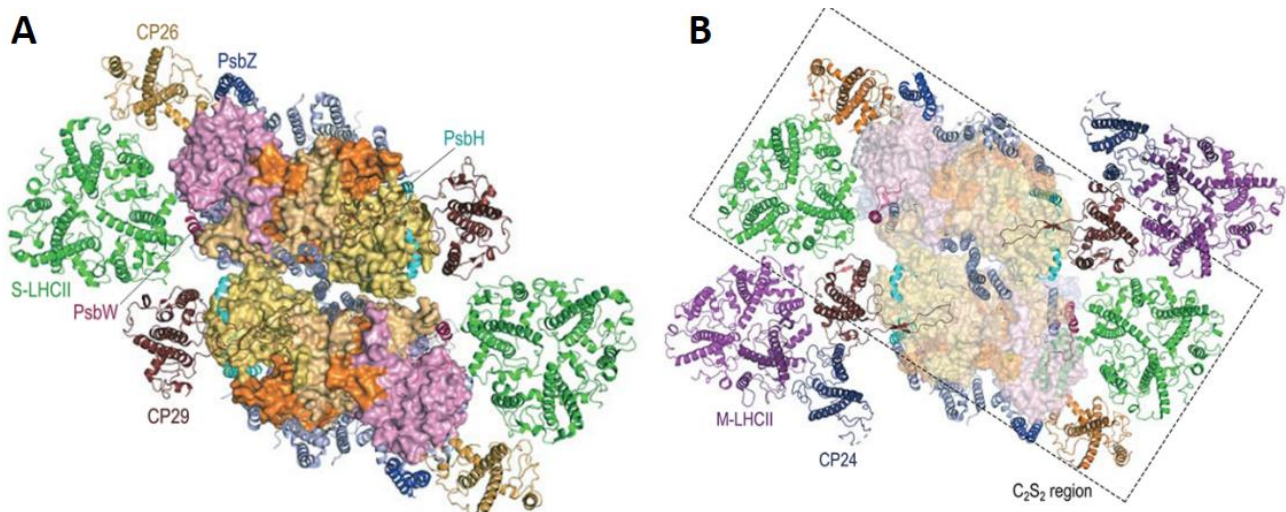


Figure 6: Example of structure diversity of PSII-LHCII supercomplexes in higher plants

A. Top view of the C_2S_2 supercomplex from spinach (PDB ID code 3JCU) from the stromal side. PSII core dimer is surrounded by two S-LHCII (green) major antennae and two CP29 (red) and CP26 (yellow) minor antennae. PsbH (cyan) is thought to be important for CP29 binding. The same is true for PsbZ (dark blue) with CP26. PsbW is believed to be important for CP43 binding which is an inner light harvesting protein. **B.** Top view of the $C_2S_2M_2$ supercomplex from pea (PDB ID code 5XNL) from the stromal side. Added to the previous image are the two major antennae M-LHCII (magenta) as well as two minor antennae proteins CP24 (dark grey). Images and inspired legends from Sheng *et al.*, 2021.

The reaction centre is composed of at least 20 subunits depending on the species, the inner light harvesting proteins (CP43 and CP47), a dozen of transmembrane subunits of low molecular weight as well as several extrinsic subunits named PsbO, P and Q (Figure 7). The highest molecular weight proteins are D1 and D2. Together, they bind the direct contributors to the electron flow through the core: the P680 chlorophylls of the PSII reaction centre, the initial electron acceptor, the pheophytin, the primary and secondary quinone acceptors, Q_A and Q_B , as well as the manganese cluster.

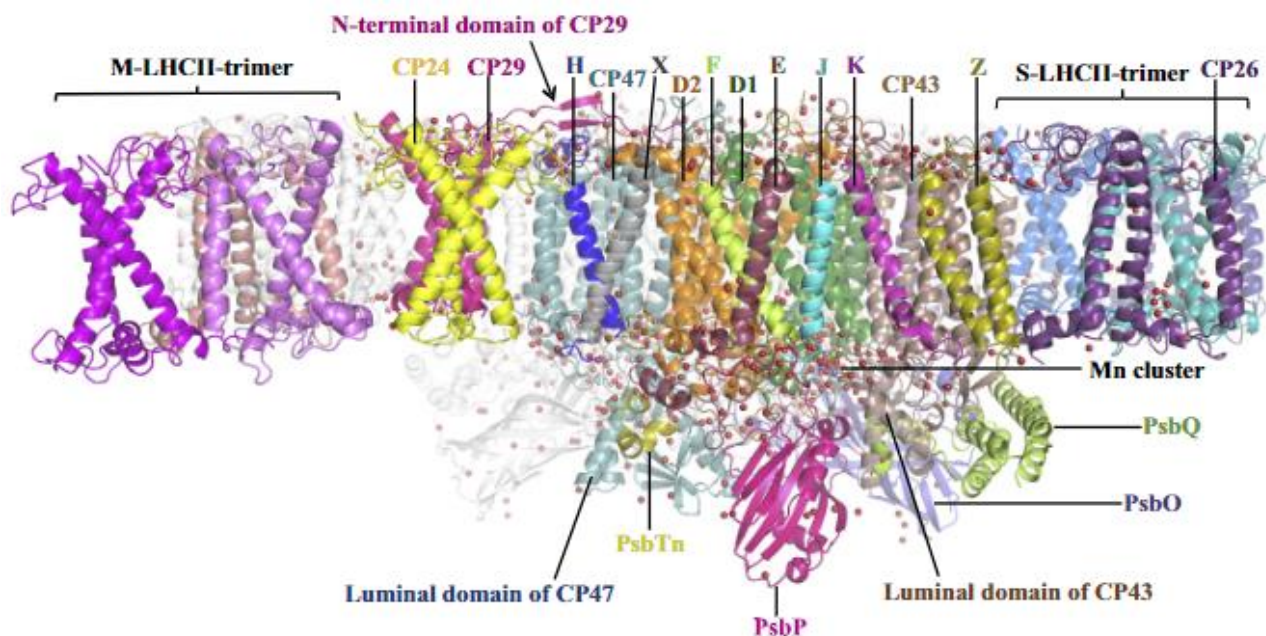


Figure 7: PSII structure of *Pisum sativum*

Side view along the membrane plane. The sub-units are coloured in one PSII monomer and shown in white in the other (PDB ID: 3JCU/5XNM). The water molecules and the Mn_4CaO_5 cluster are presented as filled circles. The other cofactors are omitted for clarity. The N-terminal domain of CP29 is indicated by an arrow. The M and S-LHCII are part of the major collector antennae. CP24, CP29 and CP26 are the minor antennae. CP43 and CP47 are the inner light harvesting proteins. D1 and D2 are the two high molecular weight subunits of the PSII reaction centre. The subunits surrounding the manganese cluster are PsbP, PsbO and PsbQ. The role of the other subunits will not be detailed in this study.

Structure and inspired legend from Cao et al., 2018.

The orientation of PSII across the membrane helps to determine donor and acceptor sides (Figure 8, **A**). On the reaction centre stromal side are the primary and secondary quinone acceptors Q_A and Q_B as well as the non-heme iron coordinated by a bicarbonate and 4 histidine residues, two coming from D1 and two from D2 (Figure 8, **B**). Q_A , a one-electron acceptor, is a quinone strongly bound to the D1 protein whereas the PQ of the Q_B -site, a two-electron acceptor called Q_B , is more weakly bound and is able to diffuse after complete reduction and protonation into the membrane joining the PQ pool. Q_B can also be replaced by exogenous molecules allowing its study such as artificial quinones or herbicides (*e.g.* DCMU). It is known that the bicarbonate ion affects forward electron transfer.

On the luminal side the manganese cluster (Mn_4CaO_5) is located whose role is to catalyse water oxidation and allows the return to the P680 ground state (see "Oxygen Evolving Complex", page 23).

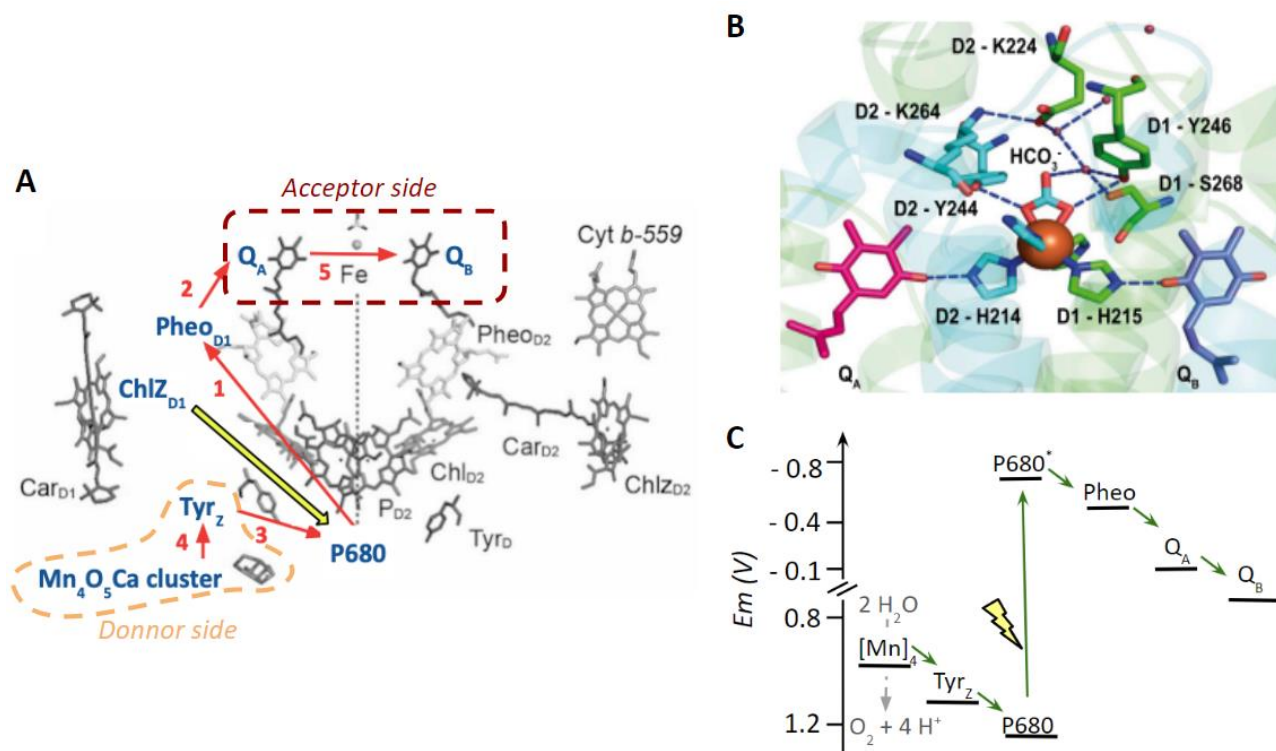


Figure 8: Electron transfer through PSII

A. PSII core cofactors, for one PSII monomer, involved in electron transfer. The acceptor side formed by the quinones Q_A and Q_B as well as the non-heme iron are circled in brown. The donor side composed of Tyr_Z and the manganese cluster are circled in orange. The excited Chl_{D1} transmits its excitation to the Chl_{D1} (yellow arrow) where charge separation takes place. Then, the positive charge is stabilised on P₆₈₀, a weakly coupled chlorophyll dimer, P_{D1}P_{D2}, with the positive charge mainly on P_{D1}. Then, pheophytin is reduced (1), Pheo⁻ reduces then the primary quinone acceptor Q_A (2). The positive charge of P680 is filled by an electron coming from Tyr_Z (3) which is itself reduced by an electron coming from water oxidation carried out by the Mn₄CaO₅ cluster (4). Finally, two successive electrons coming from Q_A reduce the quinone at the Q_B site (5). *Image from Lubitz et al., 2019.* **B.** Detailed structure of the acceptor side. In orange is the non-heme iron coordinated by a bicarbonate (HCO₃⁻) and two residues of D1 and D2. Here, only D1-H215 and D2-H214 are visible. The bicarbonate ion is also ligated to residues of the D1 and D2 proteins. Q_A and Q_B quinones are shown in pink and blue respectively. *Image from Brinkert et al., 2016.* **C.** Energetic scheme of redox reactions explained in **A** (Merry et al., 1998 ; Shibuya et al., 2010 ; Krieger and Weis, 1992 ; Krieger et al., 1995 ; Johnson et al., 1995 ; Shibamoto et al., 2009 ; Shibamoto et al., 2010).

Concerning the electron transfer (Figure 8, **A** and **C**), when the chlorophylls of the PSII light harvesting complexes are excited, the excitation is transferred to Chl_{D1} and then to Chl_{D1} where charge separation takes place. The positive charge is distributed over P_{D1} and two chlorophylls, all together named P680⁺, while the negative charge is transmitted to the pheophytin which becomes Pheo⁻. Pheo⁻ reduces the first quinone acceptor Q_A, which in turn reduces Q_B, the secondary quinone acceptor. Two successive electron transfer steps are required to allow the complete reduction and protonation of the second quinone Q_B producing plastoquinol (PQH₂). This PQH₂ will then be replaced by an oxidised quinone from the plastoquinone pool.

On the donor side, tyrosine Z (Tyr_Z) reduces P680⁺. This allows the return to the fundamental state of P680. Finally, the Tyr_Z⁺ extracts an electron from the Mn cluster, allowing, in subsequent steps, water

oxidation after in total four charge separation and electron transfer reactions (see “Oxygen Evolving Complex”, page 23).

In PSII Reactive Oxygen Species (ROS) can be formed such as singlet oxygen by charge recombination reactions or also reduced forms of O₂ such as the superoxide anion radical and hydrogen peroxide. This happens in particular upon exposure to strong light intensities. This stress has the consequence of over-reducing the plastoquinone pool which in turn leads to a slowdown in the electron flow between Q_A and Q_B. This has the effect of encouraging charge recombination reactions causing the generation of a chlorophyll triplet (³P680) which reacts rapidly with oxygen generating the highly reactive singlet oxygen (Johnson *et al.*, 1995; Rutherford and Krieger-Liszkay, 2000). This has the major consequence of degrading the D1 protein of the reaction centre (Keren and Ohad *et al.*, 1998; Rokka *et al.*, 2005). It has recently been shown that Q_A⁻ can catalyse oxygen reduction to superoxide under certain circumstances (Fantuzzi *et al.*, 2022).

There are many protection mechanisms that allow the limitation of this damage, the most important ones are explained in article 4, page 150.

In addition, studies show that there could be a protective mechanism of PSII based on a slowing down of the forward electron transfer between Q_A and Q_B. Indeed, it has been shown in certain photosynthetic organisms that the bicarbonate ion present on the PSII acceptor side could be replaced by small carboxylic acids. In *Arabidopsis thaliana*, the study of a the *hpr1* (hydroxypyruvate reductase-1) photorespiratory mutant able to accumulate the glycolate shows that the replacement of the bicarbonate by glycolate shifts the midpoint redox potential of the redox couple Q_A/Q_A⁻ to a more positive value. This lowers the yield of the production of singlet oxygen and promotes the protection of PSII (Messant *et al.*, 2018). The same phenomenon was also observed in a mixotrophic culture of the green alga *Chlamydomonas reinhardtii* in the presence of acetate (Roach *et al.*, 2013). However, no study has yet demonstrated the physiological role of this regulatory mechanism in wild-type organisms under stressed conditions. However, drought evokes a slowdown of electron transport between Q_A and Q_B, indicating that redox tuning of Q_A may indeed occur *in vivo* (Leverne and Krieger-Liszkay, 2021).

2) Oxygen-Evolving Complex

The manganese cluster (Mn_4CaO_5) or Oxygen Evolving Complex (OEC, with extrinsic proteins) is the only biocatalyst on Earth able to catalyse water oxidation and the production of oxygen. The cluster is located on the donor side of PSII and is absolutely necessary to complete its maturation and allow it to be functional. It is coordinated by seven ligands coming from the reaction centre, the majority of which come from D1 (Figure 9, A). The cluster is composed of four Mn atoms and one calcium. Its structure has a cubic shape with three Mn and the Ca. The fourth Mn is nicknamed “the soaker” because it is located slightly outside (Bao and Burnap, 2016). Nixon and Diner, 1992 and others after them (Boerner *et al.*, 1992) has defined, by directed mutagenesis, that D1-Asp170 is an essential residue for Mn cluster assembly. Then, they called it High Affinity Site (HAS) by assuming that it is the place where Mn(II) bound during photoactivation.

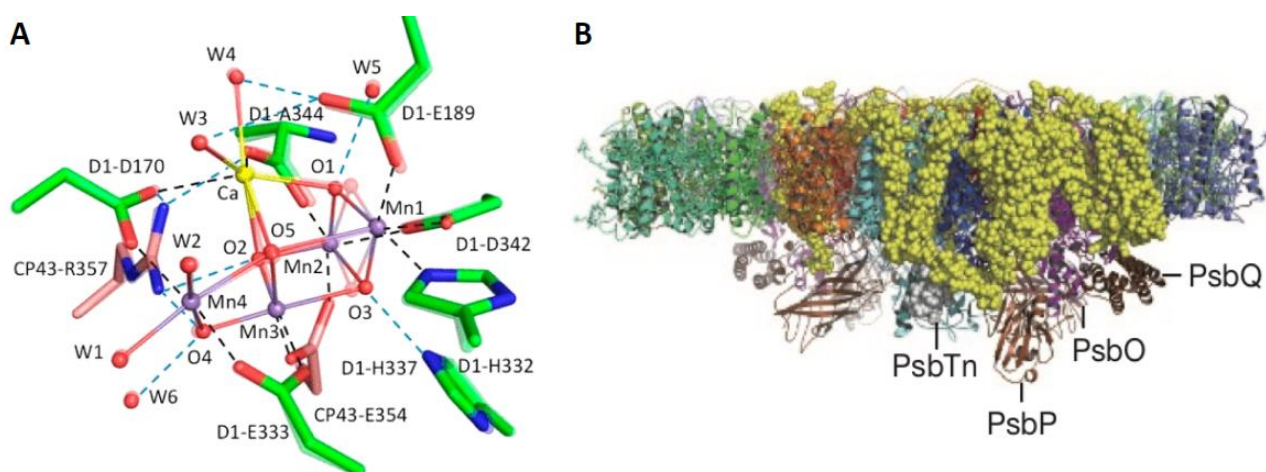


Figure 9: Manganese cluster cubane structure and extrinsic stabilising proteins

A. Superposition of the structure of two different OEC monomers. Broken lines in black and blue indicate the valence bonds and the hydrogen bonds respectively. *Image and inspired legend from Tanaka et al., 2017.* **B.** Structure of the spinach C_2S_2 -type PSII-LHCII supercomplex. Side view along the membrane plane. Dashed lines indicate estimated interfacial regions between the two monomers. The major components are shown as cartoon and stick models in different colours and the 12 small intrinsic subunits of PSII core are shown as yellow sphere models. *Image and legend from Wei et al., 2016.*

The manganese cluster assembly process is a light-dependent mechanism named photoactivation (Bao and Burnap, 2016). Photoactivation occurs in two distinct physiological conditions: in the last maturation step of a new PSII reaction centre but also when the D1 protein is damaged, during the repair process. In the first case, it allows the quinone Q_A to be photochemically active by causing a change in its electrochemical potential (Krieger and Weis, 1993). Then the cluster must be deconstructed to allow D1 replacement (Krieger *et al.*, 1998) and then reassembled (see article 4, page 165). This observation also highlighted a difference in localisation between photoactivated and non-photoactivated PSII in the grana stacks and stroma lamellae, respectively (Rantala *et al.*, 2020) (see part “Chloroplast membrane dynamic”, page 37). The photoactivation steps and the structural details of the cluster will be presented in more detail in part I, page 50.

Three extrinsic proteins are attached to the cluster: PsbP, PsbO and PsbQ (Figure 9, B). Over the years, several hypotheses have been formulated about their assembly. It has been proposed that their attachment was sequential. For example, PsbO would attach first because it contains residues necessary for PsbP attachment (Bricker and Frankel, 2003). Today, once favour the hypothesis of an independent assembly even if their expressions are correlated with each other. It has been shown in mutants of higher plants depleted in PsbP (Ifuku *et al.*, 2005) and PsbO (Yi *et al.*, 2005), an almost complete absence of PsbQ. Finally, it has been demonstrated that the binding of the three proteins involves minor PSII subunits such as PsbK, PsbJ and PsbR (Suorsa *et al.*, 2004; 2006). In particular, PsbR is required for PsbP attachment.

The attachment of these proteins is necessary to allow the stabilisation of the cluster. PsbP is known to be important for calcium binding. It also allows, with PsbQ the coordination between PSII donor and acceptor sides while guaranteeing the stabilisation of PSII-LHCII supercomplexes (Ifuku *et al.*, 2011). For more details on the roles of PsbP, PsbO and PsbQ see Suorsa and Aro, 2007; Bricker and Frankel, 2011; Suorsa *et al.*, 2016.

The water oxidation model was established by Kok and Joliot in the seventies of the last century (Kok *et al.*, in 1970). It corresponds to five S-states, from S_0 to S_4 , which represents a succession of four water oxidation steps. The S_0 state is the most reduced state while the S_4 is a transient state that decays spontaneously to S_0 by releasing a molecule of dioxygen. Four charge separations are needed to complete the cycle, and each corresponds to a removal of an electron from a water molecule and to a release of a proton. The oxidation state of the Mn ions as well as the mechanisms of each of the S-states are still under debate. An example is presented in Figure 10. Here, I will just present some recently highlighted facts on this topic.

The S_1 state is stable in the dark. Thus it is the easiest state to obtain and the first that has been crystallized (Umena *et al.*, 2011, Suga *et al.*, 2015)(Figure 9, A). The most accepted Mn oxidation state proposed for this step is $Mn(III)_2-Mn(IV)_2$ (Figure 10) (Vinyard *et al.*, 2015) or $Mn(III)_4$ or $Mn(II)-Mn(III)_2-Mn(IV)$ (Gatt *et al.*, 2012; Vinyard *et al.*, 2013). The transition to S_2 is marked by the oxidation of one of the Mn(III) to Mn(IV) and no protons are released. The S_2 state shows two paramagnetic signals by Electron Paramagnetic Resonance (EPR) spectroscopy. The two spin isoforms are: $S_{GS}=1/2$ low spin (S_2^{LS}) and $S_{GS}\geq 5/2$ high spin (S_2^{HS}). During this step, it is assumed that only one Mn(III) remains in the structure which is suggested to be present at either Mn1 or Mn4 in the cluster. The presence of a Mn(III) at Mn1 place forms the open cubane structure (Pantazis, 2012) which corresponds to S_2^{LS} while at Mn4 place, it forms the closed cubane structure and corresponds therefore to S_2^{HS} . At the experimental level, S_2^{LS} is known to represent a multiline EPR spectrum whereas the S_2^{HS} has a derivative-like EPR signal. Thus, it has recently been shown that S_3 is formed only from S_2^{HS} . Boussac (2019) proposes that S_2 to S_3 transition is triggered by the generation of tyrosine Z radical which favors deprotonation (of W1 by Asp61) as well as water binding. So far, all the structures presented for S-states result from theoretical models based on the S_1 crystallographic structure

(Guo *et al.*, 2017; Wang *et al.*, 2017; Narzi *et al.*, 2018; Siegbahn *et al.*, 2018) although the field is advancing (Suga *et al.*, 2017; Kern *et al.*, 2018). Finally, S_4 is experimentally obtained by applying three flashes of light to dark-adapted PSII. It corresponds to the oxidation of two water molecules attached to the cluster and the release of oxygen to allow the return to S_0 (Yano and Yachandra, 2014; Shen, 2015; Dau *et al.*, 2012; Vineyard and Brudvig, 2017).

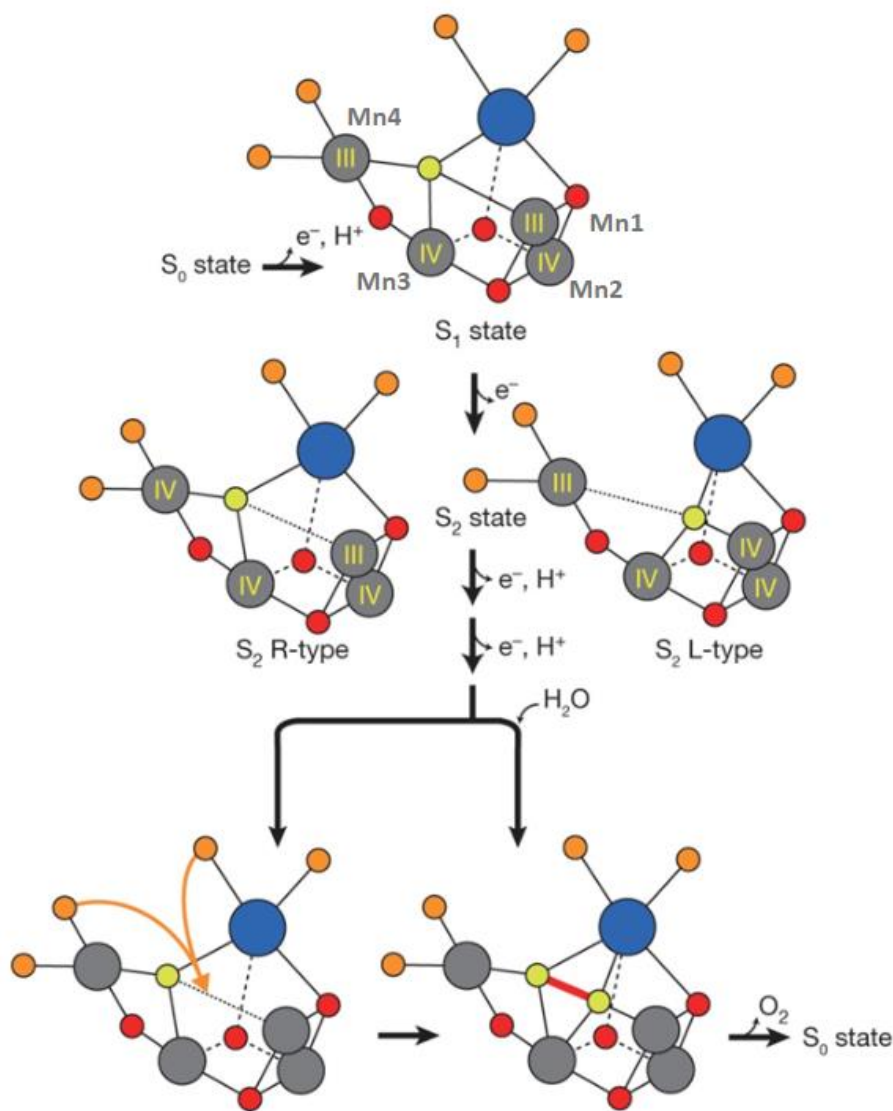


Figure 10: Example of OEC manganese ion oxidation mechanisms

O5 (yellow) in the S_1 state is connected to both Mn1(III) and Mn4(III). Upon transition from S_1 to S_2 , an electron may be removed from Mn4, leading to a right-side open structure ('R-type'), or from Mn1, leading to a left-side open structure ('L-type'). Both structures will allow insertion of a new water molecule during the subsequent S-state transition, preparing for the transition state immediately before O=O bond (indicated by a red bond in the right-hand structure in the bottom row) formation. Alternatively, the transition state ready for O=O bond formation may be formed by moving either W2 or W3 toward O5 (indicated by orange arrows in the left-hand structure in the bottom row). Manganese ions are shown with their assumed oxidation states (grey). The oxygen atoms are colored in red, the calcium ion in blue and water molecules in orange. *Image and legend from Suga et al., 2015.*

3) Photosystem I

In higher plants, PSI supercomplexes also designate the association of the reaction centre with its antennae. The PSI antennae is composed of Lhca proteins. Lhca1 to 4 form a belt around the reaction centre (Figure 11, **A**). They are arranged in the following order: Lhca1, Lhca4, Lhca2 and Lhca3. Their conserved N-terminal (Nter) regions allow them to interact with each other. They are also each linked to the reaction centre proteins PsaB, PsaF, PsaJ and PsaA, respectively. PsaA and PsaB are the two central proteins of the reaction centre that bind the cofactors involved in electron flow together with PsaC, localised on the stromal side. In contrast to D1 and D2 in PSII, PsaA and PsaB contain many pigments. PsaF is involved in the plastocyanin docking. PsaC, PsaD and PsaE form the docking site of Fd, and PsaG participates in the regulation of electron flow by stabilising the core (Sétif *et al.*, 2002; Varotto *et al.*, 2002). Under certain physiological conditions, such as light stress, it is possible that the PSII antennae (LHCII) migrate and bind to the PSI supercomplex, a process called state transition (article 4, page 150). Together, the PsaL, PsaH and PsaO proteins form the domain allowing the PSI-LHCII association. Thereby, PSI has the ability to receive energy from two pools of antennae: LHCI and LHCII (Rantala and Tikkanen, 2018).

Electron transfer involves chlorophyll P700, the chlorophyll *a* A₀, the phylloquinone A₁ and F_x which is an iron-sulfur (4Fe-4S) cluster linked to four cysteine residues, two from PsaA and two from PsaB (Figure 11, **B**). PSI also has two other 4Fe-4S clusters that are linked to the PsaC protein, named F_A and F_B.

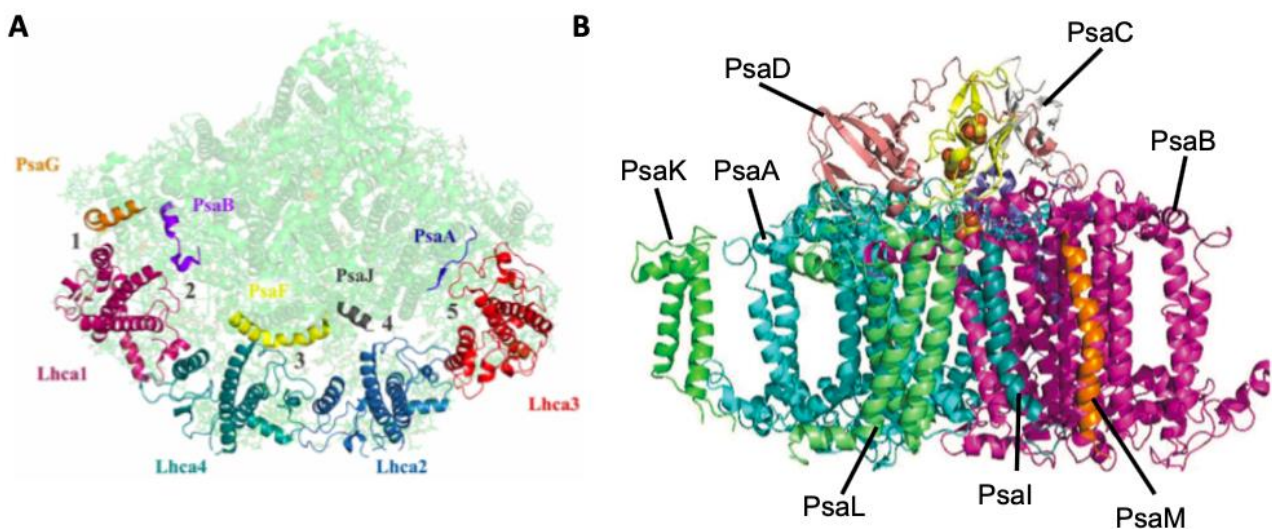


Figure 11: Structure of PSI antennae and the PSI-supercomplex

A. Stromal view of Lhca subunits interactions and association with PSI core (Mazor *et al.*, 2017 ; PDB 5L8R). Lhca1, pink; Lhca4, dark green; Lhca2, skyblue; Lhca3, red. Contact sites of PsaA, blue; PsaB, purple; PsaJ, grey; PsaF, yellow; PsaG, orange. **1:** helix C of Lhca1 interacts with the first transmembrane helix of PsaG. **2:** PsaB stromal loop and Lhca1 Nter. **3:** Lhca4 Nter and PsaF C-terminus (Cter). **4:** Lhca2 first transmembrane helix and PsaJ Nter. **5:** Lhca3 stromal loop and PsaA Nter. *Image and legend from Caspy and Nelson, 2018.* **B.** PSI reaction centre structure from *T. elongatus*. *Image from Gordiichuk et al., 2017.*

The P700 dimer receives energy from the antennae resulting in $P700^*$ that undergoes charge separation (Figure 12). An electron is transmitted to the primary acceptor chlorophyll a A_0 then to phylloquinone A_1 . It successively reduces the three Fe-S clusters F_X , F_A and F_B and finally ferredoxin. The Ferredoxin-NADP⁺-Reductase (FNR) catalyses the production of reducing power as NADPH from reduced ferredoxin (for a review, see Hanke and Mulo, 2013). At the same time, the positive charge generated ($P700^+$) returns to its ground state by accepting electrons from the reduced plastocyanin (Caspy *et al.*, 2020). Different to PSII, both branches containing the cofactors are active in electron transport.

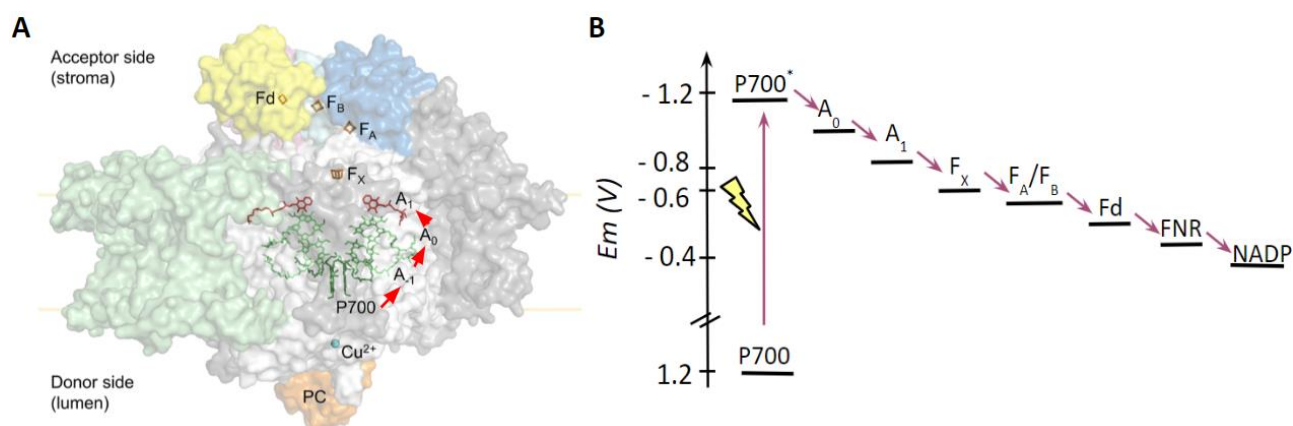


Figure 12: PSI reaction centre scheme and energetic diagram of electron transfer

A. Simplified tertiary structure of the PSI:plastocyanin:ferredoxin complex (PDB accession 6YEZ; Caspy *et al.*, 2020), showing protein subunits PsaA and PsaB (white), PsaC (cyan), PsaD (blue), PsaE (pink) and LHCI subunits (green). Other PSI subunits are coloured in grey. Also shown are plastocyanin (orange) at the PSI donor side and ferredoxin (yellow) at the PSI acceptor side. Cofactors involved in electron transport are shown; Cu^{2+} (blue), P700 (dark green), A_{-1} and A_0 chlorophylls (lime), A_1 phylloquinone (red) in PSI, as well as the PSI 4Fe4S clusters F_X , F_A , F_B (orange) and the ferredoxin (Fd) 2Fe-2S cluster (orange). *Image and legend from Lima-Melo et al., 2021.* **B.** Energy Diagram of redox reactions from the PSI reaction centre to the production of energy in the form of NADPH that is used in the Calvin-Benson cycle reactions (Brettel and Leibl, 2001 ; Mamedov *et al.*, 2015).

4) Cytochrome b_6f

Plastoquinol (PQH_2) diffuses from the Q_B site of PSII to the next closest contributor of the photosynthetic electron transport chain: cytochrome b_6f . Cyt b_6f is analogous to complex III of the respiratory chain of mitochondria. It is able to accept electrons and also has a proton pumping activity which contributes to the acidification of the lumen, essential for the synthesis of ATP. Each monomer of cytochrome b_6f (Figure 13, A) is composed of two type b cytochromes (b_H , b_L), one type c cytochrome (c_i), a Rieske protein containing a Fe-S cluster, a cytochrome f and two quinone oxidation-reduction sites (Q_i , Q_0) (Malone *et al.*, 2019). It also contains 4 small subunits named PetG, M, N and L. Mutants generated in tobacco have shown that plants lacking PetG and N are almost completely deficient in cytochrome b_6f and that PetL appears to stabilise the conformation of Rieske proteins allowing the dimerization (Schwenkert *et al.*, 2007).

For linear electron flow (Figure 13, **B**) a cytochrome b_6f dimer is needed. The PQH₂ molecule transfers one of its electrons to the Fe-S centre of a Rieske protein and another to a b_L cytochrome which allows the expulsion of two protons towards the lumen (Laisk *et al.*, 2016). Meanwhile, the electron transferred to the Rieske protein passes to the level of cytochrome f and to the plastocyanin. The reduced b_L cytochrome transfers an electron to the second b_H cytochrome which in turn reduces the quinone to semiquinone. To complete the Q cycle, a second reduced plastoquinone is needed. Again, an electron will be transferred from the Rieske protein to the plastocyanin and then to PSI. The second electron will successively reduce b_L and b_H to reduce the semiquinone to PQH₂. This causes the translocation of two additional protons. Thus, four protons enter the lumen for every two electrons transferred to the PSI reaction centre.

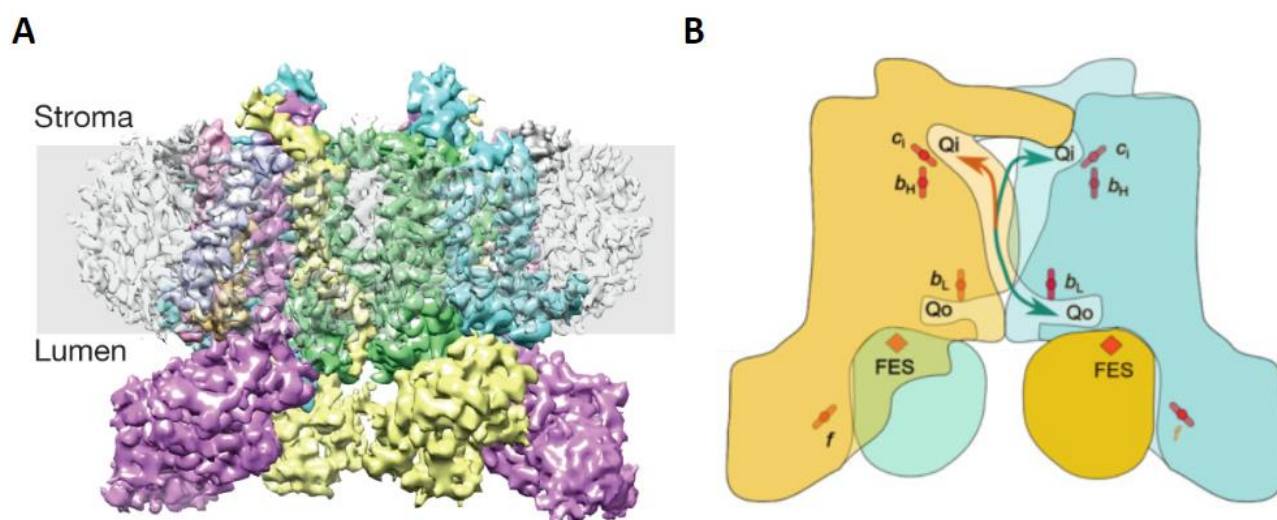


Figure 13: Cytochrome b_6f structure and Q-cycle

A. Cytochrome b_6f structure from spinach: cytochrome b_6 (green), cytochrome f (magenta), Rieske proteins (yellow), subunit IV (cyan) and small subunits PetG, M, N and L (grey, pale purple, orange and pink respectively). *Image from Malone et al., 2019.* **B.** Q-cycle. Two cytochrome b_6f monomers are embedded in the thylakoid membrane (yellow and blue). Each monomer is composed of two reduced quinone binding sites (Q_0 , Q_i), two cytochromes b (b_H , b_L), a cytochrome c (c_i), a cytochrome f (f) and a Rieske protein with an Fe-S centre. The blue arrow represents the migration of reduced quinone between the Q_i and Q_0 sites within the same monomer while the orange one shows a cross migration between the two. *Scheme from Nawrocki et al., 2019.*

B) Alternative Electron Transports and different protection mechanisms

Previously I described LEF under optimal physiological conditions. Nevertheless, photosynthetic organisms and in particular land plants have to adapt rapidly to a changing environment. To protect the photosynthetic chain against over-reduction of the PQ pool and thereby ROS generation; photosynthetic organisms have developed protective mechanisms.

In this part, I will discuss two alternative electron flows: Cyclic Electron Flow (CEF) and chlororespiration. Furthermore, of interest are other mechanisms that protect the photosynthetic chain such as the various components of Non-Photochemical Quenching (NPQ) and finally I shall introduce a family of proteins, the Plastid Terminal Oxidases (PTOX), whose activity seems to act as a “safety-valve” to protect PSII. All the mechanisms discussed in this section are detailed in article 4, page 165.

1) Cyclic Electron Flow

Cyclic Electron Flow (CEF) leads to the generation of a proton gradient and permits ATP synthesis without generating NADPH (Joliot *et al.*, 2022; Miyake, 2010; Gonzalès *et al.*, 2021; Takahashi, 2022) (Figure 14). CEF is important under different physiological conditions: 1. When the demand of ATP is higher than the amount generated only by LEF; 2. when the PQ pool is very reduced allowing to unclog the chain of excess electrons and 3. to protect PSII against photoinhibition (Suorsa *et al.*, 2016). This condition can be caused by high light stress for example. In high light, carbon fixation can be limited leading to the accumulation of NAD(P)H. Also at the onset of photosynthesis when the redox-regulated enzymes of the Calvin-Benson cycle are still inactive or in the case where the regeneration of NADP⁺ by other metabolic pathways is weak, CEF is of physiological importance. CEF takes place around the PSI. The principle is the use of reduced Fd as an electron source allowing in turn to reduce the PQ pool. Historically, two pathways contributing to CEF have been described, one involving the cytochrome *b₆f* complex and the other the NAD(P)H dehydrogenase-like complex (NDH). The NDH complex accepts electrons from ferredoxin and results in the reduction of the plastoquinone pool. It is able to form supercomplexes with PSI, which allows it to contribute to the electron flow under specific conditions (Yamamoto *et al.*, 2011; Peng *et al.*, 2009). It has been proven that the low abundance of the NDH complex as well as its electron flux and its proton pumping activity in the light period is too low to be the major contributor to CEF (Burrows *et al.*, 1998; Joliot *et al.*, 2004; Joliot and Johnson, 2011). It is now widely accepted that cytochrome *b₆f* is the major component of CEF and that its activity is responsible for a large part of the ΔpH required for ATP synthesis. This has the consequence of CEF coming into direct conflict with LEF and of greatly changing the ATP/NADPH ratio that is available for general metabolism.

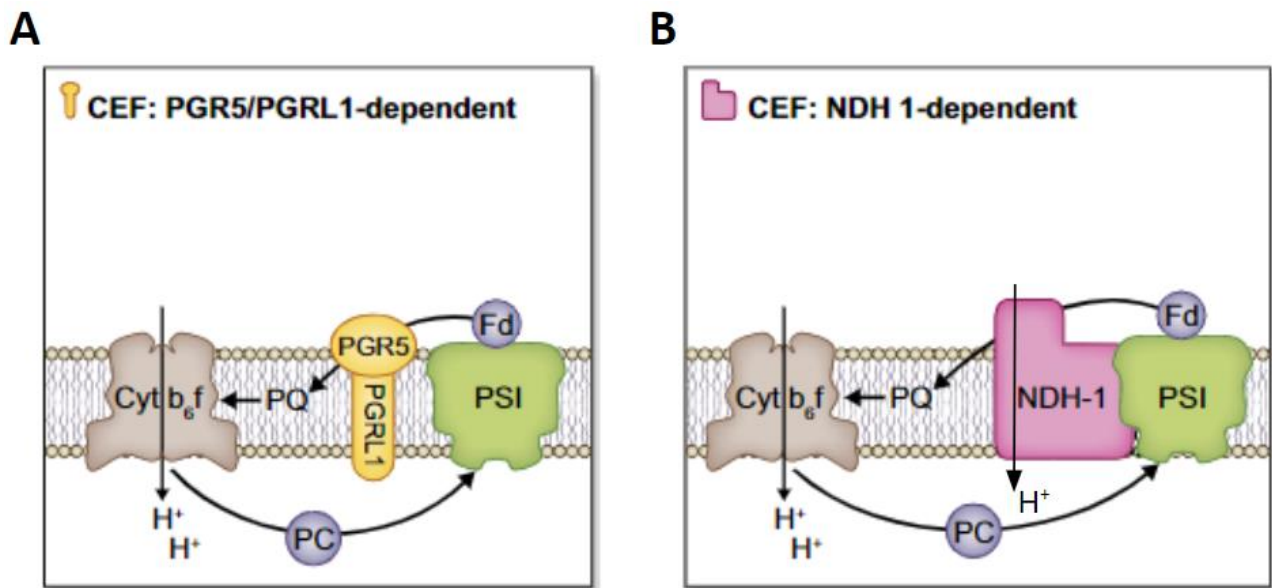


Figure 14: Two cyclic electron flow pathways

A. CEF using the PGR5/PGRL1-dependent pathway. Alternatively, Fd may also reduce directly a heme at Cyt b_6f and does not require PGR5/PGRL1 **B.** NDH-1-dependent cyclic electron flow. *Images from Alboresi et al., 2019.*

It remains to be elucidated how reduced Fd is able to come into contact with the cytochrome b_6f and transmit its electron. Studies carried out in *Chlamydomonas reinhardtii* seem to indicate that FNR and Fd would be able to form a complex with cytochrome b_6f (Zhang *et al.*, 2001; Szymańska *et al.*, 2010). In addition, mutants of *Arabidopsis thaliana* mutated in the proteins PGR5 (Proton Gradient Regulation 5) and PGRL1 (Proton Gradient Regulation-like 1) lead to a strong reduction in the dissipation of energy as heat (qE, see next chapter) and therefore an alteration in lumen acidification (Munekage *et al.*, 2002; DalCorso *et al.*, 2008). PGR5 is a small soluble protein present on the stromal side which can bind to the transmembrane protein PGRL1. It has recently been proposed that in *Arabidopsis thaliana*, the accumulation of PGR5 would allow the stabilisation of PGRL1 while PGRL2 (homolog to PGRL1) would allow the degradation of PGR5 (Rühle *et al.*, 2021). In addition, in *Chlamydomonas*, a complex composed of FNR, Fd, cytochrome b_6f and the two proteins PGR5/PGRL1 was isolated (Iwai *et al.*, 2010). Thus, it is assumed that these two proteins play a role in the regulation of CEF but their direct implication is an ongoing discussion (Takahashi, 2022). Alternatively, PGR5/PGRL1 may also play a structural role in the formation of supercomplexes between PSI and Cyt b_6f and do not participate directly in CEF.

2) Chlororespiration

Chlororespiration (Peltier and Cournac, 2002; Ibáñez *et al.*, 2010) (Figure 15) is also an alternative electron flow and allows, like CEF, to protect the photosynthetic chain under conditions that could limit the linear electron flow. It involves the NDH complex and although it plays a role in light, its activity is very small compared to the contribution of CEF. On the other hand, its role becomes predominant in the dark where it uses the energy stored in the form of NAD(P)H during the light phase to allow the re-generation of a proton gradient. FNR catalyses the oxidation of NAD(P)H to NADP⁺ and reduces Ferredoxin. The latter is able to donate its electron to the NDH complex (Schuller *et al.*, 2019) which, like cytochrome *b₆f*, has a proton pumping activity towards the lumen and reduces plastoquinone. Finally, the Plastid Terminal Oxidase (PTOX) re-oxidizes the plastoquinone pool (see “Plastid Terminal Oxidase”, page 33).

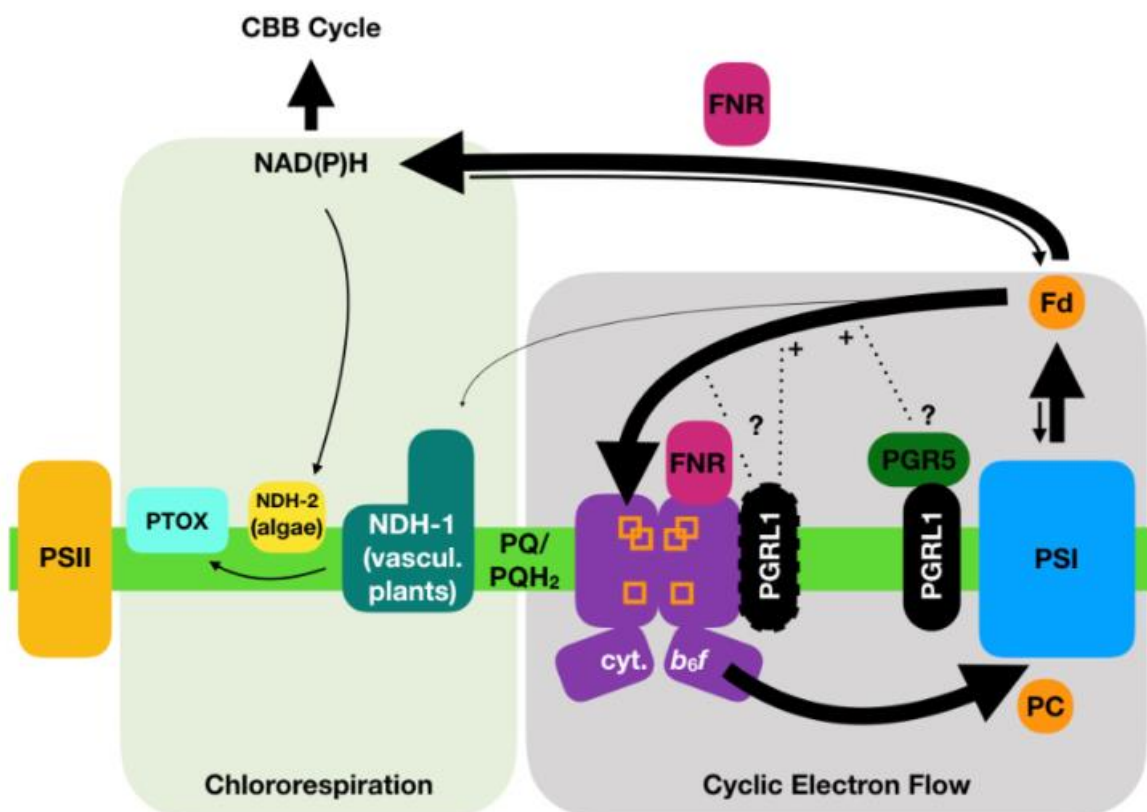


Figure 15: Cyclic Electron Flow and Chlororespiration

Scheme representing chlororespiration (green background), mainly taking place in the dark, and cyclic electron flow (CEF, grey background). CEF allows the use of Ferredoxin (Fd, orange) as an electron donor to initiate a new Q cycle at the cytochrome *b₆f* (purple). The latter again reduces the plastocyanin (PC, orange) which diffuses in the lumen to PSI. The contribution of the PGR1 (black) and PGR5 (dark green) proteins remains a debate. It is proposed that the FNR (pink) and the protein PGR1 are able to bind the cytochrome *b₆f* in order to regulate the CEF. Chlororespiration uses the energy produced by photosynthesis in the form of NADPH to allow the reduction of the NDH-1 complex (dark green) in plants or NDH-2 (yellow) in algae. Next, the plastoquinone pool (PQ/PQH₂) is reduced and then electrons are used in the rest of the photosynthetic chain. At the same time, the Plastid Terminal Oxidase (PTOX, cyan) re-oxidises the PQ pool. Scheme from Nawrocki *et al.*, 2019.

3) Non-Photochemical Quenching

Non-Photochemical Quenching (NPQ) brings together the defence systems put in place to safeguard photosynthetic activity under physiological stress (Stirbet *et al.*, 2020; Ruban and Wilson, 2021; Navakoudis *et al.*, 2022; Shi *et al.*, 2022). There are five main components of NPQ and their activation depends on the severity of the stress caused. The different components can be distinguished by their kinetics during relaxation of fluorescence quenching in the dark: qE, qZ, qT, qI and the very recently highlighted qH.

The dissipation of energy as heat, qE, is activated only a few seconds after the detection of a significantly high ΔpH . The implementation of qE reduces the excitation of the antennae by transferring the energy of the over-excited chlorophylls to the carotenoids associated with them: this is the xanthophyll cycle (qZ). The arrangement of xanthophylls in the LHC allows an energy transfer with excited chlorophylls. The conversion of violaxanthin to antheraxanthin and finally zeaxanthin mediated by the violaxanthin de-epoxidase enzyme in the lumen helps to protect PSII against photodamage. qE also involves the PSBS (PSII subunit S) protein of PSII. Details on qE and the other mechanisms of NPQ are given in article 4 (page 165) and not detailed here.

State-transition, qT, is a more difficult process to implement than qE. This is why its effectiveness is only significant a few minutes after the establishment of stress. The state transition is the migration of antennae from PSII to PSI with the aim of reducing excitation of the former and therefore protecting it against photodamage. This transition involves phosphorylation of LHCII and several other proteins including kinases and an acetylase that is necessary to allow the separation of LHCII from PSII core.

Photoinhibition, qI, corresponds to the slowest process of NPQ since it designates the damage of the PSII reaction centres and therefore the repair of the latter. It is the D1 protein which is the main site of damage at the level of PSII. Its repair involves proteins necessary for the migration of the damaged PSII, as well as, its partial disassembly allowing the degradation and re-synthesis of the D1 protein, the turn-over of which is widely known to be approximately 20 min.

Finally, qH is a recently discovered mechanism that belongs, like qI and qZ, to slowly relaxing quenching. It protects the PSII and its action is localised at the level of the latter's peripheral antenna. Only three molecular intervenants have been identified and their interactions are described in article 4.

4) Plastid Terminal Oxidases

The enzyme Plastid Terminal Oxidase (PTOX) was first discovered by Rédei in 1975 who produced a mutation in *Arabidopsis thaliana* by bombarding seeds with X-rays. Named *Immutans*, the mutant has a variegating phenotype whose proportion of white parts depends on the light intensity under which it is grown (Figure 16, A; Wu *et al.*, 1999). As the light intensity increases the variegation phenotype becomes more pronounced. In addition, electron microscopy images were able to highlight heteroplasty within the cells, that is to say a mixture of malformed and correctly formed chloroplasts (Figure 16, B; Wetzel *et al.*, 1994). PTOX is nuclear encoded and its expression is ubiquitous at the plant level. It is located in mature (chloroplasts, chromoplasts, etioplasts) and immature plastids (proplastids) where its main role is to ensure carotenoid biosynthesis and to participate in the electron flow to counter oxidative stress.

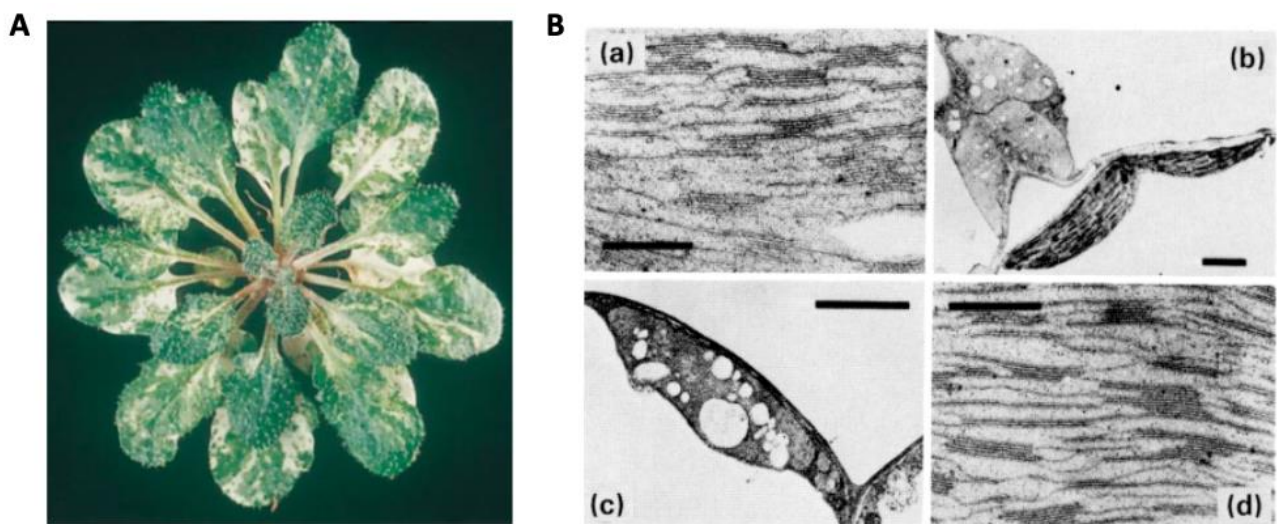


Figure 16: *Immutans* phenotype

A. Picture of *Immutans* variegation phenotype. Image from Wu *et al.*, 1999. **B.** transmission electron microscopy. Micrograph of thylakoids of a wild-type chloroplast (a). Scale bar: 500 nm. Normal and abnormal chloroplasts of two adjacent cells in the white sector (b). Scale bar: 2 μ m. Abnormal chloroplast in white sector (c). Scale bar: 2 μ m. Chloroplast thylakoids in white sector (d). Scale bar: 500 nm. Image from Wetzel *et al.*, 1994.

Three main roles are attributed to PTOX: the protection of PSII under stress, in the biosynthesis of carotenoids as well as in chlororespiration. It has been established that PTOX never conflicts with linear electron flow, however it appears to activate due to salt-stress (Stepien and Johnson, 2009) and excessive light which has earned it the nick-name of “safety valve” (Figure 17, A). Although its activation mechanism still remains mysterious, It is known that it is the over-reduction of the plastoquinone pool which is at the origin of the PTOX activation. In addition, it was recently shown in *Arabidopsis thaliana* that the protein has a different location depending on darkness or light (Bolte *et al.*, 2020). These results suggest that PTOX localisation and thereby its activity depends on the proton motive force across the thylakoid membrane. The PTOX will anchor itself at the level of the membrane close to the acceptor side of PSII where it has access to

its substrates, PQH₂ and oxygen, which are used to reinject oxidised plastoquinones into the linear flow avoiding the degradation of PSII.

On the other hand, it has been shown that *ptox* mutants are not able to produce carotenoids in high light and instead accumulate one of the precursors of the biosynthetic pathway: phytoene (Wetzel *et al.*, 1994). Carotenoids play a major role in photosynthesis since they are part of the constitution of the PSII (2 β -carotenes for the reaction centre) but also of the antennae where they participate in energy dissipation as heat (qE). In addition, carotenoids have an important role as ROS scavengers. It has been proposed in the literature (Carol and Kuntz, 2001) that Phytoene Desaturase uses oxidised plastoquinones from the pool as an electron acceptor to carry out the desaturation steps (Figure 17, **B**). In this case, PTOX would allow reoxidation of the plastoquinone pool and regenerate the electron acceptor PQ. It is the dysfunction of this biosynthetic pathway that is the cause of the variegation phenotype in *Immutans* as well as the discoloration of tomato fruits in the *Ghost* mutant (Barr *et al.*, 2004; Shahbazi *et al.*, 2007). It could also be the cause of heteroplasty. It is hypothesised that the natural but very slow reaction of plastoquinol with oxygen may be sufficient to compensate for the lack of PTOX in the mutants if they are grown at very low light intensity. It is suggested that within the same cell, certain chloroplasts are “sacrificed” to allow healthy chloroplasts to develop despite the absence of PTOX.

Finally, as explained above, the plant can consume energy in the dark for its metabolism through the process of chlororespiration. In this case, it is able to use the energy stored in the form of NAD(P)H. The electrons are transferred to the NDH complex which generates a proton gradient and reduces the quinones in the PQ pool. PTOX regenerates an oxidised pool (Peltier and Cournac, 2002).

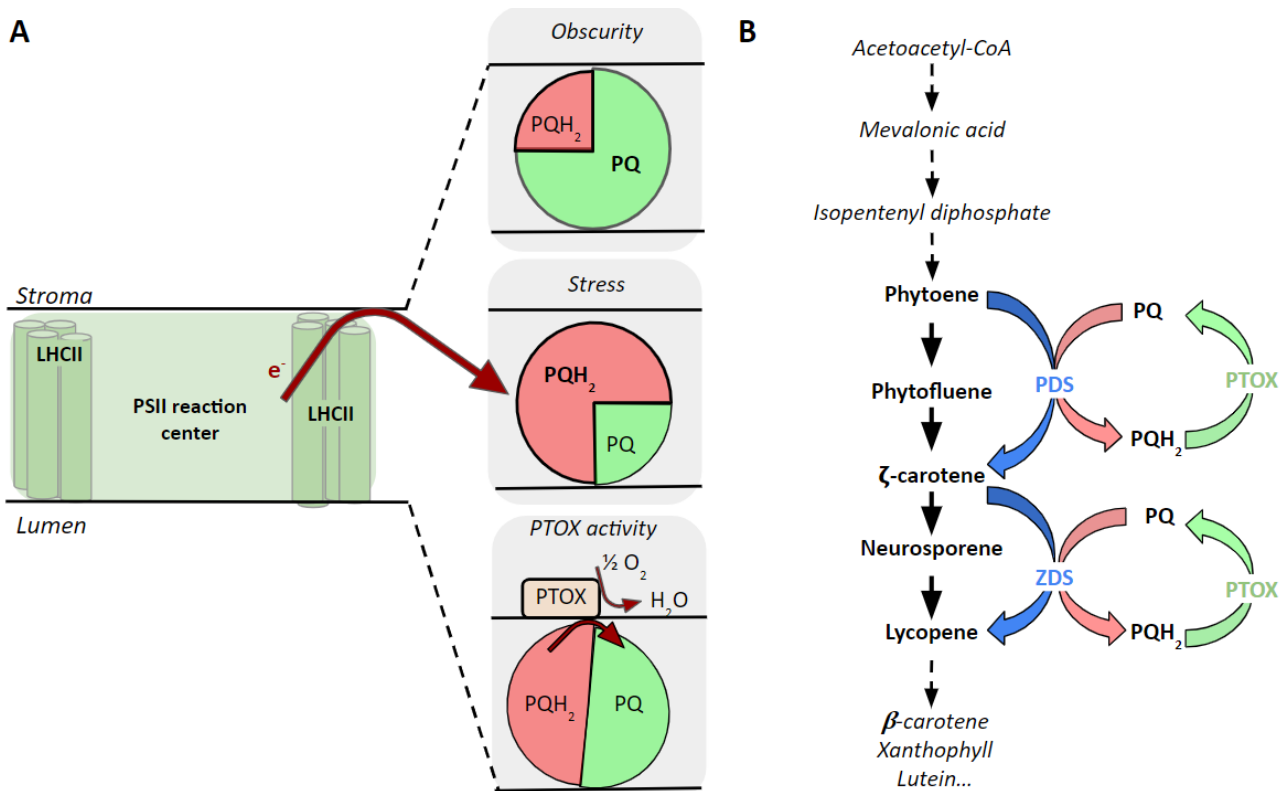


Figure 17: PTOX involvement in photosynthetic electron flow and carotenoid biosynthesis

A. Redox state of the PQ pool in different physiological conditions. In the dark (top), the PQ pool is mostly oxidised. In the light, the pool is reduced by electrons coming from the PSII reaction centre. During a stress (in the middle) such as high light intensity, the PQ pool is greatly reduced. In this case, protective mechanisms are put in place and the PTOX is activated (bottom). This results in the oxidation of the PQ pool using O_2 as a substrate. (McDonald *et al.*, 2011) **B.** Summary of major steps in carotenoid biosynthesis. Phytoene desaturase (PDS) catalyses the desaturation of phytoene and ζ -carotene desaturase catalyses the desaturation of ζ -carotene. It is assumed that they lead to the reduction of the PQ pool which is re-oxidised thanks to PTOX activity (Foudree *et al.*, 2012).

The PTOX *in vitro* structure has not been elucidated. It is known that, like certain complexes of the photosynthetic chain, it has a homologous protein in the mitochondria: Alternative OXidase (AOX). AOX is able to catalyse the oxidation of ubiquinol to ubiquinone. The superimposition of the predicted protein of *Chlamydomonas* PTOX2 (CrPTOX2) on the experimentally determined structure of *Trypanosoma* AOX (TbAOX) revealed the characteristics of the catalytic site of PTOX (Nawrocki *et al.*, 2015). Indeed, PTOX has a catalytic site consisting of six iron binding sites, essential for its activity. In addition, it also has six helices, two of which are necessary for the attachment to the membrane (α -1 and α -4) and the other four of which are important for iron coordination (α -2, α -3, α -5 and α -6) (Figure 18). The production of rice PTOX *in vitro* allows the measurement of the kinetic parameters of this recombinant protein (Yu *et al.*, 2014).

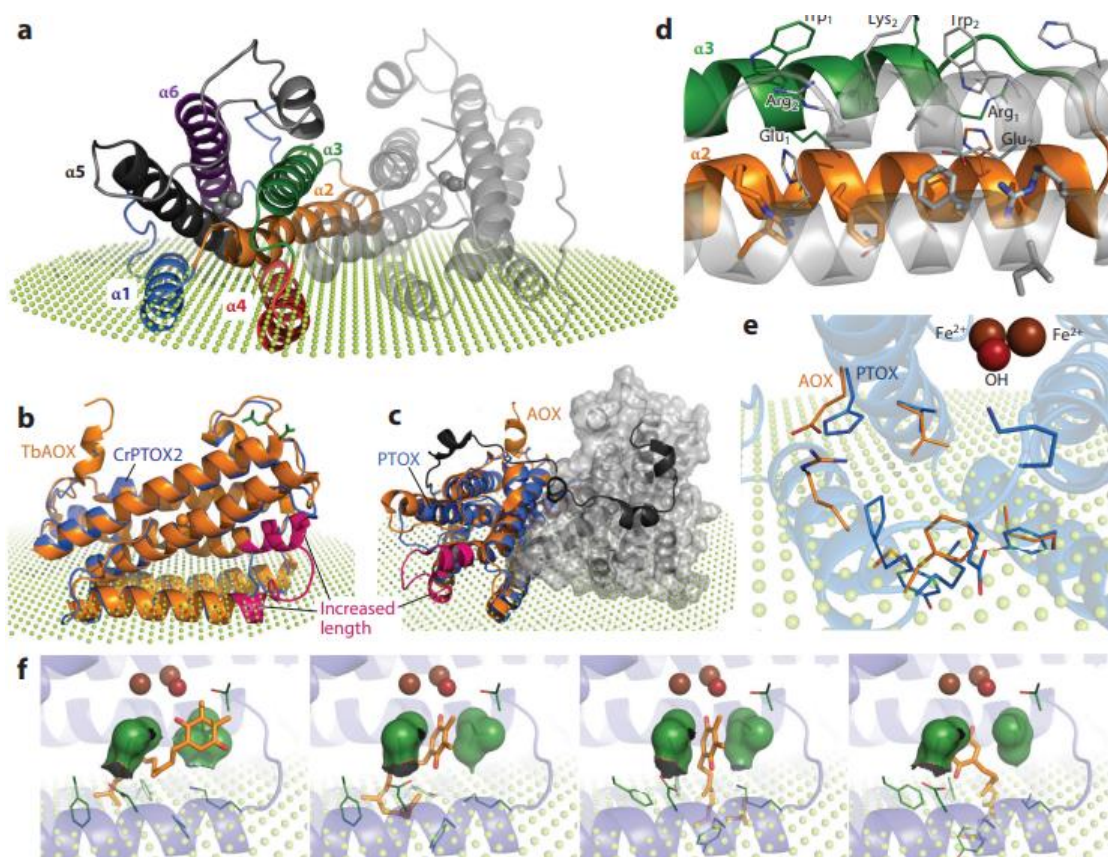


Figure 18: Simulation of *Chlamydomonas reinhardtii* Plastid Terminal Oxidase 2 structure superimposed of those of Alternative Oxidase from *Trypanosoma brucei*

A model structure of CrPTOX2. The stromal surface of the membrane is schematically depicted as light green spheres. **(a)** Overview of the PTOX dimer in the membrane. Helix numbering is from N- to C-terminus. **(b)** Major structural differences between CrPTOX2 (*blue*) and TbAOX (*orange*; Protein Data Bank ID 3VV9). Green sticks show the last residue before and first residue after the loop in PTOX. The increased length of the helices next to the binding pocket in AOX is shown in pink. **(c)** PTOX (*blue*) superimposed on AOX (*orange*). The dimerization domain of AOX (*black*) spans the second AOX monomer (*grey surface*). Because of its low sequence homology, the corresponding domain of PTOX was not included in the model. **(d)** The interface of two monomers. The colours of the helices in one monomer correspond to the colours in panel *a*; helices from the other monomer are shown in transparent grey. Conserved residues (in 93% of PTOX sequences) in the interface are shown as thick sticks; other residues that could make contact are shown as thin sticks. The distance between two pairs of phenylalanine residues between the monomers does not exceed 4 Å. Note the two pairs of glutamic acid and arginine opposite one another and the two pairs of lysine opposite the tryptophan. **(e)** Differences in the binding pocket between PTOX (*blue*) and AOX (*orange*). **(f)** Docking software model of plastoquinol (PQH₂)–binding modes in PTOX. Residues flexible during the docking are shown as sticks. Residues orienting PQH₂ with regard to the diiron active site by hydrophobic stacking are shown as surfaces. *Images and legends from Nawrocki et al., 2015.*

Finally, it is known in the literature that many photosynthetic organisms possess not one but two PTOX isoforms. This is the case of the green algae *Chlamydomonas reinhardtii* (Houille-Vernes *et al.*, 2011) while angiosperms like *Arabidopsis thaliana* have only one. In this study, I was interested in characterising the differences between these isoforms in the liverwort *Marchantia polymorpha* (Part II, page 121).

II) Chloroplast membrane dynamic

Depending on the physiological condition in which they evolve, photosynthetic organisms must adapt their photosynthetic activity. At the level of the chloroplast, different mechanisms are able to take place, such as the avoidance reaction. Indeed, in high light, chloroplasts which are normally located in the centre of the cells, can stick against the cell wall in order to receive less light. In this part, I will focus more particularly on the dynamics of chloroplast membranes as well as the supramolecular rearrangement of these, in other terms, the reorganisation of photosynthetic complexes (Kirchhoff, 2019).

Under favourable light conditions, thylakoid membranes have condensed parts called grana and loose parts in the stroma called stroma lamellae. This configuration allows efficient linear electron transfer, in particular by optimising the diffusion of plastoquinone and plastocyanin. Nevertheless, under stress (i. e. highlight), the thylakoid structure changes to allow the establishment of the various protective mechanisms mentioned above (for details see article 4, page 165). In particular, the presence of a bulge on the edges of the grana has been observed with a slight loosening of the latter (Puthiyaveetil *et al.*, 2014; Yoshioka-Nishimuro *et al.*, 2014). It was hypothesised that it could help the repair process making damaged PSII more accessible for degradation by proteases.

In parallel, supramolecular rearrangements are observed (Pribil *et al.*, 2014). It has been established that the distribution of photosynthetic complexes is heterogeneous in the thylakoids. This implies that the electron transfer is not as linear as the schemes suggest. Under physiological light conditions, PSII are present in grana whereas PSI are present in stroma lamellae (Figure 19, **A**). It is also assumed that the *b₆f* cytochromes are located at the junction between the grana and the stroma lamellae to allow the transfer of electrons between the two photosystems. When the light intensity is too high changes occur. For example, the state transition (qT) is characterised by the migration of LHClI antennae from the PSII localised in the grana to the PSI localised in the stroma lamellae (Betterle *et al.*, 2009; Johnson *et al.*, 2011) and the relocalisation of cytochrome *b₆f*. Moreover, a new complex, cytochrome *b₆f*-LHCl-PSI, was recently discovered in *Arabidopsis thaliana* (Yadav *et al.*, 2017). More concretely, if we take the example of PSII, its location is different depending on its state of assembly (Figure 19, **B**) but also depending on the environmental conditions (Danielsson *et al.*, 2006). Properly assembled and photoactivated PSII are present in the grana core, while damaged PSII migrate to the margins for the repair. This is also where the PSII are photoactivated, whether they are newly assembled or repaired.

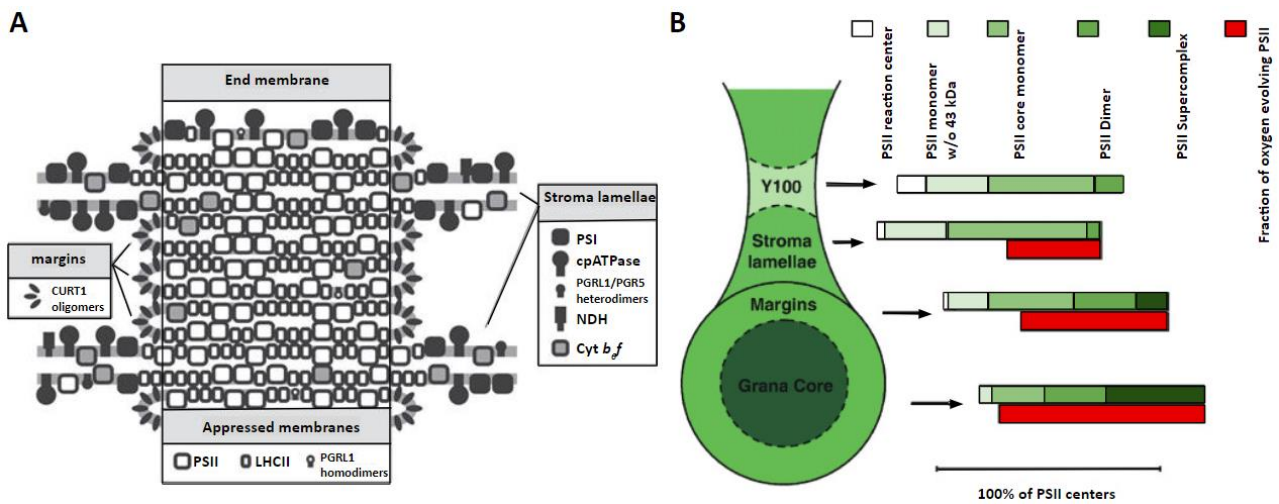


Figure 19: Photosynthetic complexes and super-complexes arrangement across the membrane

A. Scheme showing the distribution of major photosynthetic complexes on the thylakoid membrane. The PSII reaction centres and their antennae are mainly located at the level of the appressed membrane with the protein PGRL1 supposed to be involved in cyclic electron flow. At the level of the margins is the CURT1 protein. Finally, the stroma lamellae are mainly occupied by PSII, ATPases, cytochromes *b₆f* and proteins involved in alternative electron flows (PGRL1/PGR5 and NDH). The role of the CURT1, PGRL1, PGR5 and NDH proteins are discussed in article 4: Messant *et al.*, 2021 (see below). *Scheme from Pribil et al., 2014.* **B.** Quantitative distribution of the various PSII complexes in the different domains of the thylakoid membrane. *Scheme and legend from Danielsson et al., 2006.*

To conclude, in this part I have mainly taken light stress as an example, but there are a multitude of signals and signalling cascades that lead to this kind of change such as the redox state of the plastoquinone pool, ion homeostasis (Aranda Sicilia *et al.*, 2021), phosphorylation and acetylation (Staehein and Arntzen, 1983; Tikkanen and Aro, 2011; Koskela *et al.*, 2018) just to cite a few others. Thus, membrane dynamics are important in all physiological processes relating to the photosynthesis reaction including the establishment and maintenance of the linear electron flow under favourable conditions and for the implementation of all the protective mechanisms mentioned above (article 4, page 165) and investigated in this study.

III) Super-resolution microscopy: an *in vivo* way to study dynamic of photosynthetic complexes

For decades, the origin of chloroplast evolution has been an important topic in the literature. It is now widely accepted that the appearance of the first photosynthetic cells from which species of the green lineage resulted from primary endosymbiosis between a heterotrophic eukaryote and a photosynthetic cyanobacterium followed by gene transfer events between them (McFadden, 1999). Thus, the structure and number of chloroplasts in the photosynthetic organisms cells have been widely studied. The majority of unicellular green algae, the common ancestor of the green lineage, have a single chloroplast (e.g. *Chlamydomonas reinhardtii*). Whereas in Angiosperms, considered as the most evolved plants, the photosynthetic cells have a multitude of chloroplasts. Furthermore, the structure of the thylakoids has been observed, mainly by electron microscopy. Differences in their architecture could be highlighted depending on the species. Nevertheless, as explained previously, the structure of thylakoids is complex and the dynamics of both membranes and photosynthetic complexes through it is very difficult to study *in vivo*. This is explained in particular by the resolution limit of the microscopy methods used until today.

The principle of super-resolution fluorescence microscopy (SRM) is to exceed the “classical” diffraction limit of optical resolution by about half the wavelength of the emitted light when using modern high-quality optics, a concept initially conceived by Abbe. The objective is the observation of cellular structures with a level of detail approaching electron microscopy (Schermelleh *et al.*, 2019). There are three main SRM techniques where each has their limits. Photoactivated Localization Microscopy (PALM) and its derivatives mostly require the labelling of biological molecules. Structured Illumination Microscopy (SIM) involves a complex reconstruction of images. Finally, the Stimulated Emission Depletion (STED) microscopy whose high photon fluxes necessary can cause the bleaching of the fluorophores. The SRM microscope conceived and developed at Saclay primarily studies photosynthetic organisms. This experimental method is based on the use of a wide-field microscope whose modifications allow the attainment of a resolution of 126 nm in *xy* and 320 nm in *z* with the use of a 100X objective with immersion oil (Streckaïté, 2021; Streckaïté *et al.*, 2022). The methodology, called Single Pixel Reconstruction Imaging method (SPiRi), is relatively easy-to-use and requires a minimum of processing to reconstruct the final image.

A wide range of photosynthetic organisms were used to test the SRM microscopy at Saclay. The comparison of two organisms is particularly interesting for this present study: the green alga *Chlamydomonas reinhardtii* and the angiosperm *Arabidopsis thaliana* (Figure 20). Both are the most used organisms in the study of photosynthesis in the green lineage. Since the advent of the first electron microscope in 1931 and until its most recent improvements, this technique allows to highlight the internal structures of chloroplasts (grana and stroma lamellae) with an unequalled resolution.

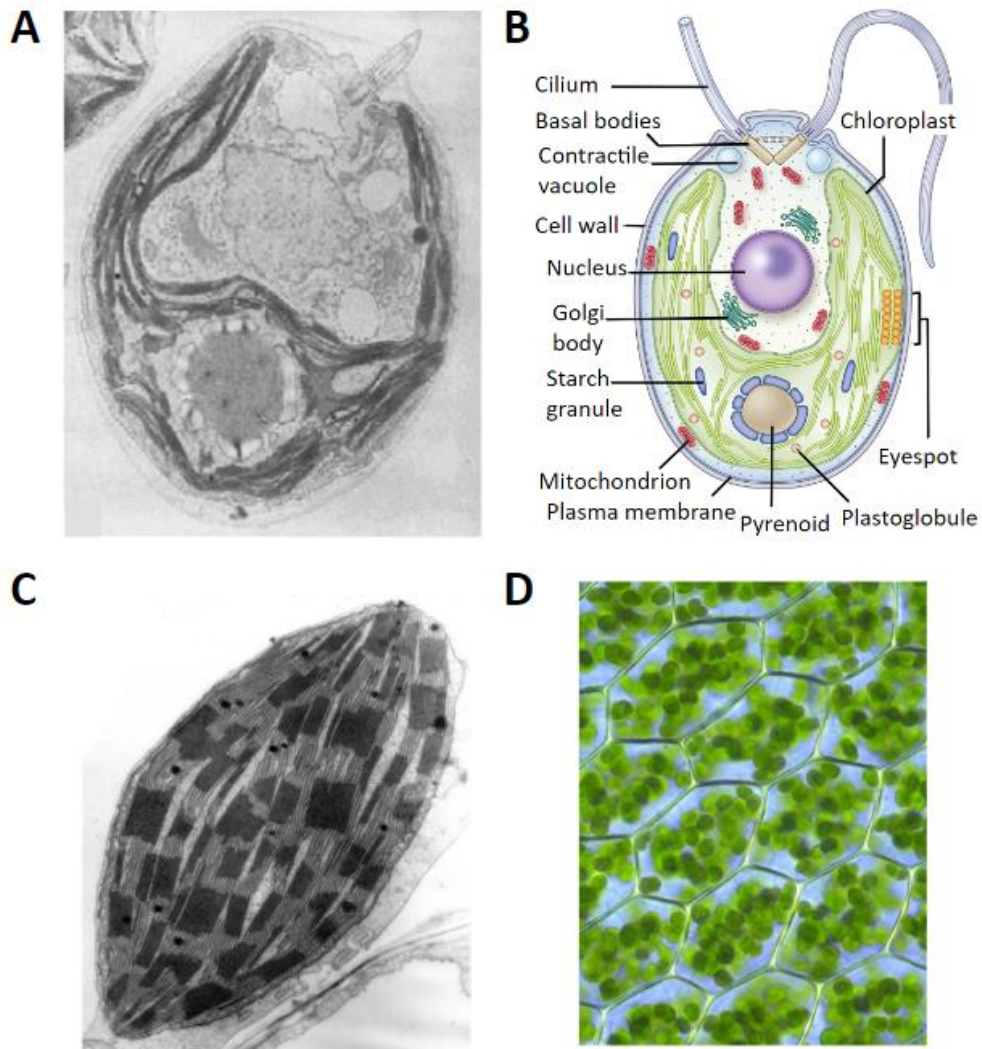


Figure 20: Structure of green algae and higher plant cells and chloroplasts

A. Electronic microscopy image of a *Chlamydomonas reinhardtii* cell (Gershuny Rachel, 2005). **B.** *Chlamydomonas reinhardtii* cell scheme. Image from Sasso et al., 2018. **C.** Electronic microscopy image of higher plant chloroplast. Image from Shutova, 2007. **D.** Microscopy image of higher plant photosynthetic tissue with cells containing chloroplasts. Image by Kristian Peters.

Nevertheless, SRM images offer new views of these chloroplasts (Figure 20, **A** and **C**). It is possible to establish the ultrastructure of chloroplasts in 3D (Figure 21, **B** and **D**). Technically, it is possible to carry out precise statistical measurements on the size of the grana. Theoretically, it allows us to formulate new hypotheses regarding the structure and function of different parts of the thylakoid membrane.

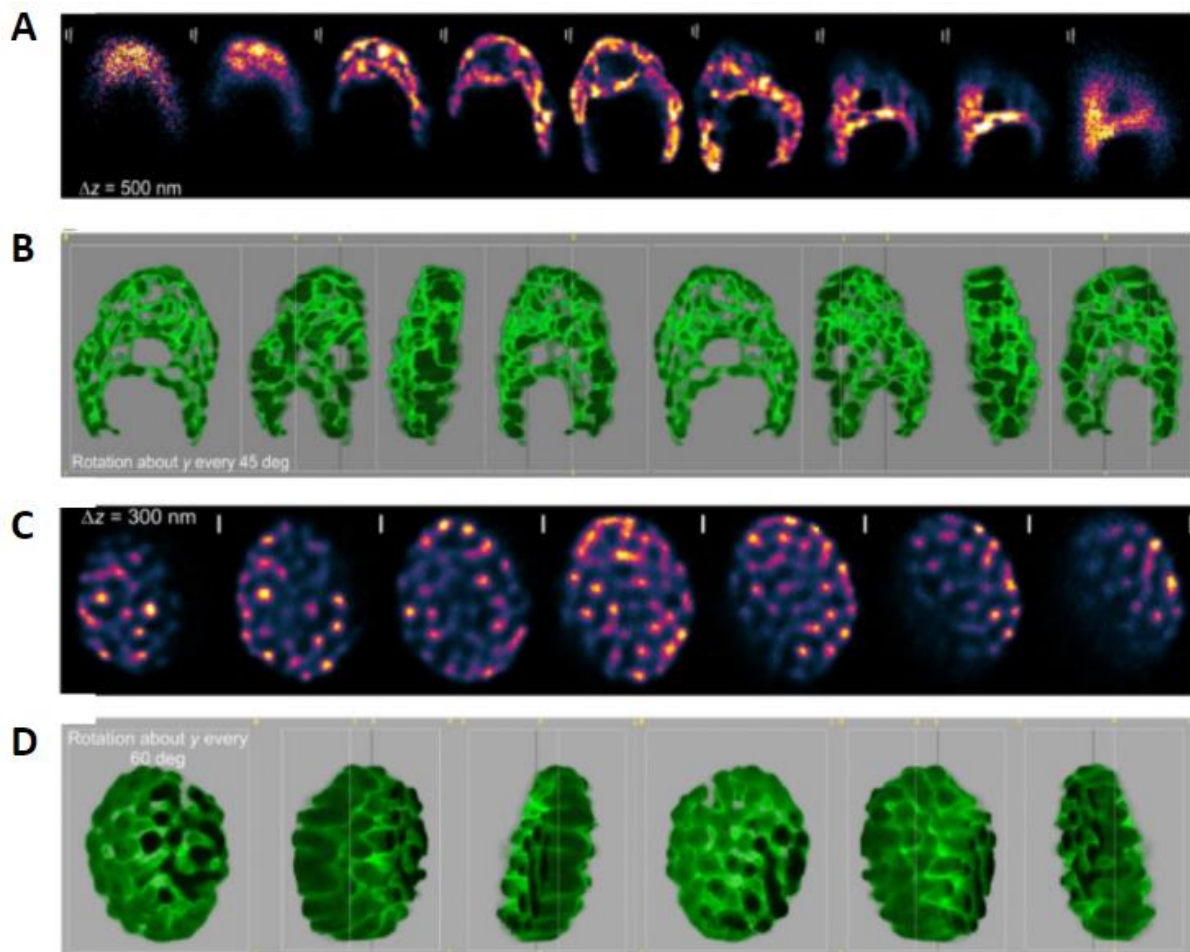


Figure 21: Chloroplast ultrastructure of *Chlamydomonas reinhardtii* and *Arabidopsis thaliana* by Super-resolution microscopy

A. An axial scan of *C. reinhardtii* cell *in vivo* by SPiRi. **B.** Cross-sections of the 3D reconstruction of *C. reinhardtii* cell every 45 degrees rotating it around y axis. **C.** SPiRi images of an axial scan of arabidopsis chloroplast. **D.** Cross-sections of the 3D reconstruction (obtained from the images shown in panel (C)) every 60 degrees around y axis. *Images and legends from Streckaitė, 2019.*

Today, the future of this technique is to exploit the biodiversity to show different organisations of the chloroplast. I have used SPiRi microscopy to follow changes in the organisation of the *Marchantia polymorpha* thylakoid membranes *in vivo*. As a first step, I hope to be able to understand the dynamics of thylakoid membrane (un)stacking as a function of physiological conditions using this simple method. This is the case in the study observing *in vivo* photoactivation in *Marchantia polymorpha* (see Part I, page 50). On the other hand, it may also be possible to study the different yield of chlorophyll fluorescence of PSI and PSII to determine the location of these centres in the thylakoids in different culture conditions. Furthermore, mapping of photosystems could allow the use of plant material expressing tagged photosynthetic proteins in order to study the colocalization of photosynthetic complexes/photosystems. One could hope to observe supercomplexes *in vivo*. So far, these latter perspectives have not been tested although they are technically feasible.

IV) *Marchantia polymorpha*, an emerging model plant

Marchantia polymorpha is one of the liverworts, considered to be the first plants to have colonised the land. Its genome was sequenced in 2008 (Bowman *et al.*, 2017) and then made available on the Marpolbase platform. Molecular tools allowing its study, such as CRISPR/Cas9 directed mutagenesis, were developed in 2014 (Sugano *et al.*, 2014). It is only very recently that the genes have been renamed with the MpXgXXXXX nomenclature and annotated according to the knowledge acquired in other organisms. Finally, the last advance was the online release of gene expression data and the construction of small co-expression networks (MBEX). *Marchantia* is therefore an organism that is beginning to gain popularity within the scientific community.

To understand the positionment of *Marchantia* in the evolutionary tree, its comparison with already known organisms is essential. Here, I will mention the green alga *Chlamydomonas reinhardtii* as an ancestor, *Arabidopsis thaliana* as an evolved organism and the moss *Physcomitrium patens* as the evolutionary closest organism. In this part, I will first describe the morphological characteristics and in a second part the molecular mechanisms of *Marchantia* with a particular interest in photosynthesis.

A) General characteristics




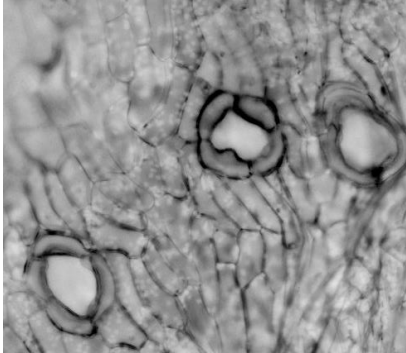
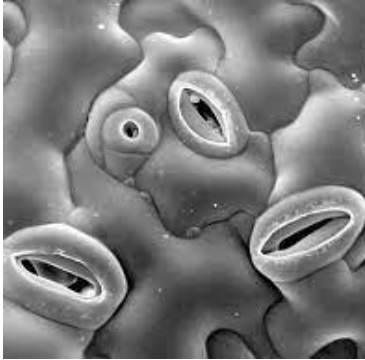
Bryophytes have a thallus-like morphology which keeps them close to the ground due to the absence of lignin. They are very dependent on external conditions, in particular the presence of water. It is necessary for their sexual reproduction since it allows male gametes to move to access females. Regarding their way of life, the diploid phase is very reduced, preferring a haploid phase. Polyploidy is known to protect organisms against unfavourable genetic mutations. In *Marchantia*, the thalli have 9 chromosomes including one sexual. It has been shown that gene expression depends on the sex of the thallus. On the other hand, asexual reproduction, mainly used in the laboratory, involves organs called gemmae cup which form on the top of the thalli. They contain clones of miniature thalli (gemmae) whose dispersal is also dependent on water. Gemmae are not able to germinate in the dark (Bowman, 2016).

Compared to *Arabidopsis*, *Marchantia* does not have specific leaf or root apparatus, nor stomata and flowers or seeds (Table I). *Marchantia* therefore has a very simple morphology with which it must adapt to environmental changes.

Table I: Comparison of major morphological traits between liverworts and angiosperms

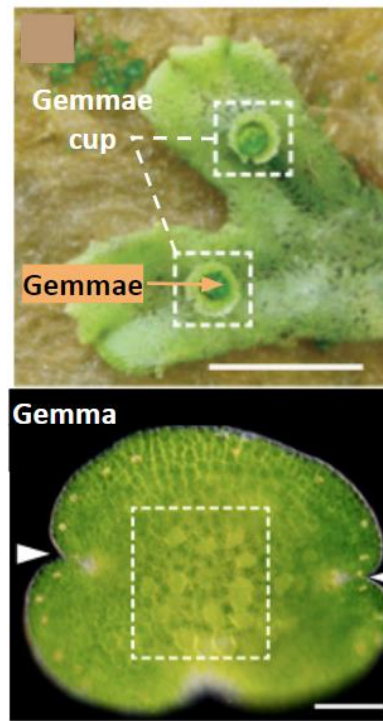
The first character is always referring to liverworts and the second to angiosperms.

I obtained liverworts rhizoid and air pore complexes images by brightfield microscopy from *Marchantia polymorpha* thalli. The thallus image comes from MNHN&OFB [Ed]. 2003-2022, Inventaire National du Patrimoine Naturel (INPN). Gemmae cup and gemmae pictures are modified from Kato *et al.*, 2019. References for angiosperms images: roots (F. Ditengou, T. Haser, AG. Palme, University of Freiburg) and stomata (D. Mosquin, University of British Columbia).

Characters	Liverworts	Angiosperms
<p><u>Rhizoids</u>: no specialised cells, uncontrolled water movement and absorption [1], [2]</p> <p><u>Roots</u>: polarised with specific zones and specialised transporters for absorption [1], [2]</p>		
<p><u>Thallus</u>: flat and close to the ground with bifurcation into dyads or tryads [3]</p> <p><u>Aerial part</u>: vascular tissues and development in height thanks to lignin, branches with evolved bifurcations, leaves with various shapes [3]</p>		<p>Different arborescence, inflorescence</p>
<p><u>Air pore complexes</u>: uncontrolled pores [4]</p> <p><u>Stomata</u>: opening and closing controlled by different signals [4]</p>		
<u>Life cycle</u>	Long haploid phase [5], [6]	Long di/polyploid phase [5]
<u>Sexual reproduction</u>	Gendered individuals [7]	Hermaphroditic flowers

Vegetative reproduction: gemmae dispersion, layering [8]

Vegetative reproduction: very different mechanisms with sometimes specialised organs (i. e. stolons or adventitious roots)



Bulb, tuber, rhizome, layering etc.

[1] Raven and Edwards, 2001; [2] Seago and Fernando, 2013; [3] Harrison and Morris, 2017; [4] Clark *et al.*, 2012; [5] Niklas and Kutschera, 2010; [6] Shimamura *et al.*, 2015; [7] Coelho *et al.*, 2019; [8] Kato *et al.*, 2019.

B) Peculiarities of photosynthesis

Two main evolutionary events interest me in this part. First, the terrestrial colonisation of plants suggests that this adaptation leads to many changes in regulatory proteins, in particular to help protect the photosynthetic chain. Second, it is known that the appearance of angiosperms is marked by the loss of many regulatory proteins that are still present in gymnosperms, mosses and liverworts.

At the level of the chloroplast, the light avoidance mechanism allows them to agglutinate at the level of the wall of the photosynthetic cells in order to protect themselves under conditions of light stress. In higher plants, this process is notably regulated by blue light receptors called phototropins (PHOT1 and PHOT2). In lower plants, neochrome, red light receptors are also involved (Pribil *et al.*, 2014).

At the level of the thylakoid membrane, the lipid composition is also changing. A study conducted on *Marchantia polymorpha* revealed a 3 times higher concentration of the lipid Sulfoquinovosyl Diacylglycerol (SQDG) than in other photosynthetic organisms and its content increases drastically after high light stress (Zaitsev *et al.*, 1998). SQDG plays a role in the interaction with peripheral membrane proteins. It has been shown to influence the assembly of the PSII core and antennae (Schaller *et al.*, 2011).

In addition, the biosynthesis of chlorophyll is also different. The reduction of protochlorophyllide to chlorophyll is catalysed by the enzyme Pchlide reductase (Amstrong, 1998; Schoefs and Frank, 2003) which exists in two versions. The first is light-dependent, Light-Dependent NADPH-Pchlide (LPOR) and the second is light-independent, Light-Independent Pchlide oxidoreductase (DPOR). LPOR is encoded by a gene present in the nucleus while the gene encoding DPOR is present in the chloroplast genome. The latter is completely absent in angiosperms and has been lost by some lineages of Pteridophytes and Gymnosperms (Ueda *et al.*, 2014). *Marchantia polymorpha* has both genes which allows it to grow in the dark. This property allowed us to follow the photoactivation of PSII *in vivo* (Part I, page 50).

Evolution has also brought changes at the level of photosynthesis complexes such as the oligomerization of PSI as a trimer (cyanobacteria) to a monomer (Yang *et al.*, 2015). The antennae can also be different. In *Physcomitrium* the LHClI are only composed of Lhca1-3 proteins and only one minor Lhca is present: Lhca5 (Busch *et al.*, 2013). In *Marchantia polymorpha*, Harrer (2003) showed that more than half of the PSII observed under electron microscopy possess an LHClI trimer and probably one more chlorophyll *a/b* binding protein than the other species mentioned. Differences in protein sequences have also been shown in *Marchantia*, which has been hypothesised to change protein regulation, as it is the case for CP29 (Kilian *et al.*, 1998).

The atmospheric conditions under which the Bryophytes arose also resulted in significant differences in RuBisCo content. It is reasonable to suggest that the high concentration of CO₂ allowed more efficient photosynthesis by favouring the carboxylase activity of the enzyme. It has also been suggested that the adaptability of Bryophytes to light conditions is due to the increased amounts of RuBisCo (Gerrotto, 2011). The light intensity also modulates their chlorophyll *a*/chlorophyll *b* ratio. In particular, that of mosses is between 1 and 2.5 depending on the species, which characterises them as shade plants.

At the level of linear and alternative electron flows as well as mechanisms of energy dissipation as heat, many proteins have been affected. Two proteins are involved in the induction of a strong protective mechanism of energy dissipation as heat: PSBS and LHCSR (Light Harvesting Complex Stress Related). PSBS is a protein able to sense the pH in the lumen and to bind to the PSII antennae but it does not bind pigments itself (see article 4, page 150). In *C. reinhardtii*, it seems to contribute to photoprotection independently of energy dissipation (Redekop *et al.*, 2020). In vascular plants, it is constitutively expressed and controls the pH-dependent part of NPQ: qE (Li *et al.*, 2000). PSBS acts as a pH sensor, its activation depends on the protonation of two glutamate residues (Li *et al.*, 2002; 2004). It activates qE by interaction with LHClI (Sacharz *et al.*, 2017). In *Physcomitrium patens*, the mechanisms of energy dissipation as heat emitted by PSBS and LHCSR are additive. PSBS and LHCSR have been shown to form megacomplexes with PSI-PSII in stromal lamellae (Furukawa *et al.*, 2019). It has been hypothesised that mechanisms mediated by PSBS and LHCSR contributed to the adaptation of early land plants to intense and fluctuating light conditions (Alboresi *et al.*, 2010).

Concerning Cyclic Electron Flow, there are two isoforms of the PGRL protein (PGRL1 and PGRL2) in *Arabidopsis thaliana*. In this organism, PGR5 is stabilised by PGRL1 whereas PGRL2 seems to cause the degradation of PGR5 (Rhüle *et al.*, 2021). In *Chlamydomonas reinhardtii* and *Physcomitrium patens* PGRL2 is absent, suggesting the involvement of another PGR5 regulatory mechanism (Rühle *et al.*, 2021).

An important change from cyanobacteria to angiosperms in the P700 oxidation strategy is the presence of Flavodiiron Proteins (FLVs). FLVs keep the acceptor side of PSI oxidised since they catalyse the reduction of O₂ to H₂O using Fd⁻ as electron donor (Sétif *et al.*, 2020). In angiosperms, they have been functionally replaced by photorespiration as the dominant electron sink (Shimakawa *et al.*, 2021). The transient activity of FLVs therefore avoids the accumulation of electrons on the acceptor side of the PSI when the LEF is limited and the consumption of NAD(P)H is slow (Alboresi *et al.*, 2019). In *Marchantia polymorpha*, they play the same role as in cyanobacteria (Shimakawa *et al.*, 2017).

Finally, Plastid Terminal Oxidases are known to act as a “safety valve” to allow the oxidation of the plastoquinone pool under stress conditions to avoid the generation of ROS. In *Chlamydomonas reinhardtii*, two PTOX isoforms are present. Until today, only one mutant affected in CrPTOX2 was obtained and could be studied. CrPTOX2 has been shown to be involved in chlororespiration (Houille-Vernes *et al.*, 2011). In *Arabidopsis thaliana*, only one isoform remains and seems not to fulfil the same functions and to be regulated in the same way as CrPTOX2 (Bolte *et al.*, 2020). In this thesis the presence of two PTOX isoforms has been highlighted in *Marchantia polymorpha*, one of which is close to green algae and the other one to angiosperms (article 2, page 117).

C) Photosynthesis study in *Marchantia polymorpha*

Marchantia polymorpha was chosen for its morphological characteristics, its place in evolution and its photosynthetic particularities. Indeed, the thin and slightly cut thallus of *Marchantia* compared to other Bryophytes (i. e. *Physcomitrium patens*) makes it easier to perform *in vivo* fluorescence measurements to detect photosynthetic activity. Moreover, its ploidy makes it easier to carry out CRISPR/Cas9 mutations than in angiosperms, most of which are polyploid. On the other hand, two biological particularities are important for my thesis. First, the presence of light-independent chlorophyll biosynthetic pathway allows *Marchantia* to be grown in the dark to track for the first time photoactivation, light-dependent Manganese cluster assembly, *in vivo* and to study its consequences on the organisation of the thylakoid membrane. Finally, the presence of all these protective mechanisms, which had disappeared in angiosperms, made it possible to highlight the presence of two types of PTOX isoforms in *Marchantia*: alga and plant-type. Thus, we were able to study the role of these proteins *in vivo* and determine their enzymatic characteristics in order to understand the evolutionary interest of the conservation of these two proteins in *Marchantia* and the disappearance of one of them in angiosperms.

Aims

The aim of the thesis was to investigate two mechanisms conserved at the level of photosynthesis: the photoactivation which is the light-dependent assembly of the Mn cluster as well as the role of PTOX proteins, involved in the protection of the photosynthetic chain. For this purpose, *Marchantia polymorpha* was chosen as a model system because of its capability to assemble PSII in the dark and the feasibility of doing super-resolution microscopy on the whole thallus. Furthermore, *M. polymorpha* offers the possibility to study regulation mechanisms of photosynthesis that are absent in angiosperms.

The first part concerns **photoactivation**.

1. The first objective was to characterise the impact of chloroplast manganese transporters mutations in *Marchantia polymorpha*, but this could not be achieved (presumed lethal mutations).
- 1'. Characterise the impact of Mn excess and deficiency on photosynthesis and metabolism in *M. polymorpha*
2. Determine the *in vitro* photoactivation conditions of isolated PSII from spinach using the oxygen electrode
3. Use EPR and derived methods to study the different stages of photoactivation and in particular the binding of the first Mn(II)
4. Find the conditions for cultivating *Marchantia polymorpha* in the dark and the analytical methods for monitoring photoactivation *in vivo* and as a function of time of illumination

The second part concerns **PTOX** proteins.

1. Studying the role of the two isoforms of PTOX in *Marchantia polymorpha* compared to other organisms of the green lineage: characterization of single and double mutants.
2. Compare and generate the structures of the two isoforms *in silico*.

A last part consisted in carrying out a theoretical reflection on the **dynamics of the thylakoids** and photosynthetic complexes within the chloroplast necessary to understand and explain certain results of the previous parts.

Part I : Photosynthesis regulation at PSII donor side

Study of Manganese homeostasis and Photoactivation

In this section, various issues will be addressed. First, I characterised the effect of manganese excess or deficiency on the development of *Marchantia polymorpha* and in particular the impact on photosynthesis and metabolism. Then, I used PSII isolated from spinach to achieve photoactivation *in vivo*. I first tried to find the best conditions for photoactivation by measuring the release of oxygen. Finally, still with isolated PSII, I approached photoactivation in a more mechanistic way using High-Field EPR spectroscopy and derived methods to determine the ligands of the first manganese ion used for photoactivation. Finally, I used *Marchantia* to try to follow photoactivation *in vivo* and to track changes in thylakoid dynamics in real time using SRM (Super-resolution fluorescence microscopy).

I) Impact of Manganese excess and deficiency on Photosynthesis and metabolism of *Marchantia polymorpha*

Manganese is an essential metal for plant survival. In particular, it plays an important role in photosynthesis since it is the major constituent of the Manganese cluster also called Oxygen Evolving Complex (Mn_4CaO_5). The light-dependent assembly of this cluster, termed photoactivation, is required for PSII activation and function.

Furthermore, it is known that manganese is not evenly distributed to the soil. Indeed, in some regions of the world, it is very abundant (Australia, China) and in others very poor (Scandinavia, Turkey), which in both cases leads to significant yield losses. In particular, it has been shown that excess Mn mainly leads to competition with the absorption of other metals such as iron. It is strongly assumed that this is the consequence of a decrease in the amount of PSI in these plants due to the presence of Fe-S clusters. On the other hand, Mn deficiency has been shown to mainly affect PSII because of the presence of Mn cluster at donor side.

Regarding *Marchantia polymorpha*, very little is known about metal homeostasis. Nevertheless, it has been defined as being a bio-indicator of heavy metals in its natural state and shown to be able to hyperaccumulate heavy metals (Samecka-Cymerman *et al.*, 1997; Ares *et al.*, 2018).

In this article, I defined Mn excess and Mn deficiency culture conditions for *Marchantia polymorpha* in order to study the homeostasis of this metal at the whole plant and chloroplast scale. In addition, we have performed a metabolomics analysis and highlighted a strong alteration of plant metabolism in excess condition while the deficiency rather targets photosynthesis.

Article 1: Manganese Excess and Deficiency affect chloroplast structure and photosynthesis in *Marchantia polymorpha* (accepted)

In this article, I have established the culture conditions of *Marchantia polymorpha* and carried out most of the experiments. I did the quantification of metals in thalli and chloroplasts in collaboration with Sébastien Thomine. Super-resolution microscopy and image processing was done with Andrew Gall. I personally collected and derived the metabolomic samples, processed the data and analysed the results in collaboration with Florence Guérard. I performed the photosynthetic measurements, i. e. chlorophyll fluorescence, P700 absorption measurements, pigment determination and activity of PSI and PSII and of antioxidant enzymes. In addition, I had the chance to supervise a student, Thaïs Henebelle, for 6 months on this project. Finally, I actively participated in writing with Anja Krieger-Liszkay.

Manganese concentration affects chloroplast structure and the photosynthetic apparatus in *Marchantia polymorpha*

Marine Messant,¹ Umama Hani ,¹ Thaïs Hennebelle ,¹ Florence Guérard ,² Bertrand Gakière,² Andrew Gall ,¹ Sébastien Thomine ,¹ and Anja Krieger-Liszky ^{1,*}

¹ Institute for Integrative Biology of the Cell (I2BC), CEA, CNRS, Université Paris-Saclay, 91198 Gif-sur-Yvette cedex, France

² Institute of Plant Sciences Paris-Saclay, CNRS, Université Paris-Sud, Institut National de la Recherche Agronomique, Université d'Evry, Université Paris-Diderot, Université Paris-Saclay, 91405 Orsay Cedex, France

*Author for correspondence: anja.liszky@i2bc.paris-saclay.fr (A.K.-L.)

The author responsible for distribution of materials integral to the findings presented in this article in accordance with the policy described in the Instructions for Authors (<https://academic.oup.com/plphys/pages/General-Instructions>) is A.K.-L. (anja.liszky@i2bc.paris-saclay.fr).

Abstract

Manganese (Mn) is an essential metal for plant growth. The most important Mn-containing enzyme is the Mn_4CaO_5 cluster that catalyzes water oxidation in photosystem II (PSII). Mn deficiency primarily affects photosynthesis, whereas Mn excess is generally toxic. Here, we studied Mn excess and deficiency in the liverwort *Marchantia polymorpha*, an emerging model ideally suited for analysis of metal stress since it accumulates rapidly toxic substances due to the absence of well-developed vascular and radicular systems and a reduced cuticle. We established growth conditions for Mn excess and deficiency and analyzed the metal content in thalli and isolated chloroplasts. In vivo super-resolution fluorescence microscopy and transmission electron microscopy revealed changes in the organization of the thylakoid membrane under Mn excess and deficiency. Both Mn excess and Mn deficiency increased the stacking of the thylakoid membrane. We investigated photosynthetic performance by measuring chlorophyll fluorescence at room temperature and 77 K, measuring P700 absorbance, and studying the susceptibility of thalli to photoinhibition. Nonoptimal Mn concentrations changed the ratio of PSI to PSII. Upon Mn deficiency, higher non-photochemical quenching was observed, electron donation to PSI was favored, and PSII was less susceptible to photoinhibition. Mn deficiency seemed to favor cyclic electron flow around PSI, thereby protecting PSII in high light. The results presented here suggest an important role of Mn in the organization of the thylakoid membrane and photosynthetic electron transport.

Introduction

Manganese (Mn) is an essential element for plant growth. Mn homeostasis is disturbed under suboptimal or excessive Mn availability (Schmidt et al. 2016; Alejandro et al. 2020). The most important Mn-containing enzyme is the Mn_4CaO_5 cluster at photosystem II (PSII) that catalyzes water oxidation. Although Mn is involved as a cofactor in a range of biochemical pathways, the primary effect of Mn deficiency in photosynthetic organisms is a decrease in photosynthetic activity (Marschner 1995). Furthermore, Mn is involved in reactive oxygen species (ROS) metabolism and

in the antioxidant response. Manganese is the cofactor of the manganese superoxide dismutase (MnSOD) found in mitochondria and peroxisomes (Bowler et al. 1994; Corpas et al. 2017). Oxalate oxidase (OxOx) present in the apoplast also requires Mn. This enzyme catalyzes the oxidation of oxalate to carbon dioxide coupled with the reduction of oxygen to hydrogen peroxide (Requena and Bornemann 1999), the latter having an essential role in the defense against pathogens (Lane 2002). When accumulated in excess, Mn can be toxic causing oxidative stress (Marschner 1995; Pittman 2005; Delhaize et al. 2007; Peiter et al. 2007; Eroglu et al. 2016).

In the presence of excess Mn in the soil, there is a competition between the uptake of Mn and other metals that are also essential for the plant (Alam et al. 2005; St. Clair and Lynch, 2005; Blamey et al. 2015; Lešková et al. 2017). Indeed, at the level of the roots, plants do not have transporters that are completely selective for a single metal. Thus, a high abundance of Mn can lead to a decrease in the absorption of other essential metals such as calcium, magnesium, iron, or even phosphorus, thereby negatively affecting photosynthesis (Nable et al. 1988; Amao and Ohashi 2008) and inhibiting chlorophyll synthesis (Clairmont et al. 1986; Subrahmanyam and Rathore 2001). Manganese excess causes chlorosis followed by necrosis leading to plant death, but these symptoms are very variable and species dependent (Millaleo et al. 2010). To overcome Mn toxicity, plants have developed different ways of Mn storage in vacuoles (Ducic and Polle 2007), cell walls (Führs et al. 2010), and even Golgi vesicles (Marschner 1995; Pittman 2005). In the literature, plant species have been divided into tolerant and non-tolerant to Mn excess. Some species can hyperaccumulate Mn at levels above 10,000 mg.kg⁻¹ dry weight (DW) (Van der Ent et al. 2013).

The effect of Mn deficiency on photosynthetic electron transport and chloroplast structure has been studied for decades in a number of different organisms ranging from cyanobacteria to angiosperms (e.g. Homann 1967; Salomon and Keren 2011). In general, a decline in PSII activity is observed although symptoms of Mn deficiency are species dependent (Homann 1967). Depending on the severity of Mn deficiency, the ultrastructure of chloroplasts may be perturbed. In slightly Mn-deficient spinach (*Spinacia oleracea*) plants, the stroma lamellae are affected, while the grana stacks are normal. Under more severe Mn deficiency, grana stacks are also disorganized (Mercer et al. 1962). More recently, similar observations were reported in the Arabidopsis (*Arabidopsis thaliana*) knockout mutant chloroplast Mn transporter1 (CMT1), a transporter localized in the inner envelope membrane, where chloroplast development was abnormal and thylakoids appeared disorganized, with either hypo- or hyper-stacked grana lamellae (Eisenhut et al. 2018; Zhang et al. 2018). In this mutant, a large heterogeneity between the chloroplasts was observed with chloroplasts containing a well-structured, normal organization of the thylakoid membranes next to chloroplasts with completely disorganized architectures (Eisenhut et al. 2018). The consequences of the loss of PSII activity and the disorganization of the thylakoid membrane on the ratio of linear and cyclic photosynthetic electron transport have not been investigated in previous studies.

In this present study, we investigated the consequences of both excess and deficiency of Mn on photosynthesis in the liverwort *Marchantia polymorpha*, an emerging model system. *Marchantia* has been described in the 1990s as being able to hyperaccumulate certain metals such as, for example, lead (Samecka-Cymerman et al. 1997). Due to the morphology of the thalli, the ventral part and hyaline parenchyma

of the plant are in direct contact with the substrate allowing the uptake of the metals from the medium without having to pass through the root system as occurs in vascular plants. Compared to vascular plants, the leaf anatomy of *Marchantia* is simpler and the tissues are thinner. Chloroplasts are less structured than in vascular plants (Tanaka et al. 2017) with smaller grana stacks, making these chloroplasts an ideal system for super-resolution fluorescence microscopy.

We have established conditions for cultivating *Marchantia* on plates under Mn deficiency and excess. The metal content, metabolome, and antioxidant activities as well as photosynthetic activity and chloroplast structure were determined to investigate the response of *Marchantia* to non-optimal Mn supply. Manganese excess and deficiency affect these processes in different ways. Manganese excess led to a strong response of the metabolome but subtle defects in photosynthesis, whereas, in contrast, Mn deficiency affected the activity of PSII and promoted cyclic electron transport around PSI. Under Mn deficiency, an increase in non-photochemical fluorescence quenching was observed, protecting PSII against photoinhibition.

Results

Part I: Mn excess induces a stress response and affects the photosynthetic apparatus

In order to determine the effect of Mn excess on *M. polymorpha*, plants were cultivated on media containing different MnCl₂ concentrations, ranging from 33 μM (Agar Control) to 6.5 mM (200×) manganese. Gemmae were cultured on a standard Gamborg's B5 medium (33 μM MnCl₂) for 2 weeks before being transferred for 1 week to the different Mn concentrations before analysis. Figure 1A shows that thalli were able to grow normally up to 1 mM Mn. However, thalli showed reduced growth from 2 up to 6.6 mM Mn, with signs of stress visible as brown spots. The chlorophyll content of the thalli was significantly decreased in excess Mn conditions (SI Table 1). The determination of Mn concentration in thalli (Figure 1B) showed that there is a positive correlation between Mn accumulation and Mn concentration in the medium. In addition to Mn, we determined Fe and Mg content since high Mn may negatively impact Fe import into the chloroplasts and thereby the assembly of FeS clusters in PSI (Millaleo et al. 2013), and Mg is important for stacking of the thylakoid membranes. Neither Fe nor Mg content was affected by the high Mn concentrations.

In the following, we focus on the conditions of Mn excess 30× and 200×. The first being the highest concentration at which *Marchantia* showed no obvious signs of stress and the second being the most stressful condition. We conducted a metabolomic analysis by gas chromatography–mass spectrometry (GC-MS) on thalli. In total, 94 metabolites have been identified and quantified (Supplemental Figure S1, Tables S2 and S3). Regarding the

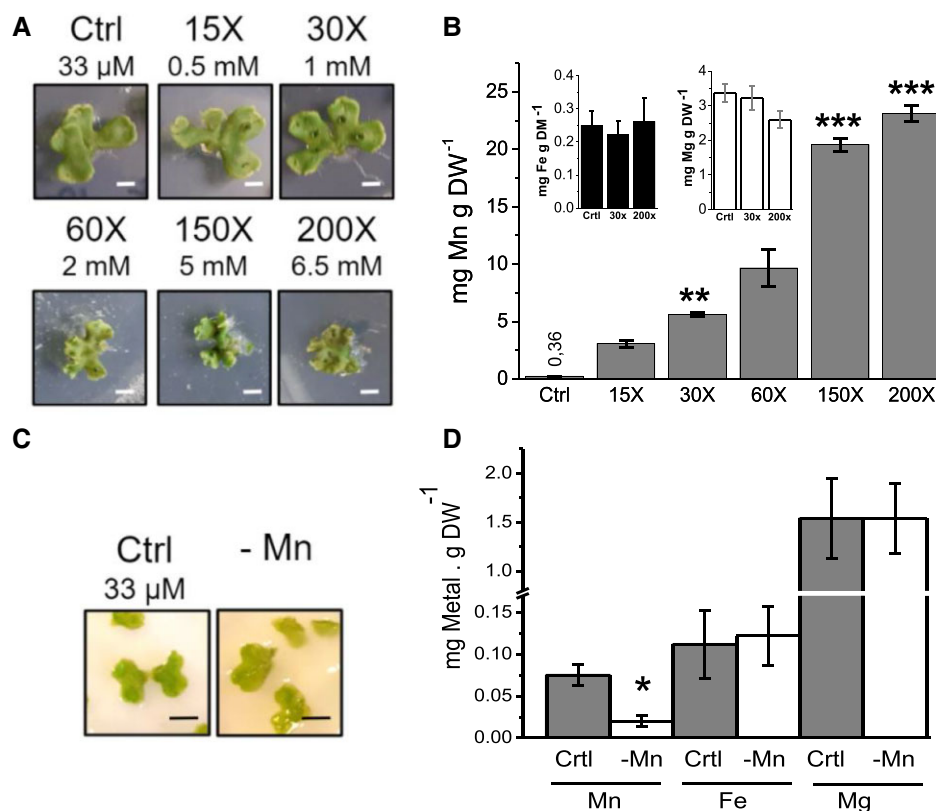


Figure 1. Effect of nonoptimal Mn supply on growth and metal content of *Marchantia polymorpha*. Mn excess: **A**) 2-wk-old thalli were transferred for 1 week to agar plates containing 33 μM (control, Ctrl), 0.5 mM (15 \times), 1 mM (30 \times), 2 mM (60 \times), 5 mM (150 \times), and 6.5 mM (200 \times) MnCl_2 , respectively. White scale bars represent 1 cm. **B**) Manganese, iron, and magnesium concentrations were determined after 1-week growth with the given Mn concentrations. Mn deficiency: **C**) 2-week-old thalli were transferred and grown for 1 week on starch plates with or without the addition of 33 μM MnCl_2 . Black scale bars represent 1 cm. **D**) Manganese, iron, and magnesium concentrations in thalli were measured after 1 week of growth on starch plates with (Ctrl, hatched bars) or without MnCl_2 (-Mn, white bars) in the medium. Error bars in **B** and **D** represent standard errors. Stars in **B** and **D** indicate significant differences, compared to the control condition, based on a Mann–Whitney test (* $P < 0.05$, ** $P < 0.01$, *** $P < 0.001$; $N \geq 3$ biological replicates).

200 \times condition, certain metabolites involved in the response to heavy metal or oxidative stresses were strongly increased, while all other metabolites decreased compared to the control. A very high concentration of Mn was associated with a strong induction of polyamine synthesis with an accumulation of ornithine, citrulline, and putrescine (Table 1). Among sugars and their derivatives, strong increases in trehalose, rhamnose, and galacturonic acid were also observed. All these compounds are known to accumulate in plants and other organisms upon exposure to heavy metals (Sharma and Dietz 2006; Singh et al. 2016; Liu et al. 2017; Hasanuzzaman et al. 2019; Alejandro et al. 2020). Most striking, *N*-methylalanine content was 30 and 50 times higher in 30 \times and 200 \times conditions, respectively. To further investigate the response to oxidative stress, the activity of a few antioxidant enzymes was measured (Table 2). A 2-fold increase in superoxide dismutase (SOD) activity was observed at the highest Mn concentration. The activity of class III peroxidases was also slightly increased at 200 \times , while catalase activity gradually decreased.

Table 1. Increase in metabolites involved in oxidative stress response upon growth on high Mn concentration

Metabolite	Experimental condition		
	Ctrl	30 \times	200 \times
Citrulline	0.001 \pm 0	0.001 \pm 0	0.003 \pm 0.001
Galacturonic acid	0.004 \pm 0	0.004 \pm 0.001	0.008 \pm 0.001
L-ornithine	0.003 \pm 0.001	0.003 \pm 0	0.007 \pm 0.001
<i>N</i> -Methylalanine	0.021 \pm 0.002	0.67 \pm 0.237	1.101 \pm 0.038
Putrescine	0.003 \pm 0.001	0.002 \pm 0	0.008 \pm 0.001
Rhamnose	0.004 \pm 0	0.004 \pm 0.001	0.008 \pm 0.001
Trehalose	0.053 \pm 0.003	0.049 \pm 0.008	0.083 \pm 0.012

List of selected metabolites showing an increase in plants grown in 200 \times condition. The mean value and SD are given ($N = 4$). $P < 0.05$ for all values, according to the 2-way ANOVA test. See Supplemental Table S2 for the full list.

Next, we studied the impact of Mn excess on chloroplast ultrastructure and photosynthetic activity. The concentration of Mn, Fe, and Mg was measured in isolated intact chloroplasts (Figure 2A). The results show a gradual and significant increase of Mn comparable with the observation made in the

Table 2. Antioxidant enzymes activities in thalli from control and manganese excess and deficiency conditions

Parameter	Experimental condition				
	Ctrl	30×	200×	Starch + Mn	Starch – Mn
SOD activity	3.01 ± 0.63	4.19** ± 0.86	6.00*** ± 1.48	5.63 ± 1.43	5.08 ± 0.63
CAT activity	1.18 ± 0.16	0.87** ± 0.26	0.54*** ± 0.12	0.72 ± 0.16	0.70 ± 0.13
PRX activity	1.27 ± 0.38	1.17 ± 0.25	1.59* ± 0.42	1.52 ± 0.20	1.04** ± 0.40
ROS	—	—	—	44.4 ± 4.2	100 ± 1.4

Superoxide dismutase, Catalase, and peroxidase activities ($\mu\text{mol substrate mg proteins}^{-1} \text{ min}^{-1}$) were measured in crude extracts. $\cdot\text{OH}$ derived from $\text{H}_2\text{O}_2/\text{O}_2^{\bullet-}$ was measured using electron paramagnetic resonance (EPR) as a hydroxyethyl-*N*-tert-butyl- α -(4-pyridyl)nitron *N'*-oxide.

(4-POBN) adduct. Mean value and SD are given. Stars indicate a significant difference compared to the control condition, based on a Mann–Whitney test (* $P < 0.01$, ** $P < 0.01$, *** $P < 0.001$, $N = 3$ biological replicates).

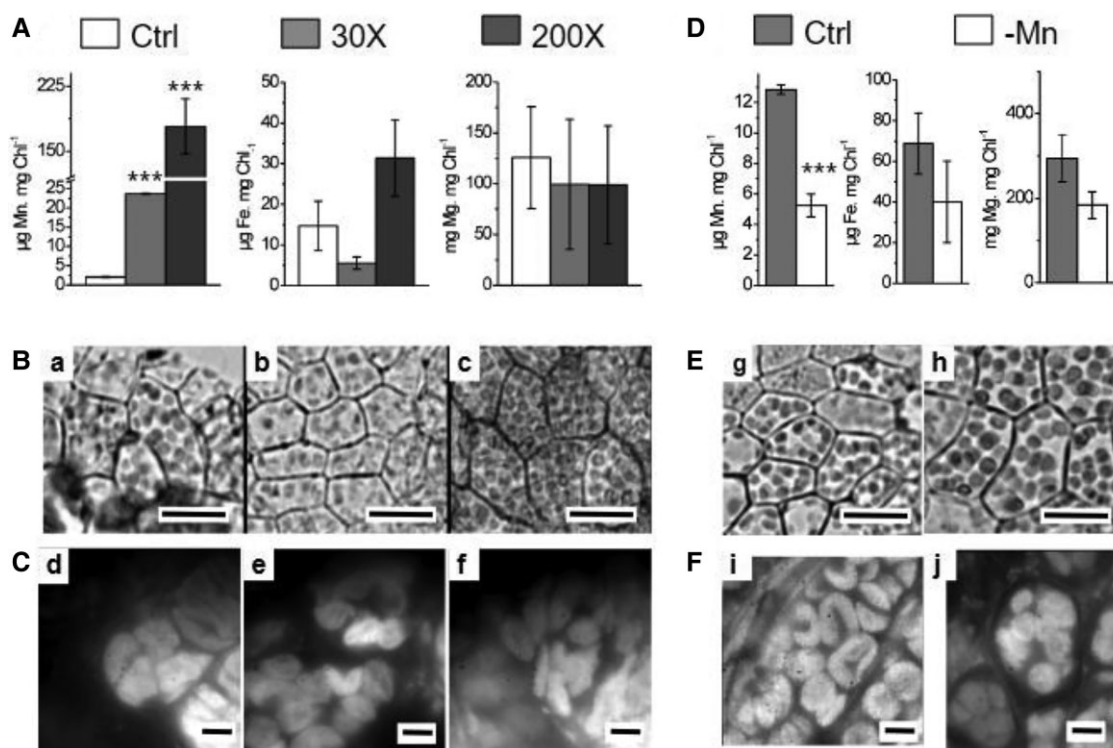


Figure 2. Chloroplast metal content and structure in *Marchantia polymorpha* grown on nonoptimal Mn supply. Mn excess: **A**) Metal content of intact chloroplasts isolated from thalli cultured on agar (control, 33 μM ; 30 \times , 1 mM; 200 \times , 6.5 mM MnCl_2). **B**) Microscopy images of thalli cultured on agar (a, Control; b, 30 \times ; c, 200 \times). **C**) Epifluorescence microscopy images of chloroplast surfaces of thalli (d, Control; e, 30 \times ; f, 200 \times). Mn deficiency: **D**) Metal content of intact chloroplasts isolated from thalli cultured on starch (Starch + Mn, 33 μM Mn; Starch – Mn, without Mn). **E**) Microscopy images of chloroplasts in thalli (g, Starch + Mn; h, Starch – Mn). **F**) Epifluorescence microscopy images of chloroplast surfaces of thalli (i, Starch + Mn; j, Starch – Mn). Scale bars in B and E represent 200 μm ; scale bars in C and F represent 10 μm . Error bars in A and D represent standard errors. Stars in A and D indicate significant differences, compared to the control condition, based on a Mann–Whitney test (*** $P < 0.001$; $N \geq 3$ biological replicates).

whole thalli. We observed an increase from 2 to 175 $\mu\text{g Mn mg Chl}^{-1}$ in the 200 \times condition compared to the Control. We determined the total chlorophyll content of the thalli to determine the proportion of Mn allocated to chloroplasts (Figures 1B and 2A; Supplemental Table S1). About 7% to 13% of the total Mn content of the thalli was detected inside the isolated chloroplasts with 13% in Control and 30 \times and 7% in 200 \times . There were no significant changes in the chloroplast Fe and Mg concentrations under Mn excess.

We used first bright-field and epifluorescence microscopy to see whether Mn excess changes the morphology of the cells as well as the number of chloroplasts (Figure 2B). In Control Agar, most chloroplasts show typical plant-type spherical morphology, while in 30 \times , there was a divergence from this typical architecture. Some chloroplasts had a deformed shape. In 200 \times , this progression of deformation of the morphology was further enhanced and the chloroplasts were smaller on average (Figure 2C, Supplemental Figure S2). Next, we used

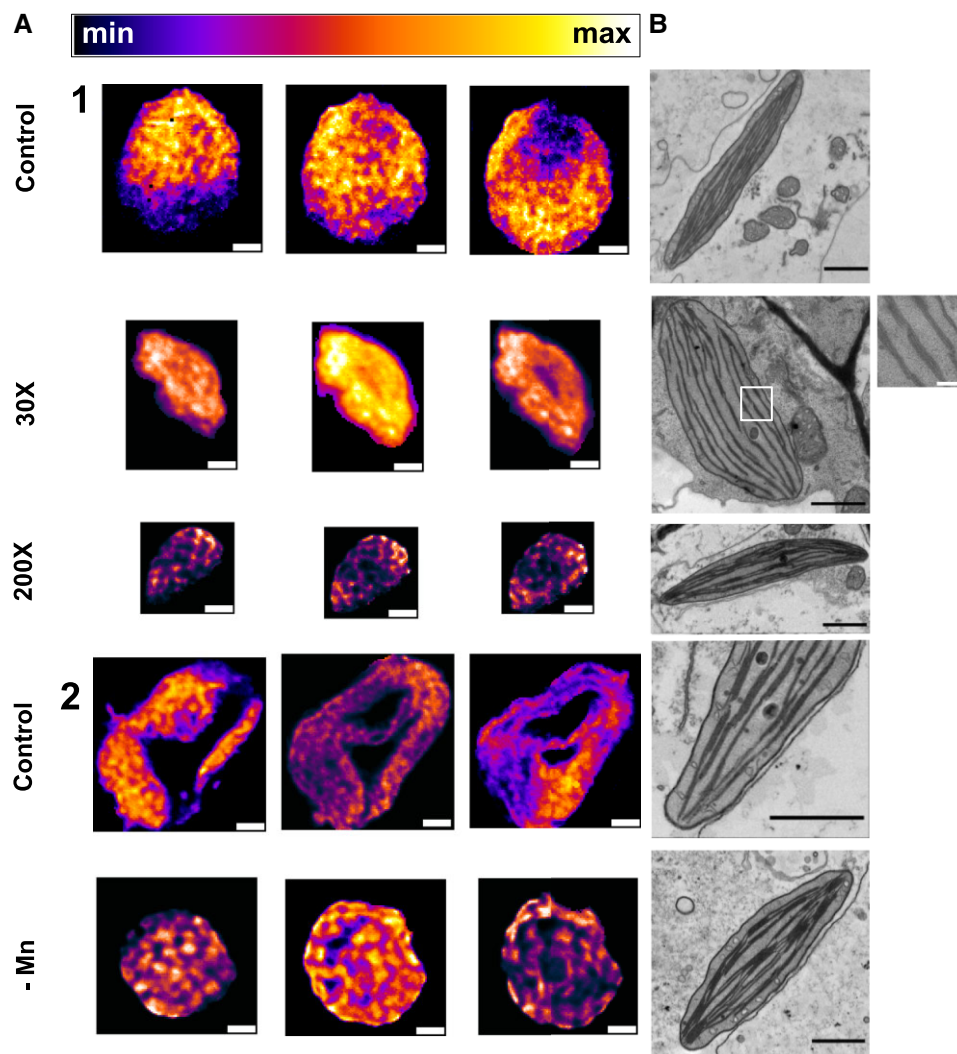


Figure 3. Organization of chloroplast membranes as evidenced by room temperature in vivo super-resolution chlorophyll fluorescence emission nanoscopy and by TEM. **A)** Super-resolution fluorescence microscopy. 1) Agar Control, 30 \times and 200 \times conditions and 2) Starch Control and Starch – Mn. For each culture condition, reading from left to right, the 3 reconstructed fluorescence maps are separated by 300 nm in the axial (z) direction. The false-color scale is represented by horizontal color bar (minimum, black; maximum, white). Scale bar: 1 μ m. One chloroplast is represented by a total of 10 chloroplasts analyzed for each condition. **B)** TEM images. 10–20 chloroplasts were analyzed, exhibiting the same features for each culture condition. Scale bar: 1 μ m (except for the digitally enhanced insert, 200 nm).

super-resolution fluorescence nanoscopy and transmission electron microscopy (TEM) to determine better the change in the organization of the thylakoid membranes triggered by excess Mn (Figure 3). At physiological temperatures, chlorophyll fluorescence is mainly due to PSII emission, which is essentially concentrated in the grana lamellae (for reviews, see Dekker and Boekema 2005; Kirchhoff 2019). Hence, the fluorescence images partly represent the spatial organization and relative abundance of grana stacks in in vivo chloroplasts. The organization of the chloroplast in the Control (Figure 3A top panel) is similar to that of *Arabidopsis thaliana* (Iwai et al. 2018; Streckaite 2021) with a “round” shape and the presence of numerous grana stacks visualized as highly fluorescent yellow/orange patches in the false-color images, albeit

with a less clear separation between stroma and grana lamellae. Under the 30 \times condition, the chloroplast is smaller, indicating a more compact spatial organization of the interconnected granae. Furthermore, the presence of a non-fluorescent region was observed in the center corresponding to a void in bright-field images. In 200 \times , the smaller chloroplasts still exhibited strong chlorophyll fluorescence emissions with a well-developed distribution of patches indicative of thylakoid grana stacks. Electron microscopy images confirm clear grana stacking under control and 200 \times conditions, while the organization at 30 \times was different with 3 thylakoid membranes always attached to each other concomitant with a lack of major grana stack formation (Figure 3B, TEM insert). This uniform distribution of attached membranes under

Table 3. Chl *a/b* ratio and electron transport capacities of thylakoids from thalli cultured on manganese excess and deficiency

Parameter	Experimental condition				
	Ctrl	30×	200×	Starch + Mn	Starch – Mn
Chl <i>a/b</i>	1.23 ± 0.09	1.30 ± 0.10	0.97 ± 0.06	0.95 ± 0.22	0.91 ± 0.20
F_v/F_m	0.775 ± 0.005	0.773 ± 0.003	0.765 ± 0.004	0.772 ± 0.012	0.751* ± 0.004
PSI/PSII	1.47 ± 0.02	1.42 ± 0.01	1.19* ± 0.02	1.11 ± 0.02	1.51* ± 0.01
PSII activity	48 ± 13	43 ± 17	15.0*** ± 5.1	30 ± 9	22 ± 8
PSI activity	116 ± 20	114 ± 27	100 ± 40	59 ± 8	75* ± 16

Chlorophyll content was determined after extraction in acetone. PSI to PSII ratio was determined by integrating the area of the fluorescence at 77 K ($\lambda_{\text{max}725}/\lambda_{\text{max}685}$). PSII and PSI activities ($\mu\text{mol O}_2 \mu\text{g chl}^{-1} \text{h}^{-1}$) were measured using an O_2 electrode. PSII activity was measured as oxygen evolution in the presence of 1 mM 2,6-dichloro-1,4-benzoquinone (DCBQ), 10 mM NH_4Cl . PSI activity was measured as oxygen uptake in the presence of 10 μM DCMU, 5 mM ascorbate, 30 μM DCPIP, 500 μM methylviologen, and 10 mM NH_4Cl . Mean value and SE are given. Stars indicate significant difference compared to the control condition, based on a Mann–Whitney test (* $P < 0.01$, *** $P < 0.001$, $N = 6$).

30× Mn is in agreement with the quasi-uniform false-color chlorophyll emission maps observed using in vivo fluorescence nanoscopy, attributed to mainly PSII emission.

Since the size of the chloroplasts and the distribution of the chlorophyll fluorescence within the chloroplasts were affected by the growth conditions, photosynthesis was studied in more detail. Table 3 presents that the Chl *a/b* ratio remained unchanged at 30× but decreased at 200× Mn, indicating that the antenna size relative to the reaction center increased since Chl *b* is a major constituent of the light-harvesting complex II (LHCII). The 77 K fluorescence emission spectra (Figure 4A) showed 3 characteristic peaks at 685, 695, and 725 nm; the former 2 peaks are attributed to LHCII and PSII, and the latter to PSI with its antenna (Sato and Butler 1978). For chloroplasts isolated from thalli grown at 200×, the emission attributed to PSI decreased relative to that of PSII, while there was no change when grown at 30× (Figure 4A). In line with the lower PSI fluorescence relative to PSII fluorescence in 200×, the capacity of PSI electron transport was slightly lower although the effect was not statistically significant (Table 3). However, the capacity of PSII electron transfer was significantly decreased. A damaging effect of high Mn concentration on PSII activity was confirmed by fluorescence induction curves (Figure 4B). The appearance of the K-phase under 200× condition can be attributed to the damage to the Mn_4CaO_5 cluster at the PSII donor side according to Strasser (1997). In 200×, maximum quantum yield of PSII (F_v/F_m) and chlorophyll quenching fluorescence were altered during illumination with actinic light, but there was no increase in the susceptibility of PSII to photoinhibition (Table 3, Supplemental Figures S3 and S4).

Part II: Mn deficiency affects the photosynthetic apparatus and may favor cyclic electron flow

In the following, we investigated the effect of Mn starvation on *M. polymorpha*. Agar plates were not suitable to induce Mn deficiency since agar contains too much Mn as an impurity ($12.8 \pm 0.4 \mu\text{M}$). Therefore, we substituted agar with starch as a gelling agent. Gemmae were cultured for 2 wk on Gamborg's B5 Agar medium (33 μM MnCl_2) before young thalli were transferred to Mn-free Gamborg's B5 Starch medium with or without the addition of Mn (33 μM Mn). It was

not possible to culture gemmae directly on starch because they were not able to develop. Figure 1C shows that plants exhibited no visible growth defect after 1 week culturing on Starch Control or without Mn. However, chlorophyll fluorescence showed a clear decrease in the quantum yield of PSII (F_v/F_m) was lower when no MgCl_2 had been added to the medium (Supplemental Figure S5). The amount of metals in thalli was measured (Figure 1D). The use of starch allowed a reduction of Mn content from 75 μg Mn g DW^{-1} (Starch Control) to 20 μg Mn g DW^{-1} (Starch – Mn). Fe and Mg contents were not affected.

As for Mn excess, a metabolic analysis was carried out. No significant difference in the metabolomics profiles was observed between the 2 starch conditions (Supplemental Table S1), while there were clear differences between Agar Control and Starch Control (Supplemental Table S2). The activity measurements of the antioxidant enzymes showed a significant decrease in the activity of type III peroxidases (Table 2). Using a spin-trapping assay, the generation of $\cdot\text{OH}$ derived from $\text{H}_2\text{O}_2/\text{O}_2^{\cdot-}$ was detected in starch-grown plants. ROS levels were 2 times higher in the Starch – Mn condition.

Next, the impact of Mn deficiency on chloroplasts was investigated. The measurements (Figure 2D) revealed a decrease in the Mn content by about 50% in the Starch – Mn condition compared with the Starch Control. There was a tendency that the Starch – Mn growth condition lowers slightly the Fe and Mg content; however, the differences were not statistically significant. Overall, the metal content (Mn, Fe, and Mg) of the chloroplasts under starch conditions was almost double compared to chloroplasts from thalli grown under Agar Control conditions. This may be due to effects on the metal uptake and transport system or also be connected to a higher intactness of the isolated chloroplasts. The epifluorescence microscopy images (Figure 2F) showed more “horseshoe-shaped” chloroplasts under the Starch Control condition. In Starch – Mn, chloroplasts appeared rounder. These observations were confirmed by super-resolution nanoscopy (Figure 3B); however, the area of the chloroplasts was unaltered (Supplemental Figure S2). In the Starch Control, the thylakoid membranes were organized in grana/lamellae-like structures. In the Starch – Mn condition, the chloroplasts had fewer voids in the 3D volume.

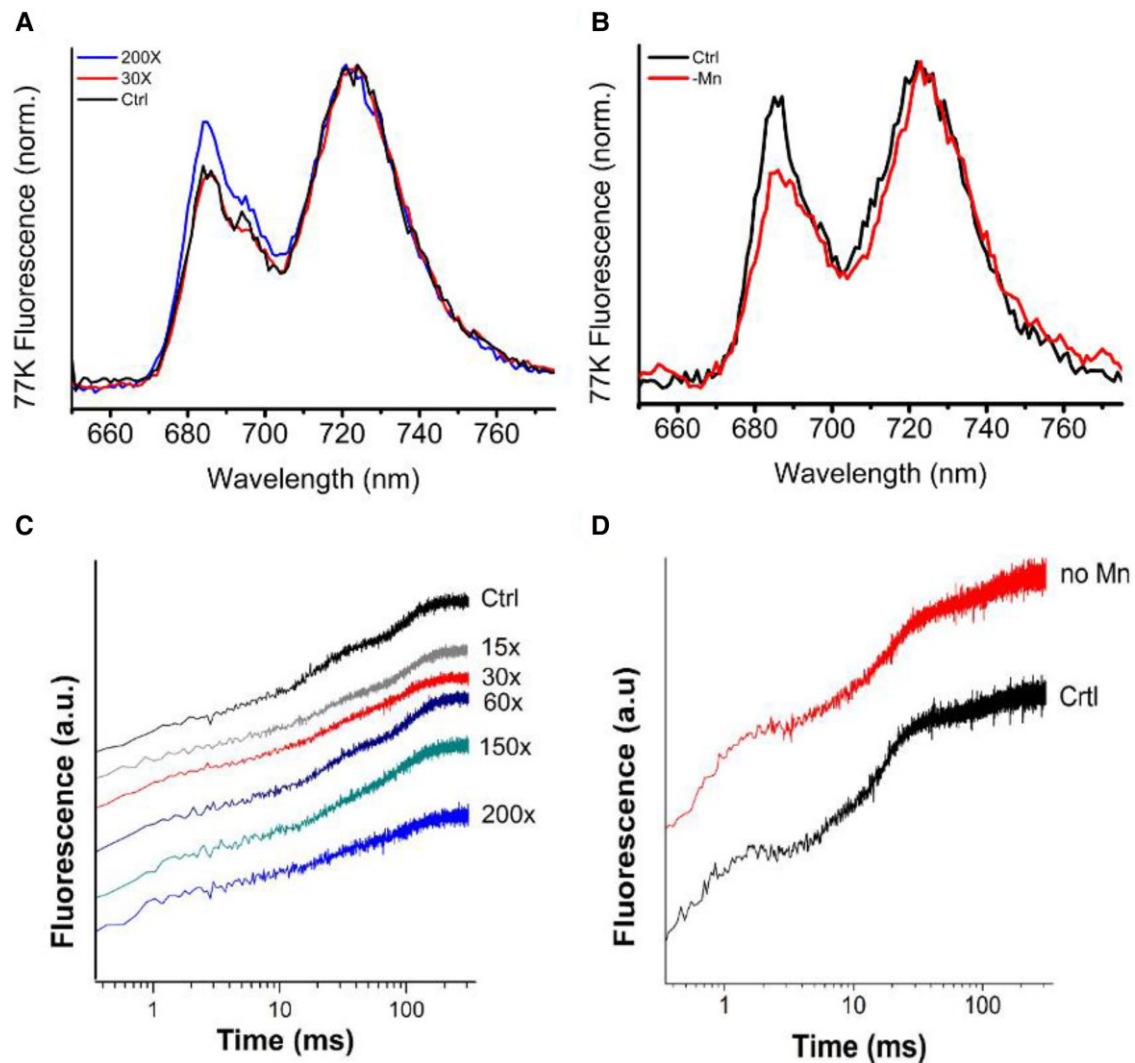


Figure 4. Chlorophyll fluorescence at 77 K and room temperature. **A)** 77 K fluorescence emission of chloroplasts extracted from thalli grown on agar: Ctrl (black), 30 × (red), and 200 × (blue, upper trace at 685 nm) ($N = 3$, biological replicates). **B)** Same as (a) carried out on starch-cultivated thalli with (Ctrl, black) or without $MnCl_2$ (–Mn, red, upper trace at 685 nm). Spectra in A and B were normalized to the maximum emission at 725 nm. **C)** Room-temperature fluorescence induction curves (OJIP) were measured on 5-min dark-adapted thalli by the application of a saturating flash with 300 ms duration. Culture conditions as in A. **D)** Fluorescence induction curves on thalli grown as in B. One representative curve is shown for each condition.

Compared with a standard chloroplast as represented in the Agar Control (Figure 3A, top panel), or Arabidopsis (Iwai et al. 2018; Streckaite 2021), the strongly fluorescent regions were localized more distinctly, indicating a change in the mesoscopic organization of the thylakoid membrane. This indicates smaller grana stacks with a more pronounced segregation between them and the stroma lamellae as confirmed by TEM. The TEM image shows a much higher degree of stacking of the thylakoid membranes (Figure 3B).

The 77 K fluorescence (Figure 4B) showed a decrease in the emission at 680 nm in chloroplasts isolated from Starch – Mn thalli, indicating a loss of PSII content compared with PSI. PSII activity was lower (Table 3). The quantum yield of PSII, F_v/F_m , was significantly lower upon Mn deficiency. PSI activity increased significantly, confirming the change in the PSI/PSII ratio under Mn deficiency seen in 77 K

fluorescence spectra. In the Starch – Mn condition, the fluorescence induction curves showed a dip phase at about 2 ms, indicative of damage to the Mn_4CaO_5 cluster at the PSII donor side (Figure 4D).

Figure 5 shows changes in room temperature chlorophyll fluorescence upon illumination with actinic light. Upon Mn deficiency, energy dissipation as the heat was enhanced (qN; Figure 5C). However, photochemical quenching (qP; Figure 5D) was not affected. Furthermore, the slightly higher minimum fluorescence level during the recovery phase (post-illumination fluorescence transient, PIFT) upon Mn deficiency indicates an increase in chlororespiratory and/or cyclic electron flow. To show whether the stability of PSII or the repair of damaged PSII was affected under Mn deficiency, photoinhibition experiments were carried out with or without the protein synthesis inhibitor lincomycin

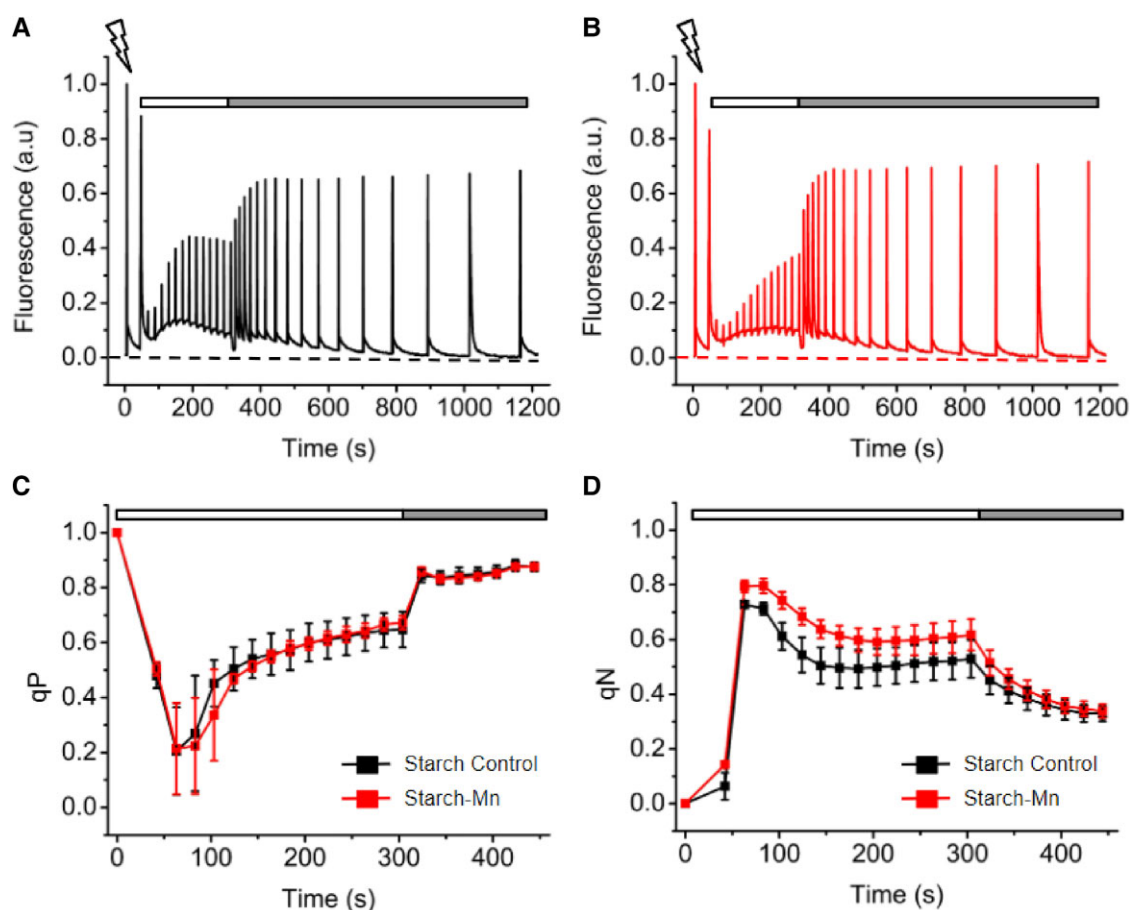


Figure 5. Analysis of variable chlorophyll fluorescence in Mn deficiency. **A)** and **B)** Induction and recovery fluorescence curves were measured on thalli transferred for 1 week to starch medium with (black) or without added MnCl_2 (red). After 5 min dark adaptation, thalli were exposed to a measuring light to determine the minimum fluorescence level (dashed lines) and to a saturating flash to obtain the maximum fluorescence level. Actinic light ($50 \mu\text{mol photons m}^{-2} \text{s}^{-1}$) was applied for 5 min (white bar). Recovery in the dark was followed (gray bar). **C)** q_P and **D)** q_N parameters were calculated, thanks to saturating flashes applied during the light and dark period. Mean values and standard deviation are given in **C** and **D** ($N = 12$, 3 biological replicates). C: lower trace, without added MnCl_2 ; D: upper trace, without added MnCl_2 .

(Figure 6). Plants cultivated on Starch – Mn were more susceptible to high light in the absence of lincomycin. In the presence of lincomycin, the opposite was observed with PSII in plants cultivated on Starch – Mn being more resistant to the photoinhibitory treatment. This may be explained by the higher nonphotochemical quenching (NPQ) protecting the photosynthetic apparatus. A higher NPQ was observed also in the presence of lincomycin (Supplemental Figure S6).

The higher PSI fluorescence at 77 K, the higher NPQ, and the protection of PSII against photoinhibition in plants cultivated on Starch – Mn may indicate that cyclic electron transport is favored under these conditions. Absorption changes of P700 show that P700 is more slowly oxidized, both in red actinic and in far-red light, in plants cultivated on Starch – Mn indicating that more electrons are available in the electron transport chain (Figure 7A). To show that indeed more electrons are available for P700⁺ reduction at the luminal side, we determined the yield of donor-side limitation, $Y(\text{ND})$ as a function of the intensity of the actinic

light. Figure 7B shows the less donor-side limitation of PSI over a wide range of light intensities in plants cultivated on Starch – Mn compared to those cultivated on Starch Control. These data further indicate a higher activity of cyclic electron flow under Mn deficiency. Under both conditions, acceptor side limitation at the stromal side of PSI was not observed because *Marchantia* possesses flavodiiron proteins that use ferredoxin as an electron donor to reduce oxygen to water (Shimakawa et al. 2021).

Discussion

In this study, we established growth conditions for manganese excess and deficiency in *M. polymorpha*. *Marchantia* can absorb up to $25 \text{ mg Mn g DW}^{-1}$ (Figure 1B) which is higher than the hyperaccumulator *Polygonum lapathifolium* that contains approximately $18 \text{ mg Mn g DW}^{-1}$ in its aerial parts (Liu et al. 2016). However, *Marchantia* shows symptoms of toxicity under the $200\times$ conditions, and thalli

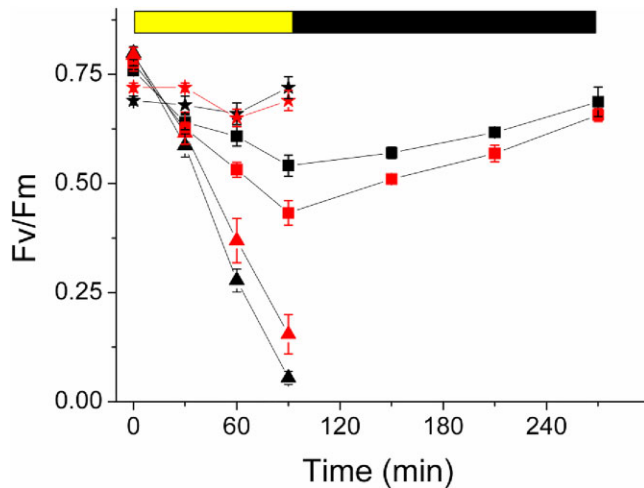


Figure 6. Photoinhibition in Mn deficiency in the absence and presence of lincomycin. Photoinhibition was measured on starch-cultivated thalli with (black symbols) or without MnCl_2 (red symbols). F_v/F_m was followed during exposure to high light ($800 \mu\text{mol photons m}^{-2}\text{s}^{-1}$) for 90 min (yellow bar) and during the recovery at room light (black bar). Squares: without lincomycin; lower trace without MnCl_2 , triangles: with lincomycin; upper trace without MnCl_2 . As a control, lincomycin samples incubated in the dark are shown (stars). Mean values and standard errors are given ($N = 6$, 2 biological replicates).

only survive for a few weeks. Therefore, *Marchantia* does not qualify as a hyperaccumulator despite its high Mn uptake capacity. Mn excess conditions induced an increase in SOD and peroxidase (PRX) activity, while catalase activity decreased (Table 2). An increase in SOD activity could reflect a higher amount of MnSOD present under Mn excess conditions. The metabolomics analysis showed that known stress-induced metabolites accumulate upon excess Mn (Table 1; Supplemental Figure S2 and Tables S2 and S3); however, the metabolomics response of *Marchantia* is distinct from that of angiosperms and requires in-depth functional analysis of metabolites and metabolic pathways. An excess of Mn affected the ratio between it and other metals (e.g. Fe and Mg) in both thalli and chloroplasts. Indeed, cation transporters are known not to be completely selective under stressed conditions (Vert et al. 2002; Ducic et al. 2005; Lei et al. 2007; Millaleo et al. 2010; Barberon et al. 2011); well-documented examples of excess of Mn in the soil are known to perturb the absorption and translocation of other elements, including iron, magnesium, and phosphorus (Ducic et al. 2005; Lei et al. 2007; Millaleo et al. 2010), causing Fe deficiency in plants. However, *Marchantia* grown at $200\times$ does not show alterations in the Fe and Mg content inside the thalli (Figures 1B and 2A). Nevertheless, an alteration in the Mn/Fe ratio may induce Fe deficiency through competitive binding. Fe deficiency is known to affect primarily PSI that is rich in 4Fe4S clusters. As shown in Figure 4B, PSI content is lowered in comparison to PSII in $200\times$. A similar reduction of PSI upon exposure to Mn excess has been reported for *Arabidopsis* (Millaleo et al. 2013). Aside PSI, the water-

splitting activity of PSII seems also to be affected in the $200\times$ condition as seen by the appearance of the K-phase in fluorescence induction curves (Figure 4C) and the decrease in PSII activity (Table 2). A toxic effect of Mn excess on PSII activity is in accordance with data on angiosperms (Liang et al. 2019); $200\times$ Mn not only negatively affected the photosynthetic apparatus but also led to a reduction in chloroplast size and an alteration of the well-separated grana stack and stroma lamellae distribution (Figures 2 and 3).

Transfer of thalli from agar to starch plates allowed to establish Mn deficiency conditions. Growth in starch allowed lowering the Mn content drastically in the thalli to $21 \mu\text{g Mn g DW}^{-1}$. According to Mengel and Kirkby (1987), the minimum Mn content required for the growth of angiosperms is about 20 to 40 mg Mn kg DW^{-1} , and most angiosperms usually contain 30 to 500 mg Mn kg DW^{-1} . Manganese deficiency led to a decrease in F_v/F_m , a change in the ratio of the activity PSI/PSII (Table 3), and less PSII content relative to PSI according to 77 K fluorescence (Figure 4B). In angiosperms, Mn deficiency lowers PSII activity while PSI activity remains unaffected (Homann 1967; for review see Schmidt et al. 2016). Furthermore, the structural organization of the thylakoids was affected (Figure 3). It is known that Mn deficiency leads to disorganization of the thylakoid membrane in angiosperms (Mercer et al. 1962; Homann 1967). In *M. polymorpha*, the smaller compartmentation of the grana stacks could be partly responsible for the changes in electron transport. In addition to a change in the stoichiometry between active PSI and active PSII, a different distribution of photosynthetic complexes may favor cyclic electron flow around PSI by allowing the formation of super-complexes likely to be required for cyclic electron flow (Iwai et al. 2010). As shown in Figure 7, thalli grown on Starch – Mn show less limitation of electron donation to P700^+ than those of the Starch Control indicating a stimulation of cyclic electron flow under Mn deprivation. Cyclic electron flow is known to be induced under specific physiological conditions like anaerobiosis in *Chlamydomonas reinhardtii* (Joliot et al. 2022). Changes in the organization of PSI complexes were also observed under Mn limitation in cyanobacteria (Salomon and Keren 2011). Increased cyclic electron flow generates a higher proton gradient across the thylakoid membrane and thereby an increase in NPQ (Figure 5C). A higher NPQ protects PSII against photoinhibition as seen when thalli grown on Starch – Mn were exposed to high light in the presence of lincomycin (Figure 6), while they were more susceptible to photoinhibition in the absence of lincomycin (Figure 6) likely due to a slowdown of PSII repair. A slowdown of PSII repair under Mn deficiency has been observed previously in the Mn transporter mutant *nramp3nramp4* in *Arabidopsis* (Lanquar et al. 2010). The repair of PSII may be slowed down in the light because of the higher ROS levels in Starch – Mn (Table 2) that affects the synthesis of the D1 protein (Nishiyama et al. 2011).

In conclusion, we show here that unfavorable Mn concentrations during the growth of *Marchantia* affect not only the

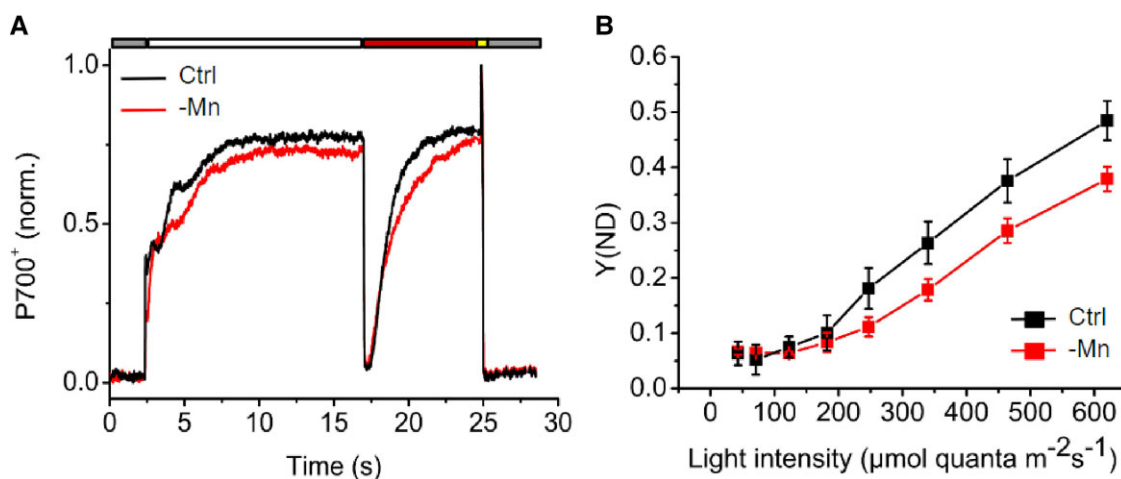


Figure 7. Activity of PSI in Mn deficiency. **A)** Normalized P700⁺ signal was obtained on thalli cultivated on Starch (+Mn, black, upper trace; -Mn, red, lower trace). The redox state of the PSI primary donor P700 was monitored through the changes in absorbance at 830 versus 875 nm. Leaves were kept in the dark for 5 min prior to the measurements. Thalli were exposed to actinic light for 15 s (white bar) and to far-red light until reaching a plateau (red bar). Then, a saturating flash was applied (yellow bar) and the decay was observed in the dark (gray bar). **B)** PSI donor-side limitation Y(ND) based on saturating pulse analyses. Following the initial determination of maximal oxidation of P700, actinic light of the indicated intensities was given for 180 s. Mean values and standard deviation are given (N = 6, 2 biological replicates).

photosynthetic apparatus but also the organization of the thylakoid membrane. Future work is needed to explore the link between changes in the organization and stacking of the thylakoid membrane and stimulation of cyclic electron flow under Mn deficiency.

Materials and methods

Plant growth conditions

Gemmae from *M. polymorpha*, Takaragaike (Tak-1) accession (male) were asexually cultured on ½ Gamborg's GB5 1% (w/v) Agar medium (Gamborg et al. 1968) for 2 weeks under a light-dark cycle of 16-h light, 22°C, 120 μmol quanta m⁻²s⁻¹, white fluorescent lamp/8 h dark, 20°C. For Mn excess condition, young thalli were transferred to ½ Gamborg's GB5 1% Agar medium containing 33 μM (control), 0.5 mM (15×), 1 mM (30×), 2 mM (60×), 5 mM (150×), or 6.5 mM (200×) MnCl₂ for 1 week before measurements. According to the metal quantification, the control medium contained 2.52 ± 0.27 μg Mn g⁻¹ fresh weight of the solid medium. For Mn deficiency, young thalli were transferred on ½ Gamborg's GB5 6% starch (w/v) medium with or without the addition of 33 μM MnCl₂ for 1 week before performing measurements. According to the metal quantification, the starch medium with MnCl₂ contained 2.03 ± 0.13 μg Mn g⁻¹, and the medium without the addition of MnCl₂ contained 0.26 ± 0.08 μg Mn g⁻¹ fresh weight of the solid medium.

Chloroplast and thylakoid isolation

About 10 g of thalli was collected, the media carefully mechanically removed, and grounded in 100 ml of GR buffer (50 mM Hepes-KOH pH 7.5, 0.33 M sorbitol, 1 mM MgCl₂,

2 mM EDTA, 5 mM Na-ascorbate) with a spatula of BSA. The slurry was filtered through 2 layers of Miracloth and centrifuged at 1,200 × g (4°C) for 7 min. Pellets were resuspended in 2 ml of GR buffer and then layered on the top of a Percoll gradient [15 ml of 30% Percoll/GR buffer (v/v) and 10 ml of 70% Percoll/GR buffer v/v], centrifuged at 7,000 × g (4°C) for 17 min (no brake). Intact chloroplasts were collected and washed in 25 ml of GR buffer; centrifugation 1,500 × g (4°C) for 5 min. The intactness was checked by light microscopy. For thylakoids, the same procedure was used without the percoll gradient.

Metal quantification

Thalli were collected and dried at 70°C for 2 days before being weighed. About 1 ml of nitric acid (65%) was added to 1 mg of plant material. For intact chloroplasts, the chlorophyll concentration was adjusted to 100 μg chl ml⁻¹ before the addition of 2.5 volume of nitric acid. After 10-fold dilution in trace-metal-free water, the metal content of the samples was determined by atomic emission spectroscopy using an MP AES 1200 spectrometer (Agilent, USA).

Super-resolution microscopy

For each sample, a small quantity of thallus was placed in a sandwich of 2 glass coverslips (22 mm diameter, Paul Marienfeld GmbH & Co. KG), sealed, and placed inside an in-house built sample holder. The sample holder was fixed to a nano-positioning system (P-733.2CD, P-725.4CD, E-725.3CD, Physikinstrumente) coupled to an inverted microscope (Ti-U, Nikon) equipped with a CFI Apochromat Lambda 100× oil immersion objective. Room-temperature fluorescence emission was recorded by an iXon ULTRA 897 camera in conventional mode, gain 3 (Andor Technology Ltd.,

Belfast), coupled to the microscope with a custom-made Optomask (Cairn Research Ltd, Faversham). The total chlorophyll fluorescence emission was isolated using a dichroic mirror/emission filter doublet (59022BS/ET655LP, Chroma Technology Corporation). Epifluorescence images were recorded using an excitation provided by a plasma light source (HPLS245 Thorlabs Inc.) and an excitation filter (MF469-35 Thorlabs Inc.). The excitation source for the laser-scanning measurements was a 445-nm emitting laser (OBIS LX, Coherent Inc.) at 100 nW intensity at the sample. Laser scanning and final image reconstruction [resolution (d) $d_{xy} = 126$ nm, $d_z = 320$ nm] were as previously described (Streckaite 2021) with a dwell time of 10 to 30 ms, 60-nm X/Y-scan steps, and 300-nm Z-scan steps.

Transmission electron microscopy

About 1-mm strips of thalli were cut under glutaraldehyde/paraformaldehyde fixative and impregnated by the 1% osmium (w/v) and 1.5% potassium hexacyanoferrate (w/v) en bloc staining protocol as described (Hawes et al. 1981; Juniper et al. 1982); 70-nm-thick sections were cut with an EM UC6 ultramicrotome (Leica Microsystems) and deposited on to copper grids. Ultrathin sections were stained with 2% uranyl acetate (w/v) (Merck) and Reynolds lead citrate according to standard procedures. Grids were examined under a JEOL 1400 TEM operating at 80 kV (JEOL, <http://www.jeol.com>). Images were acquired using a 9-megapixel high-speed camera (RIO9; Gatan, <http://www.gatan.com>) and processed using Digital Micrograph (Gatan).

Pigment analysis

Thalli were weighed and incubated in 100% acetone for 16 h in the dark. For complete pigment extraction, acetone incubation was repeated 3 times. The pigment extract was diluted to 80% acetone (v/v) before measurement. Chlorophyll *a* and chlorophyll *b* contents were calculated according to Porra and Scheer (2019).

77K Chlorophyll fluorescence measurements

Fluorescence spectra of intact chloroplasts diluted in GR buffer were measured with a Carry Eclipse fluorimeter (Agilent, USA); excitation wavelength: 430 nm. The spectra were normalized to the intensity of the PSI emission.

Chlorophyll fluorescence analysis at room temperature

Chlorophyll fluorescence analysis was performed on 5 min dark-adapted thalli using a Dual-PAM-100 fluorimeter (Walz, Effeltrich, Germany). F_m and F_m' were determined using saturating flashes (10,000 $\mu\text{mol quanta m}^{-2}\text{s}^{-1}$, duration 300 ms). F_o , minimum and F_m , maximum fluorescence in a dark-adapted sample; F_m' , maximum fluorescence and F' , fluorescence emission from a light-adapted sample. Induction and recovery curves were measured using actinic light of 50 $\mu\text{mol quanta m}^{-2}\text{s}^{-1}$: $F_v/F_m = (F_m - F_o)/F_m$,

$qN = (F_m - F_m')/(F_m - F_o')$, and $qP = (F_m' - F)/(F_m' - F_o')$. For induction curves (OJIP), one saturating flash was given.

Photoinhibition

Thalli were placed on wet filter paper and illuminated with white light (800 $\mu\text{mol quanta m}^{-2}\text{s}^{-1}$) LED panel SL3500 (Photon Systems Instrument, Drasov, Czech Republic). For recovery, samples were placed in low light (10 $\mu\text{mol quanta m}^{-2}\text{s}^{-1}$). When indicated, thalli were incubated in lincomycin (1 g L⁻¹) for 4 h prior to the photoinhibition treatment. F_v/F_m was measured using an Imaging-PAM (Walz, Effeltrich, Germany).

P700 measurements

P700 absorbance was measured using a Dual-PAM-100 fluorometer (Walz, Effeltrich, Germany). Near-infrared measuring lights (830 and 870 nm) were applied to measure the transmittance of oxidized P700. Prior to the measurements, the plants were kept in the light in the growth chamber so that the Calvin–Benson cycle enzymes were active. Five minutes dark-adapted thalli were exposed to actinic light followed by far-red light. Then, a saturating flash was given at the end of the far-red light period. To determine quantum yields of PSI donor, Y(ND), and acceptor side limitations, Y(NA), saturating pulse analysis was used (Klughammer and Schreiber 1994). Each actinic light intensity was applied for 180 s before determining Y(ND) and Y(NA).

Antioxidant enzymes activity

Thalli were harvested and ground in 50-mM HEPES buffer pH 6.5. The slurry was filtered through one layer of Miracloth, centrifuged for 5 min at 10,000 $\times g$ (4°C). Protein concentration in the crude extract was determined by amido black since the supernatant contained pigments (Schaffner and Weissmann 1973). About 10 $\mu\text{g ml}^{-1}$ protein was used for the enzymatic tests. Guaiacol peroxidase activity was determined spectrophotometrically by measuring the oxidation of guaiacol to tetraguaiacol at 470 nm (ϵ : 26.6 $\text{mM}^{-1}\text{cm}^{-1}$) (Chance and Maehly 1955). The reaction mixture contained 50 mM NaH₂PO₄/Na₂HPO₄ pH 7.5, 3 mM H₂O₂, and 0.01% (v/v) guaiacol. Catalase activity was measured polarographically at 20°C with a Clark-type electrode in 50 mM Tris buffer pH 8.5 and 1 mM H₂O₂ as substrate. SOD activity was measured using a solution of 500 μM Xanthine, 20 mM HEPES buffer pH 7, 0.2 U ml⁻¹ xanthine oxidase, and 100 μM XTT (Na₃3'-(1-(phenylaminocarbonyl)-3,4-tetrazolium)-bis-(4-methoxy-6-nitro) benzene sulfonic acid hydrate) as substrate. The kinetics of superoxide production were measured as increase in absorbance at 470 nm, and the SOD activity was determined by following the inhibition of the superoxide production after the addition of the crude extract (Molins et al. 2013). For $\cdot\text{OH}$ detection, 15 mg thalli were incubated for 1 h in 3 ml 10 mM phosphate buffer, pH 6.0, 50 mM *N*-tert-butyl- α -(4-pyridyl)nitron *N'*-oxide (4-POBN), and 4% ethanol (v/v) (Heyno et al. 2008).

Metabolite analysis

GC-MS profiling of metabolites was performed on thalli cultured on Agar Control, 30× and 200× conditions and thalli grown on Starch Control and Starch – Mn. Dried and grounded samples (5 mg of dry weight) were incubated in 1 ml of H₂O/ACN/isopropanol (2/3/3) with 4 mg l⁻¹ of ribitol for 10 min at 4°C with shaking at 250 g in an Eppendorf Thermomixer. Insoluble material was removed by centrifugation at 20,400 × g for 10 min; 700 µl of supernatant was recovered, and 70 µl of a mix of H₂O/MeOH/isopropanol (2/5/2) with 0.3 g l⁻¹ of myristic acid d27 was added as an internal standard for retention time locking. Aliquots of each extract (100 µl) extracts were dried for 4 h at 30°C in a Speed-Vac and stored at -80°C. After thawing, samples were dried again in a Speed-Vac for 1 h at 30°C before adding 10 µl of 20 mg ml⁻¹ methoxyamine in pyridine to the samples. The reaction was performed for 90 min at 30°C under continuous shaking in an Eppendorf thermomixer. A volume of 90 µl of *N*-methyl-*N*-trimethylsilyl-trifluoroacetamide was then added and the reaction continued for 30 min at 37°C. After cooling, 80 µl were transferred to an Agilent vial for injection. Four hours after derivatization, 1 µl sample was injected in splitless mode on an Agilent 7890B gas chromatograph coupled to an Agilent 5977A mass spectrometer (column: RESTEK RXI 5SIL MS 30MX0.25MMX0.25UM). An injection in split mode with a ratio of 1:30 was systematically performed for the quantification of saturated compounds. Raw Agilent data files were analyzed with AMDIS <https://chemdata.nist.gov/dokuwiki/doku.php?id=chemdata:amdis>. The Agilent Fiehn GC-MS Metabolomics RTL Library was employed for metabolite identifications. Peak areas were determined with the Masshunter Quantitative Analysis (Agilent) in splitless and split 30 modes. Peak areas were normalized to ribitol and dry weight. Metabolite contents are expressed in arbitrary units (semi-quantitative determination).

Acknowledgments

We thank Claire Boulogne (I2BC) for performing electron microscopy.

Author contributions

M.M. and A.K.-L. designed the project. M.M., U.H., T.H., F.G., B.G., A.G., S.T., and A.K.-L. performed the experiments and analyzed the data. M.M. and A.K.-L. wrote the initial version of the manuscript that was read and revised by all authors.

Supplemental data

The following materials are available in the online version of this article.

Supplemental Table S1. Chlorophyll and Mn content in thalli grown in Mn excess.

Supplemental Table S2. List of 96 metabolites identified by GC-MS in *M. polymorpha*.

Supplemental Table S3. Metabolites significantly decreased in starch condition compared with agar control in *M. polymorpha*.

Supplemental Figure S1. Metabolite analysis in *M. polymorpha* grown in Mn excess condition.

Supplemental Figure S2. Estimation of the chloroplast size under the different growth conditions.

Supplemental Figure S3. Chlorophyll fluorescence at room temperature in *M. polymorpha* grown in control and Mn excess conditions.

Supplemental Figure S4. Photoinhibition of photosystem II in *M. polymorpha* grown in control and Mn excess condition in the presence and absence of lincomycin.

Supplemental Figure S5. Chlorophyll fluorescence (F_v/F_m) in *M. polymorpha* grown on starch plates in low Mn concentrations.

Supplemental Figure S6. qN determination in the presence of lincomycin in *M. polymorpha* grown on starch in control and Mn-deficient conditions.

Funding

This work was supported by the Labex Saclay Plant Sciences-SPS (ANR-17-EUR-0007), the platform of Biophysics of the I2BC supported by the French Infrastructure for Integrated Structural Biology (FRISBI; grant number ANR-10-INBS-05), and IBI SA and France-BioImaging infrastructure supported by the Agence Nationale de la Recherche (ANR-10-INBS-04, call “investissements d’Avenir”). M.M. is supported by a CEA PhD fellowship.

Conflict of interest statement. None declared.

Data availability

Data will be made available on demand.

References

- Alam S, Akiha F, Kamei S, Huq SMI, Kawai S. Mechanism of potassium alleviation of manganese phytotoxicity in barley. *J Plant Nutr.* 2005;28(5):889–901. <https://doi.org/10.1081/PLN-20005572>
- Alejandro S, Höller S, Meier B, Peiter E. Manganese in plants: from acquisition to subcellular allocation. *Front Plant Sci.* 2020;11: article 300. <https://doi.org/10.3389/fpls.2020.00300>
- Amao Y, Ohashi A. Effect of Mn ion on the visible light induced water oxidation activity of photosynthetic organ grana from spinach. *Catal Commun.* 2008;10(2):217–220. <https://doi.org/10.1016/j.catcom.2008.08.022>
- Barberon M, Zelazny E, Robert S, Conéjéro G, Curie C, Friml J, Vert G. Monoubiquitin-dependent endocytosis of the iron-regulated transporter 1 (IRT1) transporter controls iron uptake in plants. *Proc Natl Acad Sci U S A.* 2011;108(32):E450–E458. <https://doi.org/10.1073/pnas.1100659108>
- Blamey FPC, Hernandez-Soriano M, Cheng M, Tang C, Paterson D, Lombi E, Hong Wang W, Scheckel KG, Kopittke PM. Synchrotron-based techniques shed light on mechanisms of plant sensitivity and tolerance to high manganese in the root environment. *Plant Physiol.* 2015;169(3): 2006–2020. <https://doi.org/10.1104/pp.15.00726>

- Bowler C, Van Camp W, Van Montagu M, Inzé D, Asada K.** Superoxide dismutase in plants. *CRC Crit Rev Plant Sci.* 1994;**13**(3): 199–218. <https://doi.org/10.1080/07352689409701914>
- Chance B, Maehly AC.** Assay of catalases and peroxidases. *Methods Enzymol.* 1955;**2**:764–775. [https://doi.org/10.1016/S0076-6879\(55\)02300-8](https://doi.org/10.1016/S0076-6879(55)02300-8)
- Clairmont KB, Hagar WG, Davis EA.** Manganese toxicity to chlorophyll synthesis in tobacco callus. *Plant Physiol.* 1986;**80**(1):291–293. <https://doi.org/10.1104/pp.80.1.291>
- Corpas FJ, Barroso JB, Palma JM, Rodriguez-Ruiz M.** Plant peroxisomes: a nitro-oxidative cocktail. *Redox Biol.* 2017;**11**:535–542. <https://doi.org/10.1016/j.redox.2016.12.033>
- Dekker JP, Boekema EJ.** Supramolecular organization of thylakoid membrane proteins in green plants. *Biochim Biophys Acta.* 2005;**1706**(1–2):12–39. <https://doi.org/10.1016/j.bbabi.2004.09.009>
- Delhaize E, Gruber BD, Pittman JK, White RG, Leung H, Miao Y, Jiang L, Ryan PR, Richardson AE.** A role for the AtMTP11 gene of *Arabidopsis* in manganese transport and tolerance. *Plant J.* 2007;**51**(2):198–210. <https://doi.org/10.1111/j.1365-313X.2007.03138.x>
- Ducic T, Polle A.** Manganese toxicity in two varieties of douglas fir (*Pseudotsuga menziesii* var. *viridis* and *glauca*) seedlings as affected by phosphorus supply. *Funct Plant Biol.* 2007;**34**(1):31–40. <https://doi.org/10.1071/FP06157>
- Eisenhut M, Hoecker N, Schmidt SB, Basgaran RM, Flachbart S, Jahns P, Eser T, Geimer S, Husted S, Weber APM, et al.** The plastid envelope CHLOROPLAST MANGANESE TRANSPORTER1 is essential for manganese homeostasis in *Arabidopsis*. *Mol Plant.* 2018;**11**(7): 955–969. <https://doi.org/10.1016/j.molp.2018.04.008>
- Eroglu S, Meier B, von Wiren N, Peiter E.** The vacuolar manganese transporter MTP8 determines tolerance to iron deficiency-induced chlorosis in *Arabidopsis*. *Plant Physiol.* 2016;**170**(2):1030–1045. <https://doi.org/10.1104/pp.15.01194>
- Führs H, Behrens C, Gallien S, Heintz D, Van Dorsseleer A, Braun HP, Horst WJ.** Physiological and proteomic characterization of manganese sensitivity and tolerance in rice (*Oryza sativa*) in comparison with barley (*Hordeum vulgare*). *Ann Bot.* 2010;**105**(7):1129–1140. <https://doi.org/10.1093/aob/mcq046>
- Gamborg OL, Miller RA, Ojima K.** Nutrient requirements of suspension cultures of soybean root cells. *Exp Cell Res.* 1968;**50**(1): 151–158. [https://doi.org/10.1016/0014-4827\(68\)90403-5](https://doi.org/10.1016/0014-4827(68)90403-5)
- Hasanuzzaman M, Alhathloul HA, Parvin K, Borhannuddin Bhuyan MHM, Tanveer M, Moshin SM, Nahar K, Soliman MH, Al Mahmud J, Fujita M.** Polyamine action under metal/metalloid stress: regulation of biosynthesis, metabolism, and molecular interactions. *Int J Mol Sci.* 2019;**20**(13):315. <https://doi.org/10.3390/ijms20133215>
- Hawes CR, Juniper BE, Horne JC.** Low and high-voltage electron microscopy of mitosis and cytokinesis in maize roots. *Planta.* 1981;**152**(5):397–407. <https://doi.org/10.1007/BF00385355>
- Heyno E, Klose C, Krieger-Liszskay A.** Origin of cadmium-induced reactive oxygen species production: mitochondrial electron transfer versus plasma membrane NADPH oxidase. *New Phytol.* 2008;**179**(3): 687–699. <https://doi.org/10.1111/j.1469-8137.2008.02512.x>
- Homann P.** Studies on the manganese of the chloroplast. *Plant Physiol.* 1967;**42**(7):997–1007. <https://doi.org/10.1104/pp.42.7.997>
- Iwai M, Roth MS, Niyogi KK.** Subdiffraction-resolution live-cell imaging for visualizing thylakoid membranes. *Plant J.* 2018;**96**(1): 233–243. <https://doi.org/10.1111/tpj.14021>
- Iwai M, Takizawa K, Tokutsu R, Okamoto A, Takahashi Y, Minagawa J.** Isolation of the elusive supercomplex that drives cyclic electron flow in photosynthesis. *Nature.* 2010;**464**(7292):1210–1213. <https://doi.org/10.1038/nature08885>
- Joliot P, Sellés J, Wollman FA, Verméglio A.** High efficient cyclic electron flow and functional supercomplexes in *Chlamydomonas* cells. *Biochim Biophys Acta Bioenerg.* 2022;**1863**(8):148909. <https://doi.org/10.1016/j.bbabi.2022.148909>
- Juniper BE, Hawes CR, Horne JC.** The relationships between the dictyosomes and the forms of endoplasmic-reticulum in plant-cells with different export programs. *Bot Gaz.* 1982;**143**(2):135–145. <https://doi.org/10.1086/337282>
- Kirchhoff H.** Chloroplast ultrastructure in plants. *New Phytol.* 2019;**223**(2):565–574. <https://doi.org/10.1111/nph.15730>
- Klughammer K, Schreiber U.** An improved method, using saturating light pulses for the determination of photosystem I quantum yield via P700⁺-absorbance changes at 830 nm. *Planta.* 1994;**192**(2): 261–268. <https://doi.org/10.1007/BF01089043>
- Lane BG.** Oxalate, germins, and higher-plant pathogens. *IUBMB Life.* 2002;**53**(2):67–75. <https://doi.org/10.1080/15216540211474>
- Lanquar V, Ramos MS, Lelièvre F, Barbier-Brygoo H, Krieger-Liszskay A, Krämer U, Thomine S.** Export of vacuolar manganese by AtNRAMP3 and AtNRAMP4 is required for optimal photosynthesis and growth under manganese deficiency. *Plant Physiol.* 2010;**152**(4): 1986–1999. <https://doi.org/10.1104/pp.109.150946>
- Lei Y, Korpelainen H, Li C.** Physiological and biochemical responses to high Mn concentrations in two contrasting *Populus cathayana* populations. *Chemosphere.* 2007;**68**(4):686–694. <https://doi.org/10.1016/j.chemosphere.2007.01.066>
- Lešková A, Giehl RFH, Hartmann A, Fargašová A, von Wiren N.** Heavy metals induce iron deficiency responses at different hierarchical and regulatory levels. *Plant Physiol.* 2017;**174**(3):1648–1668. <https://doi.org/10.1104/pp.16.01916>
- Liang HZ, Zhu F, Wang RJ, Huang XH, Chu JJ.** Photosystem II of *Ligustrum lucidum* in response to different levels of manganese exposure. *Sci Rep.* 2019;**9**(1):12568. <https://doi.org/10.1038/s41598-019-48735-8>
- Liu K, Yu F, Chen M, Zhou Z, Chen C, Li MS, Zhu J.** A newly found manganese hyperaccumulator – *Polygonum lapathifolium* Linn. *Int J Phytoremediation.* 2016;**18**(4):348–353. <https://doi.org/10.1080/15226514.2015.1109589>
- Liu T, Zhu L, Zhang Z, Huang H, Zhang Z, Jiang L.** Protective role of trehalose and heavy metal stress in *Aureobasidium subglaciale* F134. *Sci Rep.* 2017;**7**(1):1–9. <https://doi.org/10.1038/s41598-017-15489-0>
- Marschner H.** Mineral nutrition of higher plants. *Ann Bot.* 1995;**78**(4): 527–528. <https://doi.org/10.1006/anbo.1996.0155>
- Mengel K, Kirkby EA.** Principles of plant nutrition. *Ann Bot.* 1987;**93**(4): 479–480. <https://doi.org/10.1093/aob/mch063>
- Mercer FV, Nittim M, Possingham JV.** The effect of manganese deficiency on the structure of spinach chloroplasts. *J Cell Biol.* 1962;**15**(2):379–381. <https://doi.org/10.1083/jcb.15.2.379>
- Millaleo R, Reyes-Díaz M, Alberdi M, Ivanov AG, Krol M, Hüner NP.** Excess manganese differentially inhibits photosystem I versus II in *Arabidopsis thaliana*. *J Exp Bot.* 2013;**64**(1):343–354. <https://doi.org/10.1093/jxb/ers339>
- Millaleo R, Reyes-Díaz M, Ivanov AG, Mora ML, Alberdi M.** Manganese as essential and toxic element for plants: transport, accumulation and resistance mechanisms. *J Plant Nutr Soil Sci.* 2010;**10**(4):470–481. <https://doi.org/10.4067/S0718-95162010000200008>
- Molins H, Michelet L, Lanquar V, Agorio A, Giraudat J, Roach T, Krieger-Liszskay A, Thomine S.** Mutants impaired in vacuolar metal mobilization identify chloroplasts as a target for cadmium hypersensitivity in *Arabidopsis thaliana*. *Plant Cell Environ.* 2013;**36**(4): 804–817. <https://doi.org/10.1111/pce.12016>
- Nable RO, Houtz RL, Cheniae GM.** Early inhibition of photosynthesis during development of Mn toxicity in tobacco. *Plant Physiol.* 1988;**86**(4):1136–1142. <https://doi.org/10.1104/pp.86.4.1136>
- Nishiyama Y, Allakhverdiev SI, Murata N.** Protein synthesis is the primary target of reactive oxygen species in the photoinhibition of photosystem II. *Physiol Plant.* 2011;**142**(1):35–46. <https://doi.org/10.1111/j.1399-3054.2011.01457.x>
- Peiter E, Montanini B, Gobert A, Pedas P, Husted S, Maathuis FJ, Blaudez D, Chalot M, Sanders D.** A secretory pathway-localized cation diffusion facilitator confers plant manganese tolerance. *Proc Natl Acad Sci U S A.* 2007;**104**(20):8532–8537. <https://doi.org/10.1073/pnas.0609507104>

- Pittman JK.** Managing the manganese: molecular mechanisms of manganese transport and homeostasis. *New Phytol.* 2005;**167**(3): 733–742. <https://doi.org/10.1111/j.1469-8137.2005.01453.x>
- Porra RJ, Scheer H.** Towards a more accurate future for chlorophyll a and b determinations: the inaccuracies of Daniel Arnon's assay. *Photosynth Res.* 2019;**140**(2):215–219. <https://doi.org/10.1007/s11120-018-0579-8>
- Requena L, Bornemann S.** Barley (*Hordeum vulgare*) oxalate oxidase is a manganese-containing enzyme. *Biochem J.* 1999;**343**(1):185–190. <https://doi.org/10.1042/bj3430185>
- Salomon E, Keren N.** Manganese limitation induces changes in the activity and in the organization of photosynthetic complexes in the cyanobacterium *Synechocystis* sp. strain PCC 6803. *Plant Physiol.* 2011;**155**(1):571–579. <https://doi.org/10.1104/pp.110.164269>
- Samecka-Cymerman A, Marczonek A, Kempers AJ.** Bioindication of heavy metals in soil by liverworts. *Arch Environ Contam Toxicol.* 1997;**33**(2):162–171. <https://doi.org/10.1007/s002449900238>
- Satoh K, Butler WL.** Low temperature spectral properties of subchloroplast fractions purified from spinach. *Plant Physiol.* 1978;**61**(3): 373–379. <https://doi.org/10.1104/pp.61.3.373>
- Schaffner W, Weissmann C.** A rapid, sensitive, and specific method for the determination of protein in dilute solution. *Anal Biochem.* 1973;**56**(2):502–514. [https://doi.org/10.1016/0003-2697\(73\)90217-0](https://doi.org/10.1016/0003-2697(73)90217-0)
- Schmidt SB, Jensen PE, Husted S.** Manganese deficiency in plants: the impact on photosystem II. *Trends Plant Sci.* 2016;**21**(7):622–632. <https://doi.org/10.1016/j.tplants.2016.03.001>
- Sharma SS, Dietz K-J.** The significance of amino acids and amino acid-derived molecules in plant responses and adaptation to heavy metal stress. *J Exp Bot.* 2006;**57**(4):711–726. <https://doi.org/10.1093/jxb/erj073>
- Shimakawa G, Hanawa H, Wada S, Hanke GT, Matsuda Y, Miyake C.** Physiological roles of flavodiiron proteins and photorespiration in the liverwort *Marchantia polymorpha*. *Front Plant Sci.* 2021;**19**(12): 668805. <https://doi.org/10.3389/fpls.2021.668805>
- Singh S, Parihar P, Singh R, Singh VP, Prasad SM.** Heavy metal tolerance in plants: role of transcriptomics, proteomics, metabolomics, and ionomics. *Front Plant Sci.* 2016;**8**:1143. <https://doi.org/10.3389/fpls.2015.01143>
- St. Clair SB, Lynch JP.** Differences in the success of sugar maple and red maple seedlings on acid soils are influenced by nutrient dynamics and light environment. *Plant. Cell Environ.* 2005;**28**(7):874–885. <https://doi.org/10.1111/j.1365-3040.2005.01337.x>
- Strasser BJ.** Donor side capacity of photosystem II probed by chlorophyll a fluorescence transients. *Photosynth Res.* 1997;**52**(2): 147–155. <https://doi.org/10.1023/A:1005896029778>
- Strechaite S.** Thylakoids: from molecular to membrane organisation. A spectroscopic and nanoscopic study of the photosynthetic apparatus [PhD thesis]. [Amsterdam]: Vrije Universiteit Amsterdam; 2021.
- Subrahmanyam D, Rathore VS.** Influence of manganese toxicity on photosynthesis in ricebean (*Vigna umbellata*) seedlings. *Photosynthetica.* 2001;**38**(3):449–453. <https://doi.org/10.1023/A:1010998226323>
- Tanaka H, Sato M, Ogasawara Y, Hamashima N, Buchner O, Holzinger A, Toyooka K, Kodama Y.** Chloroplast aggregation during the cold-positioning response in the liverwort *Marchantia polymorpha*. *J Plant Res.* 2017;**130**(6):1061–1070. <https://doi.org/10.1007/s10265-017-0958-9>
- Van der Ent A, Baker AJM, Reeves RD, Pollard AJ, Schat H.** Hyperaccumulators of metal and metalloids: facts and fiction. *Plant Soil.* 2013;**362**(1–2):319–334. <https://doi.org/10.1007/s11104-012-1287-3>
- Vert G, Grotz N, Dédaldechamp F, Gaymard F, Guerinot ML, Briat JF, Curie C.** IRT1, an Arabidopsis transporter essential for iron uptake from the soil and for plant growth. *Plant Cell.* 2002;**14**(6):1223–1233. <https://doi.org/10.1105/tpc.001388>
- Zhang B, Zhang C, Liu C, Jing Y, Wang Y, Jin L, Yang L, Fu A, Shi J, Zhao F, et al.** Inner envelope CHLOROPLAST MANGANESE TRANSPORTER 1 supports manganese homeostasis and phototrophic growth in Arabidopsis. *Mol Plant.* 2018;**11**(7):943–954. <https://doi.org/10.1016/j.molp.2018.04.007>

Supplemental Material

Messant *et al.*

Manganese excess and deficiency affect chloroplast structure and the photosynthetic apparatus in *Marchantia polymorpha*

Table S1 Chlorophyll and Mn content in thalli grown in Mn excess

sample	mg Chl/g DW	mg Mn/g DW	$\mu\text{g Mn/mg Chl}$	$\mu\text{g Mn in Chloroplast/g DW}$
Crtl (agar)	$14,6 \pm 1,2$	0,231	2,1	$30,3 \pm 0,10$
30x	$10,6 \pm 1.7^*$	2,714	23,6	$250,8 \pm 0.09^{***}$
200x	$8,8 \pm 1.3^*$	23,116	178,7	$1566,2 \pm 0.06^{***}$

Chlorophyll content and dry weight was determined by three consecutive acetone extractions (N=6). Values of Mn content are the same as in Figs 1, 2 of the main manuscript. Stars indicate significant differences, compared to the control, based on a Mann and Whitney test (* $p < 0.05$, *** $p < 0.001$). Chlorophyll content was determined according to Porra and Scheer (2019).

Messant *et al.*

Manganese excess and deficiency affect chloroplast structure and the photosynthetic apparatus in *Marchantia polymorpha*

Table S2 List of 96 metabolites identified by GC-MS in *Marchantia polymorpha*

List of 96 metabolites identified and quantified in plants grown in Agar Control, 30X, 200X, Starch Control and Starch-Mn condition. N=4 biological replicates. P<0.05 for all values, according to two-way ANOVA test.

Metabolites	Control		30X		200X		Starch+Mn		Starch-Mn	
	Mean	SD	Mean	SD	Mean	SD	Mean	SD	Mean	SD
1,3-propanediol	0.011	0.000	0.012	0.000	0.011	0.000	0.011	0.001	0.011	0.001
1,6-anhydro-glucose	0.005	0.001	0.004	0.000	0.002	0.000	0.002	0.001	0.002	0.001
2,3-butanediol	0.005	0.001	0.005	0.000	0.004	0.000	0.005	0.000	0.004	0.000
2-hydroxypyridine	0.021	0.003	0.017	0.002	0.014	0.001	0.015	0.001	0.012	0.002
3,4-dihydroxymandelic acid	0.003	0.001	0.002	0.000	0.008	0.002	0.002	0.000	0.001	0.000
3-hydroxy-3-methylglutaric acid	0.005	0.000	0.004	0.000	0.003	0.000	0.003	0.001	0.002	0.001
4-hydroxypyridine	0.003	0.000	0.002	0.000	0.002	0.000	0.002	0.000	0.002	0.000
acetohydroxamic acid	0.030	0.004	0.028	0.003	0.034	0.006	0.030	0.005	0.034	0.006
allantoin	0.007	0.004	0.012	0.008	0.008	0.003	0.001	0.001	0.000	0.000
alpha ketoglutaric acid	0.029	0.004	0.006	0.006	0.000	0.000	0.011	0.010	0.010	0.009
arabinose	0.003	0.000	0.003	0.000	0.003	0.000	0.001	0.000	0.001	0.000
arbutin	0.002	0.000	0.002	0.000	0.002	0.000	0.001	0.000	0.000	0.000
aspartic acid	0.750	0.207	0.585	0.114	0.385	0.053	0.086	0.027	0.155	0.130
benzoic acid	0.003	0.000	0.003	0.000	0.003	0.000	0.003	0.000	0.003	0.000
Beta- alanine	0.004	0.001	0.003	0.001	0.004	0.001	0.001	0.000	0.001	0.001
beta-cyano-L-alanine	0.002	0.000	0.004	0.002	0.020	0.007	0.001	0.000	0.001	0.000
beta-sitosterol	0.004	0.001	0.004	0.001	0.004	0.001	0.002	0.001	0.002	0.001
citramalic acid	0.005	0.000	0.004	0.000	0.002	0.000	0.004	0.001	0.004	0.003
citric acid	0.285	0.010	0.295	0.017	0.037	0.005	0.289	0.063	0.247	0.091
citrulline	0.001	0.000	0.001	0.000	0.003	0.001	0.000	0.000	0.000	0.000
D-(+) trehalose	0.053	0.003	0.049	0.008	0.083	0.012	0.036	0.011	0.021	0.008
dehydroascorbic acid	0.007	0.001	0.004	0.000	0.005	0.001	0.001	0.000	0.001	0.000
D-glucose	0.239	0.035	0.252	0.068	0.218	0.058	0.411	0.233	0.234	0.081
D-glucose-6-phosphate	0.015	0.002	0.010	0.003	0.005	0.001	0.010	0.005	0.006	0.003
DL-isoleucine	0.060	0.015	0.061	0.010	0.046	0.014	0.028	0.006	0.023	0.009
D-malic acid	0.453	0.067	0.288	0.051	0.048	0.009	0.654	0.299	0.618	0.257
D-mannitol	0.013	0.010	0.009	0.007	0.009	0.006	0.023	0.022	0.024	0.019
D-mannose	0.005	0.000	0.004	0.000	0.004	0.000	0.045	0.042	0.002	0.000
dopamine (hydroxytyramine)	1.589	0.178	1.144	0.201	1.810	0.252	0.612	0.074	0.260	0.019
D-sorbitol	0.008	0.001	0.007	0.000	0.006	0.000	0.007	0.001	0.006	0.000

D-threitol	0.010	0.003	0.008	0.002	0.008	0.003	0.017	0.013	0.023	0.013
fructose	0.182	0.027	0.203	0.060	0.173	0.045	0.261	0.134	0.166	0.065
fructose 6-phosphate	0.008	0.001	0.006	0.001	0.003	0.001	0.005	0.002	0.003	0.001
fumaric acid	0.180	0.031	0.126	0.030	0.022	0.002	0.070	0.008	0.067	0.028
galactonic acid	0.001	0.000	0.001	0.000	0.000	0.000	0.092	0.088	0.009	0.005
galacturonic acid	0.004	0.000	0.004	0.001	0.008	0.001	0.013	0.008	0.005	0.003
gluconic acid	0.003	0.000	0.003	0.000	0.002	0.000	0.002	0.001	0.002	0.000
glyceric acid	0.016	0.001	0.014	0.001	0.006	0.001	0.016	0.005	0.013	0.006
glycerol	0.014	0.001	0.013	0.001	0.011	0.001	0.011	0.002	0.010	0.002
glycerol 1-phosphate	0.021	0.002	0.016	0.002	0.011	0.002	0.010	0.003	0.007	0.001
glycine	0.007	0.001	0.006	0.001	0.006	0.001	0.002	0.000	0.003	0.001
glycolic acid	0.013	0.001	0.015	0.001	0.014	0.001	0.009	0.000	0.009	0.002
L-(+) lactic acid	0.012	0.001	0.016	0.004	0.012	0.001	0.014	0.003	0.012	0.002
L-alanine	0.010	0.002	0.010	0.002	0.004	0.001	0.003	0.001	0.003	0.002
L-asparagine	0.372	0.021	0.461	0.074	0.478	0.085	0.059	0.036	0.108	0.095
leucrose	0.003	0.000	0.004	0.001	0.005	0.001	0.001	0.000	0.001	0.000
L-glutamic acid	2.642	0.178	2.568	0.065	2.024	0.148	1.143	0.298	1.078	0.449
L-glutamine	0.107	0.013	0.080	0.022	0.202	0.078	0.023	0.019	0.023	0.022
L-homoserine	0.002	0.000	0.002	0.000	0.002	0.000	0.001	0.000	0.000	0.000
L-leucine	0.004	0.001	0.007	0.001	0.007	0.001	0.007	0.002	0.006	0.001
L-lysine	0.003	0.001	0.002	0.001	0.004	0.002	0.001	0.000	0.000	0.000
L-methionine sulfoxide	0.001	0.000	0.001	0.000	0.001	0.000	0.000	0.000	0.000	0.000
L-norleucine	0.059	0.013	0.066	0.015	0.043	0.015	0.025	0.007	0.018	0.005
L-ornithine	0.003	0.001	0.003	0.000	0.007	0.001	0.001	0.000	0.001	0.001
L-proline	0.010	0.002	0.011	0.001	0.009	0.001	0.004	0.000	0.005	0.002
L-serine	0.625	0.028	0.617	0.037	0.616	0.113	0.157	0.040	0.138	0.069
L-threonine	0.080	0.008	0.070	0.010	0.042	0.006	0.028	0.007	0.024	0.010
L-threonine	0.025	0.005	0.036	0.018	0.070	0.019	0.005	0.001	0.004	0.000
L-tryptophan	0.043	0.019	0.036	0.017	0.134	0.035	0.005	0.002	0.003	0.002
L-valine	0.046	0.007	0.054	0.014	0.060	0.013	0.026	0.005	0.022	0.006
maltose	0.002	0.001	0.003	0.000	0.002	0.001	0.084	0.067	0.022	0.011
myo-inositol	0.042	0.003	0.041	0.001	0.031	0.003	0.022	0.005	0.018	0.004
myristic acid	0.005	0.000	0.004	0.001	0.004	0.000	0.005	0.001	0.004	0.000
N-ethylglycine	0.849	0.030	0.888	0.093	1.101	0.039	0.755	0.089	0.743	0.053
N-methylalanine	0.021	0.002	0.670	0.237	1.101	0.038	0.607	0.210	0.743	0.053
norepinephrine (noradrenalin)	0.008	0.002	0.006	0.002	0.020	0.003	0.007	0.003	0.003	0.001
norvaline	0.086	0.015	0.092	0.015	0.069	0.020	0.047	0.008	0.044	0.019
oleic acid	0.005	0.000	0.004	0.001	0.004	0.000	0.004	0.001	0.005	0.001
O-phosphocolamine	0.005	0.001	0.003	0.001	0.002	0.000	0.002	0.001	0.001	0.001
oxalic acid	0.024	0.004	0.023	0.002	0.018	0.003	0.013	0.002	0.013	0.005
palmitic acid	0.146	0.019	0.134	0.025	0.140	0.025	0.164	0.034	0.146	0.021
phenanthrene	0.007	0.001	0.006	0.001	0.007	0.001	0.006	0.000	0.007	0.001
Phenylalanine	0.018	0.002	0.019	0.002	0.009	0.002	0.006	0.003	0.005	0.001
phosphoric acid	0.615	0.138	0.318	0.124	0.093	0.019	0.589	0.176	0.510	0.280
phytol	0.050	0.002	0.046	0.006	0.089	0.024	0.016	0.007	0.011	0.005
porphine	0.032	0.003	0.030	0.002	0.039	0.002	0.029	0.001	0.024	0.001
putrescine	0.003	0.001	0.002	0.000	0.008	0.001	0.000	0.000	0.001	0.000

pyruvic acid	0.006	0.001	0.005	0.000	0.003	0.000	0.001	0.001	0.002	0.001
rhamnose	0.004	0.000	0.004	0.001	0.008	0.001	0.002	0.000	0.001	0.000
shikimic acid	0.209	0.043	0.168	0.031	0.068	0.010	0.265	0.106	0.127	0.074
stearic acid	0.076	0.017	0.073	0.021	0.087	0.019	0.098	0.022	0.098	0.023
stigmasterol	0.022	0.003	0.023	0.003	0.021	0.002	0.009	0.002	0.007	0.002
succinic acid	0.074	0.006	0.080	0.008	0.040	0.007	0.093	0.019	0.096	0.041
Sucrose	2.261	0.326	2.004	0.232	1.473	0.293	1.571	0.421	1.042	0.277
tagatose	0.005	0.000	0.004	0.000	0.074	0.071	0.079	0.046	0.085	0.084
talose	0.005	0.000	0.004	0.000	0.004	0.000	0.004	0.001	0.002	0.000
threonic acid	0.102	0.010	0.120	0.016	0.098	0.008	0.082	0.008	0.062	0.010
Threonic acid-1,4-lactone	0.007	0.001	0.008	0.001	0.016	0.003	0.004	0.000	0.003	0.001
trans-aconitic acid	0.475	0.054	0.362	0.049	0.031	0.006	0.407	0.151	0.324	0.151
tyramine	0.073	0.006	0.074	0.015	0.106	0.020	0.076	0.036	0.021	0.012
tyrosine	0.044	0.007	0.043	0.007	0.052	0.013	0.018	0.009	0.011	0.008
uracil	0.003	0.001	0.003	0.000	0.002	0.000	0.002	0.000	0.002	0.000
urea	0.011	0.002	0.010	0.002	0.003	0.001	0.005	0.002	0.002	0.001
xylitol	0.005	0.000	0.003	0.001	0.001	0.000	0.001	0.000	0.001	0.000
xylose	0.004	0.000	0.004	0.000	0.002	0.000	0.002	0.000	0.001	0.000
xylulose	0.007	0.000	0.005	0.000	0.003	0.000	0.004	0.001	0.003	0.001

Messant *et al.*

Manganese excess and deficiency affect chloroplast structure and the photosynthetic apparatus in *Marchantia polymorpha*

Table S3 Metabolites significantly decreased in Starch condition compared to Agar Control in *Marchantia polymorpha*

List of 41 metabolites significantly different between Agar Control and both Starch Control and Starch-Mn conditions combined. A statistical test ANOVA 2 was conducted. Absolute values represent the mean of 4 biological replicates for each condition. The column Starch (+/-) represents the mean between the 4 biological replicates of Starch Control and Starch-Mn conditions together.

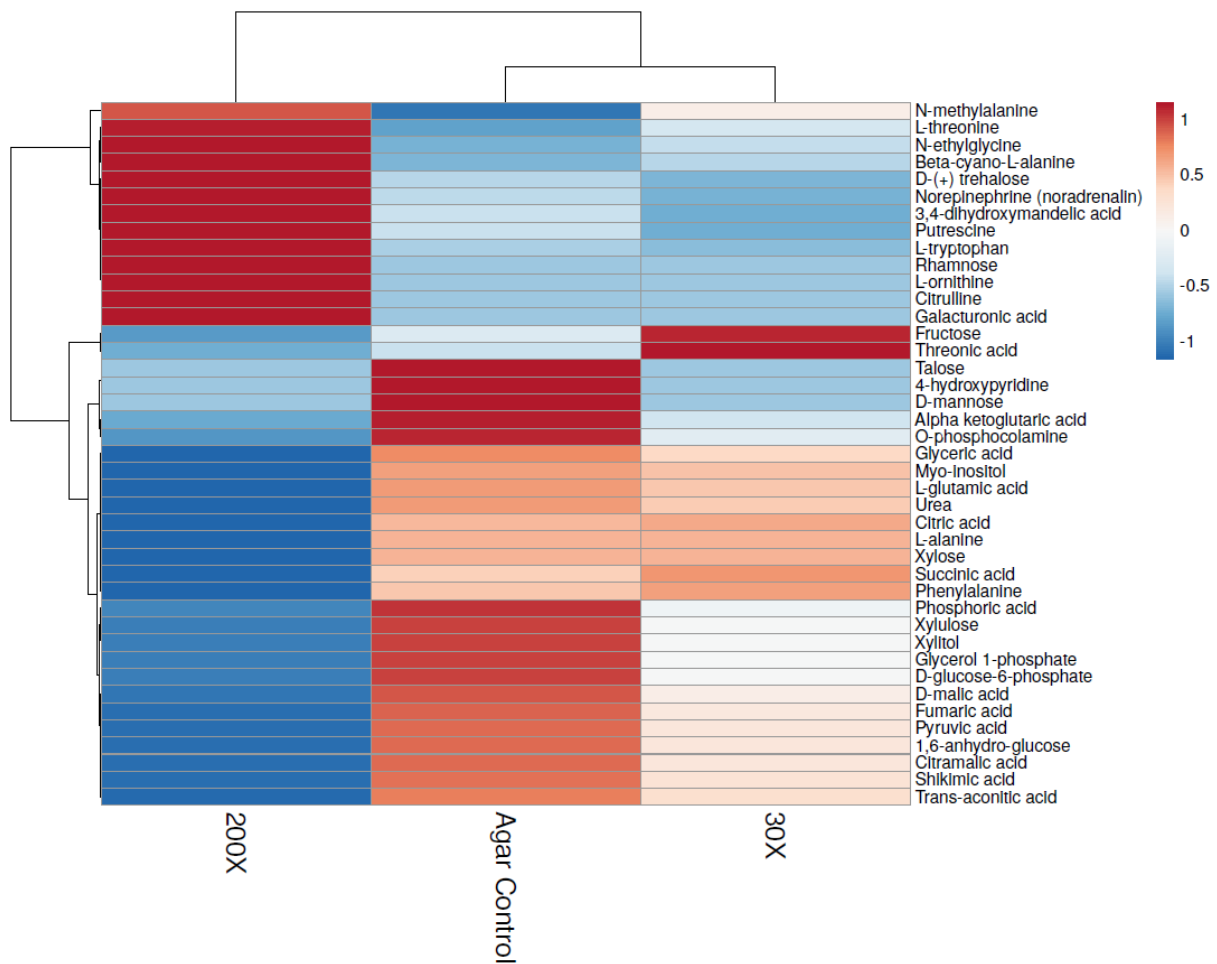
Metabolites	Agar Control		Starch (+/-)	
	Mean	SD	Mean	SD
1,6-anhydro-glucose	0.005	0.001	0.002	0.001
2-hydroxypyridine	0.021	0.003	0.013	0.003
3,4-dihydroxymandelic acid	0.003	0.001	0.001	0.001
arabinose	0.003	0.000	0.001	0.001
arbutin	0.002	0.000	0.001	0.000
aspartic acid 2	0.750	0.207	0.120	0.177
beta-cyano-L-alanine	0.002	0.000	0.001	0.000
citrulline 2	0.001	0.000	0.000	0.000
D-(+) trehalose	0.053	0.003	0.029	0.020
dopamine (hydroxytyramine)	1.589	0.178	0.436	0.213
fumaric acid	0.180	0.031	0.068	0.038
glycerol 1-phosphate	0.021	0.002	0.008	0.005
L-alanine 1	0.010	0.002	0.003	0.003
L-asparagine 2	0.372	0.021	0.083	0.136
leucrose	0.003	0.000	0.001	0.001
L-glutamic acid 3 (dehydrated)	2.642	0.178	1.110	0.707
L-glutamine 1	0.107	0.013	0.023	0.038
L-homoserine 2	0.002	0.000	0.000	0.000
L-lysine 2	0.003	0.001	0.000	0.001
L-methionine sulfoxide 3	0.001	0.000	0.000	0.000
L-norleucine 1	0.059	0.013	0.022	0.012
L-serine 1	0.625	0.028	0.148	0.105
L-threonine 1	0.080	0.008	0.026	0.016
L-valine 2	0.046	0.007	0.024	0.010
myo-inositol	0.042	0.003	0.020	0.009
N-methylalanine	0.021	0.002	0.675	0.293

O-phosphocolamine	0.005	0.001	0.002	0.001
Phenylalanine 1	0.018	0.002	0.005	0.004
phytol 1	0.050	0.002	0.013	0.012
putrescine	0.003	0.001	0.000	0.001
pyruvic acid	0.006	0.001	0.001	0.002
rhamnose 1	0.004	0.000	0.002	0.001
stigmasterol	0.022	0.003	0.008	0.005
talose 1	0.005	0.000	0.003	0.002
threonic acid	0.102	0.010	0.072	0.019
Threonic acid-1,4-lactone	0.007	0.001	0.003	0.002
tyrosine 2	0.044	0.007	0.015	0.016
urea	0.011	0.002	0.004	0.003
xylitol	0.005	0.000	0.001	0.001
xylose 2	0.004	0.000	0.002	0.001
xylulose	0.007	0.000	0.003	0.001

Messant *et al.*

Manganese excess and deficiency affect chloroplast structure and the photosynthetic apparatus in *Marchantia polymorpha*

Figure S1: Metabolite analysis in *M. polymorpha* grown in Mn excess condition.

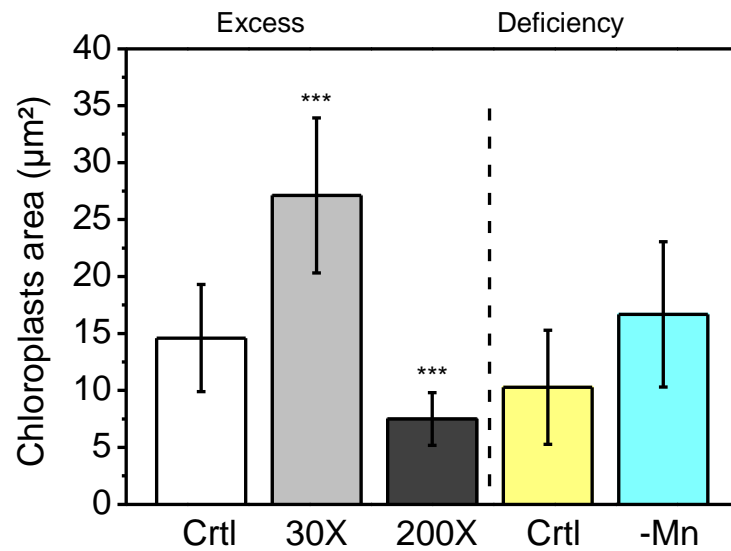


Heatmap showing significantly different metabolites in whole thalli grown under Control, 30X and 200X conditions. This figure is a result of an ANOVA 2 statistical test. The colour scale represents the changes between the three conditions taking into account the maximum and the minimum value for a given metabolite in each condition.

Messant *et al.*

Manganese excess and deficiency affect chloroplast structure and the photosynthetic apparatus in *Marchantia polymorpha*

Figure S2 Estimation of the chloroplast size under the different growth conditions

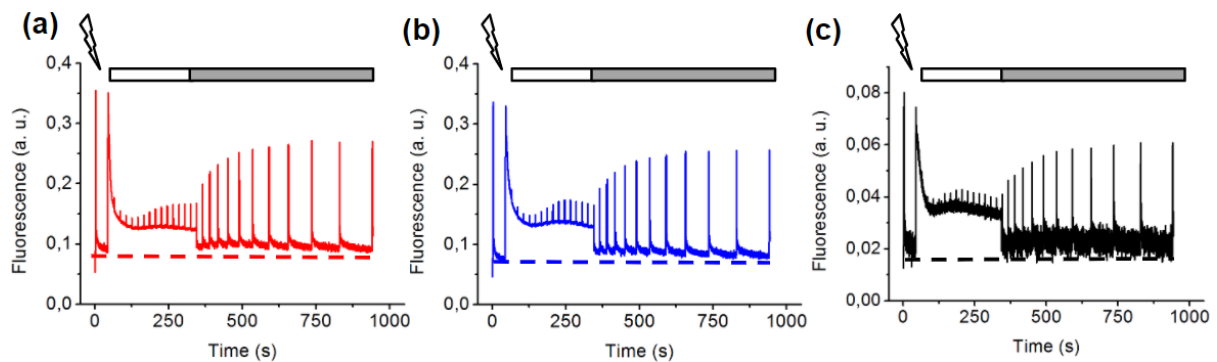


Area of the chloroplasts was determined from super-resolution fluorescence microscopy images using ImageJ. Number of images analysed: Ctrl agar: N=12, 30X: N=12; 200X: N=23; Ctrl starch: N=25, starch -Mn : N=7. Stars indicate significant differences, compared to the control, based on a Mann and Whitney test (*** p<0.001).

Messant *et al.*

Manganese excess and deficiency affect chloroplast structure and the photosynthetic apparatus in *Marchantia polymorpha*

Figure S3 Chlorophyll fluorescence at room temperature in *M. polymorpha* grown in control and Mn excess conditions

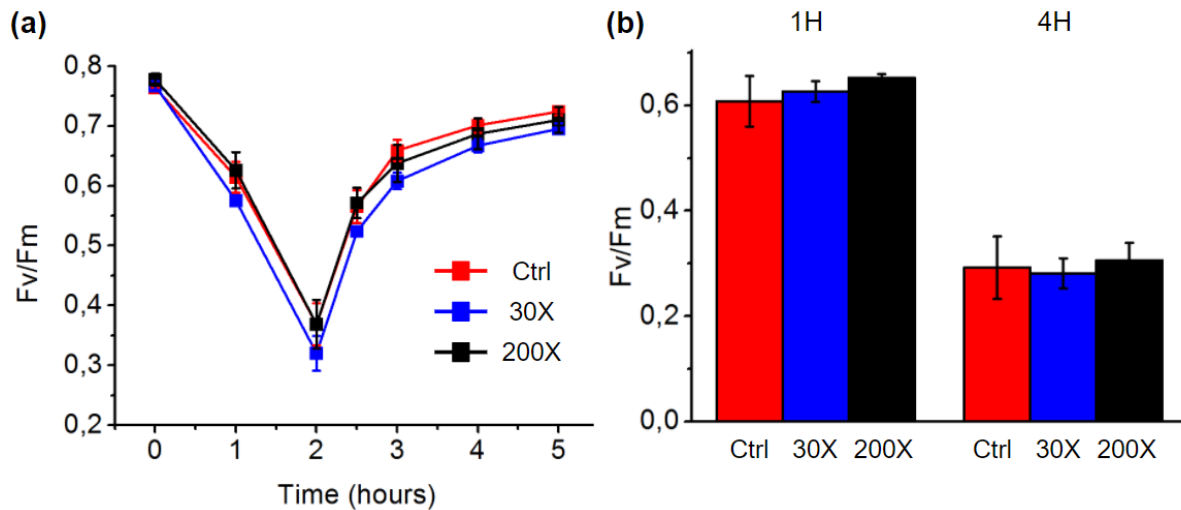


Induction and recovery of chlorophyll measured on thalli grown in Control (red), 30X (blue) and 200X (black) conditions. After 5 min dark adaptation, thalli were exposed to a measuring light to determine the minimum fluorescence level (dashed lines) and to a saturating flash to obtain the maximum fluorescence level. Actinic light ($50 \mu\text{mol photons m}^{-2} \text{s}^{-1}$) was applied for 5 min (white bar). Recovery in the dark was followed (grey bar). Representative curves are shown.

Messant *et al.*

Manganese excess and deficiency affect chloroplast structure and the photosynthetic apparatus in *Marchantia polymorpha*

Figure S4 Photoinhibition of photosystem II in *M. polymorpha* grown in control and Mn excess condition in the presence and absence of lincomycin

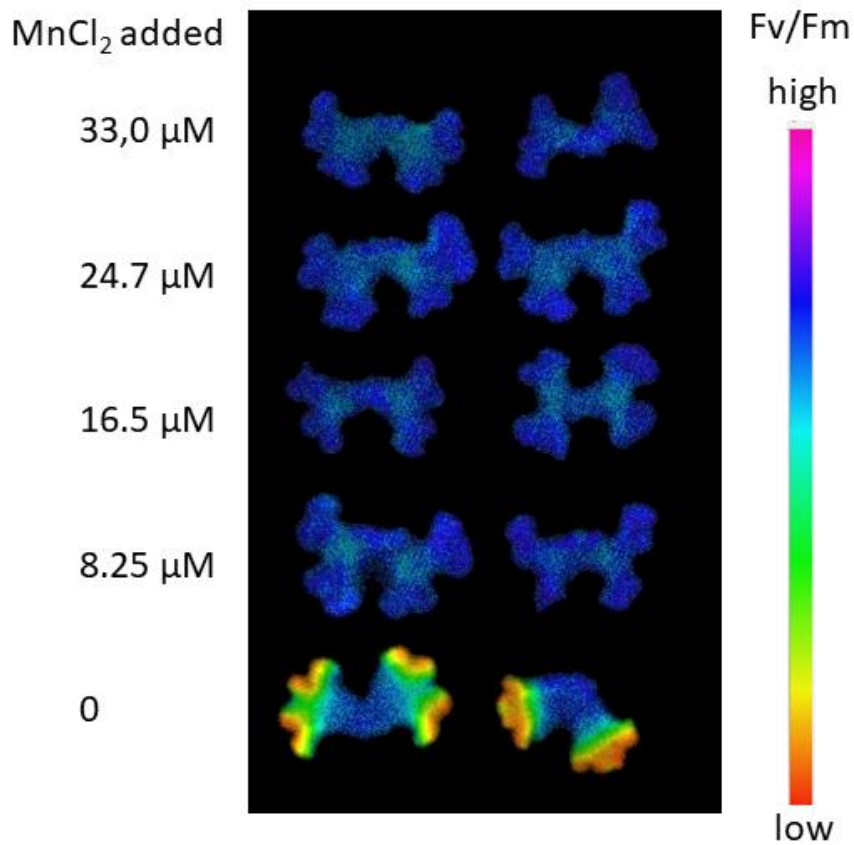


(a) Photoinhibition without lincomycin was measured in thalli cultivated in Control (red), 30X (blue) and 200X (black) conditions. F_v/F_m was followed on plants exposed to a strong light ($800 \mu\text{mol photons m}^{-2}\text{s}^{-1}$) for 3h and during the recovery at room light. (b) F_v/F_m was recorded during photoinhibition of thalli preincubated with lincomycin x (N=3, biological replicates).

Messant *et al.*

Manganese excess and deficiency affect chloroplast structure and the photosynthetic apparatus in *Marchantia polymorpha*

Figure S5 Chlorophyll fluorescence (Fv/Fm) in *M. polymorpha* grown on starch plates in low Mn concentrations

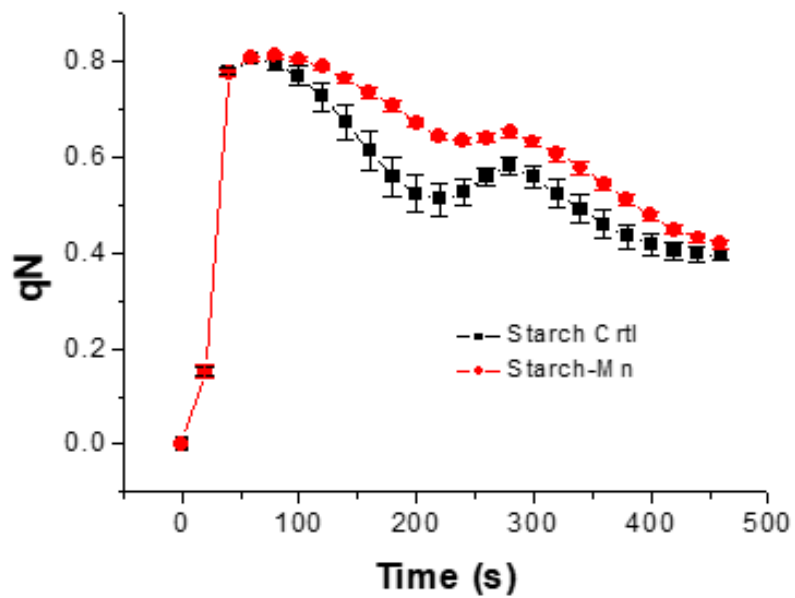


Thalli were grown for 2 weeks on standard medium before transferred for 1 week to starch media with the addition of the indicated Mn concentration. After 1 week growth on starch medium, thalli were dark-adapted for 5 min before Fv/Fm values were determined using an Imaging-PAM (Walz, Elleftrich, Germany).

Messant *et al.*

Manganese excess and deficiency affect chloroplast structure and the photosynthetic apparatus in *Marchantia polymorpha*

Figure S6 qN determination in the presence of lincomycin in *Marchantia polymorpha* grown on starch in control and Mn-deficient conditions



Thalli were incubated for 4 h in lincomycin solution (1 g L^{-1}) prior to the measurements. After 5 min dark adaptation, thalli were exposed to measuring light and to saturating flashes. Actinic light ($55\ \mu\text{mol quanta m}^{-2}\text{s}^{-1}$) was applied during 5 min. N=4.

Complementary experiments to precisely measure the parameters of the cyclic electron flow are currently in progress. In order to complete the culture conditions, measurements on *Arabidopsis thaliana* mutants affected in Mn homeostasis will also be studied. I have tried to obtain in *Marchantia polymorpha*, mutants of two Mn transporters inside the chloroplast. Indeed, CMT1 (Chloroplast Manganese Transporter 1) located on the inner membrane as well as PAM71 (Photosynthesis Affected Mutant 71) located to the thylakoid membrane have been shown in *Arabidopsis* to be responsible for Mn import (Schneider *et al.*, 2016; Eisenhut *et al.*, 2018). All our attempts to mutate these genes in *Marchantia* were unsuccessful, while other mutations could be successfully obtained in parallel. These observations suggest that simple mutations of CMT1 and PAM71 are lethal in *Marchantia polymorpha*.

II) Study of Photosystem II photoactivation

Photoactivation (Oliver *et al.*, 2021) is the light-dependent assembly of the manganese cluster at the PSII donor side. As mentioned in the general introduction, the manganese cluster is composed of four Mn, five oxygen and one calcium. Manganese ions are connected by oxo-bridges, thus forming the cubane-like structure of the cluster (see “Oxygen-Evolving Complex”, page 23). Photoactivation plays an essential role at PSII level because the latter only becomes functional in the presence of a correctly assembled Mn cluster. This mechanism takes place under two distinct conditions: activation of a newly synthesised PSII and during the D1 protein repair mechanism, where the cluster will be removed to allow degradation of the D1 protein by proteases, followed by the synthesis of a new D1 protein then re-assembly of PSII. The PSII distribution in thylakoid membranes depends on the presence of the Mn cluster (see “Chloroplast membrane dynamic”, page 37).

Photoactivation is a complex process whose different steps still need to be clarified since the intermediates are difficult to determine. It is generally accepted that the Mn ions are linked successively (Figure 22, **A**). The first Mn(II) is believed to bind to PSII in the dark. It is not currently known whether this binding occurs spontaneously or requires the presence of a protein. Then, the first light-dependent step allows the oxidation of Mn(II) to Mn(III). A dark rearrangement follows. It is supposed that it allows a change of conformation of the proteins present at the level of the PSII. This would have the consequence of favouring or allowing the attachment of the second Mn(II) and so on until a fully formed and functional cluster is obtained.

The main study method used, Electron Paramagnetic Resonance (EPR) spectroscopy, does not provide direct access to the reaction intermediates that lead to the oxidation of Mn(II) to Mn(III). On the other hand, the configuration of the residues that coordinate Mn(II) ions coming from the adjacent proteins (mainly D1, CP43) differs between the non-photoactivated PSII (apo-PSII) and the functional PSII (Figure 22, **B, C**). In apo-PSII the loops of D1 and CP43 are positioned differently. For example, D1-His337 is far away from the metal binding site in the apo-protein while it is one of the ligands of the final manganese cluster. It is difficult to predict what conformational changes can be generated by the different Mn intermediates complexes formed, especially since the mechanism requires alternatively light and dark steps. Furthermore, some have also mentioned that extrinsic proteins, especially PsbP which is able to bind Mn (Bondarava *et al.*, 2007), may play a role in the photoactivation mechanism.

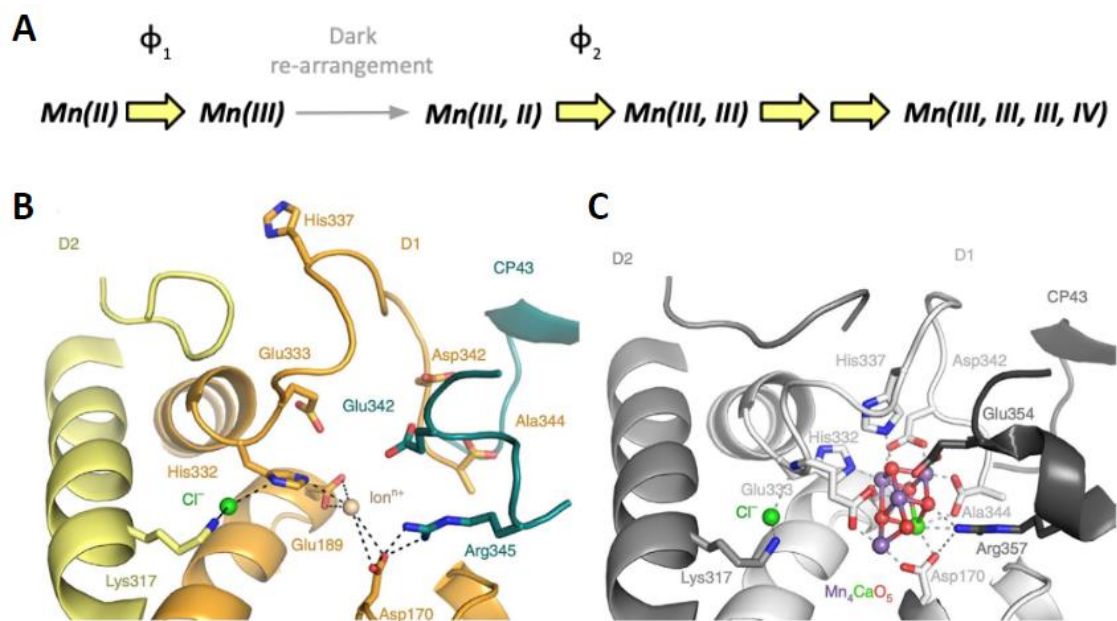


Figure 22: PSII donor side structures before and after photoactivation and general photoactivation steps
A. General scheme of photoactivation. The yellow arrows represent the light-dependent steps with ϕ_1 and ϕ_2 representing the first two photooxidation steps. The grey arrow represents the rearrangement step. **B.** The active site of the Mn_4CaO_5 cluster is resolved within our PSII-I structural model but is not yet oxygen evolving. **C.** Crystal structure of the oxygen evolving, mature PSII (PDB ID 3WU2, resolution 1.9 Å). *Images and legends from Zabret et al., 2021.*

It has been argued by Nixon *et al.*, 1992, that the initial step of photoactivation requires the presence of a HAS (High Affinity Site), the exact location of which remains to be confirmed, but the Asp170 residue of the D1 protein seems to be the most promising candidate. The mutation of D1-Asp170, which coordinates in the final cluster Mn_4 and Ca^{2+} , results in the greatest decrease in $Mn(II)$ binding affinity compared to other residues tested. Moreover, it has been shown that this $Mn(II)$ binding affinity does not depend on the Ca^{2+} . These observations suggest the presence of an intermediate oxo-bridge bond. This was demonstrated by Tyryshkin and coworkers (2006): in the dark, there is the formation of a precursor complex [$Mn^{2+} - OH^- - Ca^{2+}$] which, after light exposure, forms the first intermediate complex [$Mn^{3+} - O_2^- - Ca^{2+}$]. It is widely accepted that photoactivation involves unstable intermediates between the photooxidation steps and dark rearrangement, explaining its low quantum yield of around 1%.

The presence of calcium plays a major role in the cluster assembly. Avramov and coworkers (2020) recently demonstrated that it is important in all stages of photoactivation by stabilising certain intermediates. They also showed that a high concentration of Ca^{2+} decreases the speed of dark re-arrangement. Finally, it could also compete with the binding of the second Mn ion by taking its place at the dedicated site.

Completed by structures of isolated complexes at different photoactivation steps, a translocation mechanism of $Mn(II)$ and $Mn(III)$ has been proposed (Bao and Burnap, 2016; Zhang *et al.*, 2017). Overall, the latter suggests that each $Mn(II)$ is successively recruited at the HAS and translocated to the positions $Mn(1)$, then $Mn(2)$ and so on, when they are oxidised in $Mn(III)$.

In this part, I mainly used two different methods to study photoactivation *in vitro* and I used dark-grown *Marchantia polymorpha* to study it *in vivo*.

First, I used an oxygen electrode to study Mn catalase-like activity in solution by reproducing the experiments of Tikhonov and coworkers (2006). They demonstrated that Mn ions are able to spontaneously form complexes with bicarbonate in solution, also able to release oxygen, this is the catalase-like activity. From an evolutionary point of view, it has been hypothesised that the Mn catalase is at the origin of PSII Mn cluster development (McConnell *et al.*, 2012). Thus, Mn, Ca and HCO_3^- are able to react in solution to produce oxygen, independently of PSII photoactivation. The first experiments carried out in this part aimed to determine the precise parameters and conditions of the catalase-like activity of Mn in our experimental conditions. Then, PSII photoactivation conditions in solutions were determined (intensity/duration of illumination, solute concentration...).

The second technique used is the High Field Electron Paramagnetic Resonance (HF-EPR). This method generates a magnetic field to determine the electromagnetic radiation of electrons, i. e. their ability to absorb and then re-emit this energy. The so-called HF-EPR technique is the most advanced method in this field to date and has the main characteristic of being carried out at very low temperature and allowing a clearly defined signal to be obtained. This technique allows to determine the electromagnetic radiation of the electrons associated with Mn(II) whose signal is particularly clear at 5K and represented by 6 lines. In addition, the High Field EPR machine available at Saclay is able to carry out other derived experiments. **Sun Un** and I determined the ligands of the first Mn(II) bind to the PSII using ENDOR (Electron Nuclear Double Resonance) and ELDOR-detected NMR (Electron Double Resonance detected Nuclear Magnetic Resonance) methods which allow the determination of water molecules and identify the nuclei of other types of ligands respectively. Then, we used the Pulse Dipolar Spectroscopy (PDS) technique to calculate the distance between the Tyrosine D and the first Mn(II) to superimpose our findings to the apo-PSII structure. At last, we investigated the reversibility of photoactivation intermediates by increasing the Mn(II)/PSII ratio and follow the Mn(II) signal after photoactivation and then after 30 min dark adaptation.

Finally, I determined the culture conditions of *Marchantia polymorpha* in the dark in order to study photoactivation *in vivo*. I tested the use of two different techniques to help induce and monitor photoactivation, which are chlorophyll fluorescence measurement and SRM.

A) Measurement of Mn-catalase like activity and apo-PSII photoactivation *in vitro* using Oxygen Electrode

In solution, Mn itself is able to have a catalase-like activity using H₂O₂ as a substrate (Tikhonov et al., 2006). It has been hypothesized that it is the base for manganese cluster evolution. In these first short experiments, I determined if the Mn catalase-like activity occurs in our samples and experimental conditions to be able to interpret our further EPR data.

1) Material and methods

Measurement of catalase-like activity of Mn(II)-bicarbonate complexes

These experiments are based on the work by Tikhonov *et al.*, 2006 using an Oxygen electrode. For each measurement, the concentrations of the different stock solutions used are as follows : 100 mM H₂O₂, 10 mM MnCl₂, 1 M HCO₃⁻ et 10 mM CaCl₂. Each mixture was supplemented with Tris-HCl buffer with three different pH values : pH=6.5, pH=7.5 and pH=8.5.

2) Results

a) Characterization of oxygen evolution caused by Mn in solution: monitoring of Mn catalase-like activity

Different MnCl₂ concentrations were mixed with H₂O₂ (substrate) and Tris-HCl buffers at different pH values. The results in Table II show that there is no catalase-like activity of MnCl₂ alone when the pH is acidic. Thus, the condition of pH=6.5 will not be used further. A slight activity is observed for the pH=7.5 and pH=8.5 values. Thus, MnCl₂ alone exhibits derisory catalase-like activity under the conditions tested and does not depend on the concentration of Mn in the sample. For the rest of the experiments, only 10 μM MnCl₂ was used. Since the results obtained are similar to those already published, only a single replicate was measured to determine our conditions.

Table II: Characterization of manganese catalase-like activity depending on MnCl₂ concentration and pH

For each measurement, 10 mM H₂O₂ was added as a substrate.

	pH=6.5	pH=7.5	pH=8.5
MnCl ₂ concentrations	Oxygen Evolution (μmol O ₂ . mL ⁻¹ . h ⁻¹)		
10 μM	0	2.8	1.9
20 μM	0	2.8	1.9
50 μM	0	2.8	1.9
100 μM	0	2.8	11

I added to the previous experiment increasing concentration of bicarbonate to study its role on the activity of Mn in solution. The mixture of H₂O₂, HCO₃⁻ and MnCl₂ does induce oxygen production at pH=7.5 (catalase-like activity) and oxygen consumption at pH=8.5, as has already been shown (Tikhonov *et al.*, 2006). In addition, the increase in the bicarbonate concentration leads to an increase in the various activities observed.

Table III: Influence of bicarbonate concentration on Manganese catalase-like activity

For each measurement, 10 mM H₂O₂ was added as substrate and 10 μM MnCl₂ as a catalyst. Since the variations are the same as those published by Tikhonov *et al.*, 2006, only one replicate of each condition was conducted.

	pH=7.5	pH=8.5
HCO ₃ ⁻ concentrations	Oxygen Evolution (μmol O ₂ . mL ⁻¹ . h ⁻¹)	
15 μM	4.7	- 14.1
20 μM	9.4	- 14.1
25 μM	11.3	- 18.9

To conclude, the measurement of oxygen evolution allowing to highlight photoactivation is not likely to be compromised by the catalase-like activity of Mn by the use of a solution buffered at pH=6.5 (Table II). This pH value is also that of the lumen under conditions where the photosynthetic chain is active. On the other hand, bicarbonate has a positive effect on the catalase or superoxide dismutase activity of Mn in solution. One can therefore wonder to what extent the catalase activity of Mn resembles that of PSII cluster.

b) Apo-PSII photoactivation primary experiments

Then, I did the same experiments as before but with the aim to photoactivate isolated PSII depleted in the Mn cluster. Oxygen evolution was measured on intact PSII and inactive PSII after photoactivation in the presence of MnCl₂ and CaCl₂. Intact PSII activity was 175 μmol O₂. mg Chl⁻¹. h⁻¹ (+/- 19.01) whereas inactive PSII activity after photoactivation was only 35 μmol O₂. mg Chl⁻¹. h⁻¹ (+/- 2.80). It can be estimated that the fifth of the inactive PSII were photoactivated in these experimental conditions.

3) *Conclusions and perspectives*

The first control experiments determined that the catalase-like activity of Mn, if it does exist in plants, does not compete with the release of oxygen allowing the study of photoactivation at the pH value used in our following experiments (pH=6.5). On the other hand, these preliminary experiments show that the isolated PSII are active and that the hydroxylamine treatment to remove the Mn cluster still allows the PSII to be photoactivated. Nevertheless, the photoactivation conditions seem not to be optimal and could be improved. The resulting increase in photoactivation yield could allow us to test certain hypotheses such as: does the ligand of the non-heme iron, on the acceptor side, influence photoactivation ?

B) *In vitro* photoactivation of isolated PSII by High-Field EPR Spectroscopy

All the experiments done in this part were conducted in collaboration with **Sun Un** who is a specialist of the HF-EPR technique. As previously explained, it is assumed that the first Mn(II) binds to HAS to allow its conversion to Mn(III) by light. So far, all the accumulated evidence seems to point to the Asp170 of D1 protein, but it is still indirect. With the use of the ENDOR and ELDOR-detected NMR techniques, we were able to establish the number of water molecules as well as the nature of the other ligands bound to the first Mn(II). Then, we wondered to which structural elements these ligands can relate and for that we used a Pulse Dipolar Distance (PDS) measurement technique that measures the distance between unpaired electron spins. Finally, we aimed to do the same kind of experiment for the translocation of the other three Mn(II) atoms. So far we have succeeded in establishing a calibration curve allowing to highlight the binding of Mn(II) during the generation of the different photoactivation intermediates.

1) *Material and Methods*

PSII isolation

Spinach leaves were mixed in a solution of 0.4 M sorbitol, 10 mM NaCl, 5 mM MgCl₂, 20 mM HEPES, pH=7.5. The supernatant was filtered through 4 layers of cheesecloth and centrifuged at 8000 rpm, 4°C, 10 min. The pellet was resuspended using a brush with a 5 mM MgCl₂ solution and centrifuged at 7800 g, 4°C, 10 min. Chlorophyll concentration was measured in 80% acetone using Arnon's equation. A663 and A645 were determined by spectrophotometry. A volume of buffer 3 (15 mM NaCl, 5 mM MgCl₂, 25 mM MES, pH=6.5) was added to reach a concentration of 3 mg Chl.mL⁻¹. A third buffer 4 (buffer 3 with 100 mg.mL⁻¹ triton X-100, pH=6.5) is added to the volume previously obtained. It was covered with foil and incubated in the dark in ice water for 30 min under very gentle agitation. Then, centrifuged at 1100 g for 5 min at 4°C. The supernatant was kept and centrifuged at 35500 g for 20 min at 4°C. The pellet was resuspended in buffer 5 (0.3 M Sucrose, 10 mM NaCl, 25 mM MES, pH=6.5) and centrifuged at 40000 g for 20 min at 4°C. This centrifugation step was repeated until the supernatant was pale green and chlorophyll concentration was measured again. Isolated PSII were conserved at -80°C until their use.

Removal of the manganese cluster: hydroxylamine and EDTA treatment

PSII were suspended in a solution of 5 mM NH₂OH until a concentration of 0.5 mg chl. mL⁻¹ to remove the manganese cluster. The incubation was carried out in the dark for one hour and PSII were washed three times with buffer 5 and centrifugated 25 min, at 24100 g. The PSII were washed 3 times with buffer 5 containing 0.5 mM EDTA with successive centrifugation steps for 5 min, at 24100 g, 4°C in order to eliminate residual manganese atoms detached from PSII by NH₂OH treatment.

Photoactivation experiment and EPR High Field analysis

An aliquot of isolated PSII was thawed at room temperature and light for 5-10 min to allow irreversible oxidation of tyrosine D. Different concentrations of MnCl₂ solution are added when indicated. Less than 2 µL samples are loaded into an uncapped EPR tube. The tyrosine D signal control is measured at 55K. All experiments were carried out using a modified Bruker Elexsys II 680 EPR spectrometer equipped with an Oxford Instruments CF935 flow cryostat and 500 W Amplifier Research radio frequency amplifier.

EPR High Field spectra: First, the Mn(II) and tyrosine D signals are measured at 50K. Then, the sample warmed up to -20 °C and illuminated for 30 min with an LED optical fibre (Thorlabs) at 470 nm. A second measurement of the Mn(II) signal was done at 50K. In order to prove the reversibility of incomplete Mn cluster formation, the sample was warmed up to -20 °C and dark-adapted during 30 min. Preliminary experiments show that it works but it is difficult to determine how much light is really used.

So, to simplify the experimental procedure, samples were analysed as follows: they were illuminated for 5 min at room light and temperature to be photoactivated. Then, the first spectrum was measured at 50K. Finally, the sample was warmed up to -20 °C and dark-adapted during 30 min and another spectrum was measured at 50K.

ENDOR spectra: It has been previously shown that the number of water molecules ligated to a Mn(II) centre can be measured using ¹H ENDOR (see Bruch *et al.*, 2015; Un, 2013; Tabares and Un, 2013, for details). ¹H ENDOR spectra of the apo-PSII in the presence of 1 equivalent of Mn(II) was obtained. On average there were about 5±1 water ligands.

ELDOR-NMR: The identification of the other nuclei near to the PSII-bound Mn(II) was obtained from the ELDOR-NMR. The methodology is described in Bruch *et al.*, 2015 and Tabares and Un, 2013.

Pulse Dipolar Spectroscopy: The 94 GHz pulsed dipolar time traces were obtained using the 5-pulse RIDME technique (Milikisyants *et al.*, 2009) at 50 K. The magnetic-field position at which the measurements were made corresponded to the maximum of the Tyrosine-D spectrum. The data analysis was carried out using locally written python/Fortran-90 programs that implemented the method of Ibáñez and Jeschke (Fábregas Ibáñez and Jeschke, 2020).

2) Results

To be able to compare our samples with each other, an intensity standard signal had to be chosen and tested. In our experiments, tyrosine D was the obvious candidate. Indeed, the Tyrosine D signal is easy to obtain. The sample just needs to be illuminated for a few minutes at room temperature to generate the tyrosine D radical. As each reaction centre constrains a single Tyrosine D, it allows a precise quantification between samples. Finally, it is easily detectable and once it is present, it does not vary according to the light-dark cycles used in our experimental procedure. First, the sample was illuminated at room temperature to get the tyrosine D radical. Then, it was frozen at 50K to measure the Tyrosine D signal (Figure 23, black). The sample was warmed up at -20°C for a dark adaptation of 30 min and frozen again to measure the spectrum at 50K (red). In this case, the tyrosine D signal is not changing but 5 lines are visible in red, under the basal black line. They are corresponding to the typical Mn(II) signal, consisting in 6 lines, whose the third lines is mingled to the big tyrosine D signal. To make it more visible, the light-dark curve was calculated and multiplied by 8 (green). The Mn(II) signal is not visible after the light period because it is oxidised to Mn(III) and the latest is not visible in these conditions. As a conclusion, the tyrosine D signal is an excellent intensity standard for our experiments.

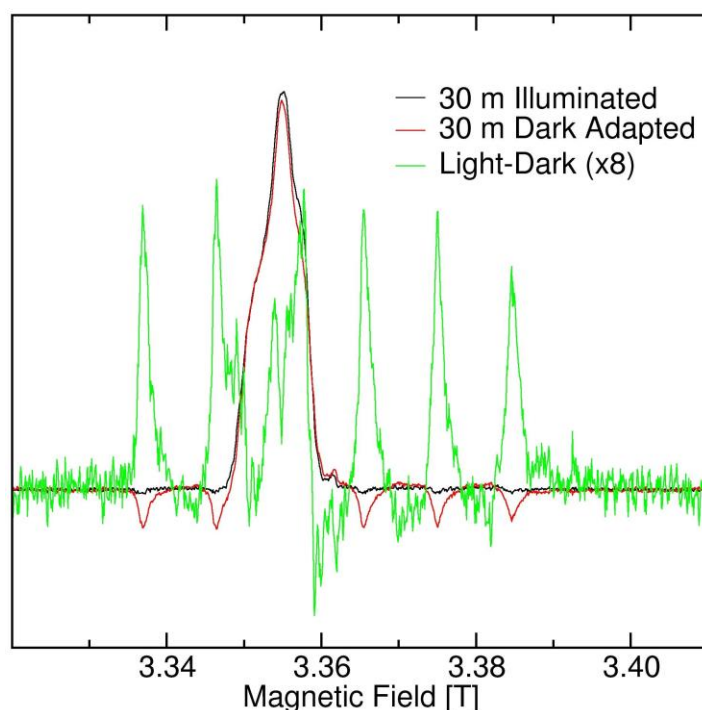


Figure 23: Tyrosine D signal, an essential element for apoPSII/Mn(II) quantification

The sample containing MnCl_2 was illuminated at room temperature to get the tyrosine D radical. It was frozen at 50K to take the “30 min illuminated” spectrum (black). It was warmed up at -20°C for dark adaptation during 30 min and frozen again at 50K to take the “30 min dark adapted” spectrum (red). In the light, Mn(II) is oxidised in Mn(III) so, no signal is visible. But, in the dark the Mn(III) is reduced to Mn(II) and this corresponds to the difference between the light and the dark spectra (green). This signal was magnified 8 times to be easily visible. EPR spectrum at 94 GHz.

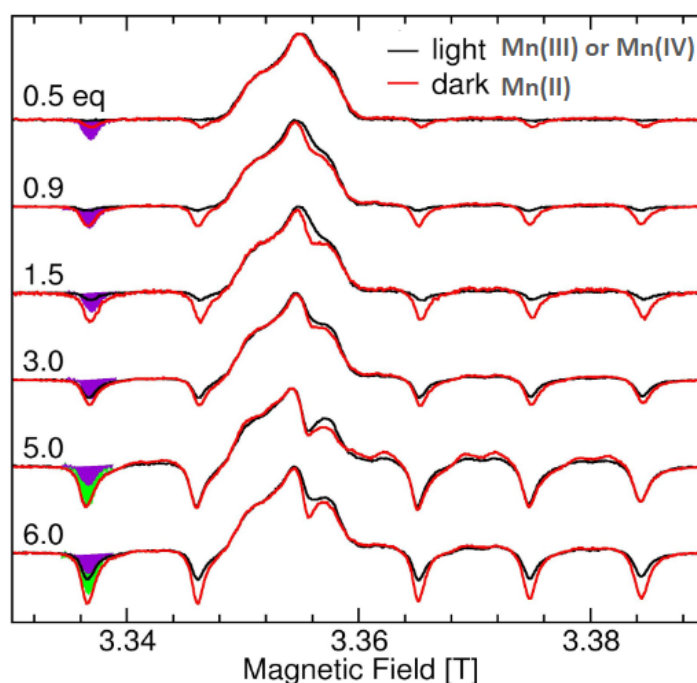


Figure 24: Evolution of Mn(II) signal at different Mn(II) concentrations during photoactivation

Samples containing different Mn(II)/PSII ratios were illuminated at room temperature and the EPR signals were measured at 50K (black). Then, samples were warmed at -20°C and dark-adapted for 30 min before the EPR signals were measured again at 50K (red). The 6 lines representative of the Mn(II) signal are present, the third is erased by the presence of the tyrosine D signal. The area in purple represents almost 1 eq and the green area 2 eq.

We were interested in the different intermediates of photoactivation. As a preliminary experiment we determined a calibration curve with different Mn(II) to PSII ratios (Figure 24). To do so, samples containing different Mn(II)/PSII equivalences were illuminated at room temperature. The light oxidation of Mn(II) to Mn(III) leads to the disappearance of the Mn(II) signal. The Mn(III) EPR signal is not visible in our experimental conditions. Then, the “light” spectra were measured at 50K (black). Samples were warmed up at -20°C and dark adapted for 30 min. Mn(III) is reduced in Mn(II), EPR signals are supposed to come back. The “dark” spectra were measured at 50K (red). The difference between light (disappearance of Mn(II) signal, converted in Mn(III)) and dark curves (Mn(III) reduction, Mn(II) signal come back) allows to determine the reversibility of the different intermediates during cluster assembly.

The first two samples have a Mn(II) content subequivalent to that of the PSII. Under these conditions (0.5 and 0.9 eq), an almost complete absence of Mn(II) signal in the light is observed. This indicates that all of the Mn(II) has been oxidised. The small residual ($\sim 10\%$) presence of Mn(II) can be explained by the presence of damaged reaction centres which cannot be photoactivated or the existence of a secondary site that does not carry photo-oxidation. After dark adaptation, we observed that Mn(II) oxidation is completely reversible since all the signals have recovered. The same behaviour is observed for the 1.5 eq.

For the 3 eq, there are 2 Mn(II) oxidised by PSII after light exposure which is not changing after 30 min of dark adaptation. It can be concluded that the intermediate composed of 2 Mn(II) oxidised is stable. It is interesting to note the parallel with native non-heme Mn catalase. The oxidation step of this intermediate can be Mn(III),Mn(III) or Mn(III),Mn(IV). It has been shown that Mn catalase enzymes are preferentially in Mn(III),Mn(III) oxidation state (Fronko *et al.*, 1988; Khagulov *et al.*, 1990; Waldo *et al.*, 1991).

For the 5 eq, there are about 3 Mn(II) oxidised by PSII after illumination and dark adaptation does not change this ratio. Finally, for the 6 eq, there are 5 Mn(II) oxidised per PSII whereas in the dark, this ratio changes to around 4 Mn(II) per PSII. It can be concluded that 4 equivalences are not sufficient to generate a complete cluster but that at least 6 are needed.

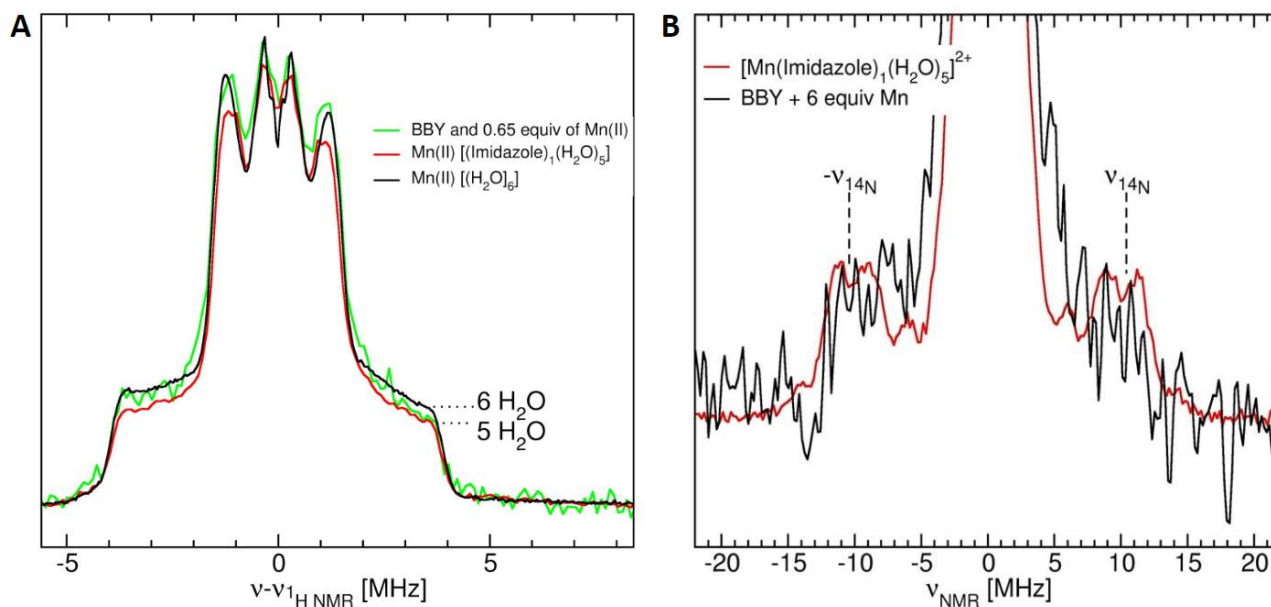


Figure 25: Determination of Mn(II) ligands

A. Spectra measured by the ENDOR and ELDOR-detected NMR techniques to allow the detection of ligands bound to Mn(II) (green). The black curve represents the standard spectrum of Mn(II) in water solution. The red curve represents the standard spectrum of Mn(II) bound to a nitrogen atom. **B.** Determination of the number of imidazole present around the first Mn(II) in the dark. On one side is the calibration curve taken from Un, 2013 (red) and on the other side the analysed sample containing 6 eq. The same thing was observed for 0.5 eq but the signal was less clear.

To go further, we focused on the attachment to the first Mn(II) to the PSII before the photoactivation. We addressed the question: what are the ligands of the first Mn(II) in the dark? To answer it, we used ENDOR and ELDOR-detected NMR techniques. The ENDOR and ELDOR-detected NMR techniques allow to determine the ligands close to the first Mn(II) bound to PSII (Figure 25). Finally, to be sure to observe only the ligands of the first Mn(II) we remain under conditions of subequivalence in Mn(II) with respect to PSII.

The ENDOR experiment (Figure 25, **A**) showed that the shoulders of the 0.65 eq (green) is between the signal of free Mn(II) in solution with 6 water and those of Mn(II) linked to an imidazole with 5 water molecules (red). It can be concluded that, on average, some Mn(II) in the dark are free or linked with one other ligand.

The ELDOR-NMR was used to identify the ligand (Figure 25, **B**). It is known that Mn(II) preferentially binds one or two nitrogen atoms with a carboxylic acid. We determined that the signal measured corresponds to one nitrogen atom according to the calibration curve of Mn(II) binding to imidazole, previously established by Un, 2013.

It is known that Mn(II) is preferentially bound to a nitrogen and a carboxylic acid. In living systems, Mn is often bound to a nitrogen coming from a histidine which is consistent with apo-PSII structure (Zabret

et al., 2019). Nevertheless, although carboxylic acids cannot be detected by this technique, none of our results suggest the presence of another ligand which should be, according to Nixon *et al.*, 1992 who assumed that the first Mn(II) binds to D1-Aps170 (the supposed HAS).

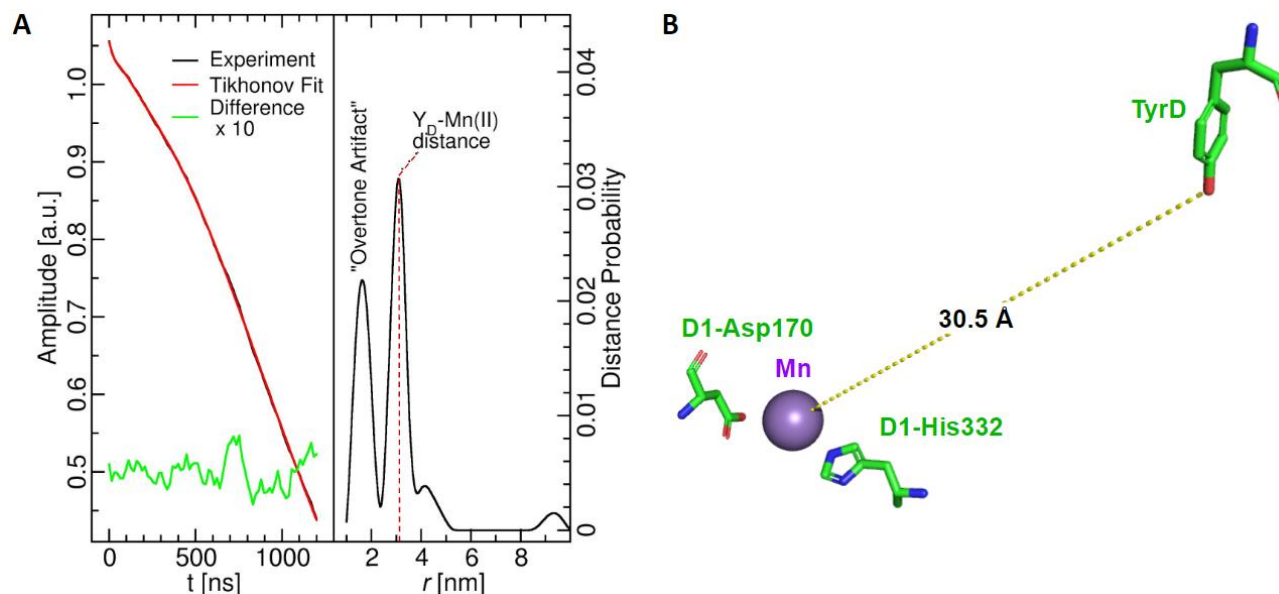


Figure 26: Distance determination between the tyrosine D radical and the first Mn(II) bound to PSII before photoactivation

A. (left) Spectrum corresponding to the experimental determination of the distance between the tyrosine D and the first Mn(II) (black) is compared to the fit obtained by the maths calculation model of the distance (red). Finally, the error/difference between the two was magnified 10 times (green). (right) Results of the mathematical calculation of the distance (previous red curve) which determines that the most probable distance corresponding to the measured spectrum (previous black curve) is 32Å (or 3.2 nm). **B.** This figure is from the cryo-EM structure of the apo-protein (Zabret *et al.*, 2021) which shows a metal ion. In the paper, authors were not able to distinguish between Ca^{2+} or Mn^{2+} . D1-Asp170, D1-His332 and Tyrosine-D (D2-Y160) were represented according to their correct localisation and distance. The distance from the structure was determined to be 30.5Å compared to 32Å (or 3.2 nm) in PDS measurement, in **A**.

The apo-PSII structure (Figure 22, **B**) shows the presence of two histidines near an ion: D1-His332 and D1-His337. To determine precisely which of them is related to the first Mn(II), the Pulse Dipolar spectroscopy (PDS) technique has been used to measure the distance between the Tyrosine D and the first Mn(II) (Figure 26, **A**). The principle of this technique is to take the measurement of the distance and then apply a maths program which estimates the most probable distance which fits to the experimental data. The distance is about 32Å (or 3.2 nm).

Compared to the structure of Zabret *et al.*, 2021 (Figure 26, **B**), we can conclude that the first Mn(II) is bound to the D1-His332 residue before the first photoactivation step. These results also provide proof that the ion present in the structure is indeed a Mn(II) (and not a calcium, as they can't distinguished). Then, it would be interesting to try to carry out the same kind of experiment with the different equivalences used before in order to detail the stages of photoactivation.

C) Photoactivation studied in dark-grown *Marchantia polymorpha* in vivo

Photoactivation plays a central role in PSII function and in the establishment of photosynthetic electron transport. It has been shown previously that photoactivation mechanisms are easier to be characterised *in vitro*. But, *in vitro* experiments erase the physiological involvements of the photoactivation at photosynthetic chain, thylakoid and even chloroplast scales. Thus, a perfect model to study photoactivation *in vivo* could be an organism able to produce complete PSII in the dark, ready to be photoactivated. This is the case of *Marchantia polymorpha*. In this part, I will describe how I cultured *Marchantia* in the dark in order to track photoactivation *in vivo* using chlorophyll fluorescence measurements and SRM method. The results obtained by the SRM method were carried out in collaboration with **Andrew Gall** who is a specialist in this technique.

1) *Material and Methods*

Culture conditions

Marchantia polymorpha gemmae from the Tarakagaike (Tak)-1 male accession were grown on ½ Gamborg's B5 agar medium containing 1% sucrose supplemented with 50 $\mu\text{g}\cdot\text{mL}^{-1}$ Spectinomycin to avoid bacteria contaminations. The gemmae were exposed for 3 days to light (16 h light, 22°C, 120 $\mu\text{mol photons}\cdot\text{m}^{-2}\cdot\text{s}^{-1}$, white fluorescent lamp/8 h dark, 20°C) in order to allow the transition between the photosynthesis and the use of sucrose as a carbon source. Then, the plates were immersed in the dark under the same culture conditions previously detailed, for a week before being analysed.

Fluorescence measurement

Fluorescence induction curves were measured on plants grown in the dark using one or more saturated light flashes of 300 ms duration with a Dual-PAM-100 fluorimeter (Walz, Effeltrich, Germany). To check the effect of the flashes, an induction curve is measured after exposing the thalli for 5 minutes under actinic light (100 $\mu\text{mol photons}\cdot\text{m}^{-2}\cdot\text{s}^{-1}$).

Super-resolution microscopy

Images were obtained from thalli cultured in the dark of 1 week. For each sample, a small quantity of thallus cultured was placed in a sandwich of two glass coverslips (22 mm diameter, Paul Marienfeld GmbH & Co. KG), sealed and placed inside an in-house built sample holder under green light. The sample holder was fixed to a nano-positioning system (P-733.2CD, P-725.4CD, E-725.3CD, Physikinstrumente) coupled to an inverted microscope (Ti-U, Nikon) equipped with a CFI Apochromat Lambda 100x oil immersion objective. Room-temperature fluorescence emission was recorded by an iXon ULTRA 897 camera (Andor Technology Ltd., Belfast) coupled to the microscope with a custom-Optomask (Cairn research Ltd, Faversham). An epi-fluorescence image was taken before photoactivation. Total chlorophyll fluorescence emission was isolated using a dichroic mirror/emission filter doublet (59022BS/ET655LP, Chroma Technology Corporation).

Epifluorescence images were recorded using an excitation provided by a plasma light source (HPLS245 Thorlabs Inc.) and an excitation filter (MF469-35 Thorlabs Inc.). The excitation source for the laser-scanning measurements was a 445 nm emitting laser (OBIS LX, Coherent Inc.). Laser-scanning and final image reconstruction (resolution (d) $d_{xy} = 126$ nm, $d_z = 320$ nm) was as previously described (Strečkaite, 2021); a ca. $3 \mu\text{m}^2$ of the thylakoid membrane was repeatably scanned with a dwell time of 30 ms at 60 nm (X/Y) intervals, giving a final frame rate of 80s.

2) Results

a) Dark-grown *Marchantia*

Marchantia gemmae were not able to survive when put directly in the dark. An acclimatation of 3 days in the sucrose medium under light is needed to allow them to survive. On the other hand, gemmae stay little after 1 week in the dark. They showed reduced growth. Finally, the limiting point of the culture was the large number of contaminations. It is certainly possible to improve the culture conditions to allow the thalli to develop more significantly and thus carry out experiments requiring more material.

b) Chlorophyll fluorescence measurement: photoactivation impact on PSII reaction centre

It has been shown that the measurement of the PSII chlorophyll fluorescence induction curves (OJIP, Stirbet and Govindjee, 2011; Stirbet *et al.*, 2014; Gupta, 2020) allow the determination of the phases corresponding to the flow of electrons through the reaction centre. The phases O to J (ends at ~ 2 ms) and J to I (ends at ~ 30 ms) correspond to the reduction of Q_A and Q_B respectively. Then, the I to P phase (ends at ~ 500 ms) is considered to be relative to the fast (I) and slow (P) reduction of the plastoquinone pool. On the other hand, under certain conditions, such as high temperature, the appearance of the K phase (~ 200 to $300 \mu\text{s}$) has been shown to be directly related to the damages at the level of the Mn cluster (Srivastava *et al.*, 1997).

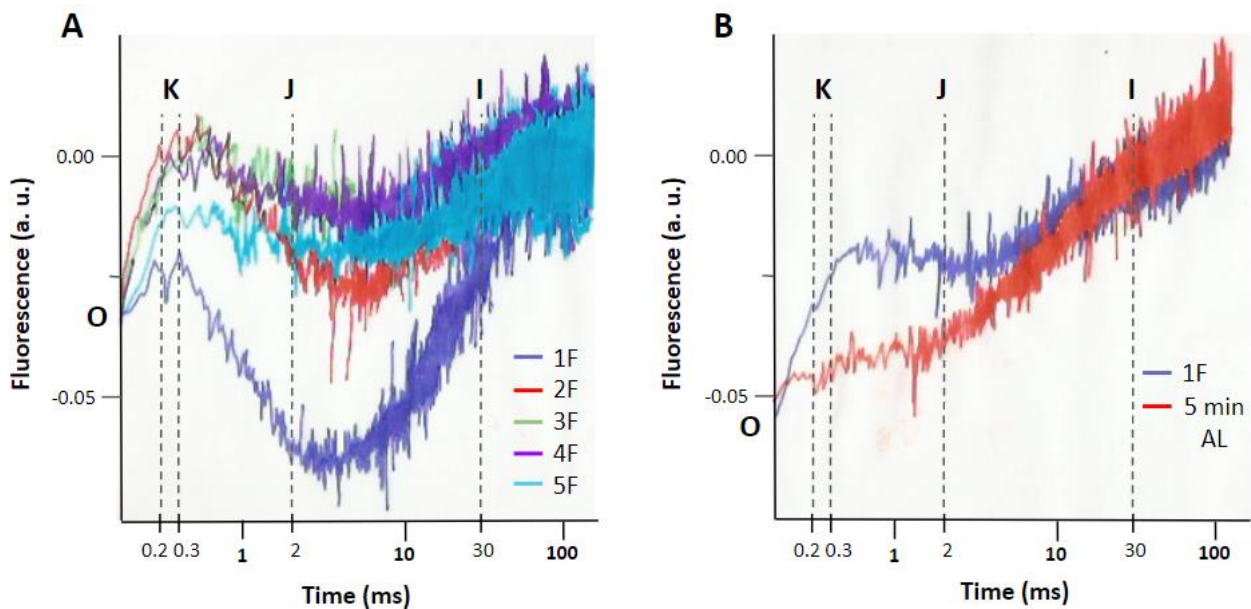


Figure 27: Photoactivation of dark-grown *Marchantia polymorpha* followed by chlorophyll fluorescence induction curves (OJIP)

A. Dark-grown *Marchantia* thalli were exposed to 1 (dark blue), 2 (red), 3 (green), 4 (purple) and 5 (cyan) successive flashes of saturating light during 300 ms. The abscissa shows the chlorophyll fluorescence (a. u.) as a function of the time (ms) in logarithmic scale. **B.** Fluorescence induction curve taken before (dark blue) and after (red) 5 min actinic light exposure of dark-grown thalli. The abscissa shows the chlorophyll fluorescence (a. u.) as a function of the time (ms) in logarithmic scale.

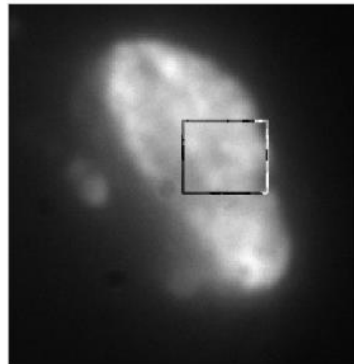
PSII chlorophyll fluorescence induction curves were measured on dark-cultured *Marchantia* thalli (Figure 27). The aim was to determine the state and the set-up of the electron flow through the reaction centre of the PSII during photoactivation. Induction curves were measured by applying a saturating flash of light lasting 300 ms. Two types of illumination were tested to induce photoactivation: application of successive flashes of 300 ms (Figure 27, **A**) or exposure to actinic light for 5 min (Figure 27, **B**). In this last condition, a flash of 300 ms was applied to the sample before and after the illumination.

The application of a single flash (Figure 27, **A**) indicates the presence of a very marked K phase (between 0.2 to 0.3 ms) then a strong decrease in fluorescence during the J phase (ends at 2 ms). The appearance of the K phase clearly shows that the PSII are not photoactivated. The ensuing decrease in fluorescence could be explained by the accumulation of $P680^+$, known to have a low fluorescence yield. This seems consistent with the fact that photoactivation must be complete to allow Q_A to be active (Krieger and Weis, 1993) and also because without a cluster there are no electrons that allow the return to the ground state of the P680. Then, the successive application of the flashes still shows the K phase but the decrease in fluorescence is more reasonable between K and J phases. It can therefore be concluded that certain clusters are formed. The difference between the induction curves after 3 up to 5 flashes does not really change which can be explained by the fact that more illumination may be necessary to photoactivate all the reaction centres. It can be hypothesised that the establishment of linear electron flow is necessary to increase the efficiency of photoactivation. As shown in Figure 27, **B**, after 5 min of actinic light, the K phase disappears completely, indicating that all the centres are photoactivated and the J-I-P phases are correctly defined, which is in agreement with the establishment of a linear electron flow through the photosynthetic chain.

c) Super-resolution fluorescence microscopy: tracking to thylakoids dynamic during photoactivation

In addition, super-resolution fluorescence microscopy has been used to observe ultrastructural changes caused by photoactivation in a region of thylakoid membrane. The use of the laser allows focussing on a small part of a chloroplast. First, a confocal image was taken rapidly with a very low light (Figure 28, **A**). Then, structural changes were tracked using PSII chlorophyll fluorescence detection for approximately 41 minutes since each scan lasted almost 80s (Figure 28, **B**). At the beginning of the experiment, the thylakoids (yellow fluorescence) are loose in the stroma and then begin to condense from around 5 minutes (Frame 3). Condensation seems to reach an intermediate level around 14 minutes (Frame 11) and seems to reach a “maximum” around 25 minutes (Frame 19). Finally, the last images, from 25 to 41 minutes still show a very slight condensation. It is reasonable to assume that the sudden light exposure of dark-grown thalli, although very low, results in significant stress which might suggest that the latter are showing conditions that are possibly not physiologically relevant. To check if damage has occurred, it would be interesting to measure F_v/F_m by chlorophyll fluorescence measurement after the photoactivation in the microscope.

A



B

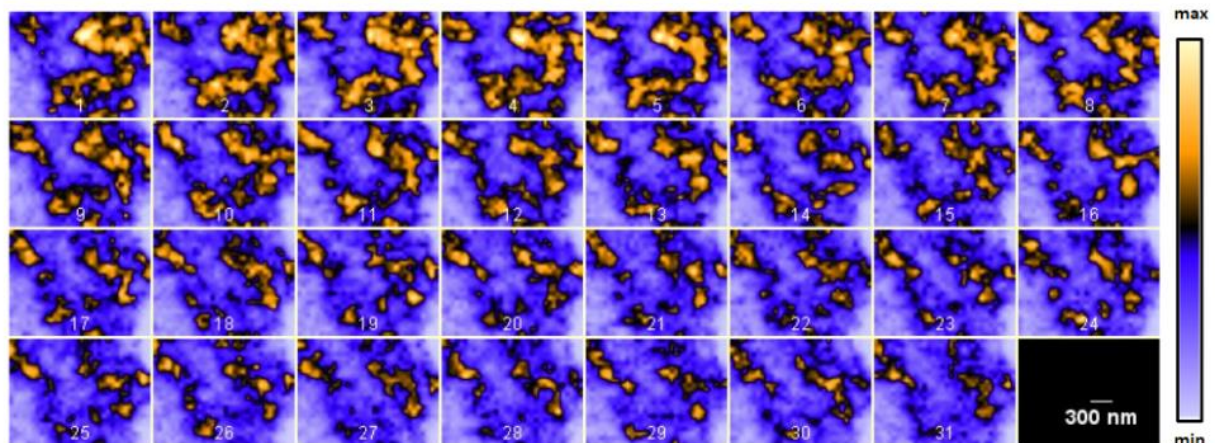


Figure 28: Evolution of chloroplasts ultra-structure of dark-grown *Marchantia polymorpha* during photoactivation

A. Confocal image of a chloroplast of a dark-grown *Marchantia* before photoactivation. The square corresponds to the area of interest followed in B. **B.** Tracking of photoactivation *in vivo* by super-resolution fluorescence microscopy. Each frame corresponds to 80s.

Thanks to all these observations, it can be hypothesised that the photoactivation of the first PSII allows the establishment of an electron flow through the membrane which will generate a gradual increase of the lumen acidification. This would have the effect of leading to the restructuring of the membranes by increasing the proportion of grana but also generating the gathering of the newly photoactivated PSII towards these compact structures in order to guarantee an efficient photosynthetic electron flow throughout the whole chain.

To conclude, chlorophyll fluorescence measurements and SRM can be used to monitor the photoactivation at different scales. To go further, the use of the chlorophyll fluorescence allows the determination of the changes which take place at the level of the PSII reaction centre during photoactivation while SRM shows it at thylakoids scale. Then, we know that it is possible to isolate the fluorescence emitted by PSII compared to that of PSI with the SRM in order to follow the changes in the localisation of photosynthetic complexes according to the photoactivation but also the first steps of the establishment of electrons flow through the chain.

D) Part I Conclusions

This first part was devoted to the donor side of the PSII and in particular to the use of Mn by *Marchantia polymorpha* and its vital importance as a catalyst for oxygen under the shape of the Mn cluster.

First, I characterised the impact of excess and deficiency of Mn on the photosynthesis and the metabolism of *Marchantia polymorpha*. I showed that *Marchantia* is able to set up protection and detoxification systems allowing it to survive to high Mn concentrations. From an evolutionary point of view, it can be hypothesised that these systems were developed to overcome the lack of regulation of Mn uptake, certainly due to the simple morphology of the plant. On the other hand, I have shown that the Mn deficiency, although difficult to establish, leads to an increase in the dissipation of energy as heat allowing to protect the PSII against photoinhibition in particular by also promoting cyclic electron flow.

The second part was particularly focused on Mn cluster-dependent light assembly, the so-called photoactivation. I have reproduced the experiments by Tikhonov *et al.*, 2006, to verify that the catalase-like activity of Mn(II) in solution does not generate the release of parasitic oxygen from photoactivation. Then, I verified apo-PSII activity after photoactivation.

To finish the *in vitro* part of the photoactivation, **Sun Un** and I carried out High Field EPR measurements and derivative experiments to determine the sequential intermediates of Mn cluster assembly during photoactivation. We have shown that the first Mn(II) is bound to D1-His332 in the dark, before the first photoactivation step.

Finally, for the first time ever, **Andrew Gall** and I tracked photoactivation and associated changes in chloroplast thylakoids structure *in vivo* in the dark-cultured organism *Marchantia polymorpha*. We have shown by different methods that photoactivation can be followed *in vivo*. It leads to the condensation of thylakoids allowing photosynthetic activity as we know it.

Part II: Regulation of Photosynthetic Electron Transport : Characterization of Plastid Terminal Oxidases a and b in *Marchantia polymorpha*

Photosynthetic organisms are subject to changing environmental conditions and have to deal with them. For this, they developed protective mechanisms, in particular at the level of the photosynthetic apparatus which is at the heart of their primary metabolism. As explained in the general introduction (page 29), many strategies have been developed such as alternative electron flows, non-photochemical quenching mechanisms and other protein families may be involved. This is the case of Plastid Terminal Oxidase (PTOX, page 33).

In this part, the model plant *Marchantia polymorpha* was used because of its place in the green lineage. Given that the most evolved plants, the angiosperms, have lost many regulatory proteins, the study of one of the first plants to have colonised the land offers new opportunities for understanding these mechanisms.

In the first two parts, the isoforms PTOXa and PTOXb in *Marchantia* were studied *in vivo* by the analysis of single and double mutants. Finally, an *in silico* analysis of the PTOX protein sequences across different photosynthetic organisms was conducted in an attempt to explain the differences between these two isoforms.

I) Characterization of PTOXa and PTOXb from *Marchantia polymorpha* *in vivo*

As explained above, the physiological role of the PTOX protein has mainly been studied in Angiosperms (i. e. *Arabidopsis thaliana*, *Solanum lycopersicum*, *Eutrema salsugineum*) as well as in the green algae *Chlamydomonas reinhardtii*. Nevertheless, it is known that the evolution of Angiosperms is marked by the disappearance of many regulatory proteins and photosynthesis is no exception. Indeed, in the following article, I have highlighted the presence of two isoforms of PTOX (PTOXa and PTOXb) in *Marchantia polymorpha*, each of which is similar to those of algae or that of Angiosperms. Single mutants $\Delta ptoxa$ and $\Delta ptoxb$ were generated in order to characterise their roles *in vivo*.

Article 2 : Evolutive differentiation between alga- and plant-type plastid terminal oxidase : study of plastid terminal oxidase PTOX isoforms in *Marchantia polymorpha*

In this article, single mutants of *Marchantia polymorpha* were generated by Ginga Shimakawa in Japan, in the laboratory of Chikahiro Miyake, Kobe University. I carried out almost all the experiments allowing the characterization of the mutants. The quantification of carotenoid content was carried out in collaboration with François Perreau, INRAE Versailles. I actively participated in writing the article.



Evolutionary differentiation between alga- and plant-type plastid terminal oxidase: Study of plastid terminal oxidase PTOX isoforms in *Marchantia polymorpha*



Marine Messant^{a,1}, Ginga Shimakawa^{a,1}, François Perreau^b, Chikahiro Miyake^c,
Anja Krieger-Liszkay^{a,*}

^a Institute for Integrative Biology of the Cell (I2BC), CEA, CNRS, Université Paris-Saclay, 91198 Gif-sur-Yvette cedex, France

^b Institut Jean-Pierre Bourgin, INRAE, AgroParisTech, Université Paris-Saclay, 78000 Versailles, France

^c Graduate School of Agricultural Science, Kobe University, 1-1 Rokkodai, Nada, Kobe 657-8501, Japan

ARTICLE INFO

Keywords:

Plastid terminal oxidase
Marchantia polymorpha
Plastoquinone pool
Chlorophyll fluorescence
P700 absorption

ABSTRACT

The liverwort *Marchantia polymorpha* contains two isoforms of the plastid terminal oxidase (PTOX), an enzyme that catalyzes the reduction of oxygen to water using plastoquinol as substrate. Phylogenetic analyses showed that one isoform, here called MpPTOXa, is closely related to isoforms occurring in plants and some algae, while the other isoform, here called MpPTOXb, is closely related to the two isoforms occurring in *Chlamydomonas reinhardtii*. Mutants of each isoform were created in *Marchantia polymorpha* using CRISPR/Cas9 technology. While no obvious phenotype was found for these mutants, chlorophyll fluorescence analyses demonstrated that the plastoquinone pool was in a higher reduction state in both mutants. This was visible at the level of fluorescence measured in dark-adapted material and by post illumination fluorescence rise. These results suggest that both isoforms have a redundant function. However, when P700 oxidation and re-reduction was studied, differences between these two isoforms were observed. Furthermore, the mutant affected in MpPTOXb showed a slight alteration in the pigment composition, a higher non-photochemical quenching and a slightly lower electron transport rate through photosystem II. These differences may be explained either by differences in the enzymatic activities or by different activities attributed to preferential involvement of the two PTOX isoforms to either linear or cyclic electron flow.

1. Introduction

One of the most important events in the evolution of photosynthetic organisms has been the colonization of lands. Alboresi et al. [1] have highlighted the great diversity of protection mechanisms that allow photosynthetic organisms to face environmental conditions that could induce oxidative stress and destruction of the photosynthetic apparatus (photoinhibition) when more light is absorbed than needed for photosynthesis. All oxygenic phototrophs ranging from algae to plants have the following regulation mechanisms in common: photosynthetic control limiting electron transport at the level of the cytochrome b_6/f complex when the pH in the lumen decreases below a certain threshold value [2]; mechanisms to dissipate excess energy in the antenna system,

the so-called non-photochemical quenching (NPQ) [3]; the proton gradient regulation 5 (PGR5) and PGR5-like 1 (PGRL1) proteins having a supposed role in the cyclic electron flow [4,5]; the chloroplast NADPH dehydrogenase (NDH) complex involved in cyclic electron flow and in chlororespiration [6,7] as well as the so-called Mehler reaction (the water-water cycle) that occurs when photosystem I (PSI) reduces O_2 to the superoxide anion radical which is then converted into O_2 and H_2O by detoxification enzymes [8]. Others, such as flavodiiron proteins (FLV) that reduce O_2 to H_2O at the acceptor side of PSI [9,10] have disappeared in angiosperms, but are present from cyanobacteria up to gymnosperms. Finally, some proteins have evolved over the time into separate subclasses such as the plastid terminal oxidase (PTOX).

PTOX oxidizes plastoquinol (PQH_2) and reduces O_2 to H_2O . It may

Abbreviations: AOX, Alternative Oxidase; DCMU, 3-(3,4-dichlorophenyl)-1,1-dimethylurea; NDH, NADH dehydrogenase-like complex; NPQ, Non-Photochemical Quenching; PGR5, Proton Gradient Regulation 5; PGRL1, PRG5-like protein; PIFT, Post-Illumination Fluorescence Transient; PQH_2 , plastoquinol; PQ, plastoquinone; PS, Photosystem; PTOX, Plastid Terminal Oxidase

* Corresponding author.

E-mail address: anja.krieger-liszkay@cea.fr (A. Krieger-Liszkay).

¹ Authors contributed equally.

<https://doi.org/10.1016/j.bbambio.2020.148309>

Received 8 April 2020; Received in revised form 2 September 2020; Accepted 14 September 2020

Available online 19 September 2020

0005-2728/ © 2020 Elsevier B.V. All rights reserved.

play an important physiological role since the redox state of the plastoquinone (PQ) pool is a key point of photosynthesis regulation in many physiological conditions. In angiosperms, PTOX is often regarded in the literature as a “safety valve”, allowing to avoid the over-reduction of PQ pool in conditions such as for example high light [11] or salt stress [12]. An increase of PTOX expression levels and of protein amounts have been observed upon exposure of plants to abiotic stress conditions like low or high temperature, drought *etc.* [13,14] Furthermore, PTOX is involved in carotenoid biosynthesis by maintaining PQ in its oxidized form [15,16]. In addition, PTOX acts as a terminal oxidase during chlororespiration [17] and in non-green plastids in etiorespiration [18] and chromorespiration [19,20]. Finally, PTOX is important in the first steps of chloroplast biogenesis, based on the publication by Wetzel et al. [15], highlighting that mutants have heteroplasmic cells.

Phylogenetic trees on PTOX evolution have been published previously focussing on amino acid sequences comparison with other oxidases [21,22]. Nawrocki et al. [23] have investigated the evolutionary relationship among PTOX isoforms in various photosynthetic organisms, which suggested that PTOX in angiosperms has been evolved along with the evolution from green algae to plants with several independent duplication events. The appearance of the ancestral protein is not clearly identified. Atteia et al. [24] hypothesized that the origin of PTOX predates primary endosymbiotic events, justifying its presence in the progeny of chlorophytes. Nevertheless, most articles agree that PTOX appears to diverge from its analogue, the mitochondrial alternative oxidase (AOX) that catalyzes the oxidation of ubiquinol by reducing O₂ to H₂O. AOXs are non-heme diiron carboxylate enzymes with six well conserved iron binding sites. It has been shown that this catalytic site including the ligands is conserved in PTOX [25] but PTOX diverges from AOX by insertion of amino acids conserved in all PTOX-containing photosynthetic organisms.

Characterization of PTOX activity *in vivo* has been mainly conducted in angiosperms by the characterization of *immutans* and *ghost* mutants in *Arabidopsis thaliana* [15,26–28] and *Solanum lycopersicum* [29], respectively. These mutants are known to have a variegated phenotype which is more important when exposed to increasing light intensities [30]. In addition, PTOX activity has been characterized *in vivo* in the green alga *Chlamydomonas reinhardtii* using a mutant affected in the isoform PTOX2 (*Crptox2*). Houilles-Vernes et al. [31] have highlighted its involvement in chlororespiration. *Crptox2* shows an over-reduction of PQ pool and is also affected in redistributing light excitation energy between photosystem II (PSII) and PSI (the so-called state transition). Using a single mutant of the cytochrome *b₆f* complex as well as a double mutant of both cytochrome *b₆f* and PTOX2, they concluded that PTOX2 is the major oxidase used to reoxidize PQ pool compared to PTOX1 in *C. reinhardtii*. *Crptox2* did not exhibit a defect in carotenoid contents and did not show a variegation phenotype such as *immutans* or *ghost*. Houille-Vernes and coworkers concluded that PTOX1 is sufficient for regenerating oxidized PQ for phytoene desaturase while being less active than PTOX2 in controlling the redox poise of PQ pool during photosynthesis. No PTOX1 mutant of *C. reinhardtii* has been characterized so far.

Liverworts can be regarded as the oldest living land plants or at least the land plants which have kept the most ancestral characters, among them *Marchantia polymorpha* has been used as a model with the sequencing of its genome and the development of genetic tools in order to better understand the evolution of land plants [32,33]. Here we demonstrate that the two *M. polymorpha* PTOX isoforms are phylogenetically significantly different and representative of algal- and angiosperm-type of PTOX respectively, and, by using mutants affected in one of the isoforms we investigated whether the isoforms differed in their activity. First, we focussed on PTOX evolution through the green lineage using *in silico* approaches. Then, mutation of both proteins independently allowed us to highlight the partial redundancy of these proteins *in vivo* by performing mainly chlorophyll fluorescence analyses.

2. Materials and methods

2.1. Phylogenetic analysis

31 amino acid sequences of PTOX and AOX in oxygenic phototrophs were aligned using Muscle [34], and then the extra N- and C-terminal regions were removed based on the comparison to cyanobacterial PTOX sequences. Thereafter, gaps in the alignment were removed using Gap Squeeze (<https://www.hiv.lanl.gov/content/sequence/GAPSTREEZE/gap.html>) with 50% of gap tolerance. The resulting sequences were compared using Muscle for building up phylogenetic trees (Supplementary material Fig. S1). The amino acid sequences of PTOX and AOX were obtained from CyanoBase (Glo, gll0601; Ana, Anacy_4546; Nos, all2096), National Center for Biotechnology Information (Coc, XP_005649673; Tha a, XP_002293901; Tha b, XP_002296917), Joint Genome Institute (Ost a, Ot11g01620; Ost b, Ot16g00910; Chl 1, Cre07.g350750; Chl 2, Cre03.g172500; Chl A, Cre09.g395950; Vol 1, Vocar.0011s0051; Vol 2, Vocar.0015s0153; Ory, Os04g57320; Zos, Zosma182g00520; Zea, Zm00008a005994; Nan a, 587833; Nan b, 605717; Pha a, 29275; Pha b, 41170; Cya 1, XM_005536341; Cya 2, XM_005536340), *Klebsormidium nitens* NIES-2285 genome project (Kle a, kfl00205_0040; Kle b, kfl00009_0280), MarpolBase (Mar a, Mapoly0050s0020; Mar b, Mapoly0003s0157), FernBase (Azo a, Azfi_s0009.g011680; Azo b, Azfi_s0070.g036665; Sal, Sacu_v1.1_s0132.g022138), and TAIR (Ara, AT4G22260; Ara A, AT3G22370).

The evolutionary history was inferred by using the Maximum Likelihood method [35]. The tree with the highest log likelihood (−8225.18) is shown. The percentage of trees in which the associated taxa clustered together is shown next to the branches. Initial trees for the heuristic search were obtained automatically by applying Neighbor-Join and BioNJ algorithms [36] to a matrix of pairwise distances estimated using a JTT model, and then selecting the topology with superior log likelihood value. The tree is drawn to scale, with branch lengths measured in the number of substitutions per site. Evolutionary analyses were conducted in MEGA X [37].

2.2. Material

A male accession of *Marchantia polymorpha*, Takaragaike (Tak)-1 and the mutants were asexually cultured on one-half-strength Gamborg's B5 agar medium [38] under a light–dark cycle (16 h-light, 22 °C, 120 μmol photons m^{−2} s^{−1}, white fluorescent lamp/8 h-dark, 20 °C). For biochemical and physiological measurements, 2–3 weeks thalli were used.

2.3. Genome editing by CRISPR/Cas9 system

The PTOX mutants of *M. polymorpha* were prepared by CRISPR/Cas9-based targeted mutagenesis [39]. The target regions (*ptoxa.1*, TTACACATGTACGAGAGCTT; *ptoxb.1*, CCAGTTGTGAGTCCCAACC; *ptoxb.2*, AAGCACCTTGGTGGATTCT) were introduced into the Gateway entry vector pMpGE_En03, and finally included in the destination vector pMpGE010 and pMpGE011. Thalli of *M. polymorpha* were infected with *Rhizobium radiobacter* C58C1 (GV2260) transformed with the resulting plasmids, and the transformants were selected on half-strength Gamborg's B5 agar medium supplemented with hygromycin or chlorsulfuron [40]. The genome DNA was extracted from the thalli of mutants, and the mutations were confirmed by DNA sequencing (Supplementary material Fig. S2). The mutants Δ *ptoxa.1* and Δ *ptoxb.1* were mainly used in this study as Δ *ptoxa* and Δ *ptoxb*. We confirmed the same phenotype of Δ *ptoxb.2* as Δ *ptoxb.1* by chlorophyll fluorescence measurements (Supplementary material Fig. S3).

2.4. Pigment analysis

Liquid chromatography-UV-absorption analysis was conducted using a HPLC column (Uptisphere Strategy C18-HQ 250 × 3 mm 3 μm, Interchim, Montluçon, France) with a liquid chromatography chain HPLC/UV (Shimadzu, Tokyo, Japan), consisting of two pumps (LC-20AD), a sample manager (SIL-20AC HT), a column oven (CTO-20A) and an UV diode array detector (UVSPD-M20A) with a flow of 0.5 mL min⁻¹. The mobile phase A was composed of 10% water and 90% acetonitrile with 0.5% acetic acid and the mobile phase B was ethyl acetate with 0.5% acetic acid. The elution gradient was as follows: initially 10% B, 1 min 10% B; 25 min 95% B. Then the column was equilibrated to initial conditions for 15 min. Absorbance was monitored at 450 nm. Peak areas were normalized by known absorption factors for each compound at 450 nm, and amounts of each pigment were calculated by normalization to chlorophyll *a*.

2.5. Chlorophyll fluorescence analysis

Chlorophyll *a* fluorescence was measured in 5 min dark-adapted thalli using an Imaging-PAM (Fig. 2 and Supplementary material Figs. S3A–C, and S4) or a Dual-PAM-100 fluorometer (Figs. 3 and 4, and Supplementary material Fig. S3D) (Walz, Effeltrich, Germany). Fluorescence parameters during illumination with blue actinic light (230 μmol photons m⁻² s⁻¹) and recovery curves were measured after the determination of F_o and F_m parameters. F_m and F_m' were determined using saturating flashes (10,000 μmol photons m⁻² s⁻¹, duration 300 ms): F_o , minimum and F_m , maximum fluorescence in a dark-adapted sample; F_m' , maximum fluorescence and F' , fluorescence emission from a light-adapted sample [41]. Post-illumination Fluorescence Transient (PIFT) was monitored in the dark after exposure to actinic red light (400 μmol photons m⁻² s⁻¹) for 10 min. When indicated, far-red light was given. Quantum yield of photochemical energy conversion in PSII, Y(II), and NPQ were determined as $(F_m' - F')/F_m'$ and $(F_m - F_m')/F_m'$, respectively. Electron transport rate through PSII was calculated as the product of Y(II) multiplied with photon flux density of red actinic light, the sample absorbance, and the ratio of the absorbance by PSII to that by both PSI and PSII [42]; we used 0.8 and 0.5, respectively, as these absorbance values which had been determined for leaves.

2.6. P700 measurement

P700 absorbance was measured using a Dual-PAM-100 fluorometer [43] (Walz, Effeltrich, Germany). Near-infrared measuring lights (830 and 870 nm) were applied to measure the transmittance of oxidized P700 (P700⁺). Five minutes dark-adapted thalli were exposed to actinic light and far-red light for 15 s. Then, a saturating flash was given in the presence of far-red light after switching off the light. First, this experiment was done on intact thalli which were then immersed for 5 min in 100 μM 3-(3,4-dichlorophenyl)-1,1-dimethylurea (DCMU) or in a combination of DCMU and 500 μM methylviologen.

2.7. Immunoblots

Thalli were grinded in 50 mM HEPES pH 7.6. The extract was filtered through cheese, centrifuged at 4000g, the pellet was resuspended in 50 mM HEPES pH 7.6, the chlorophyll concentration was determined and this membrane fraction was used for analysis by SDS-PAGE (10% acrylamide) and immunoblotting. Proteins were blotted onto nitrocellulose membrane. Labelling of the membranes with anti-PGR5, anti-NDH-B and anti-RbcL (Agrisera, Vännäs, Sweden) was carried out at room temperature in 1 × TBS (50 mM Tris-HCl pH 7.6, 150 mM NaCl), 0.1% Tween 20 and 1% non-fat powder milk. After washing, bound antibodies were revealed with a peroxidase-linked secondary anti-rabbit antibody (Agrisera, Vännäs, Sweden) and visualized by

enhanced chemiluminescence. PTOX antibodies raised against the proteins from *Arabidopsis* (gift from Marcel Kuntz, CEA Grenoble) and *Chlamydomonas reinhardtii* (gift from Xenie Johnson, CEA Cadarache) did not reveal bands in *Marchantia polymorpha*.

3. Results

Marchantia polymorpha contains two PTOX isoforms (MpPTOXs) that differ significantly in their sequences. The study of PTOX evolution has so far been limited to the comparison of their protein sequences with those of AOXs. However, the more recent evolution of different PTOX isoforms is just as interesting. Sequence comparison shows that MpPTOXa is closely related to PTOX of angiosperms that usually contain only one isoform, while MpPTOXb is more similar to PTOX isoforms found in the green alga *Chlamydomonas reinhardtii* (CrPTOXs). Since the PTOX isoform of *Arabidopsis thaliana* has been highlighted first, the isoforms resembling to it were defined here as “PTOXa” and the other isoforms as “PTOXb”. MpPTOXa shows 96% identity with PTOX in *Arabidopsis thaliana* (AtPTOX), while MpPTOXa and MpPTOXb share only 53% identity. Since the two MpPTOX isoforms are so different in respect to their sequence homology, it can be hypothesized that these proteins have different physiological functions. A closer look at the sequences revealed that MpPTOXb and CrPTOXs (hereafter defined as “alga-type PTOX”) are larger than MpPTOXa and AtPTOX (hereafter defined as “plant-type PTOX”; Fig. 1A). CrPTOX1 and CrPTOX2 are composed of 471 and 416 amino acid residues. MpPTOXb has 497 amino acid residues while MpPTOXa and AtPTOX contain only 376 and 352 ones (Supplementary material, Fig. S1).

31 amino-acid sequences of PTOX isoforms were investigated in a variety of photosynthetic organisms, including cyanobacteria, algae, and land plants. Although the C-terminal parts of the proteins are not particularly well conserved between these isoforms, the longer N-terminal part is mostly recognized in alga-type PTOX. Plant-type PTOX seems to have lost a part of the sequence between the transit peptide and the conserved motif containing the catalytic site (Fig. 1A), resulting in the shorter primary structures, although there are some exceptions such as *Zea mays* and *Nannochloropsis oceanica*. A phylogenetic tree including cyanobacterial PTOX, alga-type PTOX, plant-type PTOX, and AOX was built (Fig. 1B) based on the amino acid sequence alignment in the largely conserved region containing the catalytic site (the part “Fe-Fe” in Fig. 1A) among PTOX isoforms in a variety of photosynthetic organisms, clearly showing the three different PTOX groups. Several amino acid residues around the catalytic site are highly conserved in alga- and plant-type PTOX (Supplementary material Fig. S1). The green alga *Coccomyxa subellipsoidea* has one PTOX belonging to the alga-type. *Chlamydomonas reinhardtii* and *Volvox carteriv* have two PTOX isoforms, both belonging to the alga-type. The other green alga *Ostreococcus tauri* has both alga- and plant-type PTOX isoforms. Seed plants are proposed to be evolved from green algae through charophytes, bryophytes (liverworts, mosses, and hornworts), and pteridophytes (ferns), termed as photosynthetic green lineage [44]. Like in *Ostreococcus tauri* both alga- and plant-type PTOX isoforms are conserved in the charophyte alga *Klebsormidium nitens*, the liverwort *Marchantia polymorpha*, and the fern *Azolla filiculoides*, but alga-type one is lost in the fern *Salvinia cucullata* and in all angiosperms (Fig. 1B). In contrast to the green lineage, photosynthetic red lineage is defined as having evolved from red algae to secondary algae such as eustigmatophytes and diatoms [44]. The red alga *Cyanidioschyzon merolae* has two PTOX isoforms, both of which are closer to the alga-type ones, but the eustigmatophyte alga *Nannochloropsis oceanica* and two diatoms *Phaeodactylum tricorutum* and *Thalassiosira pseudonana* have both, alga- and plant-type PTOX (Fig. 1B).

Since the two MpPTOX isoforms are so different in respect to their sequence homology, it can be hypothesized that these proteins have different physiological functions. To characterize the physiological role of the two PTOX isoforms *in vivo*, *M. polymorpha* has been chosen since

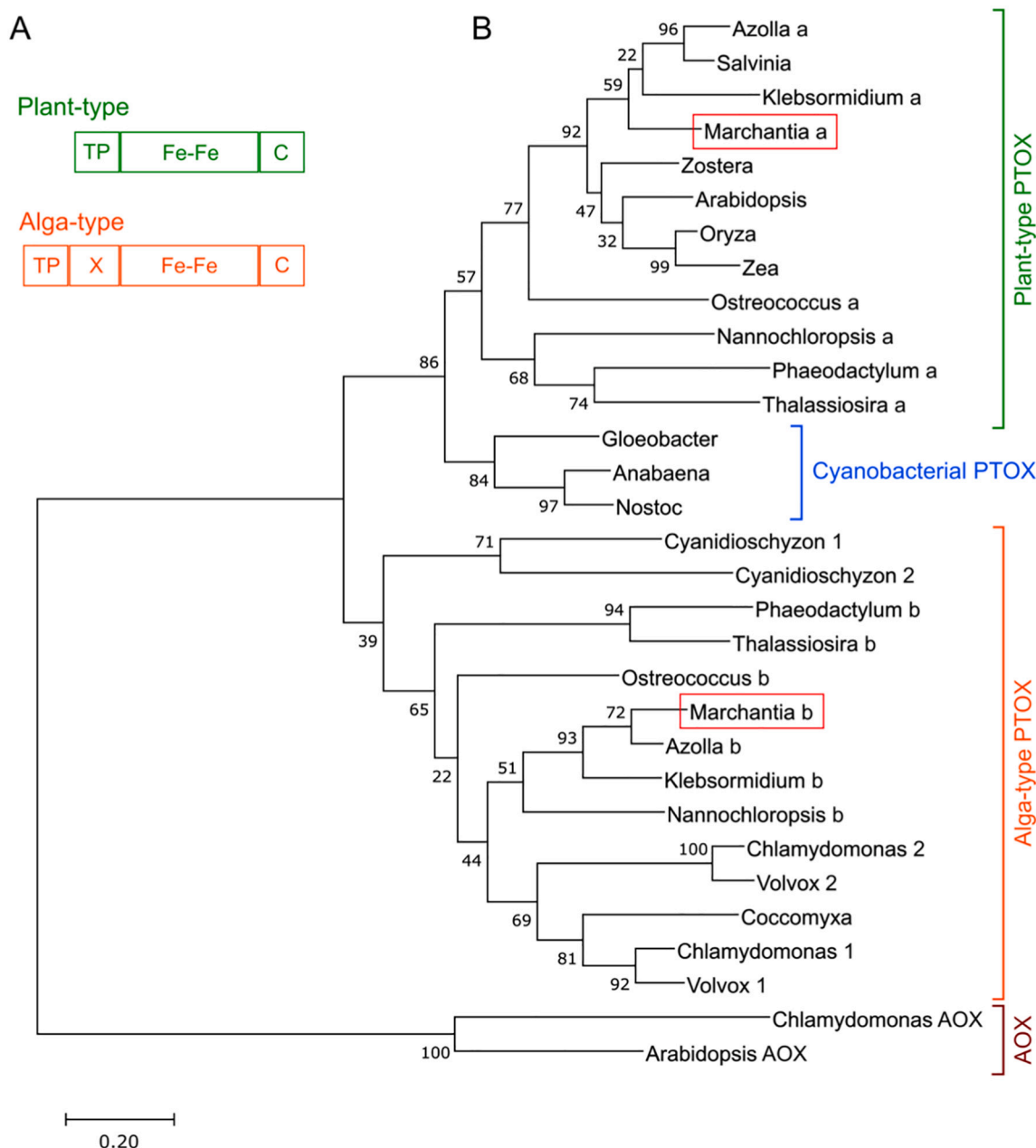


Fig. 1. Phylogenetic analysis of plastid terminal oxidase (PTOX) and alternative oxidase (AOX) isoforms in oxygenic phototrophs. (A) Typical primary structures of plant- and alga-type PTOX. TP, transit peptide; Fe–Fe, highly conserved region containing the catalytic site; C, C-terminal region; X, an extended region often observed in alga-type PTOX. (B) Phylogenetic tree of the evolutionary relationship between plastid terminal oxidase (PTOX) in oxygenic phototrophs. Each highly conserved region (Fe–Fe) was used for the alignment analysis to build the phylogenetic tree (Supplementary material Fig. S2). Branch lengths correspond to the evolutionary distances. Organisms included in this phylogenetic analysis are cyanobacteria (*Gloeobacter violaceus*, *Anabaena cylindrica*, and *Nostoc* sp.), green algae (*Coccomyxa subellipsoidea*, *Ostreococcus tauri*, *Chlamydomonas reinhardtii*, and *Volvox carteriv*), the charophyte alga *Klebsormidium nitens*, the liverwort *Marchantia polymorpha*, ferns (*Azolla filiculoides* and *Salvinia cucullata*), angiosperms (*Arabidopsis thaliana*, *Oryza sativa*, *Zostera marina*, and *Zea mays*), the eustigmatophyte alga *Nannochloropsis oceanica*, diatoms (*Phaeodactylum tricornutum* and *Thalassiosira pseudonana*), and the red alga *Cyanidioschyzon merolae*. Alternative oxidase (AOX) in *Chlamydomonas reinhardtii* (AOX1) and *Arabidopsis thaliana* (AOX1A) are also included in the analysis.

it has one PTOX belonging to the plant-type and another one of the alga-type enzyme, and its position in the evolution of the green line is intermediate between green algae and plants [33]. The mutants deficient in MpPTOXa and MpPTOXb, named hereafter $\Delta ptoxa$ and $\Delta ptoxb$, were constructed using CRISPR/Cas9-genome editing system [39]. The specific regions to MpPTOXa and MpPTOXb were determined as the target site for CRISPR/Cas9. The *Marchantia* transformants were generated by the infection of *Agrobacterium* containing binary vectors with young thalli in the presence of antibiotics (see “Materials and methods”). The gemma from the transformants was cultured on agar

plates with the antibiotics, and the frameshift mutation in the target regions were confirmed by DNA sequencing (Supplementary material Fig. S2). Concerning that the mutation occurred at the later part of the gene in the mutant $\Delta ptoxb$ ($\Delta ptoxb.1$), we constructed another line ($\Delta ptoxb.2$) to confirm that the phenotype was due to the mutation of PTOXb (Supplementary material Figs. S2 and S3). Similar to *CrptoX2*, no variegation phenotype such as *immutans* or *ghost* was seen in both $\Delta ptoxa$ and $\Delta ptoxb$ mutants.

In order to characterize the role of PTOX on photosynthetic electron transport, measurements of chlorophyll fluorescence upon illumination

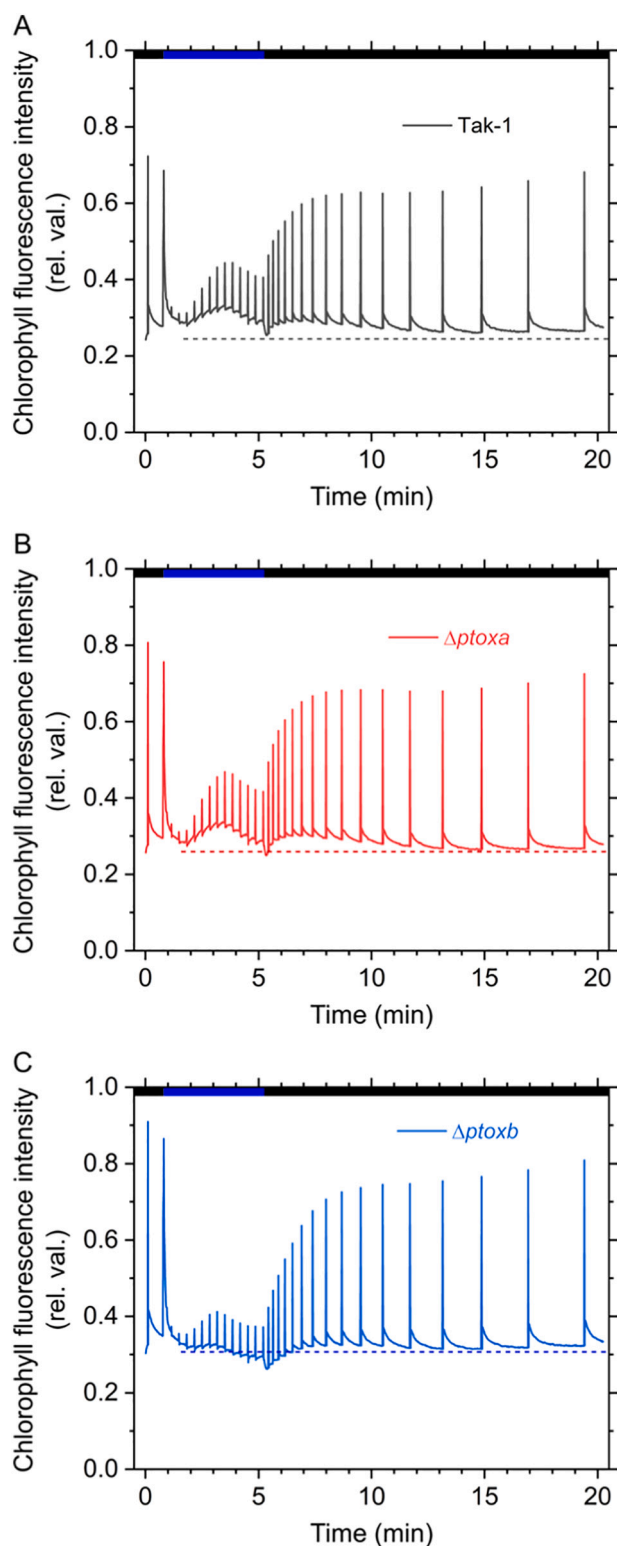


Fig. 2. Response of chlorophyll fluorescence of wild type and mutants deficient in plastid terminal oxidase to illumination by blue actinic light ($230 \mu\text{mol photons m}^{-2} \text{s}^{-1}$). A: *M. polymorpha* wild type (Tak-1), B: Δptoxa , C: Δptoxb . Before the measurements, the plants were dark-adapted for 5 min. Dashed lines indicate the chlorophyll fluorescence levels before the first saturation flash. Blue bar indicates the duration of the actinic light. Measurements were conducted independently three times (biological replicates), and representative traces are shown.

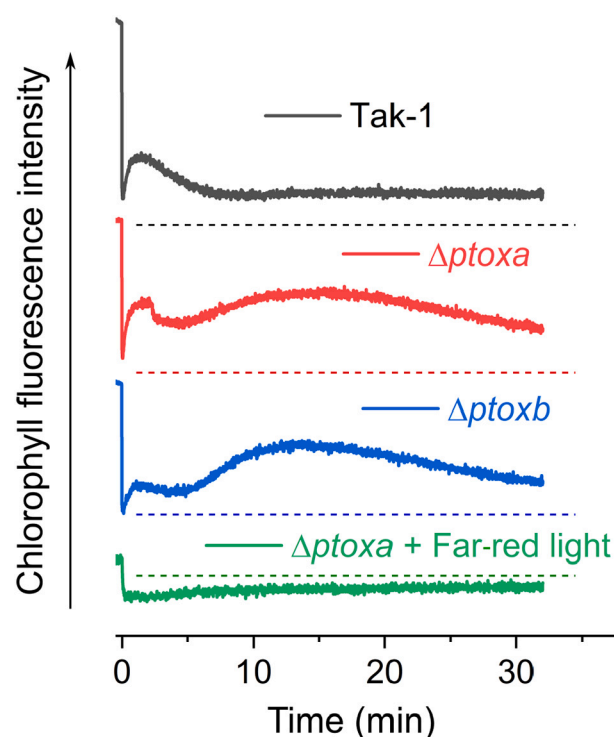


Fig. 3. Typical trace of chlorophyll fluorescence change after switching off the actinic red light ($400 \mu\text{mol photons m}^{-2} \text{s}^{-1}$, 10 min) at 0 min in wild type (Tak-1; black) and the mutants deficient in plastid terminal oxidases (Δptoxa ; red) and b (Δptoxb ; blue). Measurements were conducted independently three times (biological replicates), and representative traces are shown. Dashed lines indicate the chlorophyll fluorescence levels prior to illumination. Application of far-red light suppressed the post illumination fluorescence rise as shown here for Δptoxa (green).

and dark recovery were carried out. As shown in Fig. 2, upon illumination with actinic light Δptoxb showed a lower fluorescence level during saturating pulses while Δptoxa was very similar to Tak-1 (wild type). When the actinic light was switched off, fluorescence levels in mutants decreased below the F_0 level, more significantly for Δptoxb than for Δptoxa . This can be either caused by a higher level of NPQ leading to a quenching of F_0 or chlororespiratory activity resulting in a higher reduction state of PQ pool, Q_B and Q_A in the dark giving rise to a higher fluorescence level. In this case, dark adaptation of the material prior to the fluorescence measurement does not assure that all reaction centers are in the “open state”.

One way to determine chlororespiratory activity is to follow the so-called Post-Illumination Transient Fluorescence (PIFT) rise. Illumination with actinic light for a given time leads to the production of NADPH and ATP that can be consumed in the dark leading to a transient reduction of the PQ pool, Q_B and Q_A . Fig. 3 shows after previous illumination in the dark a strong increase in the fluorescence level (PIFT) in both mutants detected using low intensity measuring light. Applying far-red light removed the PIFT, confirming the high reduction state of the PQ pool in both mutants.

If one calculated F_v/F_m values using dark-adapted material and without taking into account that the F_0 may be not correct, one obtains values for F_v/F_m being 0.56 ± 0.04 for Δptoxa and 0.61 ± 0.04 for Δptoxb ($n = 6$). If these values were determined after far-red light illumination, 0.69 ± 0.01 and 0.71 ± 0.01 were obtained for Δptoxa and Δptoxb ($n = 6$), similar to those measured for Tak-1. F_v/F_m values determined with the Imaging-PAM system tend to be low because the intensity of the measuring light is rather high. This explains the discrepancy with the literature reporting an F_v/F_m value in Tak-1 of approximately 0.8 [45],

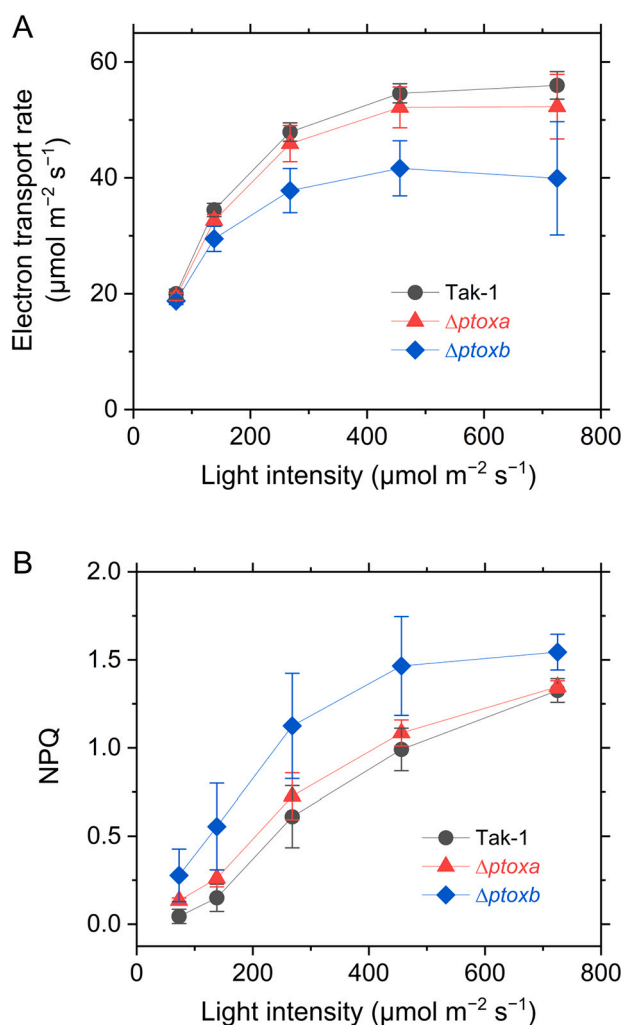


Fig. 4. Dependence of electron transport rate through PSII (A) and non-photochemical quenching (NPQ; B) on light intensity at steady-state photosynthesis (4 min after onset of actinic light) in *M. polymorpha* wild type (Tak-1; black) and the mutants deficient in plastid terminal oxidases a ($\Delta ptoxa$; red) and b ($\Delta ptoxb$; blue). Data are represented as the mean \pm SD, $n = 3$ (biological replicates).

Next, we measured NPQ and the electron transport rate as a function of actinic light intensity (Fig. 4). $\Delta ptoxb$ showed a lower electron transport rate and a higher NPQ while $\Delta ptoxa$ behaved like Tak-1. Pigment analysis showed that the amounts of certain carotenoids such as neoxanthin and violaxanthin were slightly larger in $\Delta ptoxb$ (Fig. 5). The increase in pigment content of the violaxanthin pool may explain the stronger NPQ found in this genotype. It may also indicate that $\Delta ptoxb$ is more stressed than $\Delta ptoxa$ or Tak-1, leading to a lower electron transport rate. However, no higher susceptibility to photoinhibition was observed in $\Delta ptoxb$ (Supplementary material Fig. S4).

When the PQ pool is more oxidized in the dark, it is expected that P700^+ is accumulating to a higher level in response to the illumination at a given light intensity. As can be seen in Fig. 6, more P700^+ accumulated in Tak-1 upon illumination with either actinic or far-red light. Both mutants showed the same lower level of P700^+ oxidation suggesting that PQ pool was more reduced, if we consider that there was no PSI acceptor side limitation thanks to the presence of the flavodiiron proteins (FLVs) [45]. There are nevertheless striking differences between $\Delta ptoxa$ and $\Delta ptoxb$. Upon illumination with actinic light that excites both photosystems and favours linear electron flow, the oxidation of P700 was delayed in $\Delta ptoxa$ compared with $\Delta ptoxb$, especially at the initial rise. This seems to indicate that the PQ pool was more reduced in $\Delta ptoxa$, suggesting a higher activity of this enzyme. However,

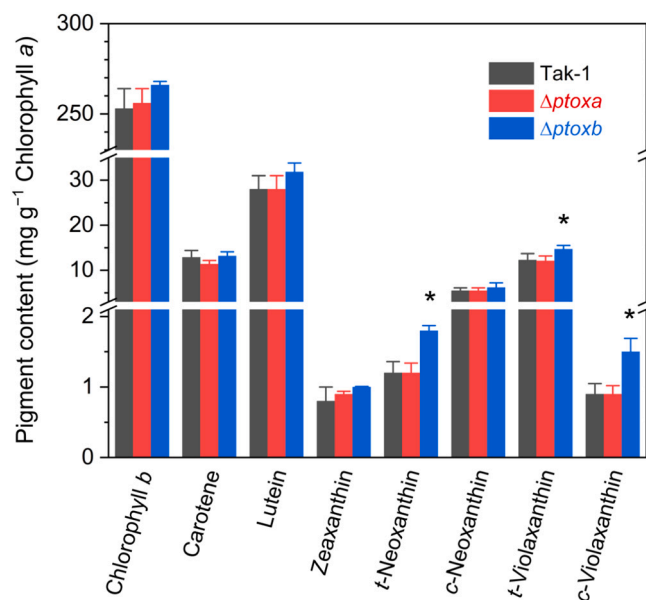


Fig. 5. Pigment content in thalli of *M. polymorpha* wild type (Tak-1; black) and the mutants deficient in plastid terminal oxidases a ($\Delta ptoxa$; red) and b ($\Delta ptoxb$; blue) determined by HPLC-UV measurement. Data are represented as the mean \pm SD, $n = 3$ (technical replicates). Statistically significant differences (*) in $\Delta ptoxb$ compared to Tak-1 were determined by Student's *t*-test ($p < 0.05$).

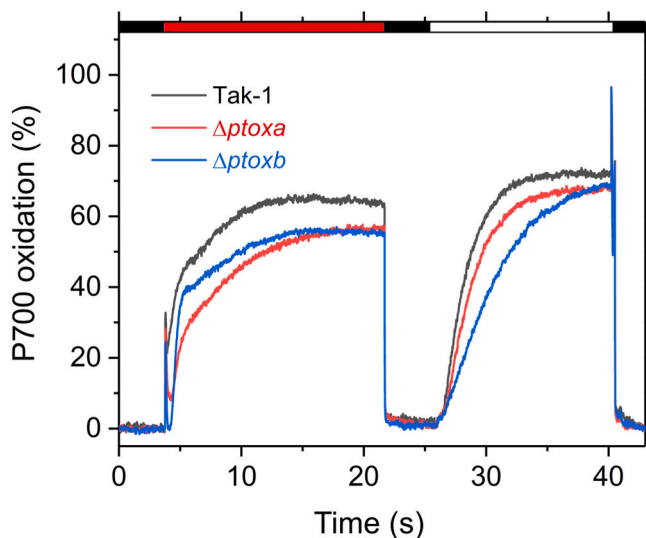


Fig. 6. Oxidation of P700 in response to light in *M. polymorpha* wild type (Tak-1; black) and the mutants deficient in plastid terminal oxidases a ($\Delta ptoxa$; red) and b ($\Delta ptoxb$; blue). Red actinic light ($500 \mu\text{mol photons m}^{-2} \text{s}^{-1}$) and far-red light were given as indicated by red and white bars. Experiments were conducted independently three times (biological replicates), and representative traces are shown. The maximum oxidation amplitude of P700 was determined by a saturation flash at the end of the far-red light at 40 s.

when illuminated with far-red light that excites preferentially PSI and favours cyclic electron flow, P700 was faster oxidized in $\Delta ptoxa$ than in $\Delta ptoxb$. To show the electron donation to P700 and the reduction state of the PQ pool in the absence of electron input from PSII, we added DCMU, an inhibitor of PSII blocking the Q_B -binding pocket. The re-reduction of P700^+ after far-red illumination was much faster in $\Delta ptoxa$ than in $\Delta ptoxb$ and Tak-1, with $\Delta ptoxb$ being slightly faster than Tak-1 (Fig. 7). This indicates again a higher reduction state of the PQ pool in $\Delta ptoxa$. In the absence of inhibitors, the re-reduction of P700^+ after far-

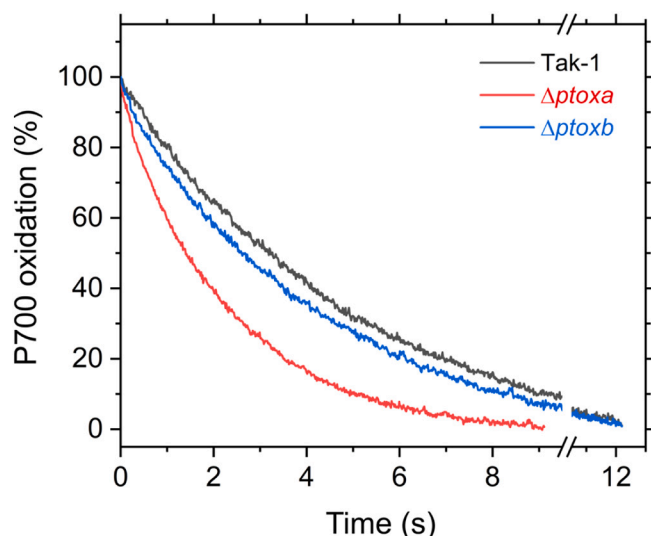


Fig. 7. P700⁺ re-reduction after illumination with far-red light in DCMU-treated thalli. Representative traces of *M. polymorpha* wild type (Tak-1, black) and the mutants deficient in plastid terminal oxidases A (Δ ptoxa; red) and B (Δ ptoxb; blue) are shown.

red illumination was slightly faster in both mutants than in Tak-1 indicating that the reduction state of the PQ pool and plastocyanin is higher. As expected, addition of the electron acceptor methylviologen together with DCMU abolished the differences between the mutants and Tak-1 (Supplementary material Fig. S5). Immunoblots probing for NDH and PGR5 showed an increase in the amount of NDH in Δ ptoxa and of PGR5 in both, Δ ptoxa and Δ ptoxb (Fig. 8).

4. Discussion

Here, we categorized PTOX isoforms in oxygenic phototrophs into three different groups (Fig. 1): cyanobacterial, alga-type, and plant-type PTOXs. Based on the present phylogenetic analysis, two different types of PTOX isoforms had been inherited to basal land plants from green algae like *Ostreococcus tauri* that is often described as one of the ancient members of the photosynthetic green lineage [46]. Both alga- and plant-type PTOXs are conserved in most basal land plants, while angiosperms have lost the alga-type PTOX. Also, the fern *Salvinia cucullata* has only a plant-type PTOX (Fig. 1B), and another fern, *Azolla filiculoides*, lost a conserved ligand of the non-heme diiron center, most probably leading to the loss or alteration in the catalytic activity in its alga-type PTOX (Supplementary material Fig. S1). These facts suggest that alga-type PTOX are already not functional in some pteridophytes. Both plant-type and alga-type PTOX are also found in secondary algae that are supposed to be derived from red algae in photosynthetic red lineage (Fig. 1B). In this study, we show that the red alga *Cyanidioschyzon merolae* has only two isoforms of alga-type PTOX. This may not be the case for all red algae and improved open genome sources of red algae may uncover the red algae species having both alga- and plant-type PTOX isoforms in near future. The appearance of the ancestral protein for PTOX has not been identified to date. However, many studies based on genomic sequence analysis seem to favor the hypothesis of PTOX acquisition during the primary endosymbiotic event, suggesting that this protein appeared much earlier than the eukaryotic lineage [21,22,24,47]. The question is when these alga- and plant-type PTOXs had been separated in the evolutionary history of photosynthetic organisms. It can be speculated that a single protein has been duplicated in eukaryotic algae, finally resulting in alga- and plant-type PTOXs, if we consider that cyanobacterial PTOX is closer to plant-type PTOX but can be clearly distinguished from both alga- and plant-type PTOXs. Interestingly, most of alga-type PTOX isoforms show

longer N-terminal regions, resulting in bigger size of proteins (Fig. 1A and Supplementary material Fig. S1). In addition, some amino acid residues are specifically conserved in each type of PTOX even in the motif containing catalytic sites (Supplementary material Fig. S1), reflected also in the phylogenetic tree (Fig. 1B). Differences in enzymatic activities of these different types of PTOX remain to be characterized in future, possibly uncovering why angiosperms had lost alga-type PTOX during the evolutionary history.

The results shown here (Figs. 2, 3, 6, 7) indicate that both MpPTOX isoforms have redundant functions and are both important for controlling the redox state of the PQ pool. Especially the PIFT showing the slow electron donation to the PQ pool via the NDH complex during chlororespiration is similar in both mutants. However, there are small differences when comparing Δ ptoxa and Δ ptoxb. Δ ptoxa shows no difference in electron transport rate and NPQ compared with Tak1, whereas in Δ ptoxb the electron transport rate is lower while NPQ is higher. The lower electron transport rate and the higher NPQ and violaxanthin amount in Δ ptoxb suggest that this mutant is slightly stressed although no obvious phenotype was visible. *Crptox2* mutant showed a lower fitness when cells were grown under phototrophic conditions and was more susceptible to photoinhibition [31]. In addition, *Crptox2* was affected in the state transition being preferentially in state 2. In contrast, Δ ptoxb in *M. polymorpha* showed neither signs of a defect in the state transition nor a higher susceptibility to high light (Supplementary material Fig. S4) suggesting that the plant-type MpPTOXa could compensate better for the absence of MpPTOXb than it was the case in *C. reinhardtii* possessing only two alga-type isoforms. In respect to carotenoid synthesis MpPTOXb seems to replace perfectly MpPTOXa since the absence of MpPTOXa did not alter the carotenoid composition neither induced a variegated phenotype as described in angiosperms for *immutans* and *ghost*.

P700 measurements show that the isoform MpPTOXa is more efficient in keeping the PQ pool oxidized since the oxidation of P700⁺ in actinic light was retarded in Δ ptoxa compared with Δ ptoxb (Fig. 6). However, under illumination with far-red light the opposite was observed with slower P700 oxidation in Δ ptoxb than in Δ ptoxa. Actinic light drives mainly reduction of the PQ pool by linear electron transport, while far-red light oxidizes the PQ pool and may also favor PQ reduction by cyclic electron flow. This leads us to hypothesize that PTOXa may be more active in linear electron transport and PTOXb more in cyclic electron transport. This different behaviour of the PTOX isoforms at the different light qualities can be rationalized by different enzymatic properties, with MpPTOXb having a higher affinity (low K_m -value) for PQH₂ but a lower V_{max} than MpPTOXa. This would make MpPTOXa the more efficient enzyme keeping the PQ pool oxidized under conditions favouring linear electron flow. The proposition of a high activity of MpPTOXa is supported by the fact that, in the presence of DCMU, the reduction of P700⁺ is accelerated in Δ ptoxa (Fig. 7). However, the amount of the NDH complex is also increased in Δ ptoxa (Fig. 8), and a higher chlororespiratory activity may also explain the higher reduction state of the PQ pool in this mutant. Since cyclic electron flow in far-red light is expected to be relatively low, the reduction state of the PQ pool may also be relatively low and MpPTOXb may become under these conditions highly efficient to keep the PQ pool oxidized. Alternatively, the two PTOX isoforms may be heterogeneously distributed within the thylakoid membrane. MpPTOXb may be preferentially associated with supercomplexes involved in cyclic flow composed of PSI, ferredoxin, cytochrome *b₆f* and a putative ferredoxin quinone reductase possibly linked to PGR5 and PGRL1 [48,49] while MpPTOXa may be preferentially associated with components of linear electron flow. A third possibility to explain the different behaviour of the two mutants may simply be a difference in the protein level of the two isoforms.

Both mutants have a higher amount of PGR5 (Fig. 8), indicating that the loss of a part of PTOX activity triggers the accumulation of higher amounts PGR5 and likely increases the capacity for cyclic electron

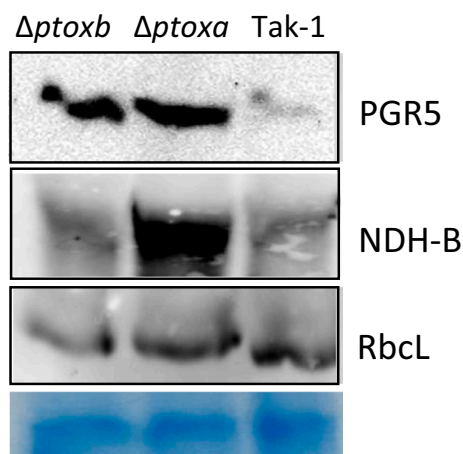


Fig. 8. PGR5 and NDH-B content in membranes fractions of *M. polymorpha* wild type (Tak-1) and the mutants deficient in plastid terminal oxidases a (*Δptoxa*) and b (*Δptoxb*) analyzed by SDS-PAGE and immunoblotting using specific antibodies. As loading controls, the signals obtained with antibodies directed against RbcL (large subunit of Ribulose-1.5-bisphosphate carboxylase/oxygenase) and a part of the Coomassie stained gel are shown.

transport. Cyclic electron transport may be important in these mutants to compensate for a reduction of the PTOX-dependent chlororespiratory activity and to keep the size of the proton motive force.

PTOX activity may also be regulated as a function of the physiological state of the chloroplast. Stepien and Johnson [12] have demonstrated that plant PTOX is localized under control conditions at the stroma lamellae while it is localized at the grana stacks under salt stress in the halophile *Eutrema salsgineum*. Furthermore, it has been shown that AtPTOX could be found partially in a soluble protein fraction and in a membrane-associated fraction. The strength of the membrane association of AtPTOX was shown to depend on the proton motive force [13,50]. A difference between plant-type and alga-type PTOX may lie in the strength of the membrane association. Nawrocki et al. [23] carried out a modelling of the structure of CrPTOX2 based on the x-ray structure of AOX from *Trypanosoma brucei* (TbAOX) [51]. Shiba et al. [51] proposed that two alpha helices upstream of the catalytic site of TbAOX are involved in the anchoring to the inner mitochondrial membrane. According to the calculation by Nawrocki et al. [23] the amphipathic helices of CrPTOX dock to a depth of approximately 8 Å into the membrane. They suggest that the N-terminal extension in CrPTOX contributes to the interaction of the two monomers of the protein. We propose here that the increase in length may as well strengthen the association of the protein to the upper membrane leaflet. Further studies are needed to investigate the difference in plant-type and alga-type PTOX regarding their attachment to the membrane and differences in the regulation of the activity of these isoforms.

Declaration of competing interest

The authors declare that they have no known competing financial interests or personal relationships that could have appeared to influence the work reported in this paper.

Acknowledgements

We thank Dr. Kimitsune Ishizaki (Kobe University, Japan) for kindly giving us the Tak-1 strain. The I2BC and the IJPB benefit from the support of Saclay Plant Sciences-SPS (ANR-17-EUR-0007) and the I2BC from the French Infrastructure for Integrated Structural Biology (FRISBI) ANR-10-INSB-05. This work has benefited from the support of IJPB's Plant Observatory technological platforms. G.S. is supported by a JSPS overseas research fellowship (201860126).

Appendix A. Supplementary data

Supplementary data to this article can be found online at <https://doi.org/10.1016/j.bbabi.2020.148309>.

References

- [1] A. Alboresi, M. Storti, T. Morosinotto, Balancing protection and efficiency in the regulation of photosynthetic electron transport across plant evolution, *New Phytol.* 221 (2018) 105–109.
- [2] C. Foyer, R. Furbank, J. Harbinson, P. Horton, The mechanisms contributing to photosynthetic control of electron transport by carbon assimilation in leaves, *Photosynth. Res.* 25 (1990) 83–100.
- [3] P. Müller, X.P. Li, K.K. Niyogi, Non-photochemical quenching. A response to excess light energy, *Plant Physiol.* 125 (2001) 1558–1566.
- [4] Y. Munekage, M. Hojo, J. Meurer, T. Endo, M. Tasaka, T. Shikanai, PGR5 is involved in cyclic electron flow around photosystem I and is essential for photoprotection in *Arabidopsis*, *Cell* 110 (2002) 361–371.
- [5] M. Suorsa, F. Rossi, L. Tadini, M. Labs, M. Colombo, P. Jahns, M.M. Kater, D. Leister, G. Finazzi, E.M. Aro, R. Barbato, P. Pesaresi, PRG5-PGR1-dependent cyclic electron transport modulates linear electron transport rate in *Arabidopsis thaliana*, *Mol. Plant* 9 (2015) 271–288.
- [6] P. Bennoun, Evidence for a respiratory chain in the chloroplast, *Proc. Natl. Acad. Sci. U. S. A.* 79 (1982) 4352–4356.
- [7] G. Peltier, E.M. Aro, T. Shikanai, NDH-1 and NDH-2 plastoquinone reductases in oxygenic photosynthesis, *Annu. Rev. Plant Biol.* 67 (2016) 55–80.
- [8] K. Asada, The water-water cycle as alternative photon and electron sinks, *Philos. Trans. R. Soc. Lond. Ser. B Biol. Sci.* 355 (2000) 1419–1431.
- [9] Y. Helman, D. Tchernov, L. Reinhold, M. Shibata, T. Ogawa, R. Schwarz, I. Ohad, A. Kaplan, Genes encoding A-type flavoproteins are essential for photoreduction of O₂ in cyanobacteria, *Curr. Biol.* 13 (2003) 230–235.
- [10] A. Alboresi, M. Storti, L. Cendron, T. Morosinotto, Role and regulation of class-C flavodiiron proteins in photosynthetic organisms, *Biochem. J.* 476 (2019) 2487–2498.
- [11] C. Laureau, R. De Paep, G. Latouche, M. Moreno-Chacon, G. Finazzi, M. Kuntz, G. Cornic, P. Streb, Plastid terminal oxidase (PTOX) has the potential to act as a safety valve for excess excitation energy in the alpine plant species *Ranunculus glacialis* L., *Plant Cell Environ.* 36 (2013) 1296–1310.
- [12] P. Stepien, G.N. Johnson, Plastid terminal oxidase requires translocation to the grana stacks to act as a sink for electron transport, *Proc. Natl. Acad. Sci. U. S. A.* 115 (2018) 9634–9639.
- [13] K. Feilke, P. Streb, G. Cornic, F. Perreau, J. Kruk, A. Krieger-Liszskay, Effect of *Chlamydomonas* plastid terminal oxidase 1 expressed in tobacco on photosynthetic electron transfer, *Plant J.* 85 (2016) 219–228.
- [14] G.N. Johnson, P. Stepien, Plastid terminal oxidase as a route to improving plant stress tolerance: known knowns and known unknowns, *Plant Cell Physiol.* 57 (2016) 1387–1396.
- [15] C.M. Wetzel, C.Z. Jiang, L.J. Meehan, D.F. Voytas, S.R. Rodermel, Nuclear-organelle interactions: the immutans variegation mutant of *Arabidopsis* is plastid autonomous and impaired in carotenoid biosynthesis, *Plant J.* 6 (1994) 161–175.
- [16] P. Carol, D. Stevenson, C. Bisanz, J. Breitenbach, G. Sandmann, R. Mache, G. Coupland, M. Kuntz, Mutations in the *Arabidopsis* gene IMMUTANS cause a variegated phenotype by inactivating a chloroplast terminal oxidase associated with phytoene desaturation, *Plant Cell* 11 (1999) 43–55.
- [17] G. Peltier, L. Courneau, Chlororespiration, *Annu. Rev. Plant Biol.* 53 (2002) 523–550.
- [18] S. Kambakam, U. Bhattacharjee, J. Petrich, S. Rodermel, PTOX mediates novel pathways of electron transport in etioplasts of *Arabidopsis*, *Mol. Plant* 9 (2016) 1240–1259.
- [19] M. Renato, I. Pateraki, A. Boronat, J. Azcón-Bieto, Tomato fruit chromoplasts behave as respiratory bioenergetic organelles during ripening, *Plant Physiol.* 166 (2014) 920–933.
- [20] M. Grabsztunowicz, P. Mulo, F. Baumann, R. Mutoh, G. Kurisu, P. Sétif, P. Beyer, A. Krieger-Liszskay, Electron transport pathways in isolated chromoplasts from *Narcissus pseudonarcissus* L., *Plant J.* 99 (2019) 245–256.
- [21] A.E. McDonald, S. Amirsadeghi, G.C. Vanlerberghe, Prokaryotic orthologues of mitochondrial alternative oxidase and plastid terminal oxidase, *Plant Mol. Biol.* 53 (2003) 865–876.
- [22] P.M. Finnegan, A.L. Umbach, J.A. Wilce, Prokaryotic origins for the mitochondrial alternative oxidase and plastid terminal oxidase nuclear genes, *FEBS Lett.* 555 (2003) 425–430.
- [23] W.J. Nawrocki, N.J. Tourasse, A. Taly, F. Rappoport, F.A. Wollman, The plastid terminal oxidase: its elusive function points to multiple contributions to plastid physiology, *Annu. Rev. Plant Biol.* 66 (2015) 49–74.
- [24] A. Atteia, R. van Lis, J.J. Van Hellemond, A.G. Tielens, W. Martin, K. Henze, Identification of prokaryotic homologues indicates an endosymbiotic origin for the alternative oxidases of mitochondria (AOX) and chloroplasts (PTOX), *Gene* 330 (2004) 143–148.
- [25] A. Fu, S. Park, S. Rodermel, Sequences required for the activity of PTOX (IMMUTANS), a plastid terminal oxidase, *J. Biol. Chem.* 280 (2005) 42489–42496.
- [26] L. Meehan, K. Harkins, J. Chory, S. Rodermel, Lhcb transcription is coordinated with cell size and chlorophyll accumulation (studies on fluorescence-activated, cell-shorter-purified single cells from wild-type and immutans *Arabidopsis thaliana*), *Plant Physiol.* 112 (1996) 953–963.
- [27] C.M. Wetzel, S.R. Rodermel, Regulation of phytoene desaturase expression is

- independent of leaf pigment content in *Arabidopsis thaliana*, *Plant Mol. Biol.* 37 (1998) 1045–1053.
- [28] D. Wu, D.A. Wright, C. Wetzel, D.F. Voytas, S. Rodermel, The IMMUTANS variegation locus of *Arabidopsis* defines a mitochondrial alternative oxidase homolog that functions during early chloroplast biogenesis, *Plant Cell* 11 (1999) 43–55.
- [29] J. Barr, W.S. White, L. Chen, H. Bae, S. Rodermel, The GHOST terminal oxidase regulated developmental programming in tomato fruit, *Plant Cell Environ.* 27 (2004) 840–852.
- [30] G.P. Rédei, Somatic instability caused by cysteine-sensitive gene in *Arabidopsis*, *Science* 139 (1963) 767–769.
- [31] L. Houilles-Vernes, F. Rapaport, F.A. Wollman, J. Alric, X. Johnson, Plastid terminal oxidase 2 (PTOX2) is the major oxidase involved in chlororespiration in *Chlamydomonas*, *Proc. Natl. Acad. Sci. U. S. A.* 108 (2011) 20820–20825.
- [32] M. Shimamura, *Marchantia polymorpha*: taxonomy, phylogeny and morphology of a model system, *Plant Cell Physiol.* 57 (2016) 230–256.
- [33] J.L. Bowman, T. Kohchi, K.T. Yamato, J. Jenkins, S. Shu, K. Ishizaki, S. Yamaoka, R. Nishihama, Y. Nakamura, F. Berger, et al., Insights into land plant evolution garnered from the *Marchantia polymorpha* genome, *Cell* 171 (2017) 287–304.
- [34] R.C. Edgar, MUSCLE: multiple sequence alignment with high accuracy and high throughput, *Nucleic Acids Res.* 32 (2004) 1792–1797.
- [35] S.Q. Le, O. Gascuel, An improved general amino acid replacement matrix, *Mol. Biol. Evol.* 25 (2008) 1307–1320.
- [36] O. Gascuel, BIONJ: an improved version of the NJ algorithm based on a simple model of sequence data, *Mol. Biol. Evol.* 14 (1997) 685–695.
- [37] S. Kumar, G. Stecher, M. Li, C. Niyaz, K. Tamura, MEGA X: molecular evolutionary genetics analysis across computing platforms, *Mol. Biol. Evol.* 35 (2018) 1547–1549.
- [38] O.L. Gamborg, R.A. Miller, K. Ojima, Nutrient requirements of suspension cultures of soybean root cells, *Exp. Cell Res.* 50 (1968) 151–158.
- [39] S.S. Sugano, R. Nishihama, M. Shirakawa, J. Takagi, Y. Matsuda, S. Ishida, et al., Efficient CRISPR/Cas9-based genome editing and its application to conditional genetic analysis in *Marchantia polymorpha*, *PLoS One* 13 (2018) e0205117.
- [40] A. Kubota, K. Ishizaki, M. Hosaka, T. Kohchi, Efficient agrobacterium-mediated transformation of the liverwort *Marchantia polymorpha* using regenerating thalli, *Biosci. Biotechnol. Biochem.* 77 (2013) 167–172.
- [41] N.R. Baker, Chlorophyll fluorescence: a probe of photosynthesis *in vivo*, *Annu. Rev. Plant Biol.* 59 (2008) 89–113.
- [42] J.P. Krall, G.E. Edwards, Relationship between photosystem II activity and CO₂ fixation in leaves, *Physiol. Plant.* 86 (1992) 180–187.
- [43] C. Klughammer, U. Schreiber, An improved method, using saturating light pulses, for the determination of photosystem I quantum yield via P700⁺-absorbance changes at 830 nm, *Planta* 192 (1994) 261–268.
- [44] P.G. Falkowski, M.E. Katz, A.H. Knoll, A. Quigg, J.A. Raven, O. Schofield, F.J.R. Taylor, The evolution of modern eukaryotic phytoplankton, *Science* 305 (2004) 354–360.
- [45] G. Shimakawa, K. Ishizaki, S. Tsukamoto, M. Tanaka, T. Sejima, C. Miyake, The liverwort, *Marchantia*, drives alternative electron flow using a flavodiiron protein to protect PSI, *Plant Physiol.* 173 (2017) 1636–1647.
- [46] E. Derelle, C. Ferraz, S. Rombauts, P. Rouzé, A.Z. Worden, S. Robbens, F. Partensky, S. Degroev, S. Echeynié, R. Cooke, et al., Genome analysis of the smallest free-living eukaryote *Ostreococcus tauri* unveils many unique features, *Proc. Natl. Acad. Sci. U.S.A.* 103 (2006) 11647–11652.
- [47] A.E. McDonald, A.G. Ivanov, R. Bode, D.P. Maxwell, S.R. Rodermel, N.P. Hüner, Flexibility in photosynthetic electron transport: the physiological role of plastocyanin terminal oxidase (PTOX), *Biochim. Biophys. Acta Bioenerg.* 1807 (2011) 954–967.
- [48] M. Iwai, K. Takizawa, R. Tokutsu, A. Okamuro, Y. Takahashi, J. Minagawa, Isolation of the elusive supercomplex that drives cyclic electron flow in photosynthesis, *Nature* 464 (2010) 1210–1213.
- [49] J. Steinbeck, I.L. Ross, R. Rothnagel, P. Gäbelein, S. Schulze, N. Giles, R. Ali, R. Drysdale, E. Sierrecki, Y. Gambin, et al., Structure of a PSI-LHCI-cyt b₆f supercomplex in *Chlamydomonas reinhardtii* promoting cyclic electron flow under anaerobic conditions, *Proc. Natl. Acad. Sci. U. S. A.* 115 (2018) 10517–10522.
- [50] S. Bolte, E. Marcon, M. Jaunario, L. Moyet, M.T. Paternostre, M. Kuntz, A. Krieger-Liszky, Dynamics of the localization of the plastid terminal oxidase PTOX inside the chloroplast, *J. Exp. Bot.* (2020) (in press) eraa074.
- [51] T. Shiba, Y. Kido, K. Sakamoto, D.K. Inaoka, C. Tsuge, R. Tatsumi, G. Takahashi, E.O. Balogun, T. Nara, T. Aoki, et al., Structure of the trypanosome cyanide-insensitive alternative oxidase, *Proc. Natl. Acad. Sci. U. S. A.* 110 (2013) 4580–4585.

Messant et al

Supplementary Material Figure S1. Amino-acid sequence comparison of the region in plastid terminal oxidase (PTOX) used for the phylogenetic analysis in Fig. 1.

Glo MIRFLVSLVFDVLYKRRPFRPYVLETVARVPYFYSLSVHLHYETLQGRKSDMLKVFHFAEWSNEHLHLLIMESLGGDNRWDRLKASLVAIVYVIVLVMISPRSAVYFMQVEEHAHPTDYDFLSDGEKRLQAPAVVAVSYITDGLDMFDEQTSRPFERRPACDLVDVFNIRDRBAEIVKTMACAKRNALQTFKSPH--
Ana MIKLVGLVLYVYVYVYKRRPFRPYVLETVARVPYFYSLSVHLHYETLQGRKSDMLKVFHFAEWSNEHLHLLIMESLGGDNRWDRLKASLVAIVYVIVLVMISPRSAVYFMQVEEHAHPTDYDFLSDGEKRLQAPAVVAVSYITDGLDMFDEQTSRPFERRPACDLVDVFNIRDRBAEIVKTMACAKRNALQTFKSPH--
Nos MIKLVGLVLYVYVYVYKRRPFRPYVLETVARVPYFYSLSVHLHYETLQGRKSDMLKVFHFAEWSNEHLHLLIMESLGGDNRWDRLKASLVAIVYVIVLVMISPRSAVYFMQVEEHAHPTDYDFLSDGEKRLQAPAVVAVSYITDGLDMFDEQTSRPFERRPACDLVDVFNIRDRBAEIVKTMACAKRNALQTFKSPH--
Osta MNEKLIASAVAVDYLKAGRSYARFVLETVARVPYFYSLSVHLHYETLQGRKSDMLKVFHFAEWSNEHLHLLIMESLGGDNRWDRLKASLVAIVYVIVLVMISPRSAVYFMQVEEHAHPTDYDFLSDGEKRLQAPAVVAVSYITDGLDMFDEQTSRPFERRPACDLVDVFNIRDRBAEIVKTMACAKRNALQTFKSPH--
Klea INHALDVFVILLDAFYADRRYARFVLETVARVPYFYSLSVHLHYETLQGRKSDMLKVFHFAEWSNEHLHLLIMESLGGDNRWDRLKASLVAIVYVIVLVMISPRSAVYFMQVEEHAHPTDYDFLSDGEKRLQAPAVVAVSYITDGLDMFDEQTSRPFERRPACDLVDVFNIRDRBAEIVKTMACAKRNALQTFKSPH--
Mara FNTFATETVKIETLVAKRLYARFVLETVARVPYFYSLSVHLHYETLQGRKSDMLKVFHFAEWSNEHLHLLIMESLGGDNRWDRLKASLVAIVYVIVLVMISPRSAVYFMQVEEHAHPTDYDFLSDGEKRLQAPAVVAVSYITDGLDMFDEQTSRPFERRPACDLVDVFNIRDRBAEIVKTMACAKRNALQTFKSPH--
Azoa FNVLIDSVLLELDALADRRYSRPFVLETVARVPYFYSLSVHLHYETLQGRKSDMLKVFHFAEWSNEHLHLLIMESLGGDNRWDRLKASLVAIVYVIVLVMISPRSAVYFMQVEEHAHPTDYDFLSDGEKRLQAPAVVAVSYITDGLDMFDEQTSRPFERRPACDLVDVFNIRDRBAEIVKTMACAKRNALQTFKSPH--
Sal FNSLIDTVIRLLDVAVYDRYARFVLETVARVPYFYSLSVHLHYETLQGRKSDMLKVFHFAEWSNEHLHLLIMESLGGDNRWDRLKASLVAIVYVIVLVMISPRSAVYFMQVEEHAHPTDYDFLSDGEKRLQAPAVVAVSYITDGLDMFDEQTSRPFERRPACDLVDVFNIRDRBAEIVKTMACAKRNALQTFKSPH--
Vna VNFILDSVKIIDLFDKRTYARFVLETVARVPYFYSLSVHLHYETLQGRKSDMLKVFHFAEWSNEHLHLLIMESLGGDNRWDRLKASLVAIVYVIVLVMISPRSAVYFMQVEEHAHPTDYDFLSDGEKRLQAPAVVAVSYITDGLDMFDEQTSRPFERRPACDLVDVFNIRDRBAEIVKTMACAKRNALQTFKSPH--
Ory VNFILDSVKIIDLFDKRTYARFVLETVARVPYFYSLSVHLHYETLQGRKSDMLKVFHFAEWSNEHLHLLIMESLGGDNRWDRLKASLVAIVYVIVLVMISPRSAVYFMQVEEHAHPTDYDFLSDGEKRLQAPAVVAVSYITDGLDMFDEQTSRPFERRPACDLVDVFNIRDRBAEIVKTMACAKRNALQTFKSPH--
Zea INSVLTSTVWVLLDLYVHDTQYRPFVLETVARVPYFYSLSVHLHYETLQGRKSDMLKVFHFAEWSNEHLHLLIMESLGGDNRWDRLKASLVAIVYVIVLVMISPRSAVYFMQVEEHAHPTDYDFLSDGEKRLQAPAVVAVSYITDGLDMFDEQTSRPFERRPACDLVDVFNIRDRBAEIVKTMACAKRNALQTFKSPH--
Nana FNIFLDSVKIMLKVYGRYARFVLETVARVPYFYSLSVHLHYETLQGRKSDMLKVFHFAEWSNEHLHLLIMESLGGDNRWDRLKASLVAIVYVIVLVMISPRSAVYFMQVEEHAHPTDYDFLSDGEKRLQAPAVVAVSYITDGLDMFDEQTSRPFERRPACDLVDVFNIRDRBAEIVKTMACAKRNALQTFKSPH--
Phaa NRKALVHQKLVDFQYVDRARFVLETVARVPYFYSLSVHLHYETLQGRKSDMLKVFHFAEWSNEHLHLLIMESLGGDNRWDRLKASLVAIVYVIVLVMISPRSAVYFMQVEEHAHPTDYDFLSDGEKRLQAPAVVAVSYITDGLDMFDEQTSRPFERRPACDLVDVFNIRDRBAEIVKTMACAKRNALQTFKSPH--
Thaa ANRFALGELKTIYFDFEDRAVYARFVLETVARVPYFYSLSVHLHYETLQGRKSDMLKVFHFAEWSNEHLHLLIMESLGGDNRWDRLKASLVAIVYVIVLVMISPRSAVYFMQVEEHAHPTDYDFLSDGEKRLQAPAVVAVSYITDGLDMFDEQTSRPFERRPACDLVDVFNIRDRBAEIVKTMACAKRNALQTFKSPH--
Coc IINVAITLVYVWVLYKRRPFRPYVLETVARVPYFYSLSVHLHYETLQGRKSDMLKVFHFAEWSNEHLHLLIMESLGGDNRWDRLKASLVAIVYVIVLVMISPRSAVYFMQVEEHAHPTDYDFLSDGEKRLQAPAVVAVSYITDGLDMFDEQTSRPFERRPACDLVDVFNIRDRBAEIVKTMACAKRNALQTFKSPH--
Ostb LLKAPYALCMLKLEKTFYARFVLETVARVPYFYSLSVHLHYETLQGRKSDMLKVFHFAEWSNEHLHLLIMESLGGDNRWDRLKASLVAIVYVIVLVMISPRSAVYFMQVEEHAHPTDYDFLSDGEKRLQAPAVVAVSYITDGLDMFDEQTSRPFERRPACDLVDVFNIRDRBAEIVKTMACAKRNALQTFKSPH--
Ch1 LKSYVLSLCLLDLYENRPFYARFVLETVARVPYFYSLSVHLHYETLQGRKSDMLKVFHFAEWSNEHLHLLIMESLGGDNRWDRLKASLVAIVYVIVLVMISPRSAVYFMQVEEHAHPTDYDFLSDGEKRLQAPAVVAVSYITDGLDMFDEQTSRPFERRPACDLVDVFNIRDRBAEIVKTMACAKRNALQTFKSPH--
Ch2 WKAPFFALCVLMDVYKKAIEKFWLETVARVPYFYSLSVHLHYETLQGRKSDMLKVFHFAEWSNEHLHLLIMESLGGDNRWDRLKASLVAIVYVIVLVMISPRSAVYFMQVEEHAHPTDYDFLSDGEKRLQAPAVVAVSYITDGLDMFDEQTSRPFERRPACDLVDVFNIRDRBAEIVKTMACAKRNALQTFKSPH--
Vol1 FIKVYFVLCVLLDLYENRPFYARFVLETVARVPYFYSLSVHLHYETLQGRKSDMLKVFHFAEWSNEHLHLLIMESLGGDNRWDRLKASLVAIVYVIVLVMISPRSAVYFMQVEEHAHPTDYDFLSDGEKRLQAPAVVAVSYITDGLDMFDEQTSRPFERRPACDLVDVFNIRDRBAEIVKTMACAKRNALQTFKSPH--
Vol2 WKAPFFALCVLMDVYKKAIEKFWLETVARVPYFYSLSVHLHYETLQGRKSDMLKVFHFAEWSNEHLHLLIMESLGGDNRWDRLKASLVAIVYVIVLVMISPRSAVYFMQVEEHAHPTDYDFLSDGEKRLQAPAVVAVSYITDGLDMFDEQTSRPFERRPACDLVDVFNIRDRBAEIVKTMACAKRNALQTFKSPH--
Kleb YILGFFVFLCLLDLYENRPFYARFVLETVARVPYFYSLSVHLHYETLQGRKSDMLKVFHFAEWSNEHLHLLIMESLGGDNRWDRLKASLVAIVYVIVLVMISPRSAVYFMQVEEHAHPTDYDFLSDGEKRLQAPAVVAVSYITDGLDMFDEQTSRPFERRPACDLVDVFNIRDRBAEIVKTMACAKRNALQTFKSPH--
Marb WILGFFVFLCLLDLYENRPFYARFVLETVARVPYFYSLSVHLHYETLQGRKSDMLKVFHFAEWSNEHLHLLIMESLGGDNRWDRLKASLVAIVYVIVLVMISPRSAVYFMQVEEHAHPTDYDFLSDGEKRLQAPAVVAVSYITDGLDMFDEQTSRPFERRPACDLVDVFNIRDRBAEIVKTMACAKRNALQTFKSPH--
Azob HILGFFVFLCLLDLYENRPFYARFVLETVARVPYFYSLSVHLHYETLQGRKSDMLKVFHFAEWSNEHLHLLIMESLGGDNRWDRLKASLVAIVYVIVLVMISPRSAVYFMQVEEHAHPTDYDFLSDGEKRLQAPAVVAVSYITDGLDMFDEQTSRPFERRPACDLVDVFNIRDRBAEIVKTMACAKRNALQTFKSPH--
Nanb FVILPYLCAFLDLYVYEGRFLARFVLETVARVPYFYSLSVHLHYETLQGRKSDMLKVFHFAEWSNEHLHLLIMESLGGDNRWDRLKASLVAIVYVIVLVMISPRSAVYFMQVEEHAHPTDYDFLSDGEKRLQAPAVVAVSYITDGLDMFDEQTSRPFERRPACDLVDVFNIRDRBAEIVKTMACAKRNALQTFKSPH--
Phab VIKIPLYLCLMDLYVYEGRFLARFVLETVARVPYFYSLSVHLHYETLQGRKSDMLKVFHFAEWSNEHLHLLIMESLGGDNRWDRLKASLVAIVYVIVLVMISPRSAVYFMQVEEHAHPTDYDFLSDGEKRLQAPAVVAVSYITDGLDMFDEQTSRPFERRPACDLVDVFNIRDRBAEIVKTMACAKRNALQTFKSPH--
Thab IIKIPLYLCLMDLYVYEGRFLARFVLETVARVPYFYSLSVHLHYETLQGRKSDMLKVFHFAEWSNEHLHLLIMESLGGDNRWDRLKASLVAIVYVIVLVMISPRSAVYFMQVEEHAHPTDYDFLSDGEKRLQAPAVVAVSYITDGLDMFDEQTSRPFERRPACDLVDVFNIRDRBAEIVKTMACAKRNALQTFKSPH--
Cya1 ISRVYTLACRFLDAPDFRVARFVLETVARVPYFYSLSVHLHYETLQGRKSDMLKVFHFAEWSNEHLHLLIMESLGGDNRWDRLKASLVAIVYVIVLVMISPRSAVYFMQVEEHAHPTDYDFLSDGEKRLQAPAVVAVSYITDGLDMFDEQTSRPFERRPACDLVDVFNIRDRBAEIVKTMACAKRNALQTFKSPH--
Cya2 ISRVYTLACRFLDAPDFRVARFVLETVARVPYFYSLSVHLHYETLQGRKSDMLKVFHFAEWSNEHLHLLIMESLGGDNRWDRLKASLVAIVYVIVLVMISPRSAVYFMQVEEHAHPTDYDFLSDGEKRLQAPAVVAVSYITDGLDMFDEQTSRPFERRPACDLVDVFNIRDRBAEIVKTMACAKRNALQTFKSPH--
Ch1a KLGKVFCLVYVYKRRPFRPYVLETVARVPYFYSLSVHLHYETLQGRKSDMLKVFHFAEWSNEHLHLLIMESLGGDNRWDRLKASLVAIVYVIVLVMISPRSAVYFMQVEEHAHPTDYDFLSDGEKRLQAPAVVAVSYITDGLDMFDEQTSRPFERRPACDLVDVFNIRDRBAEIVKTMACAKRNALQTFKSPH--
Araa LRIKAYLWRFVLETVARVPYFYSLSVHLHYETLQGRKSDMLKVFHFAEWSNEHLHLLIMESLGGDNRWDRLKASLVAIVYVIVLVMISPRSAVYFMQVEEHAHPTDYDFLSDGEKRLQAPAVVAVSYITDGLDMFDEQTSRPFERRPACDLVDVFNIRDRBAEIVKTMACAKRNALQTFKSPH--

Red brown shadings represent iron-binding sites. Green box indicates the insert specific to PTOX. Organisms included in the alignment are as follows: cyanobacteria *Gloeobacter violaceus* (Glo), *Anabaena cylindrica* (Ana), and *Nostoc* sp. (Nos); green algae *Coccomyxa subellipsoidea* (Coc), *Ostreococcus tauri* (Ost), *Chlamydomonas reinhardtii* (Chl), and *Volvox carterii* (Vol); the charophyte alga *Klebsormidium nitens* (Kle); the liverwort *Marchantia polymorpha* (Mar); ferns *Azolla filiculoides* (Azo) and *Salvinia cucullata* (Sal); angiosperms *Arabidopsis thaliana* (Ara), *Oryza sativa* (Ory), *Zostera marina* (Zos), and *Zea mays* (Zea); the eustigmatophyte alga *Nannochloropsis oceanica* (Nan); diatoms *Phaeodactylum tricornerutum* (Pha) and *Thalassiosira pseudonana* (Tha); and the red alga *Cyanidioschyzon merolae* (Cya). Alternative oxidase (AOX) in *Chlamydomonas reinhardtii* (AOX1) and *Arabidopsis thaliana* (AOX1A) are also included in the analysis (ChlA and AraA).

Supplementary Material Fig. S2. Mutations generated by CRISPR/Cas9 system in genome editing in *M. polymorpha* deficient in plastid terminal oxidases a (*ptoxa*) and b (*ptoxb*).

>PTOXa
 ATGGCGTCTGGTCTGAGGATTGCTCCTCTGAATTGTGTATATAATCGTGTGTGCCATCGGAGTCCCAAGGTTT
 TGGCTGTTGCACCCGAACGGGTCGGAATGGGCCGATTTGGCTGTGGCGGGAAAGCCCGTTCGATTCACCTCGC
 AGTTTGTGGGGTCAGGAAATCTTTGCAGCTTCTCTTGACGAGCTCGATTCGAAAGCGGGTCTCGTGTGCGC
 ACATTCAGAAGCGGGATGACCGTCCCTAAGTCAGTCTTGCAGAAGAGCCATTATTGAAATGAGGAATCGCC
 TCAAGGTTTGGAGAAGTGGGTGATTGCTGCGGAACATGGATTCAACACCTTTGCCACTGAGACTGTTGTGAAGA
 TACTAGAGACTCTGTACGCGAAGCGCTTGTACGCAAGGTTTACGTTTATAGAAACCATCGCGAGAGTTCCGTAC
 TTTGCTTTTGTATCGGTTT**TACACATGTACGAGAGCTTTGGTTG**GTGGAGACGGGCGGACTACATCAAAATTCA
 CTTTGCAGAAAGCTGGAATGAACTACATCATCTTCTGGTTATGGAGGCTCTAGGTGGAGACGAGAGGTGGATCG
 ATAGATTTTTGGCTCAGCACATTGCCGTTGCATACTATCTTCTTACTGTATTAATGTATCTCCTTAGCCCTAGA
 ATGGCATACCATTTCTCAGAATGTGTCGAGAAGCATGCTTTTCTACTTACGATAAGTTCATAAAGTCACATGG
 AGATGAGTTGAAGCTGCTTCTGCTCCGGAGGTCGAGTCCAAATATTATACTAAGGGAGATCTATACATGTTTG
 ATGAATTTCAAAGTCCATTGAACCGAACACAAGAAGACCAAGATAGAAAATCTTTATGACGTTTTCTGTGAAC
 ATTCGTGAAGACGAAGCGCAGCATTGCAAGACAATGCATGCCCTGTCAATCGGGGAAAAGTTTGAGGTCTCCACA
 TAGAGACGCTCCTTACAGAGATAGCTGATGACGAGAAGATTCTCCTCCAGCGGATTTGTGAAGGCCTATTTG
 AATGTGCCACCACAGCCACTTCGTTTCGAGACAGGGCACGGAACTAGGAGTAGAAAATCTTGTGCGAAAAATC
 GACGGATCAGAGTTATGA

Δptoxa.1 A-----

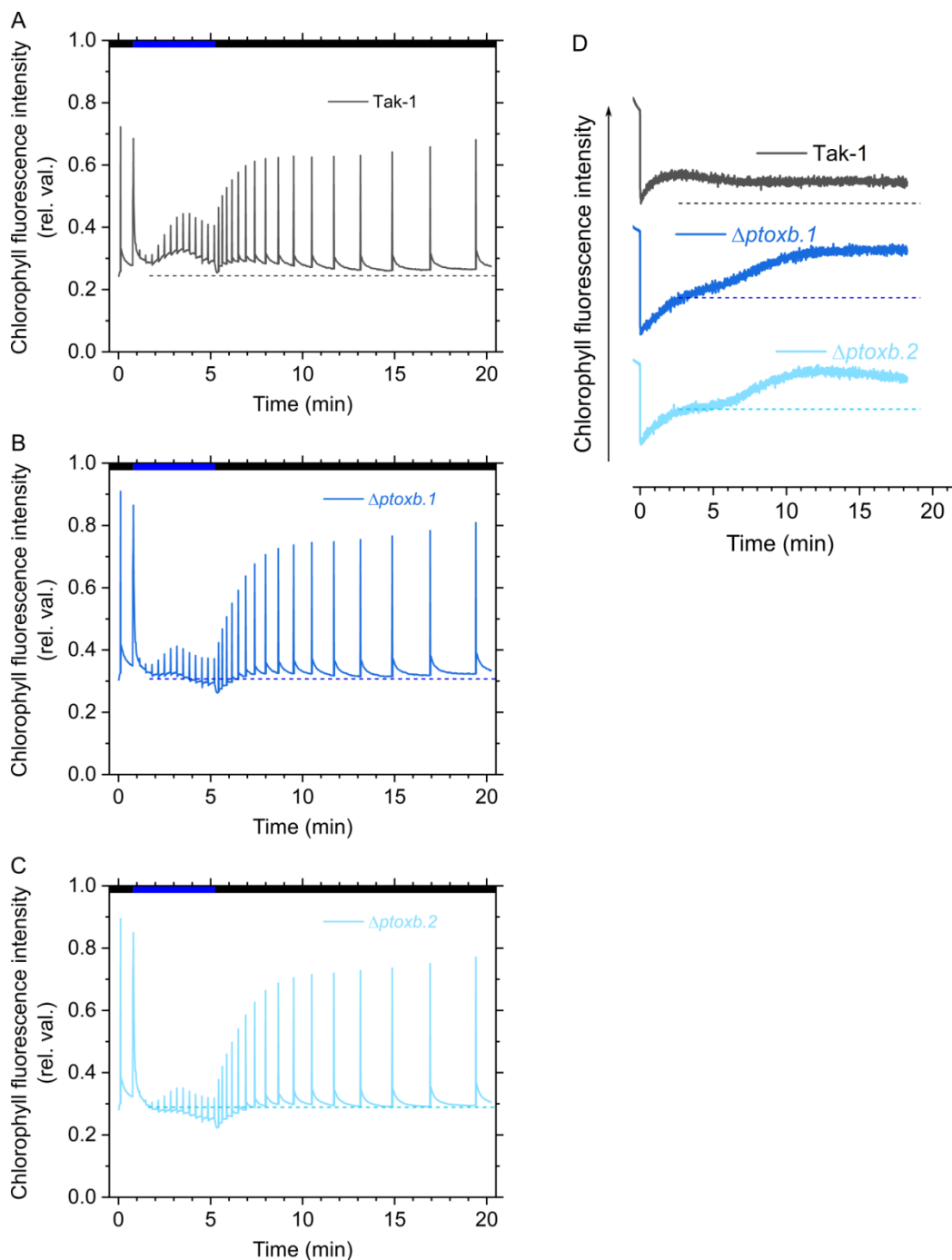
>PTOXb
 ATGGGCAGTCTGCCGCATGCATGCTTCTGGCCAGGACTGGACCGTCCGTTGCGCTTTCCACACCTCCCAGTTC
 CGCTGCTACCGACTGCACGGCTGCAGCTTCTTTGAGGTGGAGGATGCCGCTCGATTGTTGCTCATTAGGTCGG
 AGGATCATCTCTGAAGCTCTCGTTAACAGGTTTGAGCAGGCGGGAGAAAATTTGGCAGCTCTAGCTGCTCAAAC
 CTCTCAGTCCGTGCCCTTCAAAGAACGCCATATCAACAGAAGACGATAGTTCCTGTGATGAGTAGCGTCCGTTG
 GAAGGTCCTTGAGCACGAAGTGAATGAAATCACAGAGATTGGGGAGCGACGAGAGCTCTGCCGATCACTCTG
 GAACAGCAAAGCGAGGAGGCTTTGCCAAAGAGAATCCAGTTTATTACGGGTTTCAGGCAGATTTCTCCGAACG
 GGACCGACAGTTCCACAAAACGTTTTCAAGCTCGCGTTCGAGAATTTTGGGAGAGAATGGCGGGCTCTGCGACG
 AAGTTACTTATTTTCAGTATTGAAGCCAATTCGCCCCGGGAGATTGAGGGCGGCCCTTTTCAGTTAGTGGGAG
 CATAACCGGGCGAGGCTTGATTTTGTCTGCGGGGACTGGATAAGTTTGTACTTTGTATGACGGTCTGAAA
 GAGATACAGCCTGTGAAACAACAACCGAACATTGAGCAAGATGAGCTTAGGGAGCAATTAAGAAGCTGAAGTT
 AAGTAACAAAAGGTGTGGGAGAGGGAGAAAGCTCGAGAACAAGTGG**AAGCACCTTGGTGGATTCT**CGGCCAT
 ATTACTTCTGTGTTGGATGCTGGACGTGATTCGAGGACAGGCCAATTCAGCGTTTTTGGTTTTTGAAACT
 GTCGCACGGATGCCCTACTTCTCATATATTTCTATGCTCCACCTGTACGAAACGCTTGGCTGGTGGCGTTCAGG
 AGCAGAAGTGCACAAAGTCCACTTTGACAGGAGTGAATGAAATGCATCATCTCAAAAATAATGGAATCACTTG
 GAGGAGATCTTGAATGGGAGACAGATTTTTCGACAGCATGCTGCTTCTTCTACTACTGGACCTGAACGCA
 ATGTTTTTGTATACCCACGGTTCGCTACAATTTTTCAGAACTTATCGAGTCACATGCATCGATACTTACCGG
 AGAATTTGCTGATGAGAATGAAGAGCTGCTGAAAACGCTGCCCTTCTCCAGTTGCAGTAGCTACTATGAGA
 GTGGAGATTTATACATGTATGATGAGTTTCAAACAAGTCGACTCCAGAATCTCGACGGCCCAAGATGGGTAGT
 TTGTACGATGTTTTTCATGCCATTGTGGTGTGATGAAGGGGAGCATGTGAAGACAATGGTGGCTTTCACACAGCT
 TGATA**CCAGGTTGTGAGTCCAA**CGGGTCAAGTACAGTGGCCAGAAAGTAGAAACGGAAGTCCGAAATACCCG
 ACCGCTGCCGTGA

Δptoxb.1 AAA

Δptoxb.2 T-

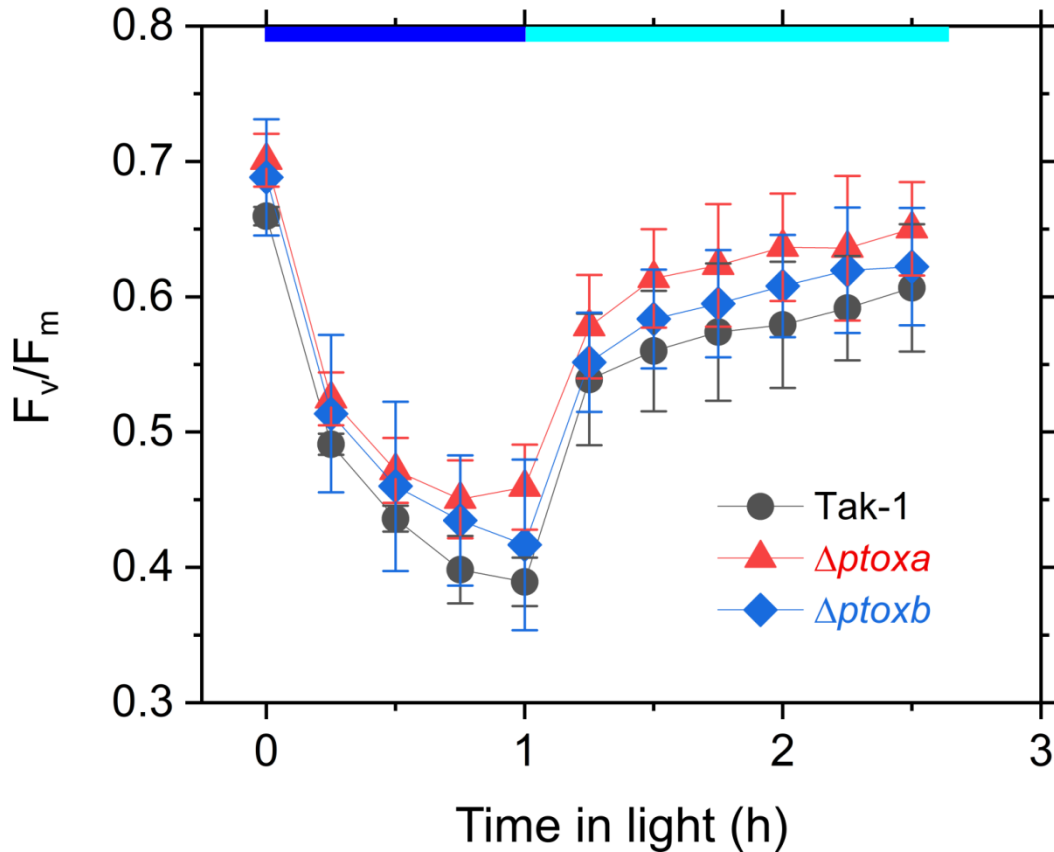
Targeted regions in open reading frames of PTOXa and b are shown by red. In the *Δptoxa.1* (so-called *Δptoxa*) and *Δptoxb.2* mutants, the mutations occurred at the motif containing the catalytic sites. In the *Δptoxb.1* mutant (so-called *Δptoxb*), the mutation occurred at the C-terminal region. We predict that the protein is expressed in a form with a part of the C-terminal region replaced 39 by different amino-acid residues if transcription and translation were not affected at all.

Supplementary Material Fig. S3. Representative results in the other line of the *M. polymorpha* mutant deficient in plastid terminal oxidases b (Δ *ptoxb.2*).

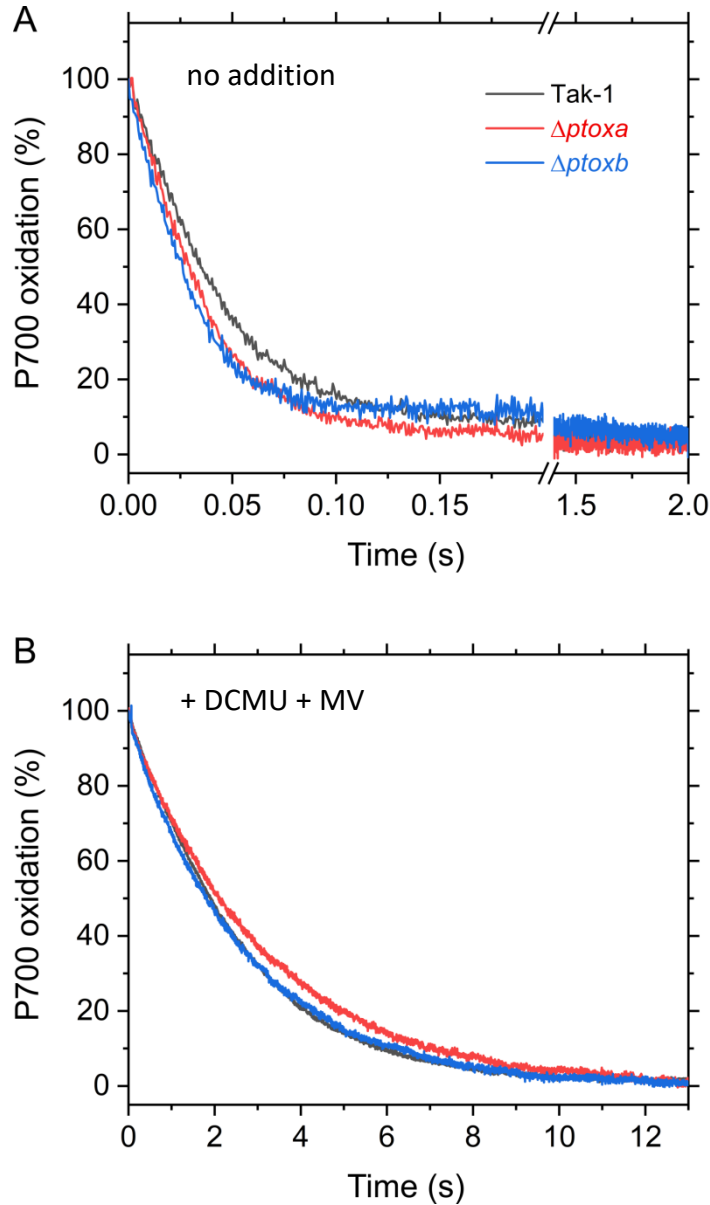


(A–C) Response of chlorophyll fluorescence to the light. An actinic blue light ($230 \mu\text{mol photons m}^{-2} \text{s}^{-1}$) was given to the *M. polymorpha* wild type (Tak-1; A), Δ *ptoxb.1* (B), and Δ *ptoxb.2* (C) as indicated by blue bars. (D) Post illumination fluorescence rise after illuminations with actinic red light ($800 \mu\text{mol photons m}^{-2} \text{s}^{-1}$, 10 min) in Tak-1 (black), Δ *ptoxb.1* (blue), and Δ *ptoxb.2* (sky blue). Before the measurements, the plants were adapted to the dark for 5 min, and dashed lines indicate the chlorophyll fluorescence levels before illumination. Experiments were conducted independently three times (biological replicates), and representative traces are shown.

Supplementary Material Fig. S4. Photoinhibition of PSII



Photoinhibition of PSII in the *M. polymorpha* wild type (Tak-1; black) and the mutants deficient in plastid terminal oxidases a ($\Delta ptoxa$; red) and b ($\Delta ptoxb$; blue). Thalli of *M. polymorpha* were exposed to high light ($600 \mu\text{mol photons m}^{-2} \text{s}^{-1}$) for 1 h and thereafter to low light ($15 \mu\text{mol photons m}^{-2} \text{s}^{-1}$) as indicated by blue and light blue bars. The chlorophyll fluorescence parameter F_v/F_m was determined after a dark adaptation for 5 min. Data are represented as the mean \pm SD, $n = 3$ (biological replicates).

Supplementary Material Fig. S5. P700⁺ reduction

P700⁺ re-reduction after illumination with far-red light. Representative traces of *M. polymorpha* wild type (Tak-1, black) and the mutants deficient in plastid terminal oxidases a ($\Delta ptoxa$; red) and b ($\Delta ptoxb$; blue) are shown. A: no inhibitors present, measurement performed in fast acquisition mode, average of 3 measures are shown; B: incubation of the thalli with 100 μ M DCMU, 500 μ M methylviologen.

To conclude, we have demonstrated the presence of two PTOX types in photosynthetic organisms: plant and alga-type PTOX, the latter of which have a N-terminus (Nter) elongation. *Marchantia polymorpha* has the particularity of having two isoforms belonging to each of the two types mentioned above, which only have 50% sequence identity between them. Fluorescence measurements have shown that the two simple mutations cause an increase in the reduction of the plastoquinone pool as well as an increase in chlororespiration and/or cyclic electron flow. These observations suggest that the two isoforms play a similar role in plants and are able to complement each other to some extent. On the other hand, the $\Delta ptox_b$ mutant is more heavily affected in the electron transport rate, non-photochemical quenching and exhibits a significant increase in the amount of certain carotenoids. Together, these data suggest that the two isoforms are not completely complementary.

II) Characterization of *Δptoxptoxb* double mutants in *Marchantia polymorpha*

As explained in the previous article (Messant *et al.*, 2021), *Marchantia polymorpha* has two distinct PTOX proteins, one of which (PTOXa) has the characteristics of the unique protein conserved in Angiosperms such as *Arabidopsis thaliana* while the other (PTOXb) resembles of both isoforms present in green algae such as *Chlamydomonas reinhardtii*. To date, it has been demonstrated that the mutation of the unique PTOX in Angiosperms leads to a visible variegation phenotype on the leaves (*Arabidopsis thaliana*) (Rédei, 1975) or even the fruits (*Solanum lycopersicum*) (Barr *et al.*, 2004). This mutation has many consequences in terms of protection of the photosynthetic chain against over reduction. Although no visible phenotype was observed in both *Marchantia polymorpha* single mutants, the two proteins impacts also the photosynthetic chain protection but in a slightly different way (see article above). On the other hand, no CrPTOX1 mutant could be obtained (Houille-Vernes *et al.*, 2011). Thus, to date, no study has highlighted the exact role of each plant and alga-type PTOX isoforms and to explain why it is the plant-type one which has been retained during evolution.

In this article, we generated two different biological materials. First, the mutant of the unique PTOX of *Arabidopsis (Immutans)* was transformed to express the bacterial desaturase CRTI, allowing to overcome the impact of the mutation on carotenoid biosynthesis. Secondly, I managed to obtain for the first time a PTOX double mutant in *Marchantia polymorpha*. Chlorophyll fluorescence of PSII and PSI absorption measurements demonstrated that PTOX protects against PSI photoinhibition and not of PSII. Finally, the activities of the recombinant proteins PTOXb and PTOXb truncated in Nter were measured.

Article 3: PTOX proteins are involved in PSI photoinhibition protection in *Marchantia polymorpha*: study of the first PTOX double mutant (submitted)

I participated in obtaining double mutants by carrying out molecular biology for CRISPR/Cas9 as well as plant transformation. I also participated in the characterization by trying to find the conditions to generate a phenotype and carried out some measurements.

1 **Plastid Terminal Oxidase (PTOX) protects photosystem I and not photosystem II against**
2 **photoinhibition in *Arabidopsis thaliana* and *Marchantia polymorpha***

3
4 Marine Messant¹, Thanh-Lan Lai¹, Adjélé Wilson¹, Ginga Shimakawa^{1,2}, Anja Krieger-Liszkay^{1,*}

5
6 ¹Université Paris-Saclay, Institute for Integrative Biology of the Cell (I2BC), CEA, CNRS, 91198 Gif-sur-
7 Yvette cedex, France

8 ²Department of Bioscience, School of Biological and Environmental Sciences, Kwansei-Gakuin
9 University, 1 Gakuen-Uegahara, Sanda, Hyogo 669-1330, Japan

10
11 *Corresponding author: phone: +33 1 6908 1803; E-mail: anja.liszkay@i2bc.paris-saclay.fr

12
13
14 **Abstract**

15 The plastid terminal oxidase PTOX controls the oxidation level of the plastoquinone pool in the
16 thylakoid membrane and acts as a safety valve upon abiotic stress, but detailed characterization of its
17 role in protecting the photosynthetic apparatus is limited. Here we used PTOX mutants in two model
18 plants *Arabidopsis thaliana* and *Marchantia polymorpha*. We created a green *Arabidopsis* PTOX
19 mutant expressing the bacterial carotenoid desaturase CRTI and a double mutant in *Marchantia*
20 lacking the plant-type and the alga-type PTOX enzymes. In both species, lack of PTOX affected the
21 redox state of the plastoquinone pool. Exposure of plants to high light intensity showed higher
22 susceptibility of photosystem I to light-induced damage in the absence of PTOX while photosystem II
23 was more stable demonstrating that PTOX plays a pro-oxidant and an anti-oxidant role *in vivo*. Our
24 results shine new light on the function of PTOX in protection of photosystem I and II.

25
26 **Introduction**

27 In nature, plants have to cope with sudden changes in light intensity. Light intensities higher than
28 needed for CO₂ assimilation saturate the photosynthetic electron transport chain and can cause
29 oxidative stress leading to damage of the photosystems. Photosynthetic organisms have a multitude
30 of regulation mechanisms to protect the photosynthetic apparatus in excess light. Among these
31 protection mechanisms there are processes that lead to the dissipation of excess energy as heat, down
32 regulation of the photosynthetic electron transport and even the degradation and repair of
33 photosystem II (PSII) that is sacrificed protecting photosystem I (PSI) against photodamage^{1,2}. PSII,
34 different to PSI, has an efficient damage repair cycle so that damage of PSII is not very costly³.
35 Alternative electron transport routes like cyclic electron flow and Mehler/Mehler-like reactions are
36 important to protect PSI against photoinhibition⁴. Furthermore, the plastid terminal oxidase PTOX has
37 been shown to be an important sink for electrons upon stress⁵⁻⁷. PTOX is a non-heme diiron carboxylate

38 enzyme that catalyzes the oxidation of plastoquinol, reducing oxygen to water. Depending on the
39 quinol availability, it can have an anti-oxidant or a pro-oxidant function as has been shown *in vitro*
40 using recombinant PTOX protein⁸. Upregulation of PTOX expression has been reported for several
41 stress-tolerant plant species acclimated to harsh environments such as drought, high light and high
42 temperature^{9, 10}, high salinity⁵, low temperature^{7, 11}, and high levels of UV light¹². PTOX is believed to
43 act as a stress-induced safety valve that keeps the acceptor side of PSII oxidized, thereby helping to
44 protect PSII from photodamage^{5,7,9-12}. However, overexpression of PTOX1 from *Chlamydomonas*
45 *reinhardtii* promotes photoinhibition via the production of reactive oxygen species^{13,14} while
46 overexpression of PTOX from *A. thaliana* does not alter the light susceptibility of PSII¹⁵.

47 The genome of angiosperms encodes one PTOX while most other photosynthetic organisms possess
48 two isoforms that can either be closely related or belong to a plant-type or an alga-type family. The
49 liverwort *Marchantia polymorpha*, the basal land plant evolutionarily located between green algae and
50 plants, contains two isoforms, a plant-type named PTOXa, and an alga-type isoform named PTOXb¹⁶.
51 PTOX mutants called *immutans* (*im*) in *Arabidopsis thaliana* and *ghost* in tomato show, depending on
52 the light intensity, a very strong variegated phenotype^{17,18}. PTOX is crucial for carotenoid biosynthesis
53 Plant desaturases¹⁸. Plant carotenoid desaturases use plastoquinone (PQ) as electron acceptor and
54 depend on PTOX for reoxidation of plastoquinol (PQH₂) to PQ. Single mutants of PTOX in *Marchantia*
55 or in *Chlamydomonas reinhardtii* show normal pigmentation^{16,19}. The regulation of PTOX activity may
56 differ between plant-type and alga-type PTOX. While the catalytic center is well conserved, alga-type
57 PTOX has an N-terminal extension probably anchoring PTOX permanently to the membrane. Plant-
58 type PTOX has been shown to migrate either within the thylakoid membrane from stroma lamellae to
59 grana stacks⁶ or associate to the thylakoid membrane only in the presence of a high proton motive
60 force where it can have access to its substrate PQH₂²⁰.

61 The importance of PTOX for protection of the photosynthetic apparatus against photoinhibition
62 remains unclear. Here we use PTOX mutants of *Arabidopsis* and *Marchantia* to study the susceptibility
63 of the photosynthetic apparatus to high light stress. To overcome the strong impact on carotenoid
64 biosynthesis in *im*, we crossed *im* with *Arabidopsis* expressing the bacterial carotene desaturase
65 (CRTI)²¹. CRTI introduces conjugation in phytoene by adding four double bonds using directly O₂ as
66 electron acceptor and, therefore, being independent of PQ. In addition, we generated double mutants
67 of PTOXa and PTOXb in *Marchantia* to show the importance of PTOX in an organism that contains,
68 different to angiosperms, flavodiiron enzymes allowing Mehler-like reaction as additional route of
69 alternative electron flow and keeping the electron transport chain oxidized. Furthermore, we
70 determined the enzymatic activity of both, PTOXa and PTOXb using an *in vitro* approach.

71

72 **Results**

73 **PTOX affects the redox state of the electron transport chain in *A. thaliana* and *M. polymorpha*.**

74 We crossed *im* with *Arabidopsis* expressing the bacterial carotene desaturase (CRTI) and used
75 chlorophyll fluorescence induction curves and post-illumination fluorescence for screening the F2
76 generation (Fig. 1). Mutants lacking PTOX in the F2 generation of the *im*CRTI lines show
77 homogeneously green leaves under normal growth light and also under fluctuating light (SI Fig. S1). Two
78 *im*CRTI lines were selected for this study hereafter called *im*CRTI_1 and *im*CRTI_2. In both lines, the
79 maximum level of chlorophyll fluorescence was reached faster in the *im*CRTI lines than in the wild type,
80 Col-0 (Fig. 1b). This shows that less PQ is available for reduction in the mutant. Moreover, the so-called
81 post-illumination fluorescence rise is higher in *im*CRTI than in Col-0, reflecting a more reduced PQ pool
82 due to the absence of PTOX activity.

83 *Marchantia* $\Delta ptoxaptobx_1$ and $\Delta ptoxaptobx_2$ construction is shown Fig. 2a. Different to *Arabidopsis*,
84 PTOX mutants in *Marchantia* do not show a phenotype independent of the light regime (Fig. 2b). When
85 the growth light intensity was doubled, all genotypes were paler. No variegated phenotype was
86 observed in the double mutants, showing that carotenoid biosynthesis was not or, if at all, very little
87 affected in the absence of PTOX in contrast to the variegated phenotype reported in the *im* mutant.
88 To challenge the photosynthetic apparatus even more, plants were grown in fluctuating light. The
89 double mutants were not more stressed than the other genotypes, only the wild type, Tak-1, was a bit
90 paler than the mutants (SI Fig. S1).

91 Both PTOX enzymes, PTOXa and PTOXb contribute to keep the redox state of the PQ pool oxidized as
92 shown by chlorophyll fluorescence induction upon illumination with actinic light (Fig. 2c). Fluorescence
93 induction was measured by applying a moderate light intensity of red light ($I=53 \mu\text{mol quanta m}^{-2}\text{s}^{-1}$).
94 When instead a saturating flash was used like usually done for determining the size of the PQ pool
95 from fluorescence induction curves, there was no difference, indicating that the size of the PQ pool
96 was the same in all genotypes. The absence of an effect in the mutants in a saturating flash can be
97 explained either by a slower reoxidation of PQH₂ by PTOX than the light-induced reduction of PQ or
98 that a certain period of actinic light is needed to provide enough substrate for PTOX. Fig. 2c shows that
99 in the first seconds after onset of light the fluorescence level remains high in $\Delta ptoxaptobx_1$, while it
100 decreases in the single mutant $\Delta ptoxa$. Tak-1 showed a slower fluorescence rise indicative for higher
101 PTOX activity. When the light was switched off, the fluorescence level remained higher in
102 $\Delta ptoxaptobx_1$ showing that the oxidation of PQH₂ was retarded in the absence of PTOX. The faster
103 fluorescence rise was observed in all mutants, also when only one PTOX isoform was lacking.

104 **PTOX activity affects the quantum efficiency of PSI.**

105 PTOX competes to a certain extent with linear electron flow from PSII via the PQ pool, the cytochrome
106 *b₆f* complex and plastocyanin to PSI. Since PTOX oxidizes PQH₂, it reduces at the same time the number
107 of electrons available for reduction of P700⁺. The number of available electrons determines the level
108 of the so-called donor-side limitation of PSI, Y(ND). When *Marchantia* thalli were exposed to
109 fluctuating light intensities, Y(ND) was high at high light intensities and low at low light intensities
110 independent of the genotype (Fig. 3a). However, the switch from high Y(ND) to low Y(ND) was
111 immediate in the double mutant while this transition was slower in Tak-1, indicating that PTOX oxidizes
112 partly the PQ pool and limits electron donation upon the change from high light to low light.
113 Accordingly, less donor side limitation (Y(ND)) was observed in the mutants when plants were
114 illuminated with increasing light intensity (Fig. 3b). Each intensity was applied for 3 min before the
115 measurement was taken to ensure that the photosynthetic apparatus was acclimated to the given light
116 intensity. At all light intensities, there was less donor-side limitation in the double mutant than in the
117 single mutant while Tak-1 showed the highest Y(ND). The lower donor side limitation in the mutants
118 resulted in a higher PSI yield (Fig. 3c), while the relative quantum yield of PSII (Y(II)) was the same in
119 all genotypes (Fig. 3d).

120 **Comparison of PTOXa and PTOXb recombinant proteins**

121 Since the double mutant had a stronger effect on PSI parameters than the single mutants, we further
122 studied the two isoforms. As shown in SI Fig. S2, there are differences in the amino acid sequence of
123 the two proteins¹⁶. In the catalytic site site, starting from α -helix 1, fully single conserved residues
124 represent 64% of the total sequences whereas conservative and semi-conservative exchanges are 26%
125 and 6% respectively. We used purified recombinant PTOXa and PTOXb proteins to determine the
126 maximum catalytic activity of the two isoforms using saturating concentrations of decylplastoquinol as

127 substrate (Table 1). The enzyme activity of PTOXa was 3 times higher than that of PTOXb. For PTOXb,
128 the N-terminal extension had been removed since the full-length gene was not expressed in *E. coli*.

129

130 **PTOX protects against photoinhibition of PSI and promotes photoinhibition of PSII**

131 Next, we investigated the protective effect of PTOX against light-induced damage of the two
132 photosystems. Both, *Arabidopsis* leaves and *Marchantia* thalli, were exposed for 3 h to high light (1250
133 $\mu\text{mol quanta m}^{-2}\text{s}^{-1}$) and photoinhibition of PSI was followed as a loss in the absorption signal at 830
134 nm, the so-called Pm value, while photoinhibition of PSII was monitored by the loss of the maximum
135 quantum yield of PSII (Fv/Fm). PSI was more susceptible to photoinhibition in *imCRTI* lines and in
136 $\Delta\text{ptoxaptob}$ mutants (Fig. 4a, c) than in the respective wild types. The opposite was observed for PSII
137 (Fig. 4b, d). It was more damaged in respective wild types than in the PTOX lacking mutants. In
138 *Marchantia*, PTOX single mutants showed no increase in PSII photoinhibition compared with the
139 double mutants, showing that one PTOX isoform is enough to allow sufficient accumulation of P700⁺
140 that protects against the destruction of the FeS clusters in PSI²². On the other hand, one PTOX isoform
141 was also sufficient to protect PSII.

142

143 **Discussion**

144 The *Arabidopsis imCRTI* lines are homogeneously green and grow well in high light. This makes this
145 mutant an ideal tool to study the effect of PTOX activity on photosynthetic electron transport in higher
146 plants. Previously the study of PTOX activity in higher plants was limited to plants grown at low light
147 intensity, a growth condition that permits to avoid the variegated phenotype²³. In *Chlamydomonas*
148 only a mutant of PTOX2 had been obtained¹⁹. The double mutant in *Marchantia* is the first mutant that
149 lacks all PTOX activity in an organism evolutionary placed below angiosperms.

150 *In vivo* experiments showed a higher PTOX activity in *C. reinhardtii*¹⁹ than in the vascular plant tomato²³
151 or in *Eutrema salsugineum*⁵. In *M. polymorpha* the deletion of PTOXb has a larger effect on the redox
152 state of the PSII acceptor side than that of PTOXa¹⁶. Purified recombinant PTOXa and PTOXb proteins
153 from *M. polymorpha* showed a higher activity than has been previously reported for rice PTOX⁸. In
154 both studies, the enzymes were expressed as MBP fusion protein to ensure their solubility. A V_{max} for
155 MBP-OsPTOX of $16.6 \pm 0.8 \mu\text{mol O}_2 \text{ mg}^{-1} \text{ min}^{-1}$ has been determined using soluble decyl-PQ at
156 saturating concentration as substrate, while here, using the same enzymatic assay, a 3-fold higher V_{max}
157 was determined for the truncated MBP-MpPTOXb and a 10-fold higher V_{max} for MBP-MpPTOXa (Table
158 1). The difference in activity may be caused by differences in substrate accessibility to the catalytic
159 center that may be caused by difference in the amino acid sequence (SI Fig. 1). The differences in
160 activities reported for *in vivo* and *in vitro* assays may be caused either by differences in the protein
161 amount relative to PSII content or in the regulation of the enzyme. The N-terminal extension in PTOXb
162 likely anchors the protein permanently to the membrane²⁴, while PTOXa is most likely only attached
163 to the thylakoid membrane in the presence of a high proton motive force²⁰ or has to move from the
164 stroma lamellae to the grana stacks to be active⁶. Anchoring of the enzyme to the membrane is
165 required for the access to its membrane-localized substrate PQH₂ and PTOXa is supposed to be
166 regulated via relocalization under conditions when photosynthetic electron transport is saturated.

167 As shown in Fig. 5, both in *Arabidopsis* and *Marchantia*, PSI is more susceptible to photoinhibition in
168 PTOX mutants while the opposite was observed for PSII. In the literature, PTOX is discussed as a safety
169 valve that protects the photosynthetic apparatus and especially PSII upon exposure of plants to

170 oxidative stress conditions such as high light, high salinity, extreme temperatures^{5,7,9}. Increase in
171 donor-side limitation to PSI and a high level of P700⁺ accumulation is known to protect PSI against
172 photoinhibition^{25,26}. We note that the PTOX mutants still can sustain P700 oxidation, which should be
173 due to the other electron sink such as Calvin-Benson cycle and flavodiiron proteins²⁷. More surprising
174 is the higher PSII damage observed in the wild types compared with the mutants. It is generally
175 assumed that a reduced PQ pool favours PSII photoinhibition. When the PQ pool is highly reduced, the
176 probability of charge recombination reactions within PSII increases leading to the generation of the
177 triplet state of P680. ³P680 react with oxygen (³O₂), a triplet in its ground state, generating singlet
178 oxygen (¹O₂), a highly reactive species that damages PSII²⁸. On the other hand, it has been shown that
179 overexpression of PTOX1 from *Chlamydomonas reinhardtii* in tobacco promotes oxidative stress and
180 PSII photoinhibition^{13,14,29}. Overexpression of *A. thaliana* PTOX, however, did not result in an increased
181 capacity to keep the plastoquinone pool oxidized and did not affect the level of PSII photoinhibition¹⁵.
182 Overexpression of PTOX1 from *C. reinhardtii* increased the production of superoxide anion radicals
183 (O₂^{•-})¹⁴. *In vitro* it has been shown that an anti-oxidant or pro-oxidant behaviour of MBP-OsPTOX
184 depends on both substrate availability and pH-value. O₂^{•-} production depends on the availability of its
185 substrate PQH₂⁸. At slightly alkaline pH, more O₂^{•-} is produced when the substrate concentration is
186 high, while PTOX plays an antioxidant role at low substrate concentration. O₂^{•-} production at pH=8.0
187 may be caused by the pH-dependent stabilization of the semiquinone PQ^{•-} or by the catalytic center
188 itself.

189 According to the data presented here, PTOX activity plays an important role under high light stress
190 stimulating PSII photoinhibition most likely via its pro-oxidant role leading to O₂^{•-} production. In high
191 light stress, PTOX activity of both PTOX isoforms is expected to be maximal *in vivo*. Photoinhibition of
192 PSII protects PSI against photoinhibition since it limits electron donation and favours the accumulation
193 of P700⁺. Sonoike and coworkers^{2,30} have proposed that PSII photoinhibition can be regarded as a
194 protection mechanism for PSI. PSI photoinhibition is irreversible in the short-term compared with the
195 efficient damage repair cycle of PSII³².

196

197 **Material and Methods**

198 **Plant material**

199 *Arabidopsis thaliana*. *Arabidopsis thaliana* (Col-0), the PTOX mutant *im*, a transgenic *Arabidopsis* line
200 expressing *CRTI* under 35S promoter control as described in Schaub *et al.*, 2005²¹ here called CRTI, and
201 two lines of crosses *im* x CRTI were grown for 3-4 weeks in soil under a light-dark cycle (16 h-light, 22
202 °C, 100 μmol photons m⁻² s⁻¹, white fluorescent lamp/8 h-dark, 20 °C). The lines of the F2 generation
203 which showed no PTOX activity were named *imCRTI_1* and *imCRTI_2*.

204 *Marchantia polymorpha*. A male accession of *M. polymorpha*, Takaragaike (Tak)-1 and all mutants
205 were asexually cultured on one-half-strength Gamborg's B5 agar medium³² in the same light conditions
206 as used for *Arabidopsis*. For physiological measurements, 2-3 weeks old thalli were used.

207 **Genome editing by CRISPR/Cas9 system**

208 The construction of plasmids allowing the transformation of *M. polymorpha* by the CRISPR/Cas9
209 method was carried out according to the method of Sugano *et al.*, 2014³³. Six target sequences of
210 interest, three for *PTOXa* and three for *PTOXb*, were inserted into pMpGE_En03 vectors which were
211 transferred into pMpGE010 or pMpGE011 vectors by gateway reaction. Each of the Δ *ptoxa* and Δ *ptoxb*
212 single mutants previously characterized¹⁶ were transformed with the vectors to mutate the remaining

213 intact PTOX gene. The final transformation of the plants was carried out using the Agar-Trap
214 method^{34,35} on thalli and gemmae. After sequencing, two double mutants were obtained from the
215 single $\Delta ptoxb$ mutant transformed with a *PTOXa* gene targeting sequence: CCTTATGGAGGCTCTAGG.
216 These different mutants do not differ in the location but in the type of mutation caused by Cas9.
217 Throughout the manuscript, these two double mutants are called $\Delta ptoxa ptoxb_1$ and $\Delta ptoxa ptoxb_2$.

218 **Vector constructions and MBP-MpPTOXa and MBP-MpPTOXb Δ Nter expression, purification from** 219 ***E.coli* and enzymatic assay**

220 *PETM-40_PTOXa construct.* The synthetic optimized gene (Eurofins) of *PTOXa* (Mp3g12150.1) from
221 *Marchantia* was amplified by PCR with the primers [F-PTOXa-Nco1 and R-PTOXa-Xho1]. The amplified
222 fragment was digested with Nco1 and Xho1 and ligated with Nco1/Xho1-digested PETM-40 to produce
223 the vector PETM-40_PTOXa.

224 *PETM-40_133-257-PTOXb (PETM-40_ Δ Nter-PTOXb) construct.* First, PTOXb gene (Mp7g11430.1) from
225 *Marchantia* was amplified by PCR using the cDNA of Tak-1 as template and the primers [F-PTOXb and
226 R-PTOXb]. The amplified fragments were cloned in PETM-40 vector linearized with Nco1 and Xho1
227 using the In-Fusion HD Cloning Kit (TaKaRa) to generate the vector PETM-40_PTOXb. Then, a deletion
228 of a large part of a sequence encoding the N terminal domain (33–257) of the PTOXb gene
229 (Mp7g11430.1) were introduced by site-directed mutagenesis using the plasmid PETM-40_PTOXb as
230 template and synthetic primers F-PET-PTOXb Del and R-PET-PTOXb Del. All plasmids were checked by
231 sequencing. List of primers in SI Table S1. The obtained plasmids were used to transform BL21 (DE3) *E.*
232 *coli* cells. 20 mL of overnight cultures was inoculated into 1L of LB, grown at 37 °C to an OD 600 nm
233 between 0.6 and 0.8 and induced with IPTG. After induction overnight at 16 °C, the cells were
234 harvested, washed in buffer A (25 mM sodium-phosphate buffer pH 7.6, MgCl₂ 2.5 mM, NaCl 300 mM,
235 glycerol 15 % V/V) and frozen at –80 °C. Purification was carried out on ice. Cells were resuspended in
236 buffer A with DNase, PMSF and lysozyme and sonicated. After centrifugation at 28,000 g for 45 min
237 the supernatant was solubilized for 30 min on ice by slowly adding 6 X CMC n-octyl β -D-
238 glucopyranoside (nOG; 1 X CMC = 25 mM) and then applied to Amylose resin. After washing thoroughly
239 with buffer A containing 2 X CMC nOG; the elution was accomplished with buffer B (50 mM Tris–HCl
240 pH 8.0, MgCl₂ 2.5 mM, glycerol, 10 % V/V, 2 X CMC nOG and 10 mM maltose). Proteins resolved by
241 SDS-PAGE were detected using Coomassie Brilliant Blue. Protein quantification was done by using the
242 Bradford reagent. The activity of recombinant PTOX was measured as described in Yu *et al.*, 2014⁸.

243 Activity was measured using a coupled enzymatic assay. PQ was reduced to PQH₂ by human DT-
244 diaphorase and PQH₂ oxidized by PTOW. Standard assay conditions containing 10 μ g protein per 700
245 μ l assay volume, 100 μ M decyl-plastoquinone, 200 μ M NADH, 10 μ g human DT-diaphorase (Sigma-
246 Aldrich), 50 mM Tris-HCl pH 8.0, 2.5mM MgCl₂ were used. Activities were determined by measuring O₂
247 consumption with a Clark-type electrode.

248 **Chlorophyll absorption and P700 measurements**

249 Chlorophyll *a* fluorescence and P700 absorption was measured using a Dual-PAM-100 fluorometer
250 (Walz, Effeltrich, Germany). Chlorophyll fluorescence curves were measured using a low actinic light
251 (38 μ mol quanta m⁻² s⁻¹). Post illumination fluorescence rise was measured after illumination of
252 *Arabidopsis* leaves for 10 min at 530 μ mol quanta m⁻² s⁻¹. PSII and PSI parameters were determined as
253 described in Messant *et al.* 2021¹⁶. Pm is the maximal P700 signal upon transformation of P700 from
254 the fully reduced to the fully oxidized state. The following definitions were used according to³⁷:
255 Effective quantum yield of PSII: $Y(II)=(Fm'-F)/Fm'$; Yield of donor side limitation: $Y(ND)=1-P700red$;
256 Yield of acceptor side limitation: $Y(NA)=(Pm-Pm')/Pm$ with Pm' being the maximal change of the P700
257 signal at a given light intensity; PSI quantum yield: $Y(I)=1-Y(ND)-Y(NA)$.

258 **Photoinhibition**

259 *Arabidopsis* leaves and *Marchantia* thalli were exposed to high light (1250 $\mu\text{mol quanta m}^{-2}\text{s}^{-1}$) for 3h.
260 Samples were kept for 15 min at room light (8 $\mu\text{mol quanta m}^{-2}\text{s}^{-1}$) before determining the maximum
261 value for P700 absorption, Pm, and the maximum quantum yield of PSII, Fv/Fm.

262

263 **Acknowledgements**

264 This work was supported by the Labex Saclay Plant Sciences-SPS (ANR-17-EUR-0007) and by the
265 platform of Biophysics of the I2BC supported by the French Infrastructure for Integrated Structural
266 Biology (FRISBI; grant number ANR-10-INSB-05). M.M. is supported by a CEA PhD fellowship.

267

268 **Author Contribution**

269 M.M, G. S. and A.K-L. designed the project. M.M, T.-L. L., A. W, G.S. and A.K-L. performed the
270 experiments and analysed the data. A.K-L. wrote the initial version of the manuscript that was read
271 and revised by all authors.

272

273 **Data availability**

274 Data will be made available on demand.

275

276 **References**

- 277 1. Oguchi, R., Terashima, I. & Chow, W.S. The effect of different spectral light quality on the
278 photoinhibition of Photosystem I in intact leaves. *Photosynth Res* **149**(1-2):83-92 (2021)
279 2. Sonoike K. Photoinhibition of photosystem I. *Physiol Plant* **142**:56-64 (2011)
280 3. Li, L., Aro, E.M. & Millar, A.H. Mechanisms of Photodamage and Protein Turnover in
281 Photoinhibition. *Trends Plant Sci.* **23**(8):667-676 (2018)
282 4. Alboresi A, Storti M, Morosinotto T. Balancing protection and efficiency in the regulation of
283 photosynthetic electron transport across plant evolution. *New Phytol* **221**:105-109 (2019)
284 5. Stepien, P. & Johnson, G.N. Contrasting responses of photosynthesis to salt stress in the
285 glycophyte *Arabidopsis thaliana* and the halophyte *Thellungiella halophila*. Role of the plastid
286 terminal oxidase as an alternative electron sink. *Plant Physiol* **149**:1154–1165 (2009)
287 6. Stepien, P. & Johnson, G.N. Plastid terminal oxidase requires translocation to the grana stacks
288 to act as a sink for electron transport. *Proc Natl Acad Sci U S A* **115**(38):9634-9639 (2018)
289 7. Streb, P., Josse, E-M., Galouët, E., Baptist, F., Kuntz, M. & Cornic, G. Evidence for alternative
290 electron sinks to photosynthetic carbon assimilation in the high mountain plant species
291 *Ranunculus glacialis*. *Plant Cell Environ* **28**:1123–1135 (2005)
292 8. Yu, Q., Feilke, K., Krieger-Liszkay, A. & Beyer P. Functional and molecular characterization of plastid
293 terminal oxidase from rice (*Oryza sativa*). *Biochim Biophys Acta* **1837**(8):1284-92 (2014)
294 9. Quiles, M.J. Stimulation of chlororespiration by heat and high light intensity in oat plants. *Plant*
295 *Cell Environ* **29**(8):1463-70 (2006)
296 10. Ibáñez, H., Ballester, A., Muñoz, R. & Quiles, M.J. Chlororespiration and tolerance to drought,
297 heat and high illumination. *J Plant Physiol* **15**;167(9):732-8 (2010)

- 298 11. Ivanov, A.G et al. Implications of alternative electron sinks in increased resistance of PSII and
299 PSI photochemistry to high light stress in cold-acclimated *Arabidopsis thaliana*. *Photosynth Res*
300 **113**(1-3):191-206 (2012)
- 301 12. Laureau, C. et al. Plastid terminal oxidase (PTOX) has the potential to act as a safety valve for
302 excess excitation energy in the alpine plant species *Ranunculus glacialis* L. *Plant Cell Environ*
303 **36**(7):1296-310 (2013)
- 304 13. Ahmad, N., Khan, M.O., Islam, E., Wei, Z.Y., McAusland, L., Lawson, T., Johnson, G.N. & Nixon,
305 P.J. Contrasting Responses to Stress Displayed by Tobacco Overexpressing an Algal Plastid
306 Terminal Oxidase in the Chloroplast. *Front Plant Sci* **11**:501 (2020)
- 307 14. Heyno, E., Gross, C.M., Laureau, C., Culcasi, M., Pietri, S. & Krieger-Liszkay, A. Plastid alternative
308 oxidase (PTOX) promotes oxidative stress when overexpressed in tobacco. *J Biol Chem*
309 **284**(45):31174-80 (2009)
- 310 15. Rosso, D. et al. IMMUTANS does not act as a stress-induced safety valve in the protection of
311 the photosynthetic apparatus of *Arabidopsis* during steady-state photosynthesis. *Plant*
312 *Physiol.* **142**, 574–585 (2006)
- 313 16. Messant, M., Shimakawa, G., Perreau, F., Miyake, C., Krieger-Liszkay, A. Evolutionary
314 differentiation between alga- and plant-type plastid terminal oxidase: Study of plastid terminal
315 oxidase PTOX isoforms in *Marchantia polymorpha*. *Biochim Biophys Acta Bioenerg*
316 **1862**(1):148309 (2021)
- 317 17. Wetzel, C.M., Jiang, C.Z., Meehan, L.J., Voytas, D.F. & Rodermel, S.R. Nuclear–organelle
318 interactions: the immutans variegation mutant of *Arabidopsis* is plastid autonomous and
319 impaired in carotenoid biosynthesis. *The Plant Journal* **6**, 161–175 (1994)
- 320 18. Carol, P. et al. Mutations in the *Arabidopsis* gene IMMUTANS cause a variegated phenotype
321 by inactivating a chloroplast terminal oxidase associated with phytoene desaturation. *The*
322 *Plant Cell* **11**, 57–68 (1999)
- 323 19. Houille-Vernes, L., Rappaport, F., Wollman, F.A., Alric, J. & Johnson, X. Plastid terminal oxidase
324 2 (PTOX2) is the major oxidase involved in chlororespiration in *Chlamydomonas*. *Proc Natl*
325 *Acad Sci U S A.* **108**(51):20820-5 (2011)
- 326 20. Bolte, S., Marcon, E., Jaunario, M., Moyet, L., Paternostre, M., Kuntz & M., Krieger-Liszkay, A.
327 Dynamics of the localization of the plastid terminal oxidase inside the chloroplast. *J Exp Bot.*
328 **71**(9):2661-2669 (2020)
- 329 21. Schaub, P., Al-Babili, S., Drake & R., Beyer, P. Why is golden rice golden (yellow) instead of red?
330 *Plant Physiol.* **138**(1):441-50 (2005)
- 331 22. Sonoike, K., Terashima, I., Iwaki, M. & Itoh, S. Destruction of photosystem I iron-sulfur centers
332 in leaves of *Cucumis sativus* L. by weak illumination at chilling temperatures. *FEBS Lett*
333 **362**:235-238 (1995)
- 334 23. Trouillard, M. et al. Kinetic properties and physiological role of the plastoquinone terminal
335 oxidase (PTOX) in a vascular plant. *Biochim. Biophys. Acta* **1817**:2140–48 (2012)
- 336 24. Nawrocki, W.J., Tourasse, N.J., Taly, A., Rappaport, F. & Wollman, F.A. The plastid terminal
337 oxidase: its elusive function points to multiple contributions to plastid physiology. *Annu Rev*
338 *Plant Biol* **66**:49-74 (2015)
- 339 25. Sejima, T., Takagi, D., Fukayama, H., Makino, A., & Miyake, C. Repetitive short-pulse light
340 mainly inactivates photosystem I in sunflower leaves. *Plant Cell Physiol* **55**, 1184-1193. (2014)
- 341 26. Cerqueira, J. V. A., Silveira, J. A. G., Carvalho, F. E. L., Cunha, J. R., & Lima Neto, M. C. The
342 regulation of P700 is an important photoprotective mechanism to NaCl-salinity in *Jatropha*
343 *curcas*. *Physiol. Plant.* **167**, 404-417 (2019)

- 344 27. Shimakawa, G., Ishizaki, K., Tsukamoto, S., Tanaka, M., Sejima, T. & Miyake, C. The Liverwort,
345 *Marchantia*, Drives Alternative Electron Flow Using a Flavodiiron Protein to Protect PSI. *Plant*
346 *Physiol* **173**(3):1636-1647 (2017)
- 347 28. Rutherford, A.W. & Krieger-Liszky, A. Herbicide-induced oxidative stress in photosystem II.
348 *Trends Biochem Sci* **26**(11):648-53 (2001)
- 349 29. Ahmad, N., Michoux, F. & Nixon, P.J. Investigating the production of foreign membrane
350 proteins in tobacco chloroplasts: expression of an algal plastid terminal oxidase. *PLoS One*
351 **7**(7):e41722 (2012)
- 352 30. Kudoh, H., & Sonoike, K. Irreversible damage to photosystem I by chilling in the light: cause of
353 the degradation of chlorophyll after returning to normal growth temperature. *Planta* **215**:
354 541–548 (2002)
- 355 31. Sonoike K. Photoinhibition of photosystem I. *Physiol Plant.* **142**(1):56-64 (2011)
- 356 32. Gamborg, O.L, Miller, R.A & Ojima, K. Nutrient requirements of suspension cultures of soybean
357 root cells. *Exp Cell Res* **50**(1):151-8 (1968)
- 358 33. Sugano, S.S., Shirakawa, M., Takagi, J., Matsuda, Y., Shimada, T., Hara-Nishimura, I. & Kohchi,
359 T. CRISPR/Cas9-mediated targeted mutagenesis in the liverwort *Marchantia polymorpha* L.
360 *Plant Cell Physiol* **55**(3):475-81 (2014)
- 361 34. Tsuboyama, S. & Kodama, Y. AgarTrap: a simplified *Agrobacterium*-mediated transformation
362 method for sporelings of the liverwort *Marchantia polymorpha* L. *Plant Cell Physiol* **55**(1):229-
363 36 (2014)
- 364 35. Tsuboyama, S., Nonaka, S., Ezura, H., Kodama, Y. Improved G-AgarTrap: A highly efficient
365 transformation method for intact gemmalings of the liverwort *Marchantia polymorpha*. *Sci*
366 *Rep* **17**;8(1):10800 (2018)
- 367 36. Klughammer, C. & Schreiber, U. An improved method, using saturating light pulses, for the
368 determination of photosystem I quantum yield via P700+-absorbance changes at 830 nm,
369 *Planta* **192**: 261–268 (1994)
- 370

371

372

373 **Table 1**

374 Activity of purified recombinant MBP-MpPTOXa and MBP-MpPtoxb- $\Delta Nter$.

	Activity ($\mu\text{mol O}_2 \text{ mg protein}^{-1} \text{ min}^{-1}$)
MBP-MpPTOXa	149 +/- 16
MBP-MpPtoxb- $\Delta Nter$	46 +/- 6

375

376 Standard assay conditions were used containing 10 μg protein per 700 μl assay volume, 100 μM decyl-
377 plastoquinone, 200 μM NADH, 10 μg DT-diaphorase, 50 mM Tris-HCl pH 8.0, 2.5 mM MgCl_2 . Activities
378 were determined by measuring O_2 consumption with a Clark-type electrode.

379

380

381

382

383

384

385

386

387

388

389

390

391

392

393

394

395

396

397

398

399

400 Figure Legends

401 Figure 1. Characterization of *Arabidopsis im* x CRTI lines. **a.** The photo shows 4 week old plants, wild-
402 type Col-0, PTOX mutant *im*, plant-expressing bacterial desaturase CRTI and *im*CRTI_1 mutant; grown
403 in long day conditions at 100 $\mu\text{mol quanta m}^{-2}\text{s}^{-1}$. **b.** Chlorophyll fluorescence induction curves of Col-
404 0 and the *im*CRTI_1 and *im*CRTI_2 lines. **c.** Post-illumination fluorescence rise of Col-0 and both *im*CRTI
405 lines after 10 min actinic light (530 $\mu\text{mol quanta m}^{-2}\text{s}^{-1}$). The flash indicates turning of the actinic light.
406 Representative curves are shown.

407 Figure 2. Characterization of *Marchantia polymorpha* PTOX mutant lines. **a.** Design of the PTOX
408 mutants using CRISP/Cas9 technology. **b.** Images of the different genotypes grown for three weeks at
409 100 $\mu\text{mol quanta m}^{-2}\text{s}^{-1}$ and at 200 $\mu\text{mol quanta m}^{-2}\text{s}^{-1}$. **c.** Chlorophyll fluorescence induction curves
410 measured at low actinic light ($I=53 \mu\text{mol quanta m}^{-2}\text{s}^{-1}$). Arrows indicate the set on/off of the measuring
411 light and of the actinic light. The inset shows a zoom of the fluorescence change upon the onset of the
412 actinic light. Black: Tak-1, blue: *Δptoxa* , violet: *$\Delta\text{ptoxaptox}_1$* . **d.** Fluorescence induction curves upon
413 onset of actinic light for all genotypes starting from the F_0 level.

414 Figure 3. Chlorophyll fluorescence and P700 absorption parameters measured with *Marchantia*. **a.**
415 Changes in PSI donor side limitation $Y(\text{ND})$ upon illumination with fluctuating light. Light intensity was
416 altered between 55 $\mu\text{mol quanta m}^{-2}\text{s}^{-1}$ (LL) and 850 $\mu\text{mol quanta m}^{-2}\text{s}^{-1}$ (HL). For clarity, only values
417 for Tak-1 (black squares) and the double mutant line *$\Delta\text{ptoxaptox}_1$* (grey triangle) are shown. **b.** PSI
418 donor side limitation $Y(\text{ND})$ as a function of the light intensity. **c.** Quantum yield of PSI, $Y(\text{I})$, as a function
419 of the light intensity. **d.** Effective quantum yield of PSII, $Y(\text{II})$ as a function of the light intensity.

420 Figure 4. Photoinhibition of PSI and PSII in *Arabidopsis* (**a, b**) and *Marchantia* (**c, d**). Leaves and thalli
421 were exposed to high light (1250 $\mu\text{mol quanta m}^{-2}\text{s}^{-1}$) for 3h. Left, percentage of the loss of maximum
422 absorption change of P700 (P_m) compared to the P_m value prior to the photoinhibition treatment.
423 Right, percentage of the loss of maximum PSII quantum yield (F_v/F_m) compared to the F_v/F_m value
424 prior to the photoinhibition treatment. F_v/F_m values were for all genotypes 0.8 ± 0.15 (100%) prior to
425 the photoinhibitory treatment. Stars indicate significant differences, compared to the control
426 condition, based on a Mann and Whitney test (* $p < 0.05$, ** $p < 0.01$; $N \geq 5$ biological replicates).

427

428

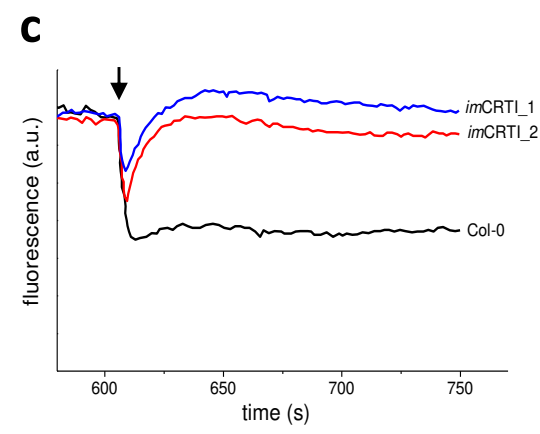
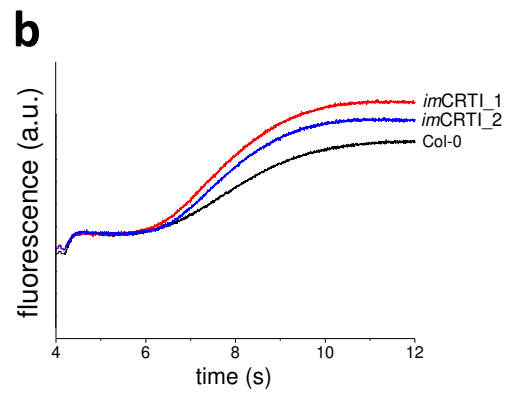
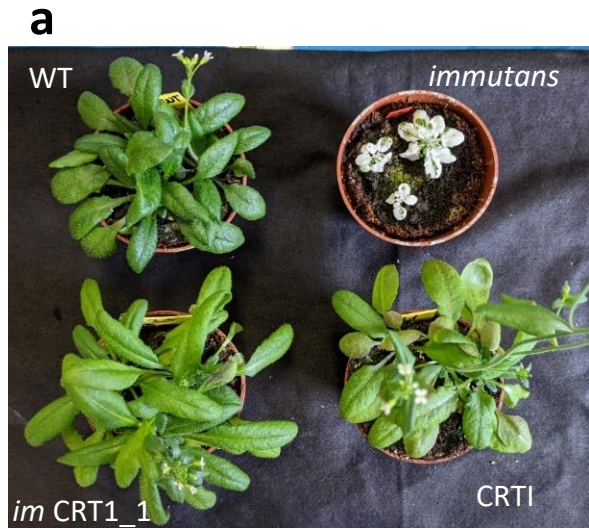


Figure 1

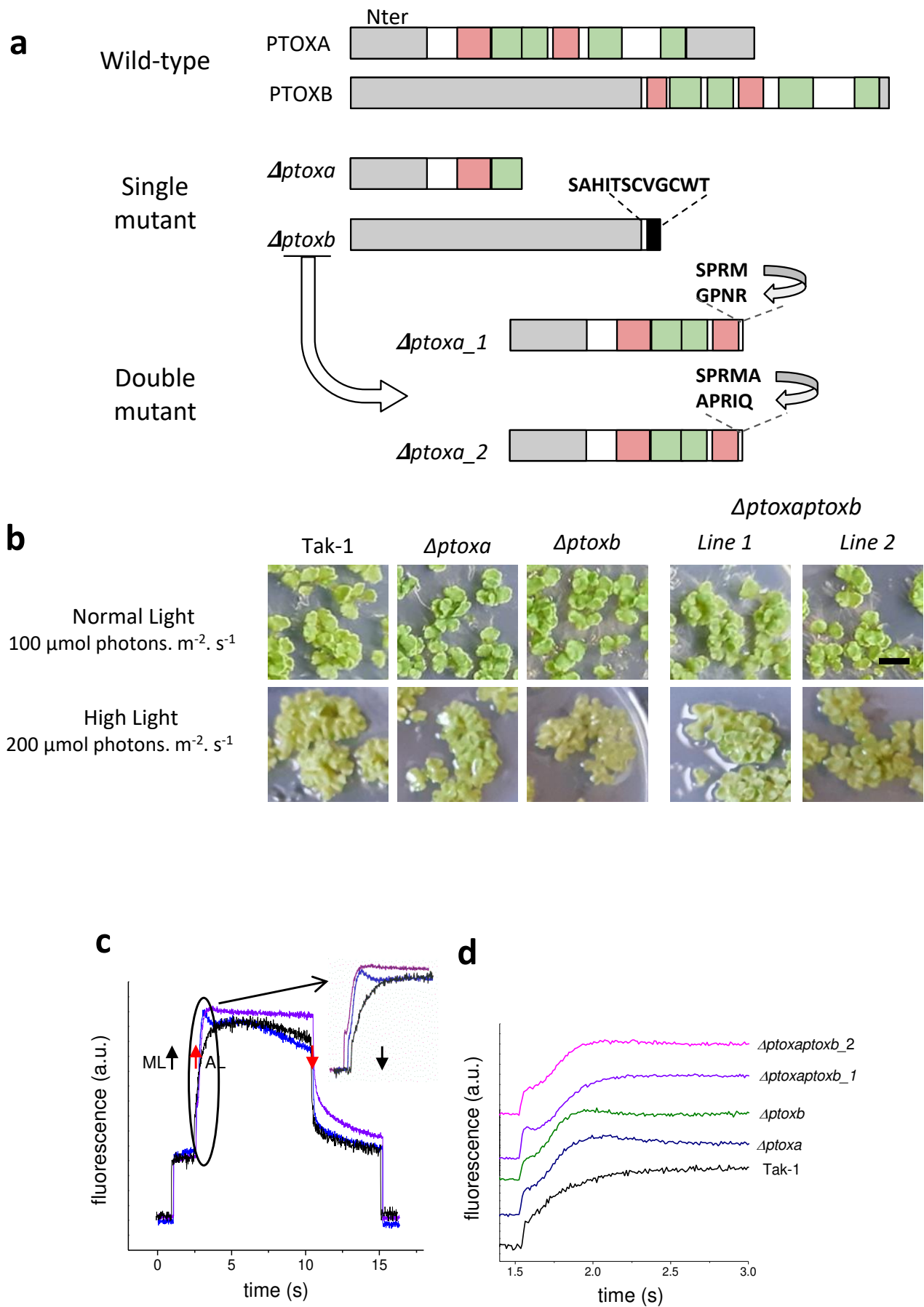


Figure 2

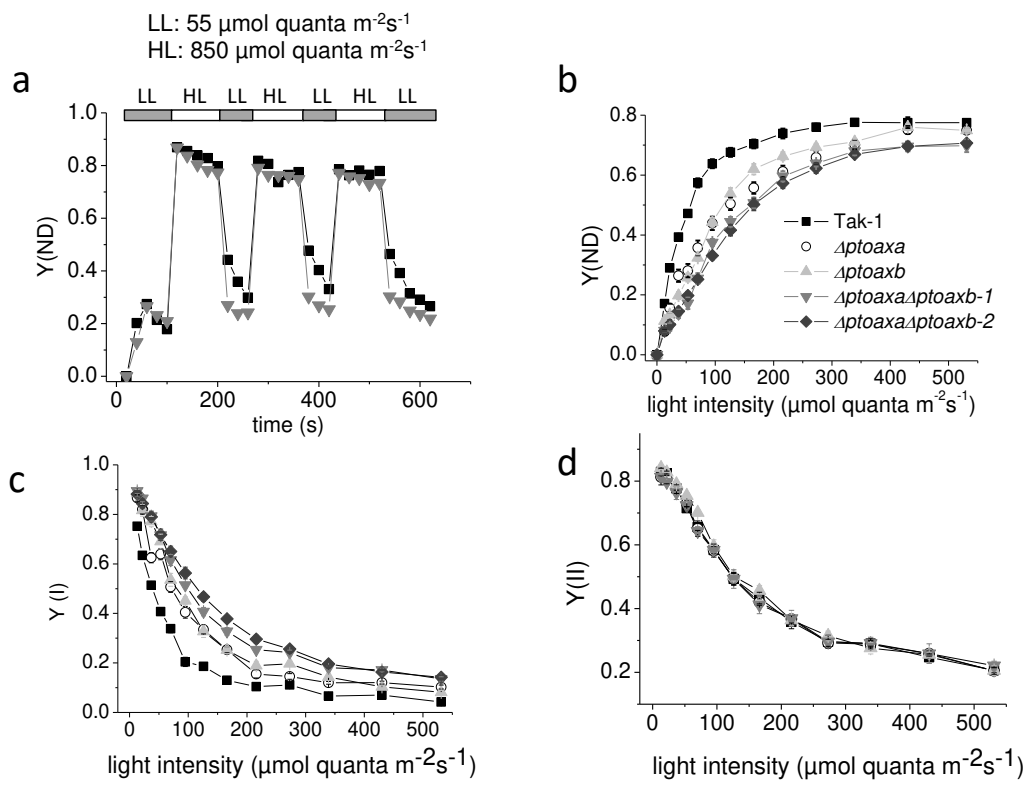
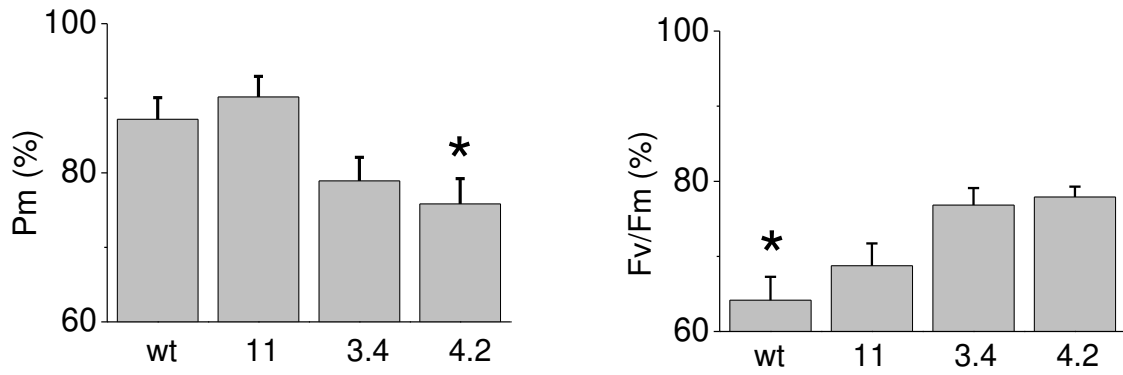


Figure 3

A. thaliana



M. polymorpha

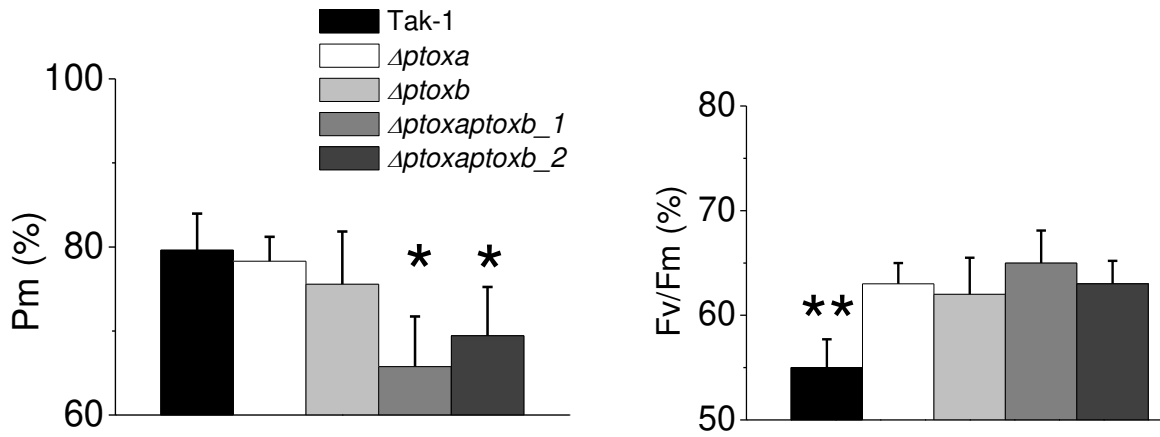
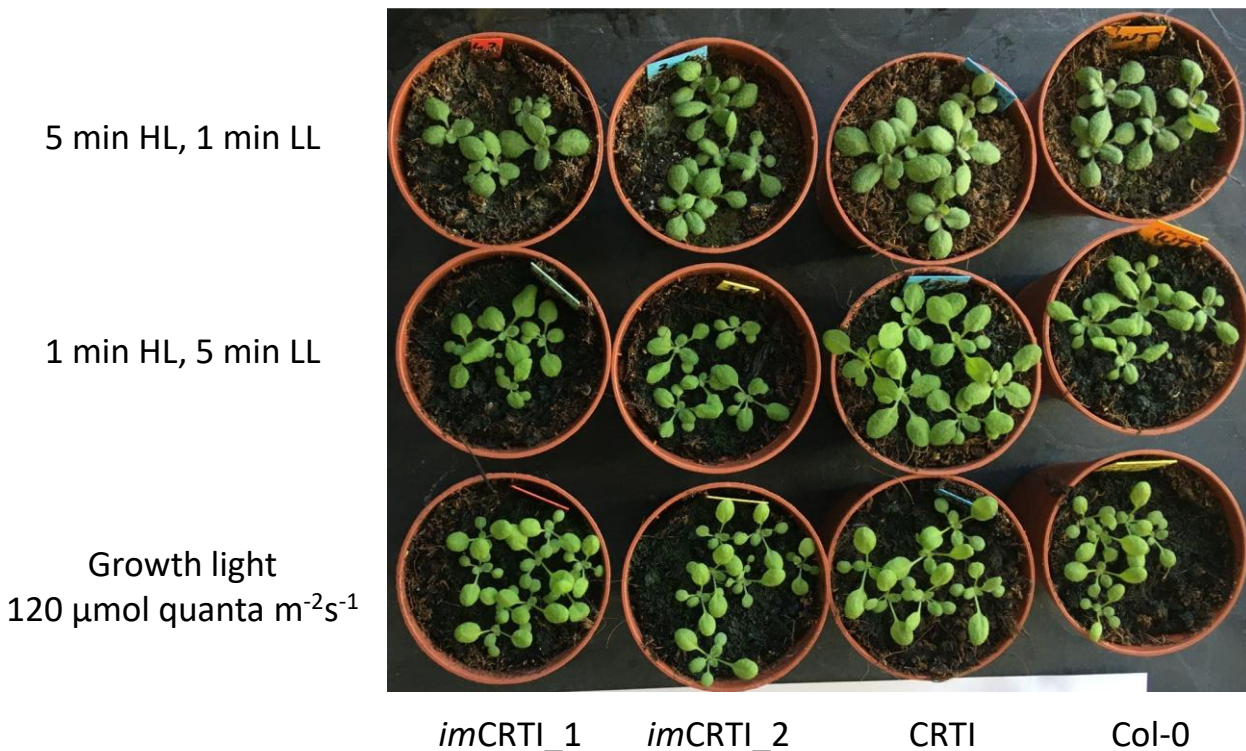


Figure 4

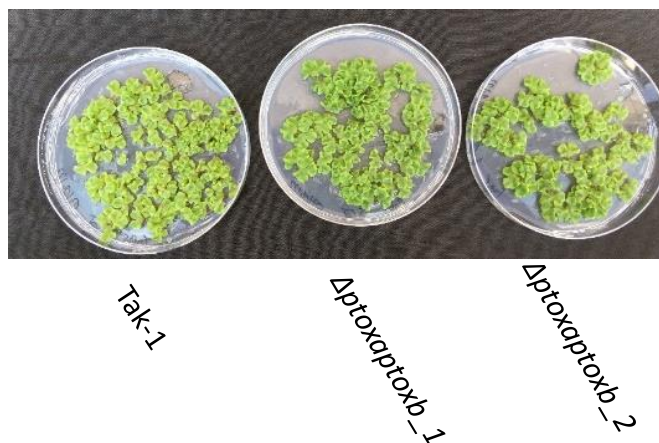
Supplementary Information

Figure 1.

Arabidopsis thaliana (3 weeks old) in long day or for 1 week in fluctuating light condition (LL = 55 $\mu\text{mol quanta m}^{-2}\text{s}^{-1}$, HL = 850 $\mu\text{mol quanta m}^{-2}\text{s}^{-1}$)

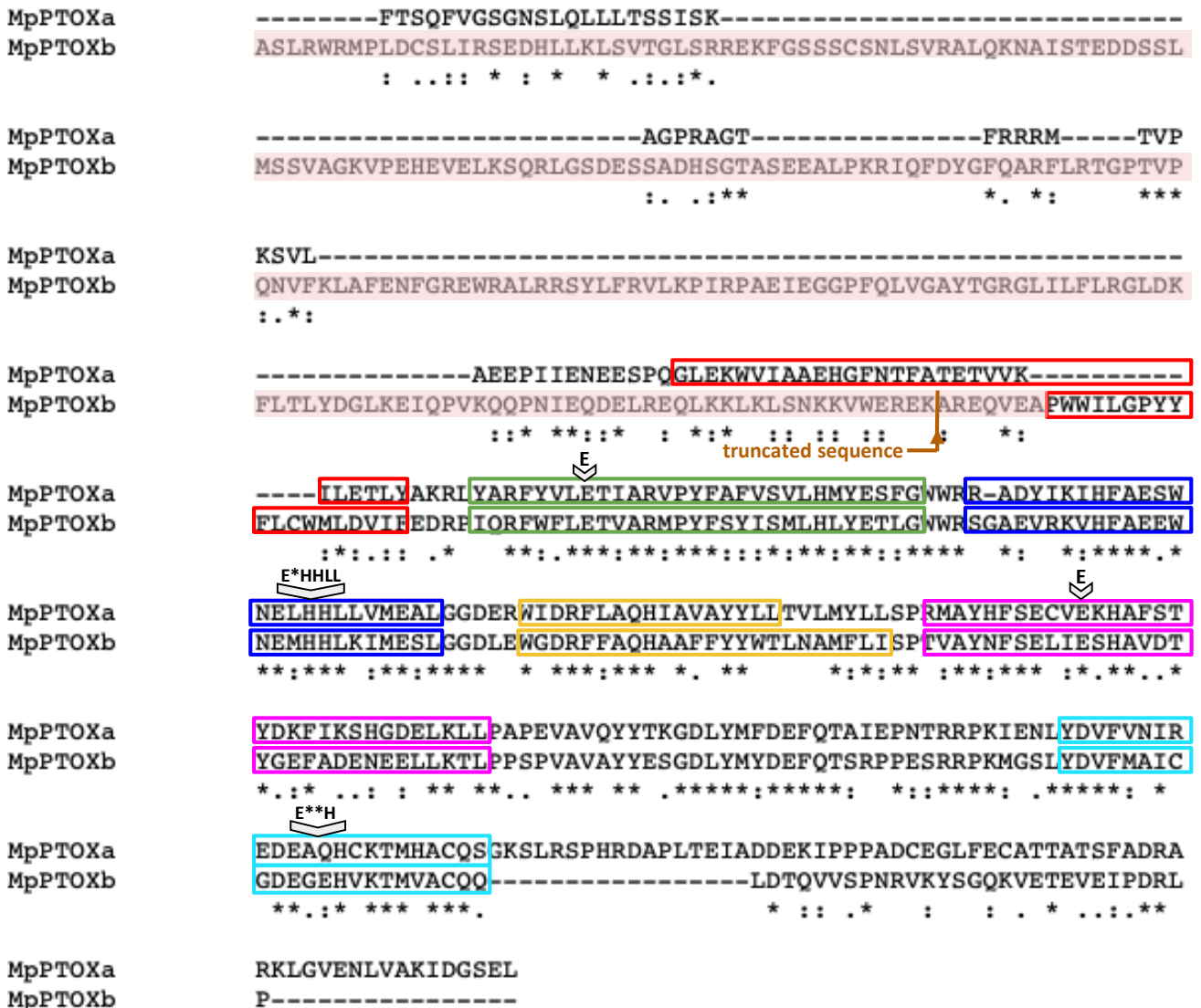


Marchantia polymorpha (2 weeks old), grown for 1 week in fluctuating light (5 min 55 $\mu\text{mol quanta m}^{-2}\text{s}^{-1}$, 1 min 850 $\mu\text{mol quanta m}^{-2}\text{s}^{-1}$)



SI Fig. 2.

Sequence alignment of MpPTOXa and Nter truncated MpPTOXb catalytic sites by MUSCLE.



Sequence alignment of MpPTOXa and Nter truncated MpPTOXb catalytic sites by MUSCLE. The six helices α -1 (red), α -2 (green), α -4 (yellow), α -5 (magenta) and α -6 (cyan) are framed and the fourth iron binding sites motifs with the six iron binding sites determined by McDonald *et al.*, 2003, are indicated in bold above sequences. The site of truncation of the recombinant protein is indicated by a flash

Ref.: McDonald AE, Amirsadeghi S, Vanlerberghe GC. Prokaryotic orthologues of mitochondrial alternative oxidase and plastid terminal oxidase. *Plant Mol Biol.* **53**(6):865-76. (2003)

Edgar RC. MUSCLE: multiple sequence alignment with high accuracy and high throughput. *Nucleic Acids Res.* **32**(5):1792-7. (2004)

Supplementary Table S1:

Primer sequences

Primer names	Primer sequences	
F-PTOX1-Nco1	F	5'- GAT ATA CCA TGG CTT CTG GCC TGC GCA TTG -3'
R-PTOX1-Xho1	R	5'- GCC GGC CTC GAG TTA TAA TTC GCT GCC ATC -3'
F-PTOX2	F	5'- TTC AGG GCG CCA TGG GCA GTC CTG CCG CAT GCA TGC TTC -3'
R-PTOX2	R	5'- GTG GTG GTG CTC GAG TCA CGG CAG ACG GTC GGG-3'
F-PET-PTOX2 Del	F	5'-GCTACCGACTGCACGGCTGCAGCTCGAGAACAAGTGGAA GCACCTTGG-3'
R-PET-PTOX2 Del	R	5'- TGCAGCCGTGCGTCGGTAGCAGCGGAAGTGGGGAGGTG -3'

Primers used for vector constructions for PTOX expression in *E.coli* as described in the Methods section.

As a conclusion, the characterization of *Δptoxaptob* double mutant by chlorophyll fluorescence and PSI absorption measurements showed that PTOX activity triggers PSI protection against photoinhibition. Our results also showed that both PTOX are regulated in a different manner and seem to be used by the plant in different physiological conditions. *In vitro* characterization of the proteins also pointed out that the plant-type PTOX is more efficient to oxidised plastoquinol which can be the cause of their selection during angiosperms evolution.

III) *In silico* comparison of the structure of Algae and Plant-type PTOX

The first *in silico* analysis carried out on proteins often said that PTOX have highly conserved catalytic sites with the six iron-binding sites as in Alternative Oxidases (McDonald *et al.*, 2003). In previous papers (Messant *et al.*, 2021; 2022 *submitted*), we highlighted the difference between Alga and Plant-type PTOX whose catalytic centres only possess 50% sequence identity. In particular, we have shown that Alga-type have an Nter extension and that the activity of the recombinant protein MpPTOXb without this extension is three times lower than that of MpPTOXa. In this part, I carried out an *in silico* study on the sequences of PTOX proteins used in Messant *et al.*, 2021 to study more precisely the characteristics of the Nter extension of Alga-type PTOX and the differences in the catalytic site of the two groups in particular in regions close to iron binding sites. The objectives of this part are to try to determine clues to understand the evolution and the regulation of the two isoforms.

A) Material and Methods

Sequence alignment and phylogenetic tree

Phylogenetic tree were generated on phylogeny.fr (Dereeper *et al.*, 2008) using the following softwares: sequence alignment were performed by MUSCLE version 3.5 (Edgar, 2004), ambiguous regions were removed using Gblocks v0.91b (Castresana, 2000) and then phylogenetic tree were generated using PhyML (Guindon *et al.*, 2010) based on the maximum likelihood principle and TreeDyn.

Protein prediction structures and visualisation

AlphaFold software (Jumper *et al.*, 2021) was used to predict the structure of proteins whose sequences were used in Messant *et al.*, 2021 to generate the phylogenetic tree. The PyMol molecular graphic system (Version 1.2r3pre, Schrödinger, LLC) was used to visualise and compare the structure of proteins with each other and to determine the potential structural differences.

Conserved Iron Binding Site motifs

The protein sequences were aligned by MUSCLE version 3.5 (Edgar, 2004). The online software Color Align conservation (Stothard, 2000) was then used to highlight the identical residues between the different proteins.

B) Results

1) Characteristics of the Nter extension of Alga-type PTOX

a) Description of the different Nter extension structures

A sequence alignment of conserved Nter parts (Figure 29, **A**) as well as the use of Alpha Fold structure predictions of complete protein sequences previously used for phylogenetic analysis from Messant *et al.*, 2021; allow to highlight the presence of protein structures potentially important for the physiological role of Alga-type PTOXs. The first group defined corresponds to the proteins of *Cyanidioschyzon* 1 and 2 which are the outermost of the Alga-type PTOX according to the phylogenetic tree (Figure 29, **B, C**). They have two helices of 24 to 27 amino acids each (dark red and blue) dubbed $\alpha 1'$ and $\alpha 3'$. Group 2 corresponds to the *Phaeodactylum* b, *Thalassiosira* b and *Ostreococcus* b proteins. They have the same two helices $\alpha 1'$, slightly shorter than the previous group and $\alpha 2'$. The absence of any notable difference in structure between these three proteins indicates that the separation of the branches between the *Phaeodactylum* b and *Thalassiosira* b proteins with that of *Ostreococcus* depends on differences in amino acids. Finally, all the proteins present in group 3 have not two but three helices in their Nter parts. A helix renamed $\alpha 2'$ has interspersed between helices $\alpha 1'$ and $\alpha 3'$. The branching differences observed in the tree for all group 3 proteins are not due to differences in protein structure but rather are related to differences in amino acids. Nevertheless, a 3' group could be identified corresponding to the proteins of *Coccomyxa*, *Chlamydomonas* 1 and *Volvox* 1. These proteins do have the three helices of group 3, however, the $\alpha 1'$ is longer and seems to be in two parts. One can therefore conclude that the $\alpha 3'$ helix is the most conserved through the evolution of the green lineage of Alga-type PTOX, which suggests a major physiological importance. Moreover, the helix $\alpha 1'$ seems the most variable but also the most ancestral. Finally, the $\alpha 2'$ helix seems to have acquired physiological importance later in evolution.

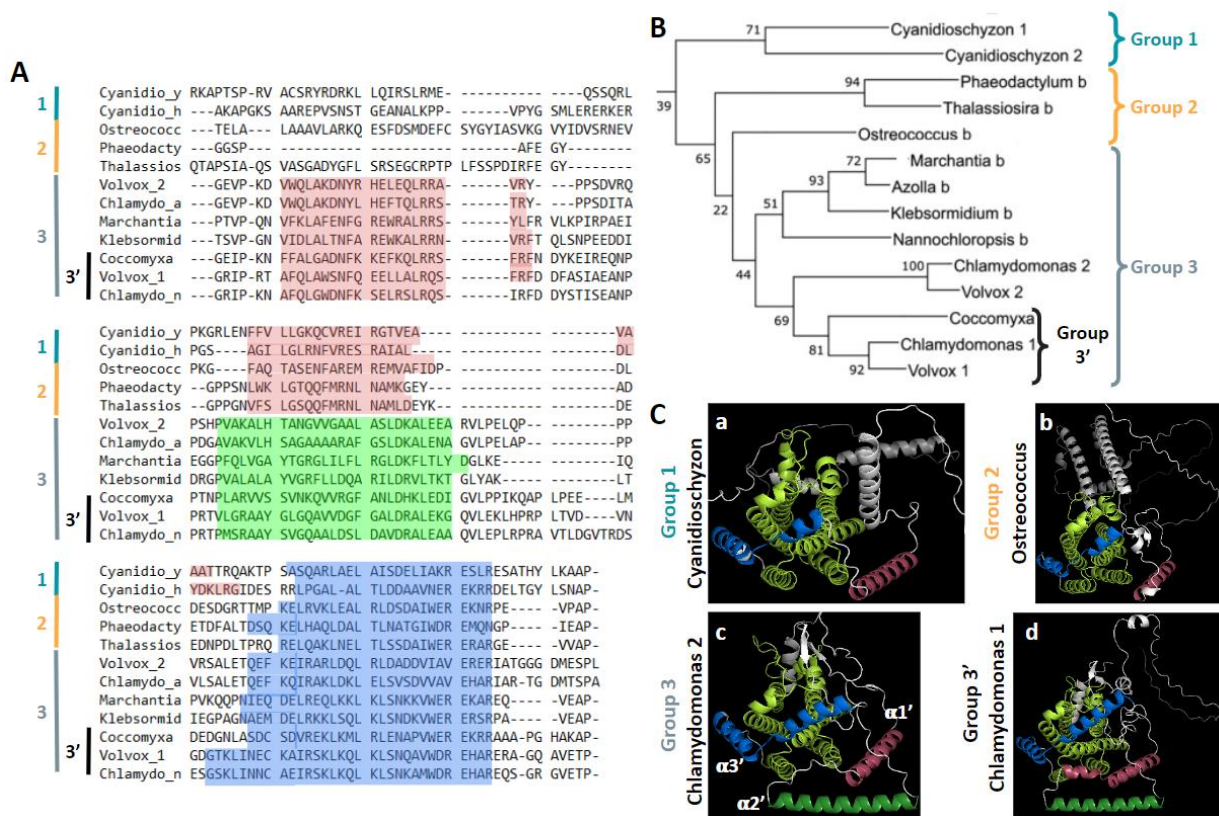


Figure 29: Comparison of Nter sequences of PTOX proteins according to phylogenetic analysis of Messant *et al.*, 2021

A. Sequence alignment of conserved Nter parts of the majority of protein sequences used for phylogenetic analysis performed in Messant *et al.* 2021. Sequence differences result in differences in Nter part structures. Three main groups have been defined : group 1 (light blue) includes the two proteins of *Cyanidioschyzon*, group 2 (orange) contains the proteins of *Ostreococcus* b, *Phaeodactylum* b and *Thalassiosira* b. Finally, group 3 (grey) regroups the rest of the proteins with a subcategory called group 3' containing the Nter parts of *Coccomyxa*, *Volvox* 1 and *Chlamydomonas* 1. The particular structures of the Nter parts are helices defined as follows : helix $\alpha 1'$ (red), hélice $\alpha 2'$ (green) et hélice $\alpha 3'$ (blue). **B.** Phylogenetic tree from the article Messant *et al.*, 2021. The establishment of groups through sequence alignment corresponds to the order of sequences during phylogenetic analysis. **C.** Complete protein sequence prediction by Alphafold and visualised by PyMol. Only one protein from each previously established group is shown here : group 1 (a) is characterised by the presence of a fairly large $\alpha 1'$ helix (dark red) and a $\alpha 3'$ helix (blue). Group 2 (b) has the same characteristics with just a shortening of the helix $\alpha 1'$ (dark red). Group 3 is marked by the appearance of the $\alpha 2'$ helix (dark green). Finally, the 3' group has a two-part $\alpha 1'$ (dark red) helix. For each of the 4 images, the conserved catalytic site is colored in light green and the rest of the protein in white.

Further experiments are needed to determine the importance of the Nter part of Alga-type PTOX. It has been shown in Messant *et al.*, 2022 (*submitted*) that its absence does not abolish catalytic activity *in vitro*. On the other hand, it could play a role in the attachment of the membrane or in the regulation of the catalytic activity by activating the protein or by regulating the accessibility of the enzyme for its substrate. Regarding membrane attachment, it is observed that the first α -1 helix (catalytic site) of Alga-type PTOX is generally shorter than that of Plant-type PTOX. For example, for MpPTOXa it contains 29 amino acids against only 18 for MpPTOXb. This seems to be largely the case for the different photosynthetic organisms studied (Table VI).

Table VI: Comparison of helices of the catalytic centre of Alga-type PTOX

Quantification of the number of amino acids forming the helices of the reaction centre of the proteins used for the phylogenetic analysis of Messant *et al.*, 2021. For each of these proteins the helices α -1 and α -4 corresponds to the amphipathic helices (AH) which dock the protein to the membrane while the helices α -2, α -3, α -5 and α -6 contain the 6 iron binding sites allowing the catalytic activity of proteins. The size of the linker between helices α -5 et α -6 was also quantified.

Species by phylogenetic order	Catalytic centre						
	α -1 (AH)	α -2 (Fe)	α -3 (Fe)	α -4 (AH)	α -5 (Fe)	linker	α -6 (Fe)
<i>Cyanidioschyzon</i> 1	17	29	24	24	32	38	22 - 33
<i>Cyanidioschyzon</i> 2	17	29	24	24	32	39	23 - 33
<i>Phaeodactylum</i> b	18	29	24	23	31	43	22
<i>Thalassiosira</i> b	18	29	24	23	32	44	22
<i>Ostreococcus</i> b	18	29	24	23	32	37	22
<i>Marchantia</i> b	18	29	24	23	32	36	23
<i>Klebsormidium</i> b	18	29	24	24	32	37	22
<i>Chlamydomonas</i> 2	17	29	24	25	32	41	23
<i>Volvox</i> 2	17	29	24	24	32	38	24
<i>Coccomyxa</i>	17	29	24	25	32	37	23
<i>Chlamydomonas</i> 1	17	30	24	24	33	38	24
<i>Volvox</i> 1	17	29	24	24	32	38	24

Thus, one could suppose that a part of the Nter extension would help for the attachment to the membrane which ended up being shortened during evolution to generate the isoform of the plant-types with a longer α -1 helix. To verify this theory, a sequence alignment was performed between the Nter part of the Alga-type PTOX and the first α -1 helix of the plant-type PTOX (Figure 30). It is observed that even if a sequence alignment has been generated, no similarity is observed between the two types of sequences. In particular, the helix α 3' which was previously supposed to be the most conserved absolutely does not match.

Phaeodacty	-----	-----	-----	-----	GRPLDESTKQ
Thalassios	-----	-----	-----	-----	GSPLSDSVKE
Klebsorm_a	-----DSAT	GWEAG	-----	-----	LIGVERR
Zostera	-----QGTPD	LLEIW	-----	-----	AIKFEHT
Marchant_a	-----ESPQ	GLEKW	-----	-----	VIAAEHG
Zea	-----SVVPS	SDDSW	-----	-----	VVKLEQS
Arabidopsi	-PNMSS	SSTS	AFETW	-----	IIKLEQG
Oryza	-----EPLVT	AEEESW	-----	-----	VVKLEQS
Azolla	-ETEGA	ASES	GWNRM	-----	VIKAEQG
Salvinia	---SAGS	IES	VMDGW	-----	VIRAEGK
Ostreococc	-----	RDDSL	-----	-----	LANAERA
Marchant	PTVPQNVFKL	AFENFGREWR	ALRRSYLFRV	LKPIRPAEIE	GGPFQLVGAY
Klebsorm_i	TSVPGNVIDL	ALTNFAREWK	ALRRNVRFTQ	LSNPEEDDID	RGPVVALALAY
Volvox_2	GEVPKDVWQL	AKDNYRHELE	QLRRAVRYPP	----SDVRQP	SHPVAKALHT
Chlamydo_a	GEVPKDVWQL	AKDNYLHEFT	QLRRSTRYPP	----SDITAP	DGAVAKVLHS
Coccomyxa	GEIPKNFFAL	GADNFKKEFK	QLRRSFRFND	YKEIREQNPP	TNPLARVVSS
Volvox_1	GRIPRTAFQL	AMSNFQEELL	ALRQSFRFDD	FASIAEANPP	RTVLGRAAYG
Chlamydo_n	GRIPKNAFQL	GWDNFKSELR	SLRQSIRFDD	YSTISEANPP	RTPHMSRAAYS
Phaeodacty	RNRQLVHQLK	SVLFDQVY	-----	-----	-----
Thalassios	ANRFAIGFLK	GTIFDTFF	-----	-----	-----
Klebsorm_a	INHALTDFV	ILL-DAFY	-----	-----	-----
Zostera	INSVLTETV	NIL-DVLY	-----	-----	-----
Marchant_a	FNTFATETV	KIL-ETLY	-----	-----	-----
Zea	FNIFATDSVI	MVL-KGVY	-----	-----	-----
Arabidopsi	VNVFLTDSVI	KIL-DTLY	-----	-----	-----
Oryza	VNIFLTESVI	TIL-DGLY	-----	-----	-----
Azolla	FNVLLTDSVI	LFL-DALY	-----	-----	-----
Salvinia	FNSLLTDIVI	RLL-DAVY	-----	-----	-----
Ostreococc	VNERLTASAV	AVT-DYLY	-----	-----	-----
Marchant	TGRGLILFLR	GLD-KFLT	--LYDGLKEIQ	PVKQ-----	----QPNIQ
Klebsorm_i	VGRFLLDQAR	ILD-RVLT	KTGLYAKLTIEG	PAG-----	----NAEM
Volvox_2	ANGVVGAAAL	SLD-KALEEA	RVLPELQPPP	VRSA-----	----LETQEF
Chlamydo_a	AGAAAAARAFG	SLD-KALENA	GVLPELAPPP	VLSA-----	----LETQEF
Coccomyxa	VNKQVVRGFA	NLD-HKLEDI	GVLPPIKQAP	LPEE----	LM DEDGNLASDC
Volvox_1	LGQAVVDGFG	ALD-RALEKG	QVLEKLHPRP	LTVD----	VN GDGTKLINEC
Chlamydo_n	VGQAALDSDL	AVD-RALEAA	QVLEPLRPPA	VTLDGVT	RDS ESGSKLINNC

Figure 30: Sequence alignment between the Nter parts of Alga-type and the α -1 helix of Plant-type PTOXs
 Sequence alignment was performed by MUSCLE (Edgar, 2004). Automatically, the sequences have been divided according to their membership: the Plant-type above and the Alga-type below the blue line. For the Plant-type, the helix α -1 has been coloured in red as before. For Alga-type, helices α '1 and α '2 have been coloured in red and green, respectively as before.

b) Special cases of Nter region of Alga-type PTOX of Nannochloropsis b and Azolla

Two proteins were intentionally excluded from the above results because they possess particular characteristics that are difficult to explain with the previously established model. Indeed, the *Nannochloropsis b* and *Azolla b* proteins present significant structural anomalies as shown in Figure 31. First, I observe that the Nter part of the *Azolla* protein corresponds completely to the protein model of the group 3 previously defined (with α 1', α 2' and α 3'). So, the previously established model does not fit to all Alga-type PTOX. These differences can be due to punctuated evolutionary events for example. On the other hand, the *Nannochloropsis b* protein does not present any of the three helices observed previously, not even the helix α 3' that was the most conserved. Surprisingly, the catalytic site of *Azolla* does not contain the first amphipathic helix of the catalytic site.

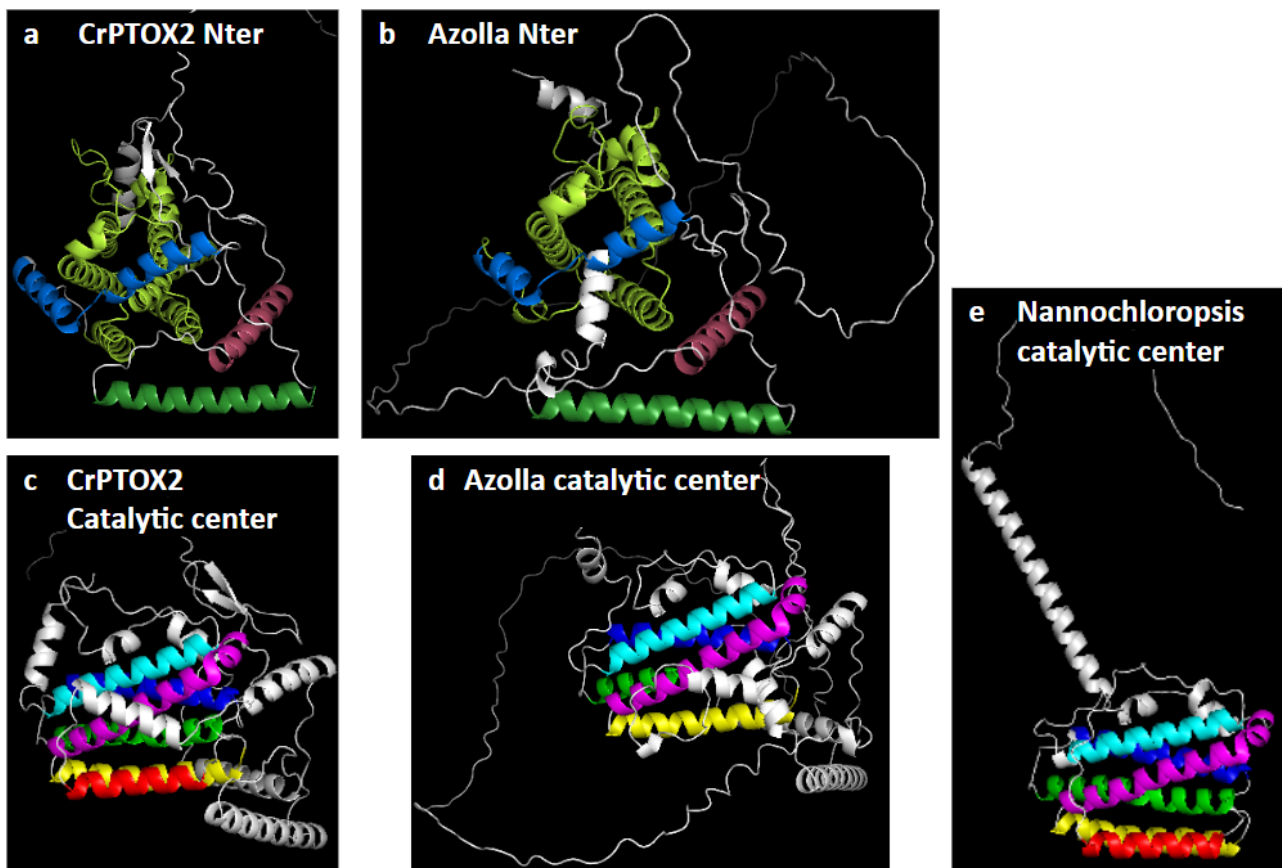


Figure 31: Comparison of protein structures of *Nannochloropsis b* and *Azolla* Alga-type PTOX with CrPTOX2
 Images **a** and **b** represent the Nter parts of the CrPTOX2 and *Azolla* proteins respectively. Helices $\alpha 1'$, $\alpha 2'$ et $\alpha 3'$ are colored in dark red, dark green and blue previously described. The catalytic site is coloured in light green in the background. Images **c**, **d** and **e** represent the catalytic sites of the CrPTOX2, *Azolla* and *Nannochloropsis b* proteins respectively. The proteins are oriented in such a way that the transmembrane helices (α -1, red and α -4, yellow) are located horizontally as they are supposed to be *in vivo*. The helices of the catalytic site are colored as follows : the helices α -1 and α -4 are in red and yellow while the helices containing the 6 iron binding sites, α -2, α -3, α -5 and α -6 are colored in green, blue, magenta and cyan. The Nter and Cter parts of the proteins as well as the linker between helices α -5 and α -6 appeared in white.

2) Comparison of Algae and Plant-type catalytic site sequences: re-definition of iron binding motifs

It has been shown that PTOX has six iron-binding sites conserved with AOX (Alternative Oxidase, McDonald *et al.*, 2003). Nevertheless, the sequence identity between Alga and Plant-type catalytic sites is only around 50% (Messant *et al.*, 2021). Moreover, activity measurements of recombinant proteins MpPTOXa and Nter truncated MpPTOXb highlight that MpPTOXa seems to be more active (Messant *et al.*, 2022, *submitted*). The sequence alignment between MpPTOXa and MpPTOXb catalytic sites revealed specific PTOX iron-binding motifs (Figure 32). So, I was interested in the comparison of the surroundings of the iron fixation sites according to those previously established by McDonald *et al.*, 2003.

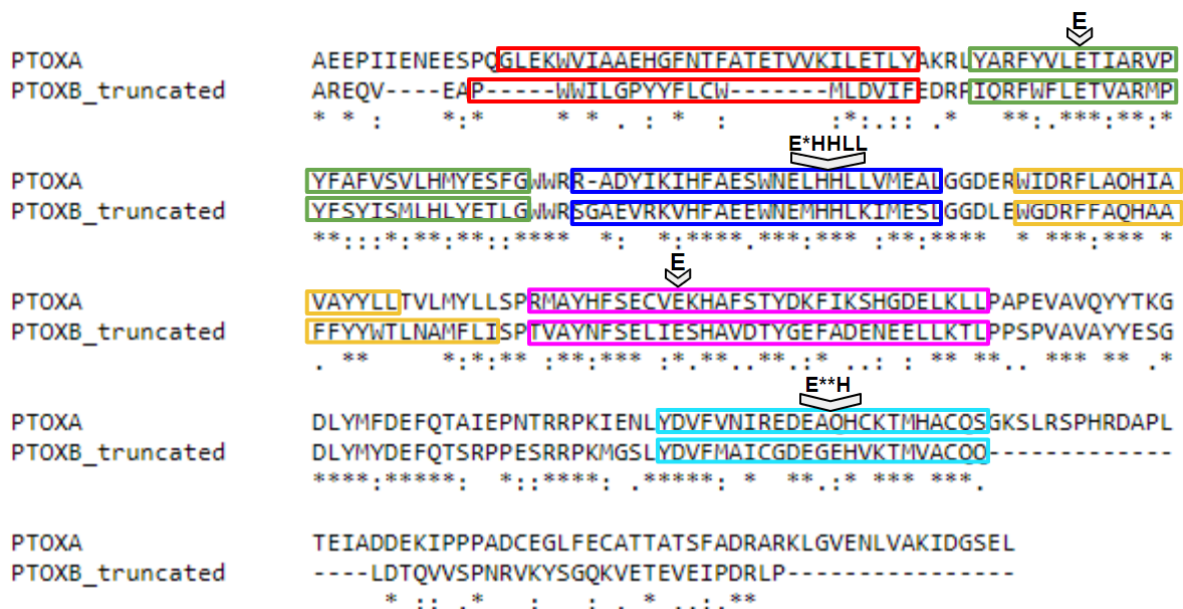


Figure 32: Sequence alignment of MpPTOXa and Nter truncated MpPTOXb catalytic sites

Sequence alignment of MpPTOXa and Nter truncated MpPTOXb catalytic sites by MUSCLE. The six helices α -1 (red), α -2 (green), α -3 (blue), α -4 (yellow), α -5 (magenta) and α -6 (cyan) are framed and the fourth iron binding sites motifs with the six iron binding sites determined by McDonald *et al.*, 2003 are indicated in bold above sequences.

The alignment of all catalytic sites sequences showed that two groups form spontaneously and correspond to the previously defined groups: The Plant and Alga-type PTOX (data not shown). To study the conserved sequences specific to each of the two groups, an alignment of the catalytic sequences was carried out separately and used to highlight the conserved regions (Figure 33). Solid arrows indicate residues only conserved in Alga-type (Figure 33, **A**) or in Plant-type (Figure 33, **B**) PTOX. The empty arrows correspond to variable residues in each of the two respective groups. It is observed that the conserved sequences in all the PTOX proteins are much greater than what was previously defined (McDonald *et al.*, 2003). The regions around the first three iron-binding sites seem to be particularly conserved in all PTOXs (helices α -2 and α -3) while for the other three, the regions seem more variable (helices α -5 and α -6). PyMol visualisation of both PTOX types (data not shown) highlight that conserved residues are localised inside catalytic sites, near to irons, or on the external side of α -2 and α -3 helices which were already hypothesised to be involved in PTOX dimerisation (Nawrocki *et al.*, 2015).

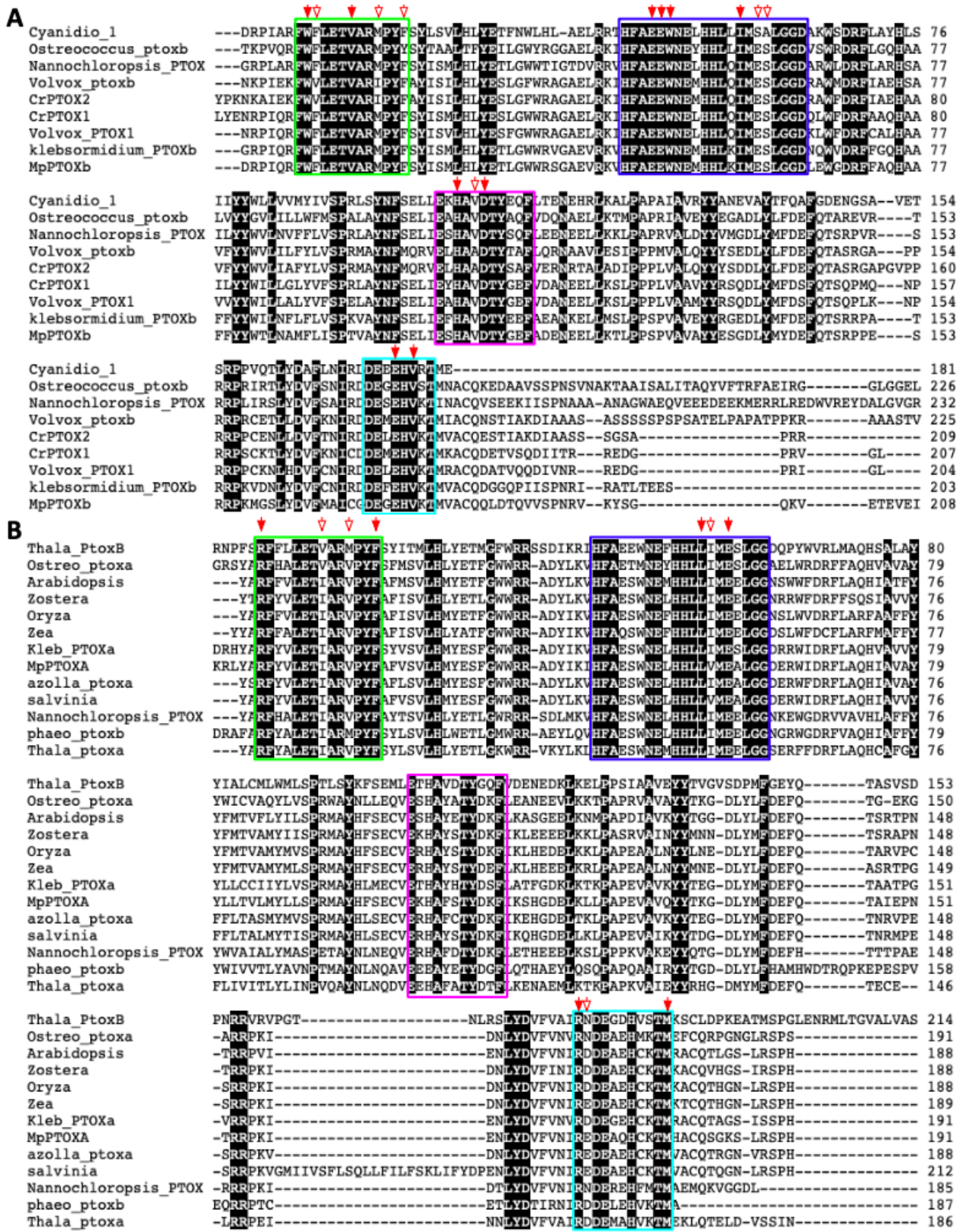


Figure 33: Sequence alignment between PTOX catalytic sites of different photosynthetic organisms
A. Alignment of the sequences of the catalytic sites of Alga-type PTOX used previously. **B.** The same alignment for Plant-type PTOX. Alignments were performed by MUSCLE and analysis of conserved sequences by Color Align Conservation software. The consensus parts of the catalytic sites are framed according to their position in the protein ($\alpha 2$, green; $\alpha 3$, blue; $\alpha 5$, magenta; $\alpha 6$, cyan). All conserved residues are highlighted in black. Solid red arrows correspond to completely conserved residues specific for Algae (**A**) or Plant-type (**B**) PTOX while empty arrows correspond to variable residues.

The results have been summarised in Figure 34 to be more readable and also to be compared with the alignment of the AOX sequence carried out by McDonald *et al.*, 2003.

First, it is observed that few residues are conserved in both oxidase families (highlighted in yellow). This is for example the case of leucine present in the first Iron-Binding Motif (IBM) considered to be important for a correct interaction between substrate and iron (Nawrocki *et al.*, 2015). But AOX and PTOX are not so close. Nawrocki *et al.*, 2015 showed that the α -1 and α -2 AOX helices are longer than those of PTOX. They suggested that this would reduce the binding pocket of the substrate and therefore give it its specificity. It can be hypothesised that the shortening of the α -1 helix in Alga-type PTOX regulate the catalytic activity by restricting the substrate binding pocket. Moreover, IBM in AOX are pretty well conserved with ~66 to 55% sequence identity (Figure 34) based on McDonald *et al.*, 2003 alignment. From another side, IBM1 and 2 are very well conserved through PTOX proteins (~70 and 66% sequence identity) while IBM3 and 4 are the most variable (~45 and 33% respectively).

Within the PTOX family, IBM from Alga-type are more conserved and those of Plant-type are more variable. The differences observed for IBM1 and 2 are amino acid substitutions having the same properties whereas it is more random for IBM3 and 4. Indeed, for IBM1 the Alga-type have the "LETVAR" motif whereas in plant-types valine can also be substituted by isoleucine which are both hydrophobic amino acids with side chains. And the conserved phenylalanine in all PTOX proteins has been hypothesised to be responsible for reducing the substrate-binding pocket.

To conclude, it could be interesting to use punctual mutations in order to determine the catalytic mechanism of PTOX and which amino acids are responsible for enzyme oligomerization.

			ID(%)	
<u>Iron-Binding Motif 1</u>				
AOX		LE (ST) (IV) A (AG)(CV) PG M	AOX	60%
AI-PTOX	*FW (FV)	LE T V A R (MI) PY (FY)	PTOX	70%
PI-PTOX	RF* * *	LE T (IV) A R (VM) PY F	Al-type	80% (57%)
			Pl-type	70% (57%)
<u>Iron-Binding Motif 2</u>				
AOX	L (LM) *E* (EY)	NERMHL	AOX	66%
AI-PTOX	H F AEE W	NE *HHL	PTOX	66%
PI-PTOX	H F A** *	NE *HHL	Al-type	91%
			Pl-type	66%
<u>Iron-Binding Motif 3</u>				
AOX	E E *A V *(ST) Y T * *		AOX	55%
AI-PTOX	E *HA (VA) D T Y * * F		PTOX	45%
PI-PTOX	E * *A * * T Y * * F		Al-type	64%
			Pl-type	45%
<u>Iron-Binding Motif 4</u>				
AOX	R *DE * *H* *V N H		AOX	58%
AI-PTOX	(RC) *DE *EHV *T (MI) *		PTOX	33%
PI-PTOX	R *DE * *H* *T M *		Al-type	50%
			Pl-type	50%

Figure 34: Comparison of iron binding sites of AOX proteins (McDonald *et al.*, 2003) and algae and plant-type PTOX

The motifs of the AOX were determined by McDonald *et al.*, 2003. The consensus sequences of the two types of PTOX were determined from the sequence alignment Figure 33. The residues in parentheses are the most frequently encountered, the stars correspond with highly variable residues. Residues conserved between the three types of proteins are highlighted in yellow and those conserved only between the PTOX proteins are highlighted in orange. On the left, the tables represent the percentage of residues conserved in AOX, (all) PTOX, Alga and Plant-type PTOX for each of the iron-binding motifs. Concerning IBM1, the values in parentheses were calculated from the “LE” motif to be able to be compared with the AOX sequence while the others take into account the entire sequence.

C) Part II conclusions and perspectives

To conclude, *Marchantia* is an ideal model to study PTOX across green lineage evolution because it has two isoforms, PTOXa, a plant-type PTOX and PTOXb, an alga-type PTOX as described in article 2. We have shown that PTOXb seems to be more important for chlororespiration. Then, the analysis of the $\Delta ptoxaptoxb$ double mutant and *imCRTI* lines (Messant *et al.*, 2022 *submitted*) highlights that PTOXs are important to protect PSI against photoinhibition and not PSII as previous studies suggested. Moreover, the activities of the recombinant proteins MpPTOXa and MpPTOXb truncated in Nter show that MpPTOXa has a catalytic activity three times greater. All our results converge towards the idea that the two types of PTOX, although catalysing the same reaction, do not play the same role within photosynthetic organisms. We suggested that the Alga-type PTOX would be present in all circumstances, finely regulated, while the plant-type would be activated only in the event of significant stress.

On the other hand, the *in silico* analysis highlights important characteristics at the level of the Nter part of the Alga-type but also of the catalytic site of the PTOX. Alga-type have up to 3 α helices in their Nter extensions. Site-directed mutagenesis experiments or the expression of truncated proteins *in vivo* could help determine their roles. For the moment, it is assumed that they are important for the regulation of catalytic activity. On the other hand, the analysis of the catalytic sites showed that the AOX and the PTOX share some essential residues which are important for iron ligation nevertheless, the regions which surround them are very variable between these two families. The IBMs of the AOX seem to be much more conserved than those of the PTOX. But this trend is not uniform among the PTOX family since the Alga-type has much more redundant IBM than those of the plant-type. Further analyses are needed to understand the catalytic activity of PTOX, but first differences highlighted by *in silico* analysis could help to explain the differences in activities already measured.

Finally, the mechanism of PTOX catalysis has never been defined. These sequence alignments could help identify amino acids important for electron transfer using mutated recombinant proteins whose activity would be analysed by transient absorption spectroscopy.

Part III : Dynamic changes in protein-membrane association for regulating Photosynthetic Electron Transport

Throughout the previous parts, the dynamics of membranes as well as photosynthetic complexes or regulatory proteins necessary for the protection of the electron transport chain have been underlying. For this, we conducted a theoretical reflection on what has already been proven of the establishment of these dynamics during alternative electron flows, non-photochemical quenching mechanisms and certain families of proteins as PTOX.

Article 4 : Dynamic changes in protein-membrane association for regulating Photosynthetic Electron Transport

In this review, we describe protective mechanisms of the photosynthetic apparatus in relation to changes in protein-membranes interactions. We have discussed cyclic electron flow, chlororespiration and the components of non-photochemical quenching. Finally, we have chosen examples of protection mechanisms involving dynamic changes of protein-membrane interactions that are not part of the major “photoprotection” schemes such as the Vesicle-Inducing Protein in Plastids (VIPP) proteins that influence nuclear gene expression and Plastid Terminal Oxidase that was thought to protect against PSII photoinhibition).

I mainly did the state transition and photoinhibition parts and I actively participated in discussions and critical reading.

Review

Dynamic Changes in Protein-Membrane Association for Regulating Photosynthetic Electron Transport

Marine Messant ¹, Anja Krieger-Liszskay ^{1,*} and Ginga Shimakawa ^{2,3} 

¹ Institute for Integrative Biology of the Cell (I2BC), CEA, CNRS, Université Paris-Saclay, CEDEX, 91198 Gif-sur-Yvette, France; marine.messant@cea.fr

² Research Center for Solar Energy Chemistry, Osaka University, 1-3 Machikaneyama, Toyonaka, Osaka 560-8531, Japan; gshimakawa@kwansai.ac.jp

³ Department of Bioscience, School of Biological and Environmental Sciences, Kwansai-Gakuin University, 2-1 Gakuen, Sanda, Hyogo 669-1337, Japan

* Correspondence: anja.krieger-liszskay@i2bc.paris-saclay.fr

Abstract: Photosynthesis has to work efficiently in contrasting environments such as in shade and full sun. Rapid changes in light intensity and over-reduction of the photosynthetic electron transport chain cause production of reactive oxygen species, which can potentially damage the photosynthetic apparatus. Thus, to avoid such damage, photosynthetic electron transport is regulated on many levels, including light absorption in antenna, electron transfer reactions in the reaction centers, and consumption of ATP and NADPH in different metabolic pathways. Many regulatory mechanisms involve the movement of protein-pigment complexes within the thylakoid membrane. Furthermore, a certain number of chloroplast proteins exist in different oligomerization states, which temporally associate to the thylakoid membrane and modulate their activity. This review starts by giving a short overview of the lipid composition of the chloroplast membranes, followed by describing supercomplex formation in cyclic electron flow. Protein movements involved in the various mechanisms of non-photochemical quenching, including thermal dissipation, state transitions and the photosystem II damage–repair cycle are detailed. We highlight the importance of changes in the oligomerization state of VIPP and of the plastid terminal oxidase PTOX and discuss the factors that may be responsible for these changes. Photosynthesis-related protein movements and organization states of certain proteins all play a role in acclimation of the photosynthetic organism to the environment.

Keywords: photosynthesis; regulation; abiotic stress; membrane association; thylakoid membrane



Citation: Messant, M.; Krieger-Liszskay, A.; Shimakawa, G. Dynamic Changes in Protein-Membrane Association for Regulating Photosynthetic Electron Transport. *Cells* **2021**, *10*, 1216. <https://doi.org/10.3390/cells10051216>

Academic Editor:
Suleyman Allakhverdiev

Received: 13 April 2021
Accepted: 13 May 2021
Published: 16 May 2021

Publisher's Note: MDPI stays neutral with regard to jurisdictional claims in published maps and institutional affiliations.



Copyright: © 2021 by the authors. Licensee MDPI, Basel, Switzerland. This article is an open access article distributed under the terms and conditions of the Creative Commons Attribution (CC BY) license (<https://creativecommons.org/licenses/by/4.0/>).

1. Introduction

The thylakoid membrane in chloroplasts is a complex three-dimensional structure that is morphologically highly dynamic, as seen by rearrangements of protein complexes under low light and high light conditions. The thylakoid membrane harbors the photosynthetic electron transport chain. It is known that several processes that regulate the efficiency of light harvesting and electron transport are linked to membrane dynamics. The electron transport chain is made out of the main protein complexes photosystem II (PSII), the site of water oxidation and oxygen release, the cytochrome *b₆f* complex (Cyt *b₆f*) and photosystem I (PSI), where ferredoxin is reduced. Reduced ferredoxin reduces NADP⁺ to NADPH, as catalyzed by the Ferredoxin NADP⁺ oxidoreductase (FNR). Both photosystems contain chlorophylls and carotenoids in their reaction centers, in the inner antenna and in the light harvesting complexes (LHC). During photosynthetic electron transport, a proton gradient (ΔpH) is established that is, together with an electrochemical gradient ($\Delta\Psi$), the driving force for the synthesis of ATP by the CF₀CF₁-ATP synthase. Regulation of light absorption efficiency of the pigment containing antenna systems and of photosynthetic electron transport is essential to allow the plant to acclimate rapidly to changes in light

intensities, which can occur, for example, in sun flecks, when shade leaves or whole plants are suddenly exposed to full sun light. Regulation of photosynthetic electron transport is also needed to fulfil the energetic demands of the chloroplast/cell/organism by optimizing the ATP/NADPH ratio. This can be achieved by changing the activity of cyclic electron transport around PSI, a process requiring formation and dissolution of supercomplexes. Well-characterized processes involved in the distribution of the LHCs between the photosystems, the so-called state transitions, depend on movements of large protein-pigment complexes within the membrane. Another well-known process that involves protein movements within the thylakoid membrane is the PSII damage–repair cycle. Furthermore, soluble proteins attach reversibly to the thylakoid, enabling their involvement in metabolic reactions and regulatory mechanisms (Figure 1).

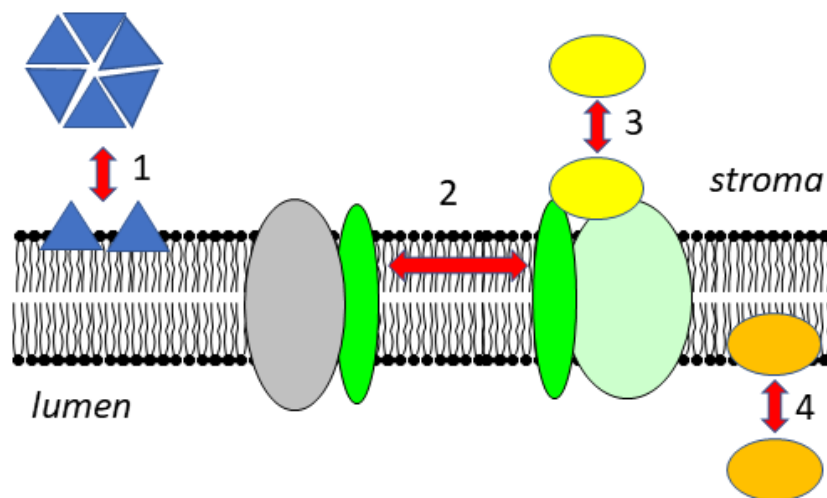


Figure 1. Dynamic changes of the association of proteins with the thylakoid membrane. In the stroma, proteins can be present in soluble forms or as peripheral membrane proteins, and their oligomerization state can change upon membrane association (1). Transmembrane proteins can move laterally within the membrane and are associated with different partner proteins (2). Soluble proteins can attach to protein complexes in the membrane (3). In the lumen, soluble proteins can attach to the membrane as a function of pH (4).

In this review, we first shortly describe the specific characteristics of the thylakoid membrane. Then, we focus on cyclic electron flow, alterations of the efficiency of light absorption and dissipation of excess energy as heat (non-photochemical quenching, NPQ), followed by a chapter on state transitions and the PSII damage–repair cycle. We will present other less well-known processes that are involved in the acclimation response of the photosynthetic apparatus and which depend on dynamic interactions with the thylakoid membrane (Figure 2). We focus mainly on processes taking place in eukaryotic photosynthetic organisms.

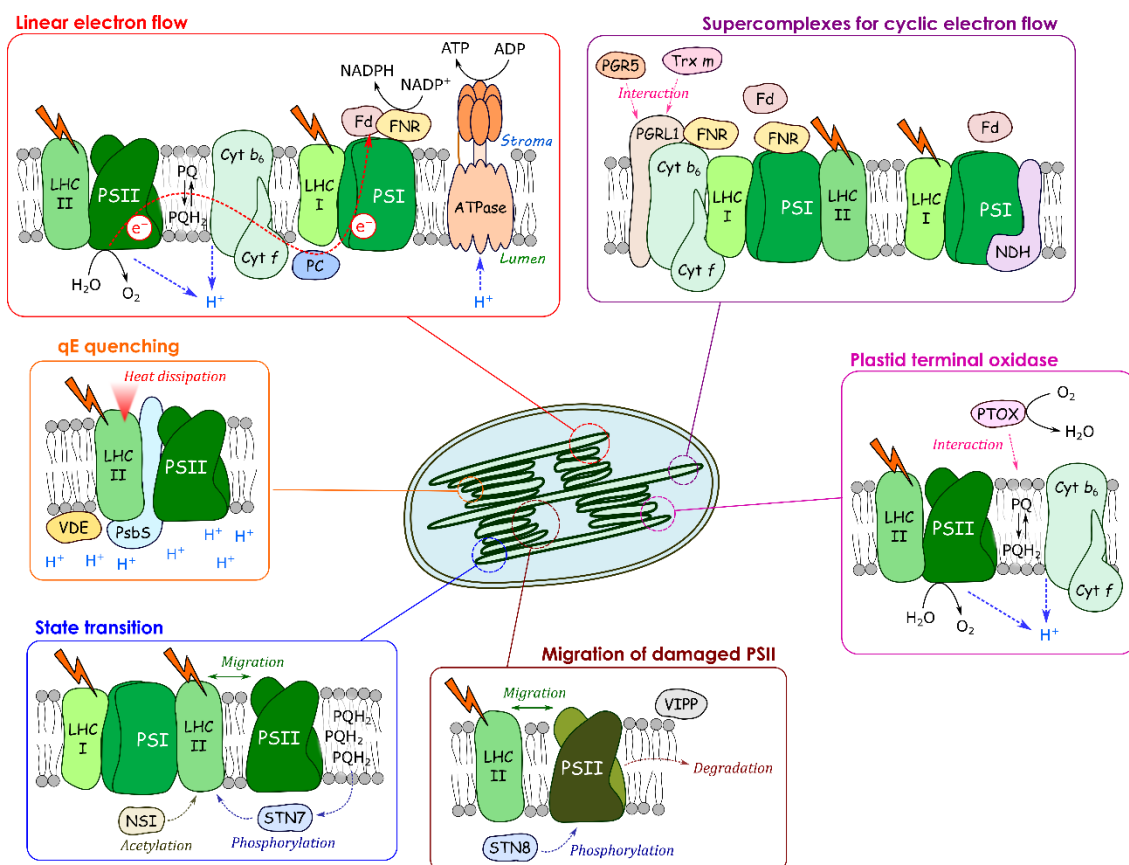


Figure 2. Dynamic changes of protein–membrane association for regulating photosynthetic electron transport. Photosynthetic linear electron flow produces NADPH and ATP for CO₂ assimilation in the grana margin. In the grana, heat dissipation at the light-harvesting complex (LHCII), the so-called qE quenching, occurs, and the damaged PSII migrates and is digested; In the grana margin, STN7 and NSI stimulate the state transition. PTOX changes its localization in response to stroma pH to maintain the PQ redox poise. A part of PSI forms supercomplexes with PGRL1, FNR and NDH in the stroma lamellae.

2. Membrane Composition

Chloroplast membranes have a very unique lipid composition with the galactolipids monogalactosyldiacylglycerol (MGDG), digalactosyldiacylglycerol (DGDG) and the glycolipid sulfoquinovosyl-diacylglycerol (SQDG) [1–4]. The external and the internal envelope membranes and the thylakoids have different lipid compositions. The outer envelope membrane is rather permeable, especially for ions, and is important for the connection between the chloroplast and the endoplasmic reticulum (ER), where protein translation principally takes place. It is composed of about 25% DGDG and 30% phosphatidylcholine, the main lipid of the ER membrane. On the contrary, the inner envelope membrane is particularly impermeable and serves as a barrier. The thylakoid membranes are mainly made of MGDG and DGDG (MGDG about 50%, DGDG about 30% of total lipid content). The lipids SQDG and phosphatidylglycerol (PG), the only major phospholipid in thylakoids, are negatively charged at neutral pH. Each represents about 10% of the total lipid content. The physicochemical properties of the head groups of the individual lipids are important for their behavior. MGDG and DGDG are neutral lipids with uncharged polar head groups. MGDG is not able to form a lipid bilayer in water because of its galactose head group [2,3]. In the thylakoid membranes, however, it forms a lipid bilayer thanks to the presence of a very high protein concentration. Compared with MGDG, DGDG has a bulkier headgroup with a cylindrical shape thanks to the presence of a second galactose residue allowing it to form a lamellar lipid bilayer. The glycolipids constitute the lipid matrix of the thylakoid membrane. As pointed out by Demé et al. [5] and Kobayashi et al. [6], the ratio of MGDG to

DGDG is important for the phase behavior of the lipid bilayer, and thereby for the structure and stability of the thylakoid membrane. The negatively charged lipids SQDG and PG may play a role in the interaction with peripheral membrane proteins.

Thylakoid membranes form distinct structures: the so-called grana stacks and stroma lamellae that differ in their protein composition. The outer layer of the grana stacks and the connection to the stroma lamellae is called the margin. Grana cores are rich in PSII and LHCII proteins. DGDG contributes to the stacking of the thylakoids in the grana [5] while PG is important for the trimerization as well as the stabilization of LHC complexes [7]. Stroma lamellae and margins are mainly composed of PSI, LHCI as well as around half of the Cyt *b₆f* complex. Margins contain more lipids per protein content than grana stacks and stroma lamellae [8]. According to Duchêne et al. [9], the distribution of the individual glycerolipids is identical in grana stacks, margins and stroma lamellae.

Lipids also have an important role as integrated components of the photosynthetic reaction centers, and are required for the optimal functioning of the photosystems. In cyanobacteria, absence of PG inhibits electron transfer between Q_A and Q_B at the acceptor side of PSII [10]. The crystal structure of PSII from cyanobacteria revealed the presence of four molecules of SQDG [11]. In the absence of SQDG, the electron flow from water to tyrosine Z is inhibited, possibly due to conformational changes in PSII [12]. According to Schaller et al. [13], SQDG influences the assembly of PSII core subunits and the antenna complexes. Several lipids were found in the structure of PSI from pea, with one being important for the connection between the Lhc subunit Lhca1 and the PSI subunit PsaF [14].

3. Dynamic Changes of Supercomplex Formation Required for Cyclic Electron Flow

Depending on the physiological conditions, a higher ATP/NADPH demand is required to fulfil the metabolic demands. Cyclic electron flow allows the generation of a proton gradient without the production of NADPH and serves to provide extra ATP. Alternatively, reduction of O₂ at PSI, the so-called Mehler reaction or pseudocyclic flow, also leads to an increase in the ΔpH and ATP synthesis. By increasing the ΔpH, cyclic electron flow contributes to the qE component of NPQ and to the regulation of linear electron flow at the level of the Cyt *b₆f* complex in so-called photosynthetic control. In addition, it may help to increase the volume of the lumen by pumping extra H⁺ into the lumen in the light. Swelling of the lumen facilitates diffusion of plastocyanin and may also allow the relocalization of luminal proteins like, for example, Deg proteases that are involved in the degradation of the D1 protein of PSII [15].

There are two pathways of cyclic electron flow, the first is insensitive to the inhibitor Antimycin A and involving the NDH complex, while the second is Antimycin-A-sensitive and involves the Cyt *b₆f* complex as well as the proton gradient regulation complex PGR5/PGRL1. A protein supercomplex composed of PSI with LHCI, LHCII, Cyt *b₆f* complex, FNR and the integral membrane protein PGRL1 has been isolated from *C. reinhardtii* and suggested to be a prerequisite for cyclic flow [16]. FNR may change its interaction partners and sub-chloroplast location as part of a mechanism to decrease CEF and increase LEF during light adaptation. FNR has been discussed for a long time to be either present in a soluble form in the stroma, or tethered to the thylakoid membrane by interaction with partner proteins. Recently, it has been demonstrated that FNR is always associated with the membrane [17]. This view that state transitions are a required for supercomplex formation was questioned by Takahashi et al. [18] who found the same protein composition of supercomplexes in *C. reinhardtii* wild type, and in a mutant incapable of performing state transitions. According to their data, there is no correlation between state transitions and cyclic electron flow, but rather between the latter and chloroplast redox state (anoxic versus oxic conditions). Furthermore, they reported the presence of PGRL1 together with FNR in high molecular weight fractions that did not contain PSI or Cyt *b₆f* complex. In this context, it is interesting to mention that thioredoxin m forms a complex with PGRL1 [19,20], which itself contains redox-active cysteine residues [21]. The formation of a complex between reduced thioredoxin m and PGRL1 may inhibit cyclic electron flow by preventing the

supercomplex formation required for cyclic flow. The work by Takahashi et al. [18], and the reports on the interaction between thioredoxin m and PGRL1 [19,20], indicate that formation of supercomplexes in the stroma lamellae depends on the redox state of the plastoquinone pool, and on the general redox state of the chloroplast.

The example of cyclic electron flow demonstrates that the protein localization is very dynamic, that it is likely under the control of the redox state of the chloroplast and that protein movements within the thylakoid membrane are needed for acclimation responses.

4. Protein Movements Involved in Non-Photochemical Quenching

One of the strategies to protect the photosynthetic apparatus from photo-oxidative damage is to dissipate excess light energy as heat at PSII, the so-called NPQ. NPQ is composed of several components that can be distinguished by their relaxation time in the darkness: q_E (seconds to minutes), state transitions, q_T (tens of minutes), and photoinhibition, q_I (hours). A long persisting quenching related to photoinhibition is called q_H . Here, we focus on the recent research progress on dynamic changes in protein–membrane association in NPQ, especially q_E , q_T (see also the recent review by Johnson and Wientjes [22]), and we will finish by introducing a newly found slowly relaxing quenching: q_H .

4.1. q_E Quenching

q_E quenching is the largest component of NPQ in short-term regulations in eukaryotic phototrophs. It occurs within the PSII antenna, the so-called LHCII. LHCII is the most abundant integral membrane protein in chloroplasts and binds 13–15 Chl *a* and Chl *b* molecules [23], 3–4 carotenoids [24] and one phospholipid [25] per monomer. Lumen acidification in the light changes the macro structure of thylakoid membranes affecting the associations between proteins and thylakoid membranes. Different models for the molecular mechanisms of q_E in plants and algae have been proposed in the last decades, and they are still a matter of debate. In the following, we describe q_E related to (a) the pH-dependent de-epoxidation of violaxanthin to the quencher zeaxanthin, (b) the protein PsbS and (c) to aggregation of LHC proteins.

(a) One proposed q_E mechanism depends on the formation of zeaxanthin as a quencher of excited states of chlorophyll. The xanthophyll cycle enzyme violaxanthin de-epoxidase (VDE), converting violaxanthin to zeaxanthin with the help of ascorbate, is an example of dynamic association of a protein to the thylakoid membranes. It is associated with the membrane depending on the pH in the lumen. VDE is localized at the luminal side of the thylakoid membrane and is attached to the membrane domain containing LHCII and being rich in MGDG when the luminal pH is approximately at 6.5 or less [26,27]. The structure of VDE at pH 7 is very different from its structure at pH 5 [28]. VDE is a monomer at pH 7 and a dimer at pH 5. At pH 5, a hydrophobic patch, likely to be involved in the membrane attachment of VDE, becomes surface exposed [28].

(b) The q_E -related pH-sensing protein PsbS affects the extent of q_E . The protein PsbS does not contain pigments itself but it is involved in zeaxanthin-dependent quenching [29,30]. PsbS has been shown to be associated to PSII, and its protonation state is essential for activating q_E . Fan et al. [29] resolved the structure of PsbS, and they discovered structural differences between the PsbS dimers at pH 7.3 and pH 5.0. According to their data, a conformational change at the luminal site may activate PsbS interaction with LHCII and thereby induce the quenching event. Kereiche and coworkers [31] proposed that PsbS controls the macro-organization of the grana membrane. PsbS was not exclusively found in LHCII-PSII supercomplexes, but was also found in PSI fractions [32]. The PsbS content seems to affect both, the grana stacks and the organization of photosynthetic complexes in the stroma lamellae, as demonstrated in freeze-fracture electron micrographs from isolated chloroplasts from wild type, *npq4* (mutant lacking PsbS) and L17 (mutant over-expressing PsbS) [33]. Haniewicz et al. [34] have shown that PsbS is mainly associated with monomeric PSII. This observation suggests that PsbS may play, in addition to

its involvement in qE, a role in the PSII repair cycle where dimeric PSII dissociates into monomeric PSII (see below).

(c) According to other models, qE is induced by aggregation of LHCII [35]. Quenching by aggregation can potentially occur in any form of LHCII but more likely it takes place within the major LHCII. LHCII aggregation is caused by the protonation of the antenna at the luminal side. Zeaxanthin is not necessary for the quenching, but may be important to couple LHCII aggregation with a change in ΔpH . The thylakoid membrane becomes thinner and hydrophobic in response to decreases in the lumen pH and the increase in NPQ [36]. Such changes may increase the probability that part of the LHCII detaches from PSII and aggregates. The lipid DGDG plays an important role in the macrostructure of the thylakoid membrane since it contributes to grana stacking [5], and it could favor the contact between LHCII trimers for excess energy dissipation [7]. Ostroumov et al. [37] recently observed a far-red emitting state in isolated aggregated LHCII and in LHCII crystals. This special state could explain how energy is dissipated. According to these authors, qE is derived from a charge transfer reaction involving a chlorophyll pair caused by a conformational change in aggregated LHCII [37]. In another model, qE is based on charge transfer between a chlorophyll-carotenoid pair. This model needs carotenoids such as zeaxanthin or lutein as the essential component for qE [38,39], and may require a closer association of PsbS with qE compared to the other models. In summary, the exact quenching mechanism is still controversial, although it is broadly accepted that qE occurs at the level of LHCII and involves carotenoids and PsbS.

4.2. qT: State Transition

State transition is defined as the migration of LHC from PSII (state 1) to PSI (state 2), increasing PSI antenna size and lowering excitation pressure in PSII (for reviews see [40–42]). The mechanism of state transition in plants involves phosphorylation of LHCII and detachment of phosphorylated LHCII from PSII. In physiological conditions, it takes place within minutes after a stress, and particularly during fluctuating light [43] or moderate heat stress [44]. State transitions can also be activated artificially by using specific wavelengths that preferentially excite PSII or PSI to change the redox state of the PQ pool (see below) [45]. In higher plants, state transition mobilizes approximately 15–20% of the LHCs.

The composition in Lhcb proteins of LHCII is complex. Arabidopsis has no fewer than 18 Lhcb proteins [46]; here, only the role of Lhcb1 to Lhcb6 is described. Lhcb 4 to 6 are known to be monomeric and interact directly with the PSII core whereas Lhcb 1 to 3 can form different combination of trimers interacting with monomeric Lhcbs, and these complexes are able to migrate differently during state transition. Three types of trimers are currently defined depending on their interaction with PSII: S-LHCs (strongly), M-LHCs (moderately), and L-LHCs (loosely bound). The latter are known to migrate more easily due to their composition of Lhcb1 and 2 [47]. They are defined as antennas shared between PSI and PSII. It has been shown that L-LHCs constitute almost 50% of the total trimers in plants cultivated in non-saturating light [40]. On the contrary, due to the presence of Lhcb3, M-LHCs are less mobile but their absence affects LHCII reorganization during state transition [48]. S-LHCs seem to be tightly associated with PSII, facilitating light harvesting at the periphery of PSII and ensuring efficient energy capture and transfer to the reaction center [49].

The specific thylakoid-bound transmembrane kinase responsible for state transitions, Stt7, was first discovered in *C. reinhardtii* [50]. Two years later, STATE TRANSITION 7 (STN7) serine/threonine kinase, the homologue of Stt7 in *A. thaliana*, was identified [51]. Activation of the kinase involves both the reduction state of the plastoquinone pool and the Cyt b_6f complex. When PSII is preferentially excited, over-reduction of the plastoquinone pool leads to the docking of a plastoquinol molecule to the Qo site of the Cyt b_6f complex. This activates the transmembrane kinase that phosphorylates LHCII [52–54]. Mutant analysis revealed that the activation of Stt7 depends on its interaction with the stromal side of Cyt b_6f complex, whereas its release for LHCII phosphorylation is controlled by

plastoquinol occupancy and turnover at the Qo site [53]. In addition, redox regulation via the reduction of a disulfide bridge plays a role in controlling the activity of the Stt7/STN7 kinases [55]. Recently, Wu and coworkers [56] showed that STN7 interacts with the Lumen Thiol Oxidoreductase 1 (LTO1), a transmembrane protein with a luminal thioredoxin domain. This interaction likely helps to keep STN7 in its oxidized active state required for LHCs phosphorylation. These data demonstrate a link between state transitions and the redox state of the chloroplast and especially that of the lumen. For a long time, phosphorylation of LHCII was the only known factor required for migration of LHCII. The STATE TRANSITION 8 kinase (STN8), an STN7 isoform, had been shown to be mainly involved in the phosphorylation of PSII core subunits such as D1, D2 and CP43 [57–59]. However, recent investigations have demonstrated that STN8 is also secondarily involved in LHCII phosphorylation at the same phosphorylated sites as the STN7 kinase, with a notable preference for Lhcb1 compared to Lhcb2 [60]. This is consistent with STN7 and phosphorylated Lhcb2 being more abundant in stroma lamellae, whereas STN8 and phosphorylated Lhcb1 locate preferentially in the grana core [61]. Recently, Koskela and coworkers [62,63] discovered that phosphorylation of LHCII is not sufficient to induce its migration alone. Plants lacking the acetyltransferase NUCLEAR SHUTTLE INTERACTING (NSI) are locked in state 1, despite phosphorylation of LHCII. NSI acetylates lysins of several proteins including subunits of PSI, PSII and LHCII. Taking together, these findings demonstrate that post-translational modifications that increase the negative charges of the LHC proteins are key elements for state transition. The return to state 1 is initiated by LHCII dephosphorylation mediated by THYLAKOID-ASSOCIATED PHOSPHATASE 38/PROTEIN PHOSPHATASE 1 (TAP38/PPH1) phosphatase [64,65].

How exactly LHCII migrate from PSII to PSI along the thylakoid membrane is still unknown. Several hypotheses can be found in the literature: (1) LHCII are transferred from grana stacks to stroma lamellae or (2) PSI approaches grana margins where, after a reorganization of the margin domain, an association of the PSI-LHCI-LHCII supercomplex takes place [66,67]. Phosphorylation of Lhcb1 could increase its mobility and the removal of peripheral antenna from PSII complexes. Furthermore, it could permit unstacking of grana [68–70]. However, other experiments revealed that phosphorylated Lhcb1 is not included in LHCII trimer binding to PSI [71,72]. Further characterization of a protein discovered 15 years ago gives new insights. CURVATURE THYLAKOID1 (CURT1) B protein, also known as TMP14, was identified by the same phosphoproteomic approaches as STN7. Initial experiments have shown that CURT1B is only localized in PSI fractions, and that it interacts with PsaL, H and O subunits [73]. Furthermore, CURT1B is present in specific regions of grana margins, i.e., the curvature of the grana edges where it is responsible for changes in grana dimensions according to light quality and quantity. CURT1B phosphorylation correlates with LHCII phosphorylation and PSI-LHCII interaction and, according to Trotta and coworkers [74], is key to modulation of thylakoid lateral heterogeneity and/or the decrease in grana diameter.

The interaction between PSI and LHCII was shown to be as strong as the binding of LHCII to PSII [75]. Structural analysis has highlighted that PSI-LHCI-LHCII complex is composed of a unique LHCII trimer, which binds to the PSI core on the opposite side of LHCI. However, it has also been reported that supercomplexes with a second LHCII trimer can bind to PSI to another site involving LHCI [76–79]. Pan and coworkers [80] recently published a structure showing interaction of PSI-LHCII of maize, involving the PSI subunits PsaO, L, H and potentially PsaK. According to this structure, PsaO, H and particularly PsaL interact directly with phosphorylated Lhcb2. PsaO seems to be involved in light energy transfer from Lhcb2 to PSI core, while PsaK could function similar for Lhcb1.

4.3. *qI*: Photoinhibition

Photoinhibition is characterized by a loss of maximum chlorophyll fluorescence and a loss of water-splitting activity in PSII. Photoinhibition is a process that occurs when the photo-oxidative damage to PSII is greater than its repair [81]. This phenomenon takes place

when plants are facing stressful conditions, such as higher light intensities than required for photosynthesis. In the most drastic cases, it is characterized by a sharp decrease in the photosynthetic capacity of the plant due to loss of linear electron transport. The D1 protein of PSII is considered in the literature to be the principal protein damaged under photoinhibitory conditions [82–84]. It is known for having a very rapid turnover in the order of 20 min [85,86], thanks to a very efficient repair system. Under photoinhibitory conditions, the acceptor side of the PSII is over-reduced, which results in the production of reactive oxygen species and, in particular, singlet oxygen that is responsible for the damage of D1 [87]. In addition, photoinhibition can also take place at the donor side of PSII inhibiting the $[\text{Mn}_4\text{CaO}_5]$ cluster, thereby limiting electron donation to Tyr_z^+ and P680^+ [88].

The movement of proteins within the thylakoid membranes and the association of proteins with the membrane/photosystems are important for not only qE and qT, but also for the PSII repair process. Active PSII dimers are located in grana stacks, whereas the PSII repair cycle occurs in grana margins. First, damaged PSII centers are phosphorylated by STN8 leading to the disassembly of LHCII-PSII complexes and PSII dimers [57,58,89]. However, a study of the *stn8* mutant highlighted that the repair is not completely dependent on phosphorylation [57] but that the later facilitates lateral mobility and, therefore, the transport of damaged PSII from the grana stacks to the margins [66]. A study of fluorescence recovery in a confocal laser-scanning microscope suggested that a limited population of chlorophyll-containing proteins can move within a 10-min time scale [90]. The population of mobile proteins increased after PSII photoinhibition in wild type but not in the *stn8* mutant of *A. thaliana*. This suggests that migration of damaged PSII depends on phosphorylation of certain subunits. In the grana margins, photoinhibited PSII is dephosphorylated again in order to allow partial disassembly of PSII monomers and to trigger degradation [91,92]. Upon arrival at grana margins, only the intermediate PSII complex RC47 remains, which is recognized by the protease FtsH [93,94]. FtsH is a complex of metalloproteases anchored to the thylakoid membrane, and it is important for the formation of thylakoid membranes during chloroplast development as well as in their maintenance [95,96]. In addition to FtsH, stromal and luminal Deg proteases act in a cooperative manner, allowing the endopeptidase cleavage of the D1 protein. It is assumed that the action of both stromal and luminal Deg proteases makes it possible to increase the number of D1 recognition sites for FtsH, and to facilitate the dissociation of the water-oxidizing complex [97–99].

A new quenching component, qH, active during photoinhibition and completely independent from the other mechanisms cited so far, has recently been reported [100,101]. qH has been described as a slowly relaxing quenching with photoprotective action which acts in concert with other quenching mechanisms involved in qI. The site of qH has been localized in the peripheral antenna of PSII. Until now, three proteins have been identified to be involved in qH: LCNP, a plastid lipocalin protein, is necessary for qH activation while for the relaxation of qH, two proteins were identified so far: SOQ1 for SUPPRESSOR OF QUENCHING 1 and the protein RELAXATION OF QH1 (ROQH1). LCNP-mediated modification of a thylakoid membrane lipid was proposed to change the conformation of LHCII and thus create a quenching site [100]. SOQ1 is a transmembrane protein that constitutively inhibits qH. LCNP is located in the thylakoid lumen and may interact with the SOQ1 domains responsible for regulating qH. ROQH1 is an atypical short-chain dehydrogenase-reductase and functions as a qH-relaxation factor. It may either directly remove the quenching conformation of the antenna or modify the hydrophobic environment at the LHCII. An *A. thaliana* *soq1roqh1* double mutant shows constitutive qH [101].

5. Proteins with Dynamic Changes in Oligomerization State and Localization at the Thylakoid Membrane

In the following, we introduce two proteins (PTOX, VIPP) that are related to the response to high light stress. These proteins are activated by perturbation of the redox

poise of the photosynthetic electron transport chain. They permit a protection of the photosynthetic electron transport chain against over reduction (PTOX), or play a role in the repair of damaged PSII (VIIP). The common point of these proteins is changes in their oligomerization state and their association with the thylakoid membrane, depending on the physiological condition.

5.1. Plastid Terminal Oxidase (PTOX)

The plastid terminal oxidase (PTOX), a plastoquinone:plastoquinone oxidoreductase of the thylakoid membranes, contains a catalytic center similar to that of the alternative oxidases of the mitochondria (AOXs), and the two enzymes share structural similarities [102]. PTOX is involved in carotenoid metabolism, it protects the photosynthetic electron transport chain against over-reduction, it participates in chlororespiration, and it may be important for setting the redox poise for cyclic electron transport. PTOX has been localized in the region of the stroma lamellae in spinach chloroplasts of non-stressed leaves [103]. It was recently demonstrated that PTOX can relocalize within the membrane [104], or can even reversibly associate to the membrane depending on the proton motive force [105]. Stepien and Johnson [104] showed that PTOX overexpressed in the halophile *Eutrema salsugineum* moved from the stroma lamellae to the grana stacks upon exposure of the plants to salt stress. Using confocal fluorescence microscopy, Bolte and coworkers [105] investigated PTOX localization in *A. thaliana* overexpressing green fluorescent protein (GFP)-PTOX. They observed a relatively homogeneous distribution of the GFP fluorescence over the whole chloroplasts when leaves had been pre-illuminated with high light intensities, a condition generating a high proton motive force. In contrast, when leaves were treated with uncouplers, or had been adapted to the dark, the GFP fluorescence was localized in spots. The spots were interpreted as PTOX oligomers. These results show that PTOX localization within the chloroplast is highly dynamic and depends on the pH in the stroma, and/or on the ion concentration. Membrane association with the grana lamellae is required to allow PTOX the access to its lipophilic substrate plastoquinol. In vitro, purified PTOX associated at slightly alkaline pH-value to liposomes composed of a lipid mixture similar to thylakoid membranes. Enzymes of the carotenoid biosynthesis pathway may behave in a similar manner like PTOX. As mentioned above, at low pH in the lumen, VDE changes its conformation, dimerizes and attaches to the membrane, thereby gaining access to the lipophilic violaxanthin. Furthermore, the phytoene desaturase that requires PTOX activity for the regeneration of its electron acceptor, plastoquinone, seems also to change its oligomeric state and thereby its activity. Gemmecker et al. [106] reported that phytoene desaturase exists in vitro in rings or stacks. The rings were composed of tetramers, which assembled into highly ordered stacked tubular structures of a length between 15–30 nm. The oligomeric stacks were soluble, while the form attached to liposomes was assigned to a single tetrameric ring. It is likely that the same distribution for phytoene desaturase is found inside the chloroplasts: a soluble form organized in stacks in the stroma and the smaller tetramers attached to the thylakoid membrane, allowing access to its substrate phytoene. Similar changes in the oligomerization state as described for the phytoene desaturase may also take place for PTOX. The catalytically functional unit of PTOX consists most likely of a dimer as it is the case for AOX [107]. Recombinant fusion protein maltose-binding protein-PTOX (MBP-PTOX) of rice tends to form different oligomeric states depending on the detergent used. In the presence of *n*-octyl β -D-glucopyranoside, MBP-PTOX was found mainly as a tetramer [108], while it was mainly in a dimeric form in the presence of β -dodecyl-maltoside [105]. Angiosperms contain one PTOX isoform, while other phylae mostly contain two isoforms; a plant-type PTOX and an algal-type PTOX [109]. The algal-type PTOX has a longer N-terminal extension that probably allows a stronger anchoring of this protein to the membrane. A dynamic association of PTOX with the thylakoid membrane may be important to permit PTOX activity only under conditions of a highly reduced electron transport chain, thereby preventing competition between PTOX and Cyt *b₆f* complex for plastoquinol under optimal conditions for photosynthesis.

The same holds for the VDE, permitting the formation of antheraxanthin and zeaxanthin only under certain physiological conditions. The activity of other carotenoid biosynthesis enzymes, such as phytoene desaturase, may be regulated in a similar way.

5.2. Vesicle-Inducing Proteins in Plastids (VIPP)

Another example of a stroma protein that changes its oligomerization state, and its membrane association, is the vesicle-inducing protein in plastids (VIPP). Plants contain only one isoform, VIPP1, while chlorophyceae have a paralog of VIPP1, called VIPP2. In chloroplasts, VIPP1 has been found at different location within the chloroplast: in a soluble form in the stroma, and in a membrane-associated form at the chloroplast envelope and at the thylakoids. In vitro, VIPP1 and VIPP2 form large oligomeric rod-like structures [110,111]. Fluorescence microscopy in vivo revealed high oligomerization states of VIPP1 as punctae, indicating that VIPP1 may assemble into higher-order oligomers not only in vitro but also in vivo [112,113]. The chloroplast chaperone system, with HSP70B-CDJ2-CGE1 being interaction partners of VIPP, plays a role in controlling the oligomerization state of VIPP [110]. A role in membrane vesicle traffic and in the biogenesis of the lipid part of thylakoid membranes had been originally attributed to VIPP1 [114] while it was later shown to be also involved in high light stress response [112,113,115]. In cyanobacteria, VIPP1 punctae dynamically form at or close to highly curved thylakoid membranes. At high light intensities, the membrane-bound form of VIPP1 was favored compared to lower light intensities when more of the cytosolic form was present [112,113]. In *C. reinhardtii*, both VIPP1 and VIPP2 accumulate under photoinhibitory conditions and likely play a role in the PSII repair cycle [115]. A certain level of VIPP1 proteins was present in all light conditions, while VIPP2 was only detectable after high light stress [116]. In *C. reinhardtii*, VIPP1 knock-down lines showed defects in PSII biogenesis and in repair of photoinhibited PSII [115]. These results indicate that VIPP1 has an important role in creating membrane domains that favor disassembly and repair of photoinhibited PSII.

6. Conclusions and Perspectives

In the present review, we give examples that show the physiological importance and the complexity of dynamic changes of protein associations to and within the thylakoid membrane. The photosynthetic electron transport components (PSII, PSI, LHCII, etc.) are heterogeneously distributed in the thylakoid membrane. The protein composition of supercomplexes changes depending on the physiological situation. Protein movements play a role in short-term regulatory mechanisms that protect the photosynthetic apparatus against photo-oxidative damage. Protein–membrane associations are required for the PSII damage–repair cycle and for the biogenesis of the photosynthetic apparatus in general. Dynamic changes of membrane association of VDE, phytoene desaturase and PTOX allow a regulation of their enzymatic activity by allowing access to their lipophilic substrates. In addition, local differences in pH and in ion concentrations are likely, creating domains which may favor membrane association of proteins. At present, it is unknown to which degree such local domains with differences in proton or ion concentration are separated or shared, and how much (how fast) changes in these heterogeneities are associated with the regulation of photosynthetic electron transport.

Many questions remain open like the effects of ions and pH on the relocalization of proteins, factors that determine the oligomerization state of proteins, associated lipids or protein partners that allow changes in oligomerization states and in the association of proteins to the membrane. Recent development of super resolution microscopy, and fluorescence lifetime imaging on plants expressing fluorescent proteins, will allow better characterization of dynamic protein localizations and structural rearrangements of the thylakoid membrane upon exposure of plants to changes in the environment.

Funding: This research received no external funding.

Acknowledgments: We thank Thomas Roach (Innsbruck University, Austria) for critical reading of the manuscript. This work benefited from the support by the LabEx Saclay Plant Sciences-SPS (grant number ANR-17-EUR-0007).

Conflicts of Interest: The authors declare no conflict of interest.

References

1. Kobayashi, K. Role of membrane glycerolipids in photosynthesis, thylakoid biogenesis and chloroplast development. *J. Plant Res.* **2016**, *129*, 565–580. [[CrossRef](#)]
2. Shipley, G.G.; Green, J.P.; Nichols, B.W. The phase behavior of monogalactosyl, digalactosyl, and sulphoquinovosyl diglycerides. *Biochim. Biophys. Acta Biomembr.* **1973**, *311*, 531–544. [[CrossRef](#)]
3. Jouhet, J. Importance of the hexagonal lipid phase in biological membrane organization. *Front. Plant Sci.* **2013**, *4*, 494. [[CrossRef](#)] [[PubMed](#)]
4. Murphy, D.J. The importance of non-planar bilayer regions in photosynthetic membranes and their stabilisation by galactolipids. *FEBS Lett.* **1982**, *150*, 19–26. [[CrossRef](#)]
5. Demé, B.; Cataye, C.; Block, M.A.; Maréchal, E.; Jouhet, J. Contribution of galactoglycerolipids to the 3-dimensional architecture of thylakoids. *FASEB J.* **2014**, *28*, 3373–3383. [[CrossRef](#)] [[PubMed](#)]
6. Kobayashi, K.; Endo, K.; Wada, H. Specific distribution of phosphatidylglycerol to photosystem complexes in the thylakoid membrane. *Front. Plant Sci.* **2017**, *8*, 1991. [[CrossRef](#)] [[PubMed](#)]
7. Liu, Z.; Yan, H.; Wang, K.; Kuang, T.; Zhang, J.; Gui, L.; An, X.; Chang, W. Crystal structure of spinach major light-harvesting complex at 2.72 Å resolution. *Nature* **2004**, *428*, 287–292. [[CrossRef](#)]
8. Koochak, H.; Puthiyaveetil, S.; Mullendore, D.L.; Li, M.; Kirchoff, H. The structural and functional domains of plant thylakoid membranes. *Plant J.* **2019**, *97*, 412–429. [[CrossRef](#)] [[PubMed](#)]
9. Duchêne, S.; Siegenthaler, P.A. Do glycerolipids display lateral heterogeneity in the thylakoid membrane? *Lipids* **2000**, *35*, 739–744. [[CrossRef](#)]
10. Itoh, S.; Kozuki, T.; Nishida, K.; Fukushima, Y.; Yamakawa, H.; Domonkos, I.; Laczkó-Dobos, H.; Kis, M.; Ughy, B.; Gombos, Z. Two functional sites of phosphatidylglycerol for regulation of reaction of plastoquinone Q_B in photosystem II. *Biochim. Biophys. Acta Bioenerg.* **2012**, *1817*, 287–297. [[CrossRef](#)]
11. Umena, Y.; Kawakami, K.; Shen, J.-R.; Kamiya, N. Crystal structure of oxygen-evolving photosystem II at a resolution of 1.9 Å. *Nature* **2011**, *473*, 55–60. [[CrossRef](#)]
12. Minoda, A.; Sato, N.; Nozaki, H.; Okada, K.; Takahashi, H.; Sonoike, K.; Tsuzuki, M. Role of sulfoquinovosyl diacylglycerol for the maintenance of photosystem II in *Chlamydomonas reinhardtii*. *Eur. J. Biochem.* **2002**, *269*, 2353–2358. [[CrossRef](#)] [[PubMed](#)]
13. Schaller, S.; Latowski, D.; Jemioła-Rzemińska, M.; Dawood, A.; Wilhelm, C.; Strzałka, K.; Goss, R. Regulation of LHCII aggregation by different thylakoid membrane lipids. *Biochim. Biophys. Acta Bioenerg.* **2011**, *1807*, 326–335. [[CrossRef](#)] [[PubMed](#)]
14. Mazor, Y.; Borovikova, A.; Nelson, N. The structure of plant photosystem I super-complex at 2.8 Å resolution. *eLife* **2015**, *4*, e07433. [[CrossRef](#)] [[PubMed](#)]
15. Kirchoff, H.; Hall, C.; Wood, M.; Herbstová, M.; Tsabari, O.; Nevo, R.; Charuvi, D.; Shimoni, E.; Reich, Z. Dynamic control of protein diffusion within the granal thylakoid lumen. *Proc. Natl. Acad. Sci. USA* **2011**, *108*, 20248–20253. [[CrossRef](#)] [[PubMed](#)]
16. Iwai, M.; Takizawa, K.; Tokutsu, R.; Okamuro, A.; Takahashi, Y.; Minagawa, J. Isolation of the elusive supercomplex that drives cyclic electron flow in photosynthesis. *Nature* **2010**, *464*, 1210–1213. [[CrossRef](#)]
17. Kramer, M.; Rodriguez-Heredia, M.; Saccon, F.; Mosebach, L.; Twachtmann, M.; Krieger-Liszka, A.; Duffy, C.; Knell, R.J.; Finazzi, G.; Hanke, G.T. Regulation of photosynthetic electron flow on dark to light transition by ferredoxin:NADP(H) oxidoreductase interactions. *eLife* **2021**, *10*, e56088. [[CrossRef](#)]
18. Takahashi, H.; Clowez, S.; Wollman, F.-A.; Vallon, O.; Rappaport, F. Cyclic electron flow is redox-controlled but independent of state transition. *Nat. Commun.* **2013**, *4*, 1954. [[CrossRef](#)]
19. Okegawa, Y.; Motohashi, K. M-type thioredoxins regulate the PGR5/PGRL1-dependent pathway by forming a disulfide-linked complex with PGRL1. *Plant Cell* **2020**, *32*, 3866–3883. [[CrossRef](#)]
20. Wolf, B.-C.; Isaacson, T.; Tiwari, V.; Dangoor, I.; Mufkadi, S.; Danon, A. Redox regulation of PGRL1 at the onset of low light intensity. *Plant J.* **2020**, *103*, 715–725. [[CrossRef](#)]
21. Hertle, A.P.; Blunder, T.; Wunder, T.; Pesaresi, P.; Pribil, M.; Armbruster, U.; Leister, D. PGRL1 is the elusive ferredoxin-plastoquinone reductase in photosynthetic cyclic electron flow. *Mol. Cell* **2013**, *49*, 511–523. [[CrossRef](#)] [[PubMed](#)]
22. Johnson, M.P.; Wientjes, E. The relevance of dynamic thylakoid organisation to photosynthetic regulation. *Biochim. Biophys. Acta Bioenerg.* **2020**, *1861*, 148039. [[CrossRef](#)]
23. Peter, G.F.; Thornber, J.P. Biochemical composition and organization of higher plant photosystem II light-harvesting pigment-proteins. *J. Biol. Chem.* **1991**, *266*, 16745–16754. [[CrossRef](#)]
24. Ruban, A.V.; Lee, P.J.; Wentworth, M.; Young, A.J.; Horton, P. Determination of the stoichiometry and strength of binding of xanthophylls to the photosystem II light harvesting complexes. *J. Biol. Chem.* **1999**, *274*, 10458–10465. [[CrossRef](#)]

25. Nußberger, S.; Dörr, K.; Wang, D.N.; Kühlbrandt, W. Lipid-protein interactions in crystals of plant light-harvesting complex. *J. Mol. Biol.* **1993**, *234*, 347–356. [[CrossRef](#)] [[PubMed](#)]
26. Goss, R.; Greifenhagen, A.; Bergner, J.; Volke, D.; Hoffmann, R.; Wilhelm, C.; Schaller-Laudel, S. Direct isolation of a functional violaxanthin cycle domain from thylakoid membranes of higher plants. *Planta* **2017**, *245*, 793–806. [[CrossRef](#)]
27. Hager, A.; Holocher, K. Localization of the xanthophyll-cycle enzyme violaxanthin de-epoxidase within the thylakoid lumen and abolition of its mobility by a (light-dependent) pH decrease. *Planta* **1994**, *192*, 581–589. [[CrossRef](#)]
28. Arnoux, P.; Morosinotto, T.; Saga, G.; Bassi, R.; Pignol, D. A structural basis for the pH-dependent xanthophyll cycle in *Arabidopsis thaliana*. *Plant Cell* **2009**, *21*, 2036–2044. [[CrossRef](#)]
29. Fan, M.; Li, M.; Liu, Z.; Cao, P.; Pan, X.; Zhang, H.; Zhao, X.; Zhang, J.; Chang, W. Crystal structures of the PsbS protein essential for photoprotection in plants. *Nat. Struct. Mol. Biol.* **2015**, *22*, 729–735. [[CrossRef](#)]
30. Li, X.-P.; Müller-Moulé, P.; Gilmore, A.M.; Niyogi, K.K. PsbS-dependent enhancement of feedback de-excitation protects photosystem II from photoinhibition. *Proc. Natl. Acad. Sci. USA* **2002**, *99*, 15222–15227. [[CrossRef](#)]
31. Kereiche, S.; Kiss, A.Z.; Kouřil, R.; Boekema, E.J.; Horton, P. The PsbS protein controls the macro-organisation of photosystem II complexes in the grana membranes of higher plant chloroplasts. *FEBS Lett.* **2010**, *584*, 759–764. [[CrossRef](#)]
32. Thidholm, E.; Lindström, V.; Tissier, C.; Robinson, C.P.; Schröder, W.; Funk, C. Novel approach reveals localisation and assembly pathway of the PsbS and PsbW proteins into the photosystem II dimer. *FEBS Lett.* **2002**, *513*, 217–222. [[CrossRef](#)]
33. Goral, T.K.; Johnson, M.P.; Duffy, C.D.P.; Brain, A.P.R.; Ruban, A.V.; Mullineaux, C.W. Light-harvesting antenna composition controls the macrostructure and dynamics of thylakoid membranes in *Arabidopsis*. *Plant J.* **2012**, *69*, 289–301. [[CrossRef](#)] [[PubMed](#)]
34. Haniewicz, P.; De Sanctis, D.; Büchel, C.; Schröder, W.P.; Loi, M.C.; Kieselbach, T.; Bochtler, M.; Piano, D. Isolation of monomeric photosystem II that retains the subunit PsbS. *Photosynth. Res.* **2013**, *118*, 199–207. [[CrossRef](#)]
35. Ruban, A.V.; Johnson, M.P.; Duffy, C.D.P. The photoprotective molecular switch in the photosystem II antenna. *Biochim. Biophys. Acta Bioenerg.* **2012**, *1817*, 167–181. [[CrossRef](#)]
36. Johnson, M.P.; Brain, A.P.; Ruban, A.V. Changes in thylakoid membrane thickness associated with the reorganization of photosystem II light harvesting complexes during photoprotective energy dissipation. *Plant Signal Behav.* **2011**, *6*, 1386–1390. [[CrossRef](#)]
37. Ostroumov, E.E.; Götze, J.P.; Reus, M.; Lambrev, P.H.; Holzwarth, A.R. Characterization of fluorescent chlorophyll charge-transfer states as intermediates in the excited state quenching of light-harvesting complex II. *Photosynth. Res.* **2020**. [[CrossRef](#)]
38. Bennett, D.I.G.; Amarnath, K.; Park, S.; Steen, C.J.; Morris, J.M.; Fleming, G.R. Models and mechanisms of the rapidly reversible regulation of photosynthetic light harvesting. *Open Biol.* **2019**, *9*, 190043. [[CrossRef](#)] [[PubMed](#)]
39. Cupellini, L.; Calvani, D.; Jacquemin, D.; Mennucci, B. Charge transfer from the carotenoid can quench chlorophyll excitation in antenna complexes of plants. *Nat. Commun.* **2020**, *11*, 662. [[CrossRef](#)] [[PubMed](#)]
40. Allen, J.F. Protein phosphorylation in regulation of photosynthesis. *Biochim. Biophys. Acta Bioenerg.* **1992**, *1098*, 275–335. [[CrossRef](#)]
41. Rochaix, J.D. Regulation and dynamics of the light-harvesting system. *Annu. Rev. Plant Biol.* **2014**, *65*, 287–309. [[CrossRef](#)]
42. Dumas, L.; Chazaux, M.; Peltier, G.; Johnson, X.; Alric, J. Cytochrome *b₆f* function and localization, phosphorylation state of thylakoid membrane proteins and consequences on cyclic electron flow. *Photosynth. Res.* **2016**, *129*, 307–320. [[CrossRef](#)] [[PubMed](#)]
43. Grieco, M.; Tikkanen, M.; Paakkanen, V.; Kangasjarvi, S.; Aro, E.M. Steady-state phosphorylation of light-harvesting complex II proteins preserves photosystem I under fluctuating white light. *Plant Physiol.* **2012**, *160*, 1896–1910. [[CrossRef](#)]
44. Nellaepalli, S.; Mekala, N.R.; Zsiros, O.; Mohanty, P.; Subramanyam, R. Moderate heat stress induces state transitions in *Arabidopsis thaliana*. *Biochim. Biophys. Acta Bioenerg.* **2011**, *1807*, 1177–1184. [[CrossRef](#)] [[PubMed](#)]
45. Haldrup, A.; Jensen, P.E.; Lunde, C.; Scheller, H.V. Balance of power: A view of the mechanism of photosynthetic state transitions. *Trends Plant Sci.* **2001**, *6*, 301–305. [[CrossRef](#)]
46. Holtzegel, U. The Lhc family of *Arabidopsis thaliana*. *Endocytobiosis Cell Res.* **2016**, *27*, 71–89.
47. Galka, P.; Santabarbara, S.; Khuong, T.T.H.; Degand, H.; Morsomme, P.; Jennings, R.C.; Boekema, E.J.; Caffarri, S. Functional analyses of the plant photosystem I–light-harvesting complex II supercomplex reveal that light-harvesting complex II loosely bound to photosystem II is a very efficient antenna for photosystem I in state II. *Plant Cell* **2012**, *24*, 2963–2978. [[CrossRef](#)]
48. Damkjær, J.T.; Kereiche, S.; Johnson, M.P.; Kovacs, L.; Kiss, A.Z.; Boekema, E.J.; Ruban, A.V.; Horton, P.; Jansson, S. The photosystem II light-harvesting protein Lhcb3 affects the macrostructure of photosystem II and the rate of state transitions in *Arabidopsis*. *Plant Cell* **2009**, *21*, 3245–3256. [[CrossRef](#)] [[PubMed](#)]
49. Su, X.; Ma, J.; Wei, X.; Cao, P.; Zhu, D.; Chang, W.; Liu, Z.; Zhang, X.; Li, M. Structure and assembly mechanism of plant C₂S₂M₂-type PSII-LHCII supercomplex. *Science* **2017**, *357*, 815–820. [[CrossRef](#)]
50. Depège, N.; Bellafiore, S.; Rochaix, J.-D. Role of chloroplast protein kinase Stt7 in LHCII phosphorylation and state transition in *Chlamydomonas*. *Science* **2003**, *299*, 1572–1575. [[CrossRef](#)]
51. Bellafiore, S.; Barneche, F.; Peltier, G.; Rochaix, J.-D. State transitions and light adaptation require chloroplast thylakoid protein kinase STN7. *Nature* **2005**, *433*, 892–895. [[CrossRef](#)]
52. Allen, J.F.; Bennett, J.; Steinback, K.E.; Arntzen, C.J. Chloroplast protein phosphorylation couples plastoquinone redox state to distribution of excitation energy between photosystems. *Nature* **1981**, *291*, 25–29. [[CrossRef](#)]
53. Zito, F.; Finazzi, G.; Delosme, R.; Nitschke, W.; Picot, D.; Wollman, F.-A. The Q_o site of cytochrome *b₆f* complexes controls the activation of the LHCII kinase. *EMBO J.* **1999**, *18*, 2961–2969. [[CrossRef](#)] [[PubMed](#)]

54. Dumas, L.; Zito, F.; Blangy, S.; Auroy, P.; Johnson, X.; Peltier, G.; Alric, J. A stromal region of cytochrome *b₆f* subunit IV is involved in the activation of the Stt7 kinase in *Chlamydomonas*. *Proc. Natl. Acad. Sci. USA* **2017**, *114*, 12063–12068. [[CrossRef](#)] [[PubMed](#)]
55. Shapiguzov, A.; Chai, X.; Fucile, G.; Longoni, P.; Zhang, L.; Rochaix, J.-D. Activation of the Stt7/STN7 kinase through dynamic interactions with the cytochrome *b₆f* complex. *Plant Physiol.* **2016**, *171*, 82–92. [[CrossRef](#)]
56. Wu, J.; Rong, L.; Lin, W.; Kong, L.; Wei, D.; Zhang, L.; Rochaix, J.D.; Xu, X. Functional redox links between Lumen Thiol Oxidoreductase1 and Serine/Threonine-protein kinase STN7. *Plant Physiol.* **2021**. [[CrossRef](#)] [[PubMed](#)]
57. Bonardi, V.; Pesaresi, P.; Becker, T.; Schleiff, E.; Wagner, R.; Pfannschmidt, T.; Jahns, P.; Leister, D. Photosystem II core phosphorylation and photosynthetic acclimation require two different protein kinases. *Nature* **2005**, *437*, 1179–1182. [[CrossRef](#)]
58. Vainonen, J.P.; Hansson, M.; Vener, A.V. STN8 protein kinase in *Arabidopsis thaliana* is specific in phosphorylation of photosystem II core proteins. *J. Biol. Chem.* **2005**, *280*, 33679–33686. [[CrossRef](#)] [[PubMed](#)]
59. Reiland, S.; Finazzi, G.; Endler, A.; Willig, A.; Baerenfaller, K.; Grossmann, J.; Gerrits, B.; Rutishauser, D.; Gruijsem, W.; Rochaix, J.-D.; et al. Comparative phosphoproteome profiling reveals a function of the STN8 kinase in fine-tuning of cyclic electron flow (CEF). *Proc. Natl. Acad. Sci. USA* **2011**, *108*, 12955–12960. [[CrossRef](#)]
60. Longoni, P.; Samol, I.; Goldschmidt-Clermont, M. The kinase state transition 8 phosphorylates light harvesting complex II and contributes to light acclimation in *Arabidopsis thaliana*. *Front. Plant Sci.* **2019**, *10*, 1156. [[CrossRef](#)]
61. Wunder, T.; Xu, W.; Liu, Q.; Wanner, G.; Leister, D.; Pribil, M. The major thylakoid protein kinases STN7 and STN8 revisited: Effects of altered STN8 levels and regulatory specificities of the STN kinases. *Front. Plant Sci.* **2013**, *4*, 417. [[CrossRef](#)]
62. Koskela, M.M.; Brünje, A.; Ivanauskaitė, A.; Grabsztunowicz, M.; Lassowskat, I.; Neumann, U.; Dinh, T.V.; Sindlinger, J.; Schwarzer, D.; Wirtz, M.; et al. Chloroplast acetyltransferase NSI is required for state transitions in *Arabidopsis thaliana*. *Plant Cell* **2018**, *30*, 1695–1709. [[CrossRef](#)]
63. Koskela, M.M.; Brünje, A.; Ivanauskaitė, A.; Lopez, L.S.; Schneider, D.; DeTar, R.A.; Kunz, H.-H.; Finkemeier, I.; Mulo, P. Comparative analysis of thylakoid protein complexes in state transition mutants *nsi* and *stn7*: Focus on PSI and LHCII. *Photosynth. Res.* **2020**, 1–16. [[CrossRef](#)] [[PubMed](#)]
64. Pribil, M.; Pesaresi, P.; Hertle, A.; Barbato, R.; Leister, D. Role of plastid protein phosphatase TAP38 in LHCII dephosphorylation and thylakoid electron flow. *PLoS Biol.* **2010**, *8*, e1000288. [[CrossRef](#)] [[PubMed](#)]
65. Shapiguzov, A.; Ingelsson, B.; Samol, I.; Andres, C.; Kessler, F.; Rochaix, J.-D.; Vener, A.V.; Goldschmidt-Clermont, M. The PPH1 phosphatase is specifically involved in LHCII dephosphorylation and state transitions in *Arabidopsis*. *Proc. Natl. Acad. Sci. USA* **2010**, *107*, 4782–4787. [[CrossRef](#)] [[PubMed](#)]
66. Tikkanen, M.; Nurmi, M.; Suorsa, M.; Danielsson, R.; Mamedov, F.; Styring, S.; Aro, E.-M. Phosphorylation-dependent regulation of excitation energy distribution between the two photosystems in higher plants. *Biochim. Biophys. Acta Bioenerg.* **2008**, *1777*, 425–432. [[CrossRef](#)]
67. Järvi, S.; Suorsa, M.; Paakkarinen, V.; Aro, E.-M. Optimized native gel systems for separation of thylakoid protein complexes: Novel super- and mega-complexes. *Biochem. J.* **2011**, *439*, 207–214. [[CrossRef](#)]
68. Fristedt, R.; Granath, P.; Vener, A.V. A protein phosphorylation threshold for functional stacking of plant photosynthetic membranes. *PLoS ONE* **2010**, *5*, e10963. [[CrossRef](#)]
69. Pietrzykowska, M.; Suorsa, M.; Semchonok, D.A.; Tikkanen, M.; Boekema, E.J.; Aro, E.-M.; Jansson, S. The light-harvesting chlorophyll *a/b* binding proteins Lhcb1 and Lhcb2 play complementary roles during state transitions in *Arabidopsis*. *Plant Cell* **2014**, *26*, 3646–3660. [[CrossRef](#)]
70. Puthiyaveetil, S.; van Oort, B.; Kirchhoff, H. Surface charge dynamics in photosynthetic membranes and the structural consequences. *Nat. Plants* **2017**, *3*, 17020. [[CrossRef](#)]
71. Crepin, A.; Caffarri, S. The specific localizations of phosphorylated Lhcb1 and Lhcb2 isoforms reveal the role of Lhcb2 in the formation of the PSI-LHCII supercomplex in *Arabidopsis* during state transitions. *Biochim. Biophys. Acta Bioenerg.* **2015**, *1847*, 1539–1548. [[CrossRef](#)] [[PubMed](#)]
72. Longoni, P.; Douchi, D.; Cariti, F.; Fucile, G.; Goldschmidt-Clermont, M. Phosphorylation of the light-harvesting complex II isoform Lhcb2 is central to state transitions. *Plant Physiol.* **2015**, *169*, 2874–2883. [[CrossRef](#)] [[PubMed](#)]
73. Khrouchtchova, A.; Hansson, M.; Paakkarinen, V.; Vainonen, J.P.; Zhang, S.; Jensen, P.E.; Scheller, H.V.; Vener, A.V.; Aro, E.-M.; Haldrup, A. A previously found thylakoid membrane protein of 14 kDa (TMP14) is a novel subunit of plant photosystem I and is designated PSI-P. *FEBS Lett.* **2005**, *579*, 4808–4812. [[CrossRef](#)]
74. Trotta, A.; Bajwa, A.A.; Mancini, I.; Paakkarinen, V.; Pribil, M.; Aro, E.-M. The role of phosphorylation dynamics of CURVATURE THYLAKOID 1B in plant thylakoid membranes. *Plant Physiol.* **2019**, *181*, 1615–1631. [[CrossRef](#)]
75. Caffarri, S.; Kouril, R.; Kereïche, S.; Boekema, E.J.; Croce, R. Functional architecture of higher plant photosystem II supercomplexes. *EMBO J.* **2009**, *28*, 3052–3063. [[CrossRef](#)] [[PubMed](#)]
76. Benson, S.L.; Maheswaran, P.; Ware, M.A.; Hunter, C.N.; Horton, P.; Jansson, S.; Ruban, A.V.; Johnson, M.P. An intact light harvesting complex I antenna system is required for complete state transitions in *Arabidopsis*. *Nat. Plants* **2015**, *1*, 15176. [[CrossRef](#)]
77. Bos, I.; Bland, K.M.; Tian, L.; Croce, R.; Frankel, L.K.; van Amerongen, H.; Bricker, T.M.; Wientjes, E. Multiple LHCII antennae can transfer energy efficiently to a single Photosystem I. *Biochim. Biophys. Acta Bioenerg.* **2017**, *1858*, 371–378. [[CrossRef](#)] [[PubMed](#)]
78. Bressan, M.; Bassi, R.; Dall’Osto, L. Loss of LHCI system affects LHCII re-distribution between thylakoid domains upon state transitions. *Photosynth. Res.* **2018**, *135*, 251–261. [[CrossRef](#)]

79. Yadav, K.N.S.; Semchonok, D.A.; Nosek, L.; Kouřil, R.; Fucile, G.; Boekema, E.J.; Eichacker, L.A. Supercomplexes of plant photosystem I with cytochrome *b₆f*, light-harvesting complex II and NDH. *Biochim. Biophys. Acta Bioenerg.* **2017**, *1858*, 12–20. [[CrossRef](#)] [[PubMed](#)]
80. Pan, X.; Ma, J.; Su, X.; Cao, P.; Chang, W.; Liu, Z.; Zhang, X.; Li, M. Structure of the maize photosystem I supercomplex with light-harvesting complexes I and II. *Science* **2018**, *360*, 1109–1113. [[CrossRef](#)]
81. Li, L.; Aro, E.-M.; Millar, A.H. Mechanisms of photodamage and protein turnover in photoinhibition. *Trends Plant Sci.* **2018**, *23*, 667–676. [[CrossRef](#)] [[PubMed](#)]
82. Mattoo, A.K.; Hoffman-Falk, H.; Marder, J.B.; Edelman, M. Regulation of protein metabolism: Coupling of photosynthetic electron transport to *in vivo* degradation of the rapidly metabolized 32-kilodalton protein of the chloroplast membranes. *Proc. Natl. Acad. Sci. USA* **1984**, *81*, 1380–1384. [[CrossRef](#)] [[PubMed](#)]
83. Aro, E.-M.; Virgin, I.; Andersson, B. Photoinhibition of Photosystem II. Inactivation, protein damage and turnover. *Biochim. Biophys. Acta Bioenerg.* **1993**, *1143*, 113–134. [[CrossRef](#)]
84. Barber, J.; Andersson, B. Too much of a good thing: Light can be bad for photosynthesis. *Trends Biochem. Sci.* **1992**, *17*, 61–66. [[CrossRef](#)]
85. Edelman, M.; Mattoo, A.K. D1-protein dynamics in photosystem II: The lingering enigma. *Photosynth. Res.* **2008**, *98*, 609–620. [[CrossRef](#)]
86. Li, L.; Nelson, C.J.; Trösch, J.; Castleden, I.; Huang, S.; Millar, A.H. Protein degradation rate in *Arabidopsis thaliana* leaf growth and development. *Plant Cell* **2017**, *29*, 207–228. [[CrossRef](#)]
87. Vass, I. Molecular mechanisms of photodamage in the Photosystem II complex. *Biochim. Biophys. Acta Bioenerg.* **2012**, *1817*, 209–217. [[CrossRef](#)] [[PubMed](#)]
88. Zavafer, A.; Cheah, M.H.; Hillier, W.; Chow, W.S.; Takahashi, S. Photodamage to the oxygen evolving complex of photosystem II by visible light. *Sci. Rep.* **2015**, *5*, 16363. [[CrossRef](#)]
89. Tikkanen, M.; Grieco, M.; Kangasjärvi, S.; Aro, E.-M. Thylakoid protein phosphorylation in higher plant chloroplasts optimizes electron transfer under fluctuating light. *Plant Physiol.* **2010**, *152*, 723–735. [[CrossRef](#)] [[PubMed](#)]
90. Goral, T.K.; Johnson, M.P.; Brain, A.P.R.; Kirchoff, H.; Ruban, A.V.; Mullineaux, C.W. Visualizing the mobility and distribution of chlorophyll proteins in higher plant thylakoid membranes: Effects of photoinhibition and protein phosphorylation. *Plant J.* **2010**, *62*, 948–959. [[CrossRef](#)]
91. Vener, A.V.; Harms, A.; Sussman, M.R.; Vierstra, R.D. Mass spectrometric resolution of reversible protein phosphorylation in photosynthetic membranes of *Arabidopsis thaliana*. *J. Biol. Chem.* **2001**, *276*, 6959–6966. [[CrossRef](#)]
92. Kato, Y.; Sakamoto, W. FtsH protease in the thylakoid membrane: Physiological functions and the regulation of protease activity. *Front. Plant Sci.* **2018**, *9*, 855. [[CrossRef](#)] [[PubMed](#)]
93. Komenda, J.; Barker, M.; Kuviková, S.; de Vries, R.; Mullineaux, C.W.; Tichý, M.; Nixon, P.J. The FtsH protease slr0228 is important for quality control of photosystem II in the thylakoid membrane of *Synechocystis* sp. PCC 6803. *J. Biol. Chem.* **2006**, *281*, 1145–1151. [[CrossRef](#)] [[PubMed](#)]
94. Kato, Y.; Miura, E.; Ido, K.; Ifuku, K.; Sakamoto, W. The variegated mutants lacking chloroplastic FtsHs are defective in D1 degradation and accumulate reactive oxygen species. *Plant Physiol.* **2009**, *151*, 1790–1801. [[CrossRef](#)] [[PubMed](#)]
95. Lindahl, M.; Tabak, S.; Cseke, L.; Pichersky, E.; Andersson, B.; Adam, Z. Identification, characterization, and molecular cloning of a homologue of the bacterial FtsH protease in chloroplasts of higher plants. *J. Biol. Chem.* **1996**, *271*, 29329–29334. [[CrossRef](#)] [[PubMed](#)]
96. Ostersetzer, O.; Adam, Z. Light-stimulated degradation of an unassembled Rieske FeS protein by a thylakoid-bound protease: The possible role of the FtsH protease. *Plant Cell* **1997**, *9*, 957–965. [[CrossRef](#)] [[PubMed](#)]
97. Kapri-Pardes, E.; Naveh, L.; Adam, Z. The thylakoid lumen protease Deg1 is involved in the repair of photosystem II from photoinhibition in *Arabidopsis*. *Plant Cell* **2007**, *19*, 1039–1047. [[CrossRef](#)]
98. Sun, X.; Fu, T.; Chen, N.; Guo, J.; Ma, J.; Zou, M.; Lu, C.; Zhang, L. The stromal chloroplast Deg7 protease participates in the repair of photosystem II after photoinhibition in *Arabidopsis*. *Plant Physiol.* **2010**, *152*, 1263–1273. [[CrossRef](#)]
99. Sun, X.; Peng, L.; Guo, J.; Chi, W.; Ma, J.; Lu, C.; Zhang, L. Formation of DEG5 and DEG8 complexes and their involvement in the degradation of photodamaged photosystem II reaction center D1 protein in *Arabidopsis*. *Plant Cell* **2007**, *19*, 1347–1361. [[CrossRef](#)]
100. Malnoë, A.; Schultink, A.; Shahrabi, S.; Rumeau, D.; Havaux, M.; Niyogi, K.K. The plastid lipocalin LCNP is required for sustained photoprotective energy dissipation in *Arabidopsis*. *Plant Cell* **2018**, *30*, 196–208. [[CrossRef](#)]
101. Amstutz, C.L.; Fristedt, R.; Schultink, A.; Merchant, S.S.; Niyogi, K.K.; Malnoë, A. An atypical short-chain dehydrogenase-reductase functions in the relaxation of photoprotective qH in *Arabidopsis*. *Nat. Plants* **2020**, *6*, 154–166. [[CrossRef](#)] [[PubMed](#)]
102. Nawrocki, W.J.; Tourasse, N.J.; Taly, A.; Rappaport, F.; Wollman, F.-A. The plastid terminal oxidase: Its elusive function points to multiple contributions to plastid physiology. *Annu. Rev. Plant Biol.* **2015**, *66*, 49–74. [[CrossRef](#)] [[PubMed](#)]
103. Lennon, A.M.; Prommeenate, P.; Nixon, P.J. Location, expression and orientation of the putative chlororespiratory enzymes, Ndh and IMMUTANS, in higher-plant plastids. *Planta* **2003**, *218*, 254–260. [[CrossRef](#)]
104. Stepien, P.; Johnson, G.N. Plastid terminal oxidase requires translocation to the grana stacks to act as a sink for electron transport. *Proc. Natl. Acad. Sci. USA* **2018**, *115*, 9634–9639. [[CrossRef](#)] [[PubMed](#)]
105. Bolte, S.; Marcon, E.; Jaunario, M.; Moyet, L.; Paternostre, M.; Kuntz, M.; Krieger-Liszskay, A. Dynamics of the localization of the plastid terminal oxidase inside the chloroplast. *J. Exp. Bot.* **2020**, *71*, 2661–2669. [[CrossRef](#)]

106. Gemmecker, S.; Schaub, P.; Koschmieder, J.; Brausemann, A.; Drepper, F.; Rodriguez-Franco, M.; Ghisla, S.; Warscheid, B.; Einsle, O.; Beyer, P. Phytoene desaturase from *Oryza sativa*: Oligomeric assembly, membrane association and preliminary 3D-analysis. *PLoS ONE* **2015**, *10*, e0131717. [[CrossRef](#)] [[PubMed](#)]
107. Shiba, T.; Kido, Y.; Sakamoto, K.; Inaoka, D.K.; Tsuge, C.; Tatsumi, R.; Takahashi, G.; Balogun, E.O.; Nara, T.; Aoki, T.; et al. Structure of the trypanosome cyanide-insensitive alternative oxidase. *Proc. Natl. Acad. Sci. USA* **2013**, *12*, 4580–4585. [[CrossRef](#)]
108. Yu, Q.; Feilke, K.; Krieger-Liszkay, A.; Beyer, P. Functional and molecular characterization of plastid terminal oxidase from rice (*Oryza sativa*). *Biochim. Biophys. Acta Bioenerg.* **2014**, *1837*, 1284–1292. [[CrossRef](#)]
109. Messant, M.; Shimakawa, G.; Perreau, F.; Miyake, C.; Krieger-Liszkay, A. Evolutionary differentiation between alga- and plant-type plastid terminal oxidase: Study of plastid terminal oxidase PTOX isoforms in *Marchantia polymorpha*. *Biochim. Biophys. Acta Bioenerg.* **2021**, *1862*, 148309. [[CrossRef](#)] [[PubMed](#)]
110. Liu, C.; Willmund, F.; Golecki, J.R.; Cacace, S.; Heß, B.; Markert, C.; Schroda, M. The chloroplast HSP70B-CDJ2-CGE1 chaperones catalyse assembly and disassembly of VIPP1 oligomers in *Chlamydomonas*. *Plant J.* **2007**, *50*, 265–277. [[CrossRef](#)]
111. Otters, S.; Braun, P.; Hubner, J.; Wanner, G.; Vothknecht, U.C.; Chigri, F. The first α -helical domain of the vesicle-inducing protein in plastids 1 promotes oligomerization and lipid binding. *Planta* **2013**, *237*, 529–540. [[CrossRef](#)] [[PubMed](#)]
112. Bryan, S.J.; Burroughs, N.J.; Shevela, D.; Yu, J.; Rupprecht, E.; Liu, L.-N.; Mastroianni, G.; Xue, Q.; Llorente-Garcia, I.; Leake, M.C.; et al. Localisation and interactions of the Vipp1 protein in cyanobacteria. *Mol. Microbiol.* **2014**, *94*, 1179–1195. [[CrossRef](#)] [[PubMed](#)]
113. Gutu, A.; Chang, F.; O’Shea, E.K. Dynamical localization of a thylakoid membrane binding protein is required for acquisition of photosynthetic competency. *Mol. Microbiol.* **2018**, *108*, 16–31. [[CrossRef](#)] [[PubMed](#)]
114. Westphal, S.; Heins, L.; Soll, J.; Vothknecht, U.C. *Vipp1* deletion mutant of *Synechocystis*: A connection between bacterial phage shock and thylakoid biogenesis? *Proc. Natl. Acad. Sci. USA* **2001**, *98*, 4243–4248. [[CrossRef](#)]
115. Nordhues, A.; Schöttler, M.A.; Unger, A.-K.; Geimer, S.; Schönfelder, S.; Schmollinger, S.; Rütgers, M.; Finazzi, G.; Soppa, B.; Sommer, F.; et al. Evidence for a role of VIPP1 in the structural organization of the photosynthetic apparatus in *Chlamydomonas*. *Plant Cell* **2012**, *24*, 637–659. [[CrossRef](#)]
116. Theis, J.; Niemeyer, J.; Schmollinger, S.; Ries, F.; Rütgers, M.; Gupta, T.K.; Sommer, F.; Muranaka, L.S.; Venn, B.; Schulz-Raffelt, M.; et al. VIPP2 interacts with VIPP1 and HSP22E/F at chloroplast membranes and modulates a retrograde signal for HSP22E/F gene expression. *Plant Cell Environ.* **2020**, *43*, 1212–1229. [[CrossRef](#)]

Discussion and Perspectives

The different aims (Figure 35) of this thesis were:

- (1) to study the light dependent assembly of the Mn cluster *in vitro* and *in vivo* using new and rare technologies (HF-EPR and SRM), Figure 35, blue box.
- (2) to characterise the roles of the different isoforms of the Plastid Terminal Oxidase family of proteins across green lineage, Figure 35, orange box.
- (3) employing the singularities of *Marchantia polymorpha* to show new research opportunities that this species can offer, Figure 35, purple box.

(1) Study of Manganese homeostasis and Photoactivation

***Marchantia polymorpha*: a future model for metal homeostasis studies**

In Messant *et al.*, 2022, we have shown that in Mn excess conditions *Marchantia* is able to absorb up to 25 mg Mn. g DW⁻¹ which can only be reached by hyperaccumulators (Liu *et al.*, 2016). This can be due to the absence of specific transporters at the level of rhizoids or maybe its protection mechanisms against metal stress are so efficient that *Marchantia* does not need to limit Mn uptake under physiological conditions. In fact, metabolomic analysis has shown that some metabolites accumulate that are known to protect against heavy metals stress. For example, tryptophan is involved in cadmium protection (Sanjaya *et al.*, 2008), putrescine and its precursor ornithine, which modulates ion transport across membranes under stress conditions (Pottosin *et al.*, 2021) or citrulline, a scavenger of hydroxyl radicals and protects against oxidative damage (Akashi *et al.*, 2001; 2004; Yokota *et al.*, 2002). For the metabolome analysis, I used a library commonly used for *Arabidopsis* metabolomic analysis, but many metabolites that were detected in *Marchantia* were absent in this library. This suggests that *Marchantia* has different and more diverse metabolites than *Arabidopsis*. For example, N-methyl-L-Alanine greatly increases under Mn excess but this molecule, according to my understanding, has never been mentioned in plants. It can be hypothesised that it plays a similar role than β -alanine. The latter has been described to be important for the resistance to abiotic stress and protection against heavy metals as well as free radicals (Klapheck *et al.*, 1988; Moran *et al.*, 2000). Accumulation of metabolites not present in *Arabidopsis* could be interesting to study in detail to see whether different metabolic pathways exist in liverworts compared with higher plants. *Marchantia* is a promising model to study heavy metal homeostasis in plants. It may also be a good candidate for phytoremediation.

On the other hand, Mn deficiency has been a very difficult condition to obtain. It is reasonable to think that gemmae have, like seeds, a quantity of Mn sufficient for their development. The substitution of agar by starch as a gelling agent highlights an alteration in the structure of the chloroplasts as well as in the level of photosynthetic activity. It is known that ion homeostasis modulates the dynamics of the thylakoid

membranes (Li *et al.*, 2021). In particular, Mn deficiency leads to condensation of the thylakoid membranes (Mercer *et al.*, 1962; Homan, 1967; Schmidt *et al.*, 2016; Messant *et al.*, 2022). Ion flows into the mesophyll cell and into the chloroplast are particularly controlled by ion channels. Two Mn transporters have recently been characterised in *Arabidopsis*: PAM71 (Photosynthesis Affected Mutant 71, Schneider *et al.*, 2016) and CMT1 (Chloroplast Manganese Transporter 1, Eisenhut *et al.*, 2018) whose mutants could not be obtained in *Marchantia* even by supplementing the medium with Mn. These mutations therefore lead to a drastic or even lethal phenotype. It would be interesting to generate RNAi mutants in the hope of obtaining an attenuated phenotype.

Regarding photosynthetic activity, measurements of PSII chlorophyll fluorescence and PSI absorption point to an increase in cyclic electron flow as well as an increase in NPQ. All these elements show a desire to protect the active PSII to avoid repair and therefore photoactivation, which in the absence of a sufficient quantity of Mn is more difficult to achieve.

To conclude, the data from Messant *et al.*, 2022 tend to show that *Marchantia* has different or possibly ancestral metal uptake, transport, regulation and protection systems to those described in higher plants. Their characterization could help to understand the great adaptability of *Marchantia* in the face of deficiency and excess of Mn but also for other heavy metals (Samecka-Cymerman *et al.*, 1997). These mechanisms could be used for phytoremediation of transplants to plants of agronomic interest.

High-Field EPR and derivative techniques: new horizons for the mechanistic study of photoactivation

I showed in the first part of the thesis that photoactivation is a difficult process to study whose intermediates have yet to be precisely determined. The preliminary experiments carried out using an O₂ electrode lead to the quantification of the Mn catalase-like activity in solution (Tikhonov *et al.*, 2006) under my experimental conditions. I was able to determine that Mn catalase-like activity is unlikely to take place in the lumen when the pH is acidic.

Moreover, Sun Un and I were interested in characterising the assembly steps of the Mn cluster. For this, we used HF-EPR and derived methods. We have determined that the photoactivation steps are reversible until the oxidation of two Mn(II) together. Moreover, by focusing more particularly on the binding of the first Mn(II), we have shown the presence of 5 water molecules (± 1) and an atom of N as ligands. The calculation of the distance between tyrosine D and the first Mn(II) allows us to confirm that the single amino acid ligand detected corresponds to the D1-His332 residue. This confirmed that the ion present in the apo-PSII structure (Zabret *et al.*, 2019) corresponds to Mn(II). Nevertheless, even if carboxylic groups are not detectable by the method used, no other ligand was detected. Interestingly, all our results can be compared with the structure of Mn catalase from *Lactobacillus plantarum* (Barynin *et al.*, 2001, Figure 35). Indeed, the two Mn atoms are linked by an oxobridge and coordinated by histidine and glutamine residues, which resembles the configuration of Mn1 and Mn2 in the final cluster (Figure 35). Mn1 is coordinated by D1-Glu189 and D1-His332 and Mn2 by D1-Asp342 and CP43-Glu354. This is an argument that seems to support the

theory of cluster evolution, derived from Mn catalase. On the other hand, the structure of apo-PSII also seems to point in this direction since the divalent ion is coordinated by D1-His332 and D1-Glu189. These observations raise the question of the proposed involvement of the D1-Asp170 residue and the presence of a HAS. The experiments of Nixon *et al.*, 1992 were carried out on mutants lacking D1-Asp170. However, its role in the final structure of the cluster (coordination of the calcium ion) could also explain its preponderant importance. Furthermore, a binding site composed of a nitrogen and a carboxylic group does not specifically form a high affinity site for Mn and could actually be suitable for any divalent ion. Thus, one can also discuss the involvement of a cargo protein, able to bind Mn(II) or of an extrinsic protein whose PSII binding could promote Mn(II) binding. It has been shown in *Synechocystis* that the tetratricopeptide protein (TRP) PrtA, that is able to bind Mn(II), is necessary to supply the first Mn(II) to the PSII precursor to initiate photoactivation. This hypothesis could be all the more favoured as it could explain more easily how photoactivation on the donor side activates Q_A on the PSII acceptor side (Krieger and Weis, 1993). It has been hypothesised that the extrinsic protein PsbP could be a Mn chaperone delivering Mn to PSII during photoactivation in higher plants (Bondarava *et al.*, 2007). Moreover, Peng *et al.* 2006, demonstrated the presence of a chloroplast TRP protein, LPA (Low PSII Accumulation), involved in the assembly of PSII and the repair of the D1 protein. These two processes are the two physiological conditions in which photoactivation takes place. It would be interesting to study the role of PsbP and LPA during both photoactivation and recovery after photoinhibition to show whether they have homologous roles to PrtA in cyanobacteria.

I have initiated a project on LPA proteins in *Marchantia*. Thalli will be transformed to obtain mutants of homologs LPA1, LPA2 and LPA3. Preliminary *in silico* analysis have shown that the expression of LPA2 is correlated with that of the Mn transporter CMT1 in *Arabidopsis* and *Marchantia*. If these mutants are obtained, it would be interesting to grow them in the dark and use the SRM to determine their involvement during photoactivation. Finally, recombinant protein production and even point mutations could be analysed by EPR to determine if and how they bind Mn.

(2) Characterization of PTOXa and PTOXb isoforms in *Marchantia polymorpha*

Alga and Plant-type PTOXs: same activity, different roles and regulations

In Messant *et al.*, 2019; I highlighted the presence of two types of isoforms in the green lineage: the alga-type and the plant-type PTOX. The Alga-type PTOX isoforms have an elongation in Nter, absent in the Plant-type isoforms. The Alga-type PTOXs are close to the two isoforms present in the green algae *Chlamydomonas*, while the plant-types are close to the single isoform of angiosperms such as *Arabidopsis*. Studying *Marchantia* allows one to investigate the function of each of the two types since it has one of each. Analysis of the single mutants demonstrated that thalli do not have variegation phenotype, unlike known angiosperms mutants (*immutans* in *Arabidopsis*, *ghost* in tomato). It is possible that the two isoforms complement each other to some extent. Unsurprisingly, the plastoquinone pool was shown to be more reduced in the two single mutants. Although both isoforms catalyse the same reaction, we have shown that they play distinct roles *in vivo*. Indeed, MpPTOXb seems to be more important for chlororespiration. Additionally, experiments performed as in Bolte *et al.*, 2020 could also help to determine the localization of the two isoforms to test the hypothesis of an always-membrane-attached isoform with access to the PQ pool, assumed to be MpPTOXb, and an isoform attaching to the thylakoid membrane only under stress conditions, assumed to be MpPTOXa. This could also offer new research perspectives concerning the transport of PTOX proteins to the membrane but also their interaction partners. It has been suggested that PTOX proteins are stored in plastoglobules. *In silico* co-expression analyses on *Arabidopsis* data have already revealed certain genes that code for proteins present in plastoglobules (van Wijk and Kessler, 2017) as well as proteins of the photosynthetic chain (data not shown).

MpPTOX isoforms are not involved in carotenoid biosynthesis and protects against PSI photoinhibition

To go further, we have for the first time succeeded in obtaining a PTOX double mutant (Messant *et al.*, 2022 submitted). We have shown that the double mutant does not possess a variegation phenotype. This proves that PTOX does not play the same role in carotenoid biosynthesis in *Marchantia polymorpha* as in *Arabidopsis*. Given the results of the analysis of metabolites for the Mn homeostasis study, it may also be possible that, in *Marchantia*, the biosynthesis of carotenoids takes place in a slightly different way to that of angiosperms. Then, we conclude that PTOX is important for PSI protection. We have shown that PTOX activity promotes PSII photoinhibition which is a protection mechanism for PSI preservation. On the other hand, obtaining *imCRTI* mutants allows to overcome the variegation phenotype and therefore offers new opportunities to understand the role of PTOX on the electron flow in high light. Microscopy images are needed to verify whether the heteroplasmic of chloroplasts is still present and therefore to study the role of PTOX in the biosynthesis of chloroplasts.

Characterization of Alga-type Nter elongation and iron binding site motifs

The *in silico* study on the Nter elongation of alga-type PTOX showed the presence of two or three helices named: $\alpha'1$, $\alpha'2$ et $\alpha'3$. The first and the last being the most preserved and the second being the one that seems to have appeared later. We propose that the helices may play a role in the attachment to the membrane, the accessibility to the substrate or the activation and regulation of the protein. To determine this, additional experiments are required, such as the production of point mutations on the recombinant protein or the complementation of the *Marchantia* double mutant with a MpPTOXb Nter truncated protein. On the other hand, even although the catalytic sites of the two isoforms are highly conserved, their comparison allows to define (1) more specific patterns of iron binding sites of PTOX proteins than those already established in comparison with AOXs (McDonald *et al.*, 2003; Fu *et al.*, 2005) and (2) to define variations between alga and plant-type PTOX. Finally, the amino acid variations between the two types of isoforms will allow to identify sites for specific point mutations that could help to understand the lower activity of purified MpPTOXb compared to MpPTOXa. In general, the catalytic mechanism of PTOX needs to be elucidated, for example using the transient absorption spectroscopy.

To conclude, the characterization of the two PTOX isoforms in *Marchantia polymorpha* has highlighted the importance of using models from other classes than higher plants. Indeed, this study allow to show the diversity of PTOX proteins and to redefine their roles by overcoming the pleiotropic effects present only in certain groups, as it seems to be the case for the role in the biosynthesis of carotenoids in certain angiosperms. On the other hand, the abundance of regulatory proteins in *Marchantia*, which explain its high adaptability, could be interesting for plant engineering.

(3) Marchantia polymorpha, an emerging plant model

In the near future, I think that *Marchantia* studies will resolve many questions regarding the evolution of plants during the green lineage, particularly at the molecular level (metabolic pathways, signalling, regulation, *etc.*). Regarding photosynthesis, it will allow the study of lost or modified regulatory systems compared to angiosperms, as is the case for PTOX and Mn homeostasis. The use of a morphologically simpler but molecularly more complex model will undoubtedly open up new perspectives on photosynthesis and its protective mechanisms.

Monitoring chloroplast membrane and photosynthetic complexes dynamic: the new opportunities of the super-resolution fluorescence Microscopy

As I showed throughout this study, *Marchantia* is a plant that can adapt to all kinds of conditions and is difficult to stress even when mutated. In addition to the fact that it is easy to cultivate and transform, this characteristic makes it an essential model organism because it allows the observation of events that are difficult to observe in less adaptive species (photoactivation, PTOX mutation, heavy metal stress *etc.*). For this, Andrew Gall and I used super-resolution fluorescence microscopy (SRM) to determine the dynamics of thylakoids in two different projects: Mn homeostasis in the chloroplast and photoactivation. For Mn homeostasis, the principle has been to observe the membranes upon excess and starvation as discussed previously. While for photoactivation, the dynamics of the membranes were followed over time. We have shown, albeit using a limited number of regions of interest, that photoactivation of PSII and the establishment of the linear electron flow leads to the condensation and thus compartmentation of thylakoid membranes. To go further, we want to use SRM to determine the dynamics of photosynthetic complexes in different physiological conditions and in particular, during the establishment of protection systems of the photosynthetic chain (Messant *et al.*, 2021). SRM has also the potential to distinguish the fluorescence of both photosystems (assuming that the experimental conditions are correct) without using modified plant material. On the other hand, *Marchantia* is easy to transform and could be used to produce tagged proteins. To cite just one example, the localization and dynamics of PGRL1/PGR5 proteins across the membrane could elucidate their roles in specific physiological conditions. Together, the technology and the emerging plant model offer new possibilities.

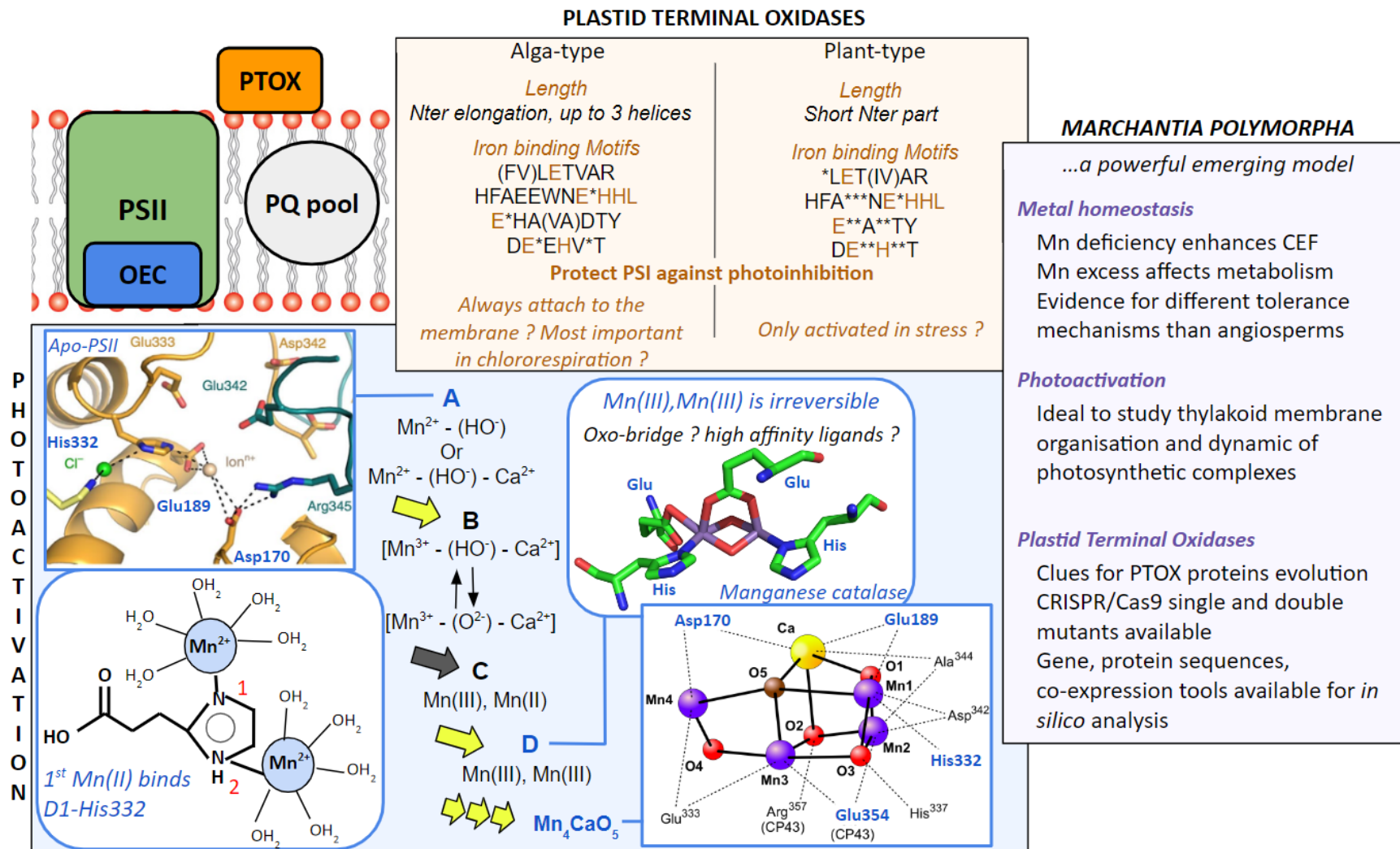


Figure 35: Summary of the importance of manganese and PTOX in photoactivation and photoinhibition processes

(top left) simplified scheme of the Mn cluster at PSII donor side and PTOX at stroma-side. (in blue) Photoactivation was carried out on apo-PSII whose structure is shown at the top left (Zabret *et al.*, 2019). Sun Un and I have shown that the first Mn(II) binds to an N atom and 5 water molecules (± 1) and that the N atom comes from D1-His332. We have demonstrated that intermediate D, formed by two Mn atoms, is stable. It is likely that their arrangements resemble the Mn catalase structure (top right, Barynin *et al.*, 2001). At the bottom right is the structure of the fully formed cluster (wikipedia, from Robertazzi *et al.*, 2014; Najapour *et al.*, 2014; Suga *et al.*, 2015). (in yellow) the characterization of PTOX from *Marchantia polymorpha* showed the presence of Alga-type PTOX with a long Nter part and of Plant-type. The protein sequence alignment helps to redefine the highly conserved iron binding motifs. PTOX protects PSI against photoinhibition. The role of each isoform remains to be defined. (In purple) *Marchantia polymorpha* has opened up new research opportunities on conserved mechanisms of photosynthesis, namely photoactivation and protection of the photosynthetic chain through the characterization of PTOX isoform.

References

- Alboresi A, Gerotto C, Giacometti GM, Bassi R, Morosinotto T. Physcomitrella patens mutants affected on heat dissipation clarify the evolution of photoprotection mechanisms upon land colonization (2010) *Proc Natl Acad Sci USA*. **107**(24):11128-33. doi: 10.1073/pnas.1002873107.
- Alboresi A, Storti M, Morosinotto T. Balancing protection and efficiency in the regulation of photosynthetic electron transport across plant evolution (2019) *New Phytol*. **221**(1):105-109. doi: 10.1111/nph.15372.
- Arabidopsis Genome Initiative. Analysis of the genome sequence of the flowering plant Arabidopsis thaliana. (2000) *Nature*. **408**(6814):796-815. doi: 10.1038/35048692.
- Ares Á, Itouga M, Kato Y, Sakakibara H. Differential Metal Tolerance and Accumulation Patterns of Cd, Cu, Pb and Zn in the Liverwort Marchantia polymorpha L. (2018) *Bull Environ Contam Toxicol*. **100**(3):444-450. doi: 10.1007/s00128-017-2241-0.
- Armstrong GA. Greening in the dark: light-independent chlorophyll biosynthesis from anoxygenic photosynthetic bacteria to gymnosperms. (1998) *Journal of Photochemistry and Photobiology*. **43**:87-100. doi: 10.1016/S1011-1344(98)00063-3.
- Aranda Sicilia MN, Sánchez Romero ME, Rodríguez Rosales MP, Venema K. Plastidial transporters KEA1 and KEA2 at the inner envelope membrane adjust stromal pH in the dark. (2021) *New Phytol*. **229**(4):2080-2090. doi: 10.1111/nph.17042.
- Archibald JM. Endosymbiosis and Eukaryotic Cell Evolution. (2015) *Curr Biol*. **25**(19):R911-21. doi: 10.1016/j.cub.2015.07.055.
- Avramov AP, Hwang HJ, Burnap RL. The role of Ca²⁺ and protein scaffolding in the formation of nature's water oxidizing complex. (2020) *Proc Natl Acad Sci USA*. **117**(45):28036-28045. doi: 10.1073/pnas.2011315117.
- Barr J, White WS, Chen L, Bae H, Rodermel S. The Ghost terminal oxidase regulates developmental programming in tomato fruit. (2004) *Plant, Cell & Environment*. **27**(7):840-852. doi: 10.1111/j.1365-3040.2004.01190.x
- Barynin VV, Whittaker MM, Antonyuk SV, Lamzin VS, Harrison PM, Artymiuk PJ, Whittaker JW. Crystal structure of manganese catalase from Lactobacillus plantarum. (2001) *Structure*. **(8)**:725-38. doi: 10.1016/s0969-2126(01)00628-1.
- Bao H, Burnap RL. Photoactivation: The Light-Driven Assembly of the Water Oxidation Complex of Photosystem II. (2016) *Front Plant Sci*. **7**:578. doi: 10.3389/fpls.2016.00578.
- Betterle N, Ballottari M, Zorzan S, de Bianchi S, Cazzaniga S, Dall'osto L, Morosinotto T, Bassi R. Light-induced dissociation of an antenna hetero-oligomer is needed for non-photochemical quenching induction. (2009) *J Biol Chem*. **284**(22):15255-66. doi: 10.1074/jbc.M808625200.
- Berner RA. GEOCARBSULF: a combined model for Phanerozoic atmospheric O₂ and CO₂. (2006) *Geochimica et Cosmochimica Acta*. **70**:5653-5664.
- Berner RA. Phanerozoic atmospheric oxygen: new results using the geocarbsultf model. (2009) *American Journal of Science*. **309**:603-606.
- Blaby IK, Blaby-Haas CE, Tourasse N, Hom EF, Lopez D, Aksoy M, Grossman A, Umen J, Dutcher S, Porter M, King S, Witman GB, Stanke M, Harris EH, Goodstein D, Grimwood J, Schmutz J, Vallon O, Merchant SS, Prochnik S. The Chlamydomonas genome project: a decade on. (2014) *Trends Plant Sci*. **19**(10):672-80. doi: 10.1016/j.tplants.2014.05.008.
- Boekema EJ, van Roon H, Calkoen F, Bassi R, Dekker JP. Multiple types of association of photosystem II and its light-harvesting antenna in partially solubilized photosystem II membranes. (1999) *Biochemistry*. **38**(8):2233-9. doi: 10.1021/bi9827161.

- Boerner RJ, Nguyen AP, Barry BA, Debus RJ. Evidence from directed mutagenesis that aspartate 170 of the D1 polypeptide influences the assembly and/or stability of the manganese cluster in the photosynthetic water-splitting complex. (1992) *Biochemistry*. **31**(29):6660-72. doi: 10.1021/bi00144a005.
- Bolte S, Marcon E, Jaunario M, Moyet L, Paternostre M, Kuntz M, Krieger-Liszkay A. Dynamics of the localization of the plastid terminal oxidase inside the chloroplast. (2020) *J Exp Bot*. **71**(9):2661-2669. doi: 10.1093/jxb/eraa074.
- Bondarava N, Un S, Krieger-Liszkay A. Manganese binding to the 23 kDa extrinsic protein of Photosystem II. (2007) *Biochim Biophys Acta*. **1767**(6):583-8. doi: 10.1016/j.bbabi.2007.01.001.
- Boussac A. Temperature dependence of the high-spin S2 to S3 transition in Photosystem II: Mechanistic consequences. (2019) *Biochim Biophys Acta Bioenerg*. **1860**(6):508-518. doi: 10.1016/j.bbabi.2019.05.001.
- Bowman JL. A Brief History of Marchantia from Greece to Genomics. (2016) *Plant Cell Physiol*. **57**(2):210-29. doi: 10.1093/pcp/pcv044.
- Bowman JL, Kohchi T, Yamato KT, Jenkins J, Shu S, Ishizaki K, Yamaoka S, Nishihama R, Nakamura Y, Berger F, Adam C, Aki SS, Althoff F, Araki T, Arteaga-Vazquez MA, Balasubramanian S, Barry K, Bauer D, Boehm CR, Briginshaw L, Caballero-Perez J, Catarino B, Chen F, Chiyoda S, Chovatia M, Davies KM, Delmans M, Demura T, Dierschke T, Dolan L, Dorantes-Acosta AE, Eklund DM, Florent SN, Flores-Sandoval E, Fujiyama A, Fukuzawa H, Galik B, Grimanelli D, Grimwood J, Grossniklaus U, Hamada T, Haseloff J, Hetherington AJ, Higo A, Hirakawa Y, Hundley HN, Ikeda Y, Inoue K, Inoue SI, Ishida S, Jia Q, Kakita M, Kanazawa T, Kawai Y, Kawashima T, Kennedy M, Kinose K, Kinoshita T, Kohara Y, Koide E, Komatsu K, Kopischke S, Kubo M, Kyojuka J, Lagercrantz U, Lin SS, Lindquist E, Lipzen AM, Lu CW, De Luna E, Martienssen RA, Minamino N, Mizutani M, Mizutani M, Mochizuki N, Monte I, Mosher R, Nagasaki H, Nakagami H, Naramoto S, Nishitani K, Ohtani M, Okamoto T, Okumura M, Phillips J, Pollak B, Reinders A, Rövekamp M, Sano R, Sawa S, Schmid MW, Shirakawa M, Solano R, Spunde A, Suetsugu N, Sugano S, Sugiyama A, Sun R, Suzuki Y, Takenaka M, Takezawa D, Tomogane H, Tsuzuki M, Ueda T, Umeda M, Ward JM, Watanabe Y, Yazaki K, Yokoyama R, Yoshitake Y, Yotsui I, Zachgo S, Schmutz J. Insights into Land Plant Evolution Garnered from the Marchantia polymorpha Genome. (2017) *Cell*. **171**(2):287-304.e15. doi: 10.1016/j.cell.2017.09.030.
- Brettel K, Leibl W. Electron transfer in photosystem I. (2001) *Biochim Biophys Acta*. **1507**(1-3):100-14. doi: 10.1016/s0005-2728(01)00202-x.
- Bricker TM, Frankel LK. Carboxylate groups on the manganese-stabilizing protein are required for efficient binding of the 24 kDa extrinsic protein to photosystem II. (2003) *Biochemistry*. **42**(7):2056-61. doi: 10.1021/bi020652v.
- Bricker TM, Frankel LK. Auxiliary functions of the PsbO, PsbP and PsbQ proteins of higher plant Photosystem II: a critical analysis. (2011) *J Photochem Photobiol B*. **104**(1-2):165-78. doi: 10.1016/j.jphotobiol.2011.01.025.
- Brinkert K, De Causmaecker S, Krieger-Liszkay A, Fantuzzi A, Rutherford AW. Bicarbonate-induced redox tuning in Photosystem II for regulation and protection. (2016) *Proc Natl Acad Sci USA*. **113**(43):12144-12149. doi: 10.1073/pnas.1608862113.
- Bruch EM, Thomine S, Tabares LC, Un S. Variations in Mn(II) speciation among organisms: what makes D. radiodurans different. (2015) *Metallomics*. **7**(1):136-44. doi: 10.1039/c4mt00265b.
- Busch A, Petersen J, Webber-Birungi MT, Powikrowska M, Lassen LM, Naumann-Busch B, Nielsen AZ, Ye J, Boekema EJ, Jensen ON, Lunde C, Jensen PE. Composition and structure of photosystem I in the moss Physcomitrella patens. (2013) *J Exp Bot*. **64**(10):2689-99. doi: 10.1093/jxb/ert126.
- Burrows PA, Sazanov LA, Svab Z, Maliga P, Nixon PJ. Identification of a functional respiratory complex in chloroplasts through analysis of tobacco mutants containing disrupted plastid ndh genes. (1998) *EMBO J*. **17**(4):868-76. doi: 10.1093/emboj/17.4.868.
- Cao P, Su X, Pan X, Liu Z, Chang W, Li M. Structure, assembly and energy transfer of plant photosystem II supercomplex. (2018) *Biochim Biophys Acta Bioenerg*. **1859**(9):633-644. doi: 10.1016/j.bbabi.2018.03.007.
- Carol P, Kuntz M. A plastid terminal oxidase comes to light: implications for carotenoid biosynthesis and chlororespiration. (2001) *Trends Plant Sci*. **6**(1):31-6. doi: 10.1016/s1360-1385(00)01811-2.

- Caspy I, Nelson N. Structure of the plant photosystem I. (2018) *Biochem Soc Trans.* **46**(2):285-294. doi: 10.1042/BST20170299.
- Caspy I, Borovikova-Sheinker A, Klaiman D, Shkolnisky Y, Nelson N. The structure of a triple complex of plant photosystem I with ferredoxin and plastocyanin. (2020) *Nat Plants.* **6**(10):1300-1305. doi: 10.1038/s41477-020-00779-9.
- Castresana J. Selection of conserved blocks from multiple alignments for their use in phylogenetic analysis. (2000) *Mol Biol Evol.* **17**(4):540-52. doi: 10.1093/oxfordjournals.molbev.a026334.
- Clark JW, Harris BJ, Hetherington AJ, Hurtado-Castano N, Brench RA, Casson S, Williams TA, Gray JE, Hetherington AM. The origin and evolution of stomata. (2022) *Curr Biol.* **32**(11):R539-R553. doi: 10.1016/j.cub.2022.04.040.
- Coelho SM, Gueno J, Lipinska AP, Cock JM, Umen JG. UV Chromosomes and Haploid Sexual Systems. (2018) *Trends Plant Sci.* **23**(9):794-807. doi: 10.1016/j.tplants.2018.06.005.
- Cullis CA, Vorster BJ, Van Der Vyver C, Kunert KJ. Transfer of genetic material between the chloroplast and nucleus: how is it related to stress in plants? (2009) *Ann Bot.* **103**(4):625-33. doi: 10.1093/aob/mcn173.
- DalCorso G, Pesaresi P, Masiero S, Aseeva E, Schünemann D, Finazzi G, Joliot P, Barbato R, Leister D. A complex containing PGRL1 and PGR5 is involved in the switch between linear and cyclic electron flow in Arabidopsis. (2008) *Cell.* **132**(2):273-85. doi: 10.1016/j.cell.2007.12.028.
- Danielsson R, Suorsa M, Paakkarinen V, Albertsson PA, Styring S, Aro EM, Mamedov F. Dimeric and monomeric organization of photosystem II. Distribution of five distinct complexes in the different domains of the thylakoid membrane. (2006) *J Biol Chem.* **281**(20):14241-9. doi: 10.1074/jbc.M600634200.
- Dau H, Zaharieva I, Haumann M. Recent developments in research on water oxidation by photosystem II. (2012) *Curr Opin Chem Biol.* **16**(1-2):3-10. doi: 10.1016/j.cbpa.2012.02.011.
- Dekker JP, Boekema EJ. Supramolecular organization of thylakoid membrane proteins in green plants. (2005) *Biochim Biophys Acta.* **1706**(1-2):12-39. doi: 10.1016/j.bbabi.2004.09.009.
- Dereeper A, Guignon V, Blanc G, Audic S, Buffet S, Chevenet F, Dufayard JF, Guindon S, Lefort V, Lescot M, Claverie JM, Gascuel O. Phylogeny.fr: robust phylogenetic analysis for the non-specialist. (2008) *Nucleic Acids Res.* **36**(Web Server issue):W465-9. doi: 10.1093/nar/gkn180.
- Donoghue PCJ, Harrison CJ, Paps J, Schneider H. The evolutionary emergence of land plants.. (2021) *Curr Biol.* **31**(19):R1281-R1298. doi: 10.1016/j.cub.2021.07.038.
- Edgar RC. MUSCLE: multiple sequence alignment with high accuracy and high throughput. (2004) *Nucleic Acids Res.* **32**(5):1792-7. doi: 10.1093/nar/gkh340.
- Eisenhut M, Hoecker N, Schmidt SB, Basgaran RM, Flachbart S, Jahns P, Eser T, Geimer S, Husted S, Weber APM, Leister D, Schneider A. The Plastid Envelope CHLOROPLAST MANGANESE TRANSPORTER1 Is Essential for Manganese Homeostasis in Arabidopsis. (2018) *Mol Plant.* **11**(7):955-969. doi: 10.1016/j.molp.2018.04.008.
- Fábregas Ibáñez L, Jeschke G. Optimal background treatment in dipolar spectroscopy. (2020) *Phys Chem Chem Phys.* **22**(4):1855-1868. doi: 10.1039/c9cp06111h.
- Fantuzzi A, Allgöwer F, Baker H, McGuire G, Teh WK, Gamiz-Hernandez AP, Kaila VRI, Rutherford AW. Bicarbonate-controlled reduction of oxygen by the QA semiquinone in Photosystem II in membranes. (2019) *Proc Natl Acad Sci USA.* **119**(6):e2116063119. doi: 10.1073/pnas.2116063119.
- Foudree A, Putarjunan A, Kambakam S, Nolan T, Fussell J, Pogorelko G, Rodermeil S. The Mechanism of Variegation in immutans Provides Insight into Chloroplast Biogenesis. (2012) *Front Plant Sci.* **3**:260. doi: 10.3389/fpls.2012.00260.
- Fronko RM, Penner-Hahn JE, Bender CJ. EPR spectral evidence for a dinuclear active site in the *Lactobacillus plantarum* manganese catalase. (1988) *J. Am. Chem. Soc.* **110**(22):7554-7555. doi: 10.1021/ja00230a055

- Fu A, Park S, Rodermel S. Sequences required for the activity of PTOX (IMMUTANS), a plastid terminal oxidase: in vitro and in planta mutagenesis of iron-binding sites and a conserved sequence that corresponds to Exon 8. (2005) *J Biol Chem*. **280**(52):42489-96. doi: 10.1074/jbc.M508940200.
- Fürst-Jansen JMR, de Vries S, de Vries J. Evo-physio: on stress responses and the earliest land plants. (2020) *J Exp Bot*. **71**(11):3254-3269. doi: 10.1093/jxb/eraa007.
- Furukawa R, Aso M, Fujita T, Akimoto S, Tanaka R, Tanaka A, Yokono M, Takabayashi A. Formation of a PSI-PSII megacomplex containing LHCSR and PsbS in the moss *Physcomitrella patens*. (2019) *J Plant Res*. **132**(6):867-880. doi: 10.1007/s10265-019-01138-2.
- Gatt P, Petrie S, Stranger R, Pace RJ. Rationalizing the 1.9 Å crystal structure of photosystem II--A remarkable Jahn-Teller balancing act induced by a single proton transfer. (2012) *Angew Chem Int Ed Engl*. **51**(48):12025-8. doi: 10.1002/anie.201206316.
- Gerotto (2011) Photoprotection mechanisms in the moss *Physcomitrella patens*: Insights on the photosynthesis adaptation during land colonization. PhD dissertation, Università degli studi di Padova, Padova.
- Gershuny Rachel (2005) 5' UTR sequence requirements for stability of rcbL transcripts in the chloroplast of *Chlamydomonas reinhardtii*.
- González MC, Cejudo FJ, Sahrawy M, Serrato AJ. Current Knowledge on Mechanisms Preventing Photosynthesis Redox Imbalance in Plants. (2021) *Antioxidants (Basel)*. **10**(11):1789. doi: 10.3390/antiox10111789.
- Gordiichuk P, Pesce D, Ocampo OEC, Marcozzi A, Wetzelaer GAH, Paul A, Loznik M, Gloukhikh E, Richter S, Chiechi RC, Herrmann A. Orientation and Incorporation of Photosystem I in Bioelectronics Devices Enabled by Phage Display. (2017) *Adv Sci (Weinh)*. **4**(5):1600393. doi: 10.1002/adv.201600393.
- Goss R, Schwarz C, Matzner M, Wilhelm C. Influence of the compatible solute sucrose on thylakoid membrane organization and violaxanthin de-epoxidation. (2021) *Planta*. **254**(3):52. doi: 10.1007/s00425-021-03699-w.
- Guindon S, Dufayard JF, Lefort V, Anisimova M, Hordijk W, Gascuel O. New algorithms and methods to estimate maximum-likelihood phylogenies: assessing the performance of PhyML 3.0. (2010) *Syst Biol*. **59**(3):307-21. doi: 10.1093/sysbio/syq010.
- Guo Y, Li H, He LL, Zhao DX, Gong LD, Yang ZZ. Theoretical reflections on the structural polymorphism of the oxygen-evolving complex in the S2 state and the correlations to substrate water exchange and water oxidation mechanism in photosynthesis. (2017) *Biochim Biophys Acta Bioenerg*. **1858**(10):833-846. doi: 10.1016/j.bbabi.2017.08.001.
- Gupta R. The oxygen-evolving complex: a super catalyst for life on earth, in response to abiotic stresses. (2020) *Plant Signal Behav*. **15**(12):1824721. doi: 10.1080/15592324.2020.1824721.
- Hanke G, Mulo P. Plant type ferredoxins and ferredoxin-dependent metabolism. (2013) *Plant Cell Environ*. **36**(6):1071-84. doi: 10.1111/pce.12046.
- Harrer R. Associations between light-harvesting complexes and Photosystem II from *Marchantia polymorpha* L. determined by two- and three-dimensional electron microscopy. (2003) *Photosynth Res*. **75**(3):249-58. doi: 10.1023/A:1023952832255.
- Harrison CJ, Morris JL. The origin and early evolution of vascular plant shoots and leaves. (2018) *Philos Trans R Soc Lond B Biol Sci*. **373**(1739):20160496. doi: 10.1098/rstb.2016.0496.
- Haworth M, Elliott-Kingston C, McElwain JC. Stomatal control as a driver of plant evolution. (2011) *J Exp Bot*. **62**(8):2419-23. doi: 10.1093/jxb/err086.
- Hetherington AJ, Dolan L. Evolution: Diversification of Angiosperm Rooting Systems in the Early Cretaceous. (2019) *Curr Biol*. **29**(20):R1081-R1083. doi: 10.1016/j.cub.2019.08.030.

- Höhner R, Aboukila A, Kunz HH, Venema K. Proton Gradients and Proton-Dependent Transport Processes in the Chloroplast. (2016) *Front Plant Sci.* 7:218. doi: 10.3389/fpls.2016.00218.
- Houille-Vernes L, Rappaport F, Wollman FA, Alric J, Johnson X. Plastid terminal oxidase 2 (PTOX2) is the major oxidase involved in chlororespiration in *Chlamydomonas*. (2011) *Proc Natl Acad Sci USA.* **108**(51):20820-5. doi: 10.1073/pnas.1110518109.
- Ibáñez H, Ballester A, Muñoz R, Quiles MJ. Chlororespiration and tolerance to drought, heat and high illumination. (2010) *J Plant Physiol.* **167**(9):732-8. doi: 10.1016/j.jplph.2009.12.013.
- Ifuku K, Yamamoto Y, Ono TA, Ishihara S, Sato F. PsbP protein, but not PsbQ protein, is essential for the regulation and stabilization of photosystem II in higher plants. (2005) *Plant Physiol.* **139**(3):1175-84. doi: 10.1104/pp.105.068643.
- Ifuku K, Ido K, Sato F. Molecular functions of PsbP and PsbQ proteins in the photosystem II supercomplex. (2011) *J Photochem Photobiol B.* **104**(1-2):158-64. doi: 10.1016/j.jphotobiol.2011.02.006.
- Iwai M, Takizawa K, Tokutsu R, Okamuro A, Takahashi Y, Minagawa J. Isolation of the elusive supercomplex that drives cyclic electron flow in photosynthesis. (2010) *Nature.* **464**(7292):1210-3. doi: 10.1038/nature08885.
- Jill Harrison C. Development and genetics in the evolution of land plant body plans. (2017) *Philos Trans R Soc Lond B Biol Sci.* **372**(1713):20150490. doi: 10.1098/rstb.2015.0490.
- Johnson GN, Rutherford AW, Krieger A. A change in the midpoint potential of the quinone QA in photosystem II associated with photoactivation of oxygen evolution. (1995) *Biochim Biophys Acta.* **1229**(2):202–207. 24.
- Johnson MP, Goral TK, Duffy CD, Brain AP, Mullineaux CW, Ruban AV. Photoprotective energy dissipation involves the reorganization of photosystem II light-harvesting complexes in the grana membranes of spinach chloroplasts. (2011) *Plant Cell.* **23**(4):1468-79. doi: 10.1105/tpc.110.081646.
- Johnson MP. Metabolic regulation of photosynthetic membrane structure tunes electron transfer function. (2018) *Biochem J.* **475**(7):1225-1233. doi: 10.1042/BCJ20170526.
- Joliot P, Béal D, Joliot A. Cyclic electron flow under saturating excitation of dark-adapted *Arabidopsis* leaves. (2004) *Biochim Biophys Acta.* **1656**(2-3):166-76. doi: 10.1016/j.bbabi.2004.03.010.
- Joliot P, Johnson GN. Regulation of cyclic and linear electron flow in higher plants. (2011) *Proc Natl Acad Sci USA.* **108**(32):13317-22. doi: 10.1073/pnas.1110189108.
- Joliot P, Sellés J, Wollman FA, Verméglio A. High efficient cyclic electron flow and functional supercomplexes in *Chlamydomonas* cells. (2022) *Biochim Biophys Acta Bioenerg.* **1863**(8):148909. doi: 10.1016/j.bbabi.2022.148909.
- Jumper J, Evans R, Pritzel A, Green T, Figurnov M, Ronneberger O, Tunyasuvunakool K, Bates R, Žídek A, Potapenko A, Bridgland A, Meyer C, Kohl SAA, Ballard AJ, Cowie A, Romera-Paredes B, Nikolov S, Jain R, Adler J, Back T, Petersen S, Reiman D, Clancy E, Zielinski M, Steinegger M, Pacholska M, Berghammer T, Bodenstein S, Silver D, Vinyals O, Senior AW, Kavukcuoglu K, Kohli P, Hassabis D. Highly accurate protein structure prediction with AlphaFold. (2021) *Nature.* **596**(7873):583-589. doi: 10.1038/s41586-021-03819-2.
- Kato H, Yasui Y, Ishizaki K. Gemma cup and gemma development in *Marchantia polymorpha*. (2020) *New Phytol.* **228**(2):459-465. doi: 10.1111/nph.16655.
- Kaur D, Khaniya U, Zhang Y, Gunner MR. Protein Motifs for Proton Transfers That Build the Transmembrane Proton Gradient. (2021) *Front Chem.* 9:660954. doi: 10.3389/fchem.2021.660954.
- Keren N, Berg A, van Kan PJ, Levanon H, Ohad I. Mechanism of photosystem II photoinactivation and D1 protein degradation at low light: the role of back electron flow. (1997) *Proc Natl Acad Sci USA.* **94**(4):1579-84. doi: 10.1073/pnas.94.4.1579.
- Kern J, Chatterjee R, Young ID, Fuller FD, Lassalle L, Ibrahim M, Gul S, Fransson T, Brewster AS, Alonso-Mori R, Hussein R, Zhang M, Douthit L, de Lichtenberg C, Cheah MH, Shevela D, Wersig J, Seuffert I, Sokaras D, Pastor E, Weninger C,

- Kroll T, Sierra RG, Aller P, Butryn A, Orville AM, Liang M, Batyuk A, Koglin JE, Carbajo S, Boutet S, Moriarty NW, Holton JM, Dobbek H, Adams PD, Bergmann U, Sauter NK, Zouni A, Messinger J, Yano J, Yachandra VK. Structures of the intermediates of Kok's photosynthetic water oxidation clock. (2018) *Nature*. **563**(7731):421-425. doi: 10.1038/s41586-018-0681-2.
- Khagulov SV, Barynin VV, Anthonyuk-Barynina SV. Manganese-containing catalase from *Thermus thermophilus* peroxide-induced redox transformation of manganese ions in presence of specific inhibitors of catalase activity. (1990) *BBA*. **1020**(1):25-33. doi: 10.1016/0005-2728(90)90089-M
- Kilian R, Bassi R, Schäfer C. Identification and characterization of photosystem II chlorophyll a/b binding proteins in *Marchantia polymorpha* L. (1998) *Planta*. **204**(2):260-7. doi: 10.1007/s004250050255.
- Kirchhoff H. Chloroplast ultrastructure in plants. (2019) *New Phytol*. **223**(2):565-574. doi: 10.1111/nph.15730. (2019) Erratum in: *New Phytol*. **224**(2):994.
- Kok B, Forbush B, McGloin M. Cooperation of charges in photosynthetic O₂ evolution-I. A linear four step mechanism. (1970) *Photochem Photobiol*. **11**(6):457-75. doi: 10.1111/j.1751-1097.1970.tb06017.x.
- Koskela MM, Brünje A, Ivanauskaite A, Grabsztunowicz M, Lassowskat I, Neumann U, Dinh TV, Sindlinger J, Schwarzer D, Wirtz M, Tyystjärvi E, Finkemeier I, Mulo P. Chloroplast Acetyltransferase NSI Is Required for State Transitions in *Arabidopsis thaliana*. (2018) *Plant Cell*. **30**(8):1695-1709. doi: 10.1105/tpc.18.00155.
- Krieger A, Weis E. Energy-dependent of chlorophyll-a-fluorescence: The involvement of proton-calcium exchange at photosystem 2. (1992) *Photosynthetica*. **27**(1-2): 89–98. 22.
- Krieger A, Weis E. The role of calcium in the pH-dependent control of Photosystem II. (1993) *Photosynth Res*. **37**(2):117-30. doi: 10.1007/BF02187470.
- Krieger A, Rutherford AW, Johnson GN. On the determination of redox midpoint potential of the primary quinone electron acceptor, QA, in photosystem II. (1995) *Biochim Biophys Acta*. **1229**(2):193–201. 23.
- Krieger A, Rutherford AW, Vass I, Hideg E. Relationship between activity, D1 loss, and Mn binding in photoinhibition of photosystem II. (1998) *Biochemistry*. **37**(46):16262-9. doi: 10.1021/bi981243v.
- Laisk A, Oja V, Eichelmann H. Kinetics of plastoquinol oxidation by the Q-cycle in leaves. (2016) *Biochim Biophys Acta*. **1857**(6):819-30. doi: 10.1016/j.bbabi.2016.03.032. Epub 2016 Apr 4. PMID: 27056771.
- Lang D, Zimmer AD, Rensing SA, Reski R. Exploring plant biodiversity: the Physcomitrella genome and beyond. (2008) *Trends Plant Sci*. **13**(10):542-9. doi: 10.1016/j.tplants.2008.07.002.
- Leverne L, Krieger-Liszkay A. Moderate drought stress stabilizes the primary quinone acceptor QA and the secondary quinone acceptor QB in photosystem II. (2021) *Physiol Plant*. **171**(2):260-267. doi: 10.1111/ppl.13286.
- Li XP, Björkman O, Shih C, Grossman AR, Rosenquist M, Jansson S, Niyogi KK. A pigment-binding protein essential for regulation of photosynthetic light harvesting. (2000) *Nature*. **403**(6768):391-5. doi: 10.1038/35000131.
- Li XP, Phippard A, Pasari J, Niyogi KK. Structure-function analysis of photosystem II subunit S (PsbS) in vivo. (2002) *Funct Plant Biol*. **29**(10):1131-1139. doi: 10.1071/FP02065.
- Li XP, Gilmore AM, Caffarri S, Bassi R, Golan T, Kramer D, Niyogi KK. Regulation of photosynthetic light harvesting involves intrathylakoid lumen pH sensing by the PsbS protein. (2004) *J Biol Chem*. **279**(22):22866-74. doi: 10.1074/jbc.M402461200.
- Lima-Melo Y, Kılıç M, Aro EM, Gollan PJ. Photosystem I Inhibition, Protection and Signalling: Knowns and Unknowns. (2021) *Front Plant Sci*. **12**:791124. doi: 10.3389/fpls.2021.791124.
- Liu Z, Yan H, Wang K, Kuang T, Zhang J, Gui L, An X, Chang W. Crystal structure of spinach major light-harvesting complex at 2.72 Å resolution. (2004) *Nature*. **428**(6980):287-92. doi: 10.1038/nature02373.

- Lubitz W, Chrysin M, Cox N. Water oxidation in photosystem II. (2019) *Photosynth Res.* **142**(1):105-125. doi: 10.1007/s11120-019-00648-3.
- Ma J, Hu X, Huang J. Plant Colonization of Land: Mining Genes from Bacteria. (2020) *Trends Plant Sci.* **25**(4):317-319. doi: 10.1016/j.tplants.2020.01.012.
- Malone LA, Qian P, Mayneord GE, Hitchcock A, Farmer DA, Thompson RF, Swainsbury DJK, Ranson NA, Hunter CN, Johnson MP. Cryo-EM structure of the spinach cytochrome b6/f complex at 3.6 Å resolution. (2019) *Nature.* **575**(7783):535-539. doi: 10.1038/s41586-019-1746-6.
- Mamedov M, Govindjee, Nadochenko V, Semenov A. Primary electron transfer processes in photosynthetic reaction centers from oxygenic organisms. (2015) *Photosynth Res.* **125**(1-2):51-63. doi: 10.1007/s11120-015-0088-y.
- Maréchal E. Primary Endosymbiosis: Emergence of the Primary Chloroplast and the Chromatophore, Two Independent Events. (2018) *Methods Mol Biol.* **1829**:3-16. doi: 10.1007/978-1-4939-8654-5_1.
- Marin B, Nowack EC, Melkonian M. A plastid in the making: evidence for a second primary endosymbiosis. (2005) *Protist.* **156**(4):425-32. doi: 10.1016/j.protis.2005.09.001.
- Martin W, Herrmann RG. Gene transfer from organelles to the nucleus: how much, what happens, and Why? (1998) *Plant Physiol.* **118**(1):9-17. doi: 10.1104/pp.118.1.9.
- Mazor Y, Borovikova A, Caspy I, Nelson N. Structure of the plant photosystem I supercomplex at 2.6 Å resolution. (2017) *Nat Plants.* **3**:17014. doi: 10.1038/nplants.2017.14.
- McConnell IL, Grigoryants VM, Scholes CP, Myers WK, Chen PY, Whittaker JW, Brudvig GW. EPR-ENDOR characterization of (17O, 1H, 2H) water in manganese catalase and its relevance to the oxygen-evolving complex of photosystem II. (2021) *J Am Chem Soc.* **134**(3):1504-12. doi: 10.1021/ja203465y.
- McDonald AE, Amirsadeghi S, Vanlerberghe GC. Prokaryotic orthologues of mitochondrial alternative oxidase and plastid terminal oxidase. (2003) *Plant Mol Biol.* **53**(6):865-76. doi: 10.1023/B:PLAN.0000023669.79465.d2.
- McDonald AE, Ivanov AG, Bode R, Maxwell DP, Rodermel SR, Hüner NP. Flexibility in photosynthetic electron transport: the physiological role of plastoquinol terminal oxidase (PTOX). (2011) *Biochim Biophys Acta.* **1807**(8):954-67. doi: 10.1016/j.bbabi.2010.10.024.
- McFadden GI (1999) Endosymbiosis and evolution of the plant cell. *Curr Opin Plant Biol* **2**: 513-519. doi: 10.1016/s1369-5266(99)00025-4.
- Merry SA, Nixon PJ, Barter LM, Schilstra M, Porter G, Barber J, Durrant JR, Klug DR. Modulation of quantum yield of primary radical pair formation in photosystem II by site-directed mutagenesis affecting radical cations and anions. (1998) *Biochemistry.* **37**(50):17439-47. doi: 10.1021/bi980502d.
- Messant M, Timm S, Fantuzzi A, Weckwerth W, Bauwe H, Rutherford AW, Krieger-Liszkay A. Glycolate Induces Redox Tuning Of Photosystem II in Vivo: Study of a Photorespiration Mutant. (2018) *Plant Physiol.* **177**(3):1277-1285. doi: 10.1104/pp.18.00341.
- Messant M, Shimakawa G, Perreau F, Miyake C, Krieger-Liszkay A. Evolutionary differentiation between alga- and plant-type plastid terminal oxidase: Study of plastid terminal oxidase PTOX isoforms in *Marchantia polymorpha*. (2021) *Biochim Biophys Acta Bioenerg.* **1862**(1):148309. doi: 10.1016/j.bbabi.2020.148309.
- Messant M, Krieger-Liszkay A, Shimakawa G. Dynamic Changes in Protein-Membrane Association for Regulating Photosynthetic Electron Transport. (2021) *Cells.* **10**(5):1216. doi: 10.3390/cells10051216.
- Milikisyants S, Scarpelli F, Finiguerra MG, Ubbink M, Huber M. A pulsed EPR method to determine distances between paramagnetic centers with strong spectral anisotropy and radicals: the dead-time free RIDME sequence. (2009) *J Magn Reson.* **201**(1):48-56. doi: 10.1016/j.jmr.2009.08.008.

- Miyake C. Alternative electron flows (water-water cycle and cyclic electron flow around PSI) in photosynthesis: molecular mechanisms and physiological functions. (2010) *Plant Cell Physiol.* **51**(12):1951-63. doi: 10.1093/pcp/pcq173.
- Munekage Y, Hojo M, Meurer J, Endo T, Tasaka M, Shikanai T. PGR5 is involved in cyclic electron flow around photosystem I and is essential for photoprotection in Arabidopsis. (2002) *Cell.* **110**(3):361-71. doi: 10.1016/s0092-8674(02)00867-x.
- Najafpour MM, Isaloo MA, Eaton-Rye JJ, Tomo T, Nishihara H, Satoh K, Carpentier R, Shen JR, Allakhverdiev SI. Water exchange in manganese-based water-oxidizing catalysts in photosynthetic systems: from the water-oxidizing complex in photosystem II to nano-sized manganese oxides. (2014) *Biochim Biophys Acta.* **1837**(9):1395-410. doi: 10.1016/j.bbabi.2014.03.008.
- Narzi D, Bovi D, Guidoni L. Pathway for Mn-cluster oxidation by tyrosine-Z in the S2 state of photosystem II. (2014) *Proc Natl Acad Sci USA.* **111**(24):8723-8. doi: 10.1073/pnas.1401719111.
- Narzi D, Capone M, Bovi D, Guidoni L. Evolution from S3 to S4 States of the Oxygen-Evolving Complex in Photosystem II Monitored by Quantum Mechanics/Molecular Mechanics (QM/MM) Dynamics. (2018) *Chemistry.* **24**(42):10820-10828. doi: 10.1002/chem.201801709.
- Navakoudis E, Stergiannakos T, Daskalakis V. A perspective on the major light-harvesting complex dynamics under the effect of pH, salts, and the photoprotective PsbS protein. (2022) *Photosynth Res.* doi: 10.1007/s11120-022-00935-6.
- Nawrocki WJ, Tourasse NJ, Taly A, Rappaport F, Wollman FA. The plastid terminal oxidase: its elusive function points to multiple contributions to plastid physiology. (2015) *Annu Rev Plant Biol.* **66**:49-74. doi: 10.1146/annurev-arplant-043014-114744.
- Nawrocki WJ, Bailleul B, Picot D, Cardol P, Rappaport F, Wollman FA, Joliot P. The mechanism of cyclic electron flow. (2019) *Biochim Biophys Acta Bioenerg.* **1860**(5):433-438. doi: 10.1016/j.bbabi.2018.12.005.
- Niklas KJ, Kutschera U. The evolution of the land plant life cycle. (2010) *New Phytol.* **185**(1):27-41. doi: 10.1111/j.1469-8137.2009.03054.x.
- Nixon PJ, Diner BA. Aspartate 170 of the photosystem II reaction centre polypeptide D1 is involved in the assembly of the oxygen-evolving manganese cluster. (1992) *Biochemistry.* **31**(3):942-8. doi: 10.1021/bi00118a041.
- Oliver N, Avramov AP, Nürnberg DJ, Dau H, Burnap RL. From manganese oxidation to water oxidation: assembly and evolution of the water-splitting complex in photosystem II. (2022) *Photosynth Res.* **152**(2):107-133. doi: 10.1007/s11120-022-00912-z.
- Pantazis DA, Ames W, Cox N, Lubitz W, Neese F. Two interconvertible structures that explain the spectroscopic properties of the oxygen-evolving complex of photosystem II in the S2 state. (2012) *Angew Chem Int Ed Engl.* **51**(39):9935-40. doi: 10.1002/anie.201204705.
- Peltier G, Cournac L. Chlororespiration. (2002) *Annu Rev Plant Biol.* **53**:523-50. doi: 10.1146/annurev.arplant.53.100301.135242.
- Peng L, Ma J, Chi W, Guo J, Zhu S, Lu Q, Lu C, Zhang L. LOW PSII ACCUMULATION1 is involved in efficient assembly of photosystem II in Arabidopsis thaliana. (2006) *Plant Cell.* **18**(4):955-69. doi: 10.1105/tpc.105.037689.
- Peng L, Fukao Y, Fujiwara M, Takami T, Shikanai T. Efficient operation of NAD(P)H dehydrogenase requires supercomplex formation with photosystem I via minor LHCl in Arabidopsis. (2009) *Plant Cell.* **21**(11):3623-40. doi: 10.1105/tpc.109.068791.
- Petersen J, Rredhi A, Szyttenholm J, Mittag M. Evolution of circadian clocks along the green lineage. (2022) *Plant Physiol.* kiac141. doi: 10.1093/plphys/kiac141..
- Pribil M, Labs M, Leister D. Structure and dynamics of thylakoids in land plants. (2014) *J Exp Bot.* **65**(8):1955-72. doi: 10.1093/jxb/eru090.

- Puthiyaveetil S, Tsabari O, Lowry T, Lenhert S, Lewis RR, Reich Z, Kirchhoff H. Compartmentalization of the protein repair machinery in photosynthetic membranes. (2014) *Proc Natl Acad Sci USA*. **111**(44):15839-44. doi: 10.1073/pnas.1413739111.
- Rantala S, Tikkanen M. Phosphorylation-induced lateral rearrangements of thylakoid protein complexes upon light acclimation. (2018) *Plant Direct*. **2**(2):e00039. doi: 10.1002/pld3.39.
- Rantala M, Rantala S, Aro EM. Composition, phosphorylation and dynamic organization of photosynthetic protein complexes in plant thylakoid membrane. (2020) *Photochem Photobiol Sci*. **19**(5):604-619. doi: 10.1039/d0pp00025f.
- Raven JA, Edwards D. Roots: evolutionary origins and biogeochemical significance. (2001) *J Exp Bot*. **52**(Spec Issue):381-401. doi: 10.1093/jexbot/52.suppl_1.381.
- Raven JA, Colmer TD. Life at the boundary: photosynthesis at the soil-fluid interface. A synthesis focusing on mosses. (2016) *J Exp Bot*. **67**(6):1613-23. doi: 10.1093/jxb/erw012.
- Rédei GP. Arabidopsis as a genetic tool. (1975) *Annu Rev Genet*. **9**:111-27. doi: 10.1146/annurev.ge.09.120175.000551.
- Redekop P, Rothhausen N, Rothhausen N, Melzer M, Mosebach L, Dülger E, Bovdilova A, Caffarri S, Hippler M, Jahns P. PsbS contributes to photoprotection in *Chlamydomonas reinhardtii* independently of energy dissipation. (2020) *Biochim Biophys Acta Bioenerg*. **1861**(5-6):148183. doi: 10.1016/j.bbabi.2020.148183.
- Rensing SA, Lang D, Zimmer AD, Terry A, Salamov A, Shapiro H, Nishiyama T, Perroud PF, Lindquist EA, Kamisugi Y, Tanahashi T, Sakakibara K, Fujita T, Oishi K, Shin-I T, Kuroki Y, Toyoda A, Suzuki Y, Hashimoto S, Yamaguchi K, Sugano S, Kohara Y, Fujiiyama A, Anterola A, Aoki S, Ashton N, Barbazuk WB, Barker E, Bennetzen JL, Blankenship R, Cho SH, Dutcher SK, Estelle M, Fawcett JA, Gundlach H, Hanada K, Heyl A, Hicks KA, Hughes J, Lohr M, Mayer K, Melkozernov A, Murata T, Nelson DR, Pils B, Prigge M, Reiss B, Renner T, Rombauts S, Rushton PJ, Sanderfoot A, Schween G, Shiu SH, Stueber K, Theodoulou FL, Tu H, Van de Peer Y, Verrier PJ, Waters E, Wood A, Yang L, Cove D, Cuming AC, Hasebe M, Lucas S, Mishler BD, Reski R, Grigoriev IV, Quatrano RS, Boore JL. The Physcomitrella genome reveals evolutionary insights into the conquest of land by plants. (2008) *Science*. **319**(5859):64-9. doi: 10.1126/science.1150646.
- Roach T, Sedoud A, Krieger-Liszkay A. Acetate in mixotrophic growth medium affects photosystem II in *Chlamydomonas reinhardtii* and protects against photoinhibition. (2013) *Biochim Biophys Acta*. **1827**(10):1183-90. doi: 10.1016/j.bbabi.2013.06.004.
- Robertazzi A, Galstyan A, Knapp EW. PSII manganese cluster: protonation of W2, O5, O4 and His337 in the S1 state explored by combined quantum chemical and electrostatic energy computations. (2014) *Biochim Biophys Acta*. **1837**(8):1316-21. doi: 10.1016/j.bbabi.2014.03.018.
- Rokka A, Suorsa M, Saleem A, Battchikova N, Aro EM. Synthesis and assembly of thylakoid protein complexes: multiple assembly steps of photosystem II. (2005) *Biochem J*. **388**(Pt 1):159-68. doi: 10.1042/BJ20042098.
- Ruban AV, Wilson S. The Mechanism of Non-Photochemical Quenching in Plants: Localization and Driving Forces. (2021) *Plant Cell Physiol*. **62**(7):1063-1072. doi: 10.1093/pcp/pcaa155.
- Rühle T, Dann M, Reiter B, Schünemann D, Naranjo B, Penzler JF, Kleine T, Leister D. PGRL2 triggers degradation of PGR5 in the absence of PGRL1. (2021) *Nat Commun*. **12**(1):3941. doi: 10.1038/s41467-021-24107-7.
- Rumak I, Gieczewska K, Kierdaszuk B, Gruszecki WI, Mostowska A, Mazur R, Garstka M. 3-D modelling of chloroplast structure under (Mg²⁺) magnesium ion treatment. Relationship between thylakoid membrane arrangement and stacking. (2010) *Biochim Biophys Acta*. **1797**(10):1736-48. doi: 10.1016/j.bbabi.2010.07.001.
- Rutherford AW, Krieger-Liszkay A. Herbicide-induced oxidative stress in photosystem II. (2001) *Trends Biochem Sci*. **26**(11):648-53. doi: 10.1016/s0968-0004(01)01953-3.

- Sacharz J, Giovagnetti V, Ungerer P, Mastroianni G, Ruban AV. The xanthophyll cycle affects reversible interactions between PsbS and light-harvesting complex II to control non-photochemical quenching. (2017) *Nat Plants*. **3**:16225. doi: 10.1038/nplants.2016.225.
- Sánchez-Baracaldo P, Cardona T. On the origin of oxygenic photosynthesis and Cyanobacteria. (2020) *New Phytol*. **225**(4):1440-1446. doi: 10.1111/nph.16249.
- Samecka-Cymerman A, Marczonek A, Kempers AJ. Bioindication of heavy metals in soil by liverworts. (1997) *Arch Environ Contam Toxicol*. **33**(2):162-71. doi: 10.1007/s002449900238.
- Sasso S, Stibor H, Mittag M, Grossman AR. From molecular manipulation of domesticated *Chlamydomonas reinhardtii* to survival in nature. (2018) *Elife*. **7**:e39233. doi: 10.7554/eLife.39233.
- Schaller S, Latowski D, Jemioła-Rzemińska M, Dawood A, Wilhelm C, Strzałka K, Goss R. Regulation of LHCII aggregation by different thylakoid membrane lipids. (2011) *Biochim Biophys Acta*. **1807**(3):326-35. doi: 10.1016/j.bbabi.2010.12.017.
- Schermelleh L, Ferrand A, Huser T, Eggeling C, Sauer M, Biehlmaier O, Drummen GPC. Super-resolution microscopy demystified. (2019) *Nat Cell Biol*. **21**(1):72-84. doi: 10.1038/s41556-018-0251-8.
- Schmidt SB, Jensen PE, Husted S. Manganese Deficiency in Plants: The Impact on Photosystem II. (2016) *Trends Plant Sci*. **21**(7):622-632. doi: 10.1016/j.tplants.2016.03.001.
- Schneider A, Steinberger I, Herdean A, Gandini C, Eisenhut M, Kurz S, Morper A, Hoecker N, Rühle T, Labs M, Flügge UI, Geimer S, Schmidt SB, Husted S, Weber AP, Spetea C, Leister D. The Evolutionarily Conserved Protein PHOTOSYNTHESIS AFFECTED MUTANT71 Is Required for Efficient Manganese Uptake at the Thylakoid Membrane in Arabidopsis. (2016) *Plant Cell*. **28**(4):892-910. doi: 10.1105/tpc.15.00812.
- Schoefs B, Franck F. Protochlorophyllide reduction: mechanisms and evolutions. (2003) *Photochem Photobiol*. **78**(6):543-57. doi: 10.1562/0031-8655(2003)078<0543:prmae>2.0.co;2.
- Schuller JM, Birrell JA, Tanaka H, Konuma T, Wulforst H, Cox N, Schuller SK, Thiemann J, Lubitz W, Sétif P, Ikegami T, Engel BD, Kurisu G, Nowaczyk MM. Structural adaptations of photosynthetic complex I enable ferredoxin-dependent electron transfer. (2019) *Science*. **363**(6424):257-260. doi: 10.1126/science.aau3613.
- Schwenkert S, Legen J, Takami T, Shikanai T, Herrmann RG, Meurer J. Role of the low-molecular-weight subunits PetL, PetG, and PetN in assembly, stability, and dimerization of the cytochrome b6/f complex in tobacco. (2007) *Plant Physiol*. **144**(4):1924-35. doi: 10.1104/pp.107.100131.
- Seago JL Jr, Fernando DD. Anatomical aspects of angiosperm root evolution. (2013) *Ann Bot*. **112**(2):223-38. doi: 10.1093/aob/mcs266.
- Sétif P, Fischer N, Lagoutte B, Bottin H, Rochaix JD. The ferredoxin docking site of photosystem I. (2002) *Biochim Biophys Acta*. **1555**(1-3):204-9. doi: 10.1016/s0005-2728(02)00279-7.
- Sétif P, Shimakawa G, Krieger-Liszka A, Miyake C. Identification of the electron donor to flavodiiron proteins in *Synechocystis* sp. PCC 6803 by in vivo spectroscopy. (2020) *Biochim Biophys Acta Bioenerg*. **1861**(10):148256. doi: 10.1016/j.bbabi.2020.148256.
- Shahbazi M, Gilbert M, Labouré AM, Kuntz M. Dual role of the plastid terminal oxidase in tomato. (2007) *Plant Physiol*. **145**(3):691-702. doi: 10.1104/pp.107.106336.
- Shen JR. The Structure of Photosystem II and the Mechanism of Water Oxidation in Photosynthesis. (2015) *Annu Rev Plant Biol*. **66**:23-48. doi: 10.1146/annurev-arplant-050312-120129.
- Sheng X, Liu Z, Kim E, Minagawa J. Plant and Algal PSII-LHCII Supercomplexes: Structure, Evolution and Energy Transfer. (2021) *Plant Cell Physiol*. **62**(7):1108-1120. doi: 10.1093/pcp/pcab072.

- Shi Y, Ke X, Yang X, Liu Y, Hou X. Plants response to light stress. (2022) *J Genet Genomics*. S1673-8527(22)00137-0. doi: 10.1016/j.jgg.2022.04.017.
- Shibamoto T, Kato Y, Sugiura M, Watanabe T. Redox potential of the primary plastoquinone electron acceptor Q(A) in photosystem II from *Thermosynechococcus elongatus* determined by spectroelectrochemistry. (2009) *Biochemistry*. **48**(45):10682-4. doi: 10.1021/bi901691j.
- Shibamoto T, Kato Y, Nagao R, Yamazaki T, Tomo T, Watanabe T. Species-dependence of the redox potential of the primary quinone electron acceptor QA in photosystem II verified by spectroelectrochemistry. (2010) *FEBS Lett*. **584**(8):1526-30. doi: 10.1016/j.febslet.2010.03.002.
- Shibuya Y, Takahashi R, Okubo T, Suzuki H, Sugiura M, Noguchi T. Hydrogen bond interactions of the pheophytin electron acceptor and its radical anion in photosystem II as revealed by Fourier transform infrared difference spectroscopy. (2010) *Biochemistry*. **49**(3):493-501. doi: 10.1021/bi9018829.
- Shimakawa G, Ishizaki K, Tsukamoto S, Tanaka M, Sejima T, Miyake C. The Liverwort, *Marchantia*, Drives Alternative Electron Flow Using a Flavodiiron Protein to Protect PSI. (2017) *Plant Physiol*. **173**(3):1636-1647. doi: 10.1104/pp.16.01038.
- Shimakawa G, Hanawa H, Wada S, Hanke GT, Matsuda Y, Miyake C. Physiological Roles of Flavodiiron Proteins and Photorespiration in the Liverwort *Marchantia polymorpha*. (2021) *Front Plant Sci*. **12**:668805. doi: 10.3389/fpls.2021.668805.
- Shimamura M. *Marchantia polymorpha*: Taxonomy, Phylogeny and Morphology of a Model System. (2016) *Plant Cell Physiol*. **57**(2):230-56. doi: 10.1093/pcp/pcv192.
- Shutova, T. (2007). Photosynthetic water oxidation : the function of two extrinsic proteins. PhD dissertation, Fysiologisk botanik. Retrieved from <http://urn.kb.se/resolve?urn=urn:nbn:se:umu:diva-1476>
- Siegbahn PEM . The S2 to S3 transition for water oxidation in PSII (photosystem II), revisited. (2018) *Phys Chem Chem Phys*. **20**(35):22926-22931. doi: 10.1039/c8cp03720e.
- Srivastava A, Guissé B, Greppin H, Strasser RJ. Regulation of antenna structure and electron transport in photosystem II of *Pisum sativum* under elevated temperature probed by the fast polyphasic chlorophyll a fluorescence transient: OKJIP. (1997) *BBA*. **1320**(1):95-106. doi: 10.1016/S0005-2728(97)00017-0.
- Staehelein LA, Arntzen CJ. Regulation of chloroplast membrane function: protein phosphorylation changes the spatial organization of membrane components. (1983) *J Cell Biol*. **97**(5 Pt 1):1327-37. doi: 10.1083/jcb.97.5.1327.
- Staehelein LA, Paolillo DJ. A brief history of how microscopic studies led to the elucidation of the 3D architecture and macromolecular organization of higher plant thylakoids. (2020) *Photosynth Res*. **145**(3):237-258. doi: 10.1007/s11120-020-00782-3.
- Standfuss J, Terwisscha van Scheltinga AC, Lamborghini M, Kühlbrandt W. Mechanisms of photoprotection and nonphotochemical quenching in pea light-harvesting complex at 2.5 Å resolution. (2005) *EMBO J*. **24**(5):919-28. doi: 10.1038/sj.emboj.7600585.
- Stepien P, Johnson GN. Contrasting responses of photosynthesis to salt stress in the glycophyte *Arabidopsis* and the halophyte *Thellungiella*: role of the plastid terminal oxidase as an alternative electron sink. (2009) *Plant Physiol*. **149**(2):1154-65. doi: 10.1104/pp.108.132407.
- Stirbet A, Govindjee. On the relation between the Kautsky effect (chlorophyll a fluorescence induction) and Photosystem II: basics and applications of the OJIP fluorescence transient. (2011) *J Photochem Photobiol B*. **104**(1-2):236-57. doi: 10.1016/j.jphotobiol.2010.12.010.
- Stirbet A, Riznichenko GY, Rubin AB, Govindjee. Modeling chlorophyll a fluorescence transient: relation to photosynthesis. (2014) *Biochemistry (Mosc)*. **79**(4):291-323. doi: 10.1134/S0006297914040014.

- Stirbet A, Lazár D, Guo Y, Govindjee G. Photosynthesis: basics, history and modelling. (2020) *Ann Bot.* **126**(4):511-537. doi: 10.1093/aob/mcz171.
- Stothard P. The sequence manipulation suite: JavaScript programs for analyzing and formatting protein and DNA sequences. (2000) *Biotechniques.* **28**(6):1102, 1104. doi: 10.2144/00286ir01.
- Streckaite S (2021) Thylakoids: from molecular to membrane organisation. A spectroscopic and nanoscopic study of the photosynthetic apparatus. PhD dissertation Vrije Universiteit Amsterdam, Amsterdam.
- Streckaite S, Frolov D, Chmeliov J, Gelzinis A, Iliaoaia C, Rinsky S, van Grondelle R, Valkunas L, Gall A, Bruno R. Single Pixel Reconstruction Imaging: taking confocal imaging to the extreme. (2022) Biorxiv. Submitted. doi:10.1101/2022.11.08.515455
- Suga M, Akita F, Hirata K, Ueno G, Murakami H, Nakajima Y, Shimizu T, Yamashita K, Yamamoto M, Ago H, Shen JR. Native structure of photosystem II at 1.95 Å resolution viewed by femtosecond X-ray pulses. (2015) *Nature.* **517**(7532):99-103. doi: 10.1038/nature13991.
- Suga M, Akita F, Sugahara M, Kubo M, Nakajima Y, Nakane T, Yamashita K, Umena Y, Nakabayashi M, Yamane T, Nakano T, Suzuki M, Masuda T, Inoue S, Kimura T, Nomura T, Yonekura S, Yu LJ, Sakamoto T, Motomura T, Chen JH, Kato Y, Noguchi T, Tono K, Joti Y, Kameshima T, Hatsui T, Nango E, Tanaka R, Naitow H, Matsuura Y, Yamashita A, Yamamoto M, Nureki O, Yabashi M, Ishikawa T, Iwata S, Shen JR. Light-induced structural changes and the site of O=O bond formation in PSII caught by XFEL. (2017) *Nature.* **543**(7643):131-135. doi: 10.1038/nature21400.
- Sugano SS, Shirakawa M, Takagi J, Matsuda Y, Shimada T, Hara-Nishimura I, Kohchi T. CRISPR/Cas9-mediated targeted mutagenesis in the liverwort *Marchantia polymorpha* L. (2014) *Plant Cell Physiol.* **55**(3):475-81. doi: 10.1093/pcp/pcu014.
- Suorsa M, Regel RE, Paakkarinen V, Battchikova N, Herrmann RG, Aro EM. Protein assembly of photosystem II and accumulation of subcomplexes in the absence of low molecular mass subunits PsbL and PsbJ. (2004) *Eur J Biochem.* **271**(1):96-107. doi: 10.1046/j.1432-1033.2003.03906.x.
- Suorsa M, Sirpiö S, Allahverdiyeva Y, Paakkarinen V, Mamedov F, Styring S, Aro EM. PsbR, a missing link in the assembly of the oxygen-evolving complex of plant photosystem II. (2006) *J Biol Chem.* **281**(1):145-50. doi: 10.1074/jbc.M510600200.
- Suorsa M, Aro EM. Expression, assembly and auxiliary functions of photosystem II oxygen-evolving proteins in higher plants. (2007) *Photosynth Res.* **93**(1-3):89-100. doi: 10.1007/s11120-007-9154-4.
- Suorsa M, Rossi F, Tadani L, Labs M, Colombo M, Jahns P, Kater MM, Leister D, Finazzi G, Aro EM, Barbato R, Pesaresi P. PGR5-PGRL1-Dependent Cyclic Electron Transport Modulates Linear Electron Transport Rate in *Arabidopsis thaliana*. (2016) *Mol Plant.* **9**(2):271-288. doi: 10.1016/j.molp.2015.12.001.
- Szymańska R, Dłużewska J, Slesak I, Kruk J. Ferredoxin:NADP⁺ oxidoreductase bound to cytochrome *b₆f* complex is active in plastoquinone reduction: implications for cyclic electron transport. (2011) *Physiol Plant.* **141**(3):289-98. doi: 10.1111/j.1399-3054.2010.01434.x.
- Tabares LC, Un S. In situ determination of manganese(II) speciation in *Deinococcus radiodurans* by high magnetic field EPR: detection of high levels of Mn(II) bound to proteins. (2013) *J Biol Chem.* **288**(7):5050-5. doi: 10.1074/jbc.C112.444992.
- Takahashi H. Cyclic electron flow A to Z. (2022) *J Plant Res.* **135**(4):539-541. doi: 10.1007/s10265-022-01402-y.
- Tanaka A, Fukushima Y, Kamiya N. Two Different Structures of the Oxygen-Evolving Complex in the Same Polypeptide Frameworks of Photosystem II. (2017) *J Am Chem Soc.* **139**(5):1718-1721. doi: 10.1021/jacs.6b09666.
- Tikhonov KG, Zastrizhnaya OM, Kozlov YN, Klimov VV. Composition and catalase-like activity of Mn(II)-bicarbonate complexes. (2006) *Biochemistry (Mosc).* **71**(11):1270-7. doi: 10.1134/s0006297906110137.
- Tikkanen M, Aro EM. Thylakoid protein phosphorylation in dynamic regulation of photosystem II in higher plants. (2012) *Biochim Biophys Acta.* **1817**(1):232-8. doi: 10.1016/j.bbabi.2011.05.005.

Tyryshkin AM, Watt RK, Baranov SV, Dasgupta J, Hendrich MP, Dismukes GC. Spectroscopic evidence for Ca²⁺ involvement in the assembly of the Mn₄Ca cluster in the photosynthetic water-oxidizing complex. (2006) *Biochemistry*. **45**(42):12876-89. doi: 10.1021/bi061495t.

Ueda M, Tanaka A, Sugimoto K, Shikanai T, Nishimura Y. chlB requirement for chlorophyll biosynthesis under short photoperiod in *Marchantia polymorpha* L. (2014) *Genome Biol Evol*. **6**(3):620-8. doi: 10.1093/gbe/evu045.

Un S. Structure and nature of manganese(II) imidazole complexes in frozen aqueous solutions. (2013) *Inorg Chem*. **52**(7):3803-13. doi: 10.1021/ic302415s.

Varotto C, Pesaresi P, Jahns P, Lessnick A, Tizzano M, Schiavon F, Salamini F, Leister D. Single and double knockouts of the genes for photosystem I subunits G, K, and H of *Arabidopsis*. Effects on photosystem I composition, photosynthetic electron flow, and state transitions. (2002) *Plant Physiol*. **129**(2):616-24. doi: 10.1104/pp.002089.

Vinyard DJ, Ananyev GM, Dismukes GC. Photosystem II: the reaction center of oxygenic photosynthesis. (2013) *Annu Rev Biochem*. **82**:577-606. doi: 10.1146/annurev-biochem-070511-100425.

Vinyard DJ, Khan S, Brudvig GW. Photosynthetic water oxidation: binding and activation of substrate waters for O-O bond formation. (2015) *Faraday Discuss*. **185**:37-50. doi: 10.1039/c5fd00087d.

Vinyard DJ, Khan S, Askerka M, Batista VS, Brudvig GW. Energetics of the S₂ State Spin Isomers of the Oxygen-Evolving Complex of Photosystem II. (2017) *J Phys Chem B*. **121**(5):1020-1025. doi: 10.1021/acs.jpccb.7b00110.

Vinyard DJ, Brudvig GW. Progress Toward a Molecular Mechanism of Water Oxidation in Photosystem II. (2017) *Annu Rev Phys Chem*. **68**:101-116. doi: 10.1146/annurev-physchem-052516-044820.

Waldo GS, Penner-Hahn JE. Mechanism of manganese catalase peroxide disproportionation: determination of manganese oxidation states during turnover. (1995) *Biochemistry*. **34**(5):1507-12. doi: 10.1021/bi00005a006.

Wang J, Askerka M, Brudvig GW, Batista VS. Crystallographic Data Support the Carousel Mechanism of Water Supply to the Oxygen-Evolving Complex of Photosystem II. (2017) *ACS Energy Lett*. **2**(10):2299-2306. doi: 10.1021/acsenenergylett.7b00750.

Wei X, Su X, Cao P, Liu X, Chang W, Li M, Zhang X, Liu Z. Structure of spinach photosystem II-LHCII supercomplex at 3.2 Å resolution. (2016) *Nature*. **534**(7605):69-74. doi: 10.1038/nature18020.

Wetzel CM, Jiang CZ, Meehan LJ, Voytas DF, Rodermeil SR. Nuclear-organelle interactions: the immutans variegation mutant of *Arabidopsis* is plastid autonomous and impaired in carotenoid biosynthesis. (1994) *Plant J*. **6**(2):161-75. doi: 10.1046/j.1365-3113x.1994.6020161.x.

Wu D, Wright DA, Wetzel C, Voytas DF, Rodermeil S. The IMMUTANS variegation locus of *Arabidopsis* defines a mitochondrial alternative oxidase homolog that functions during early chloroplast biogenesis. (1999) *Plant Cell*. **11**(1):43-55. doi: 10.1105/tpc.11.1.43.

Yadav KN, Semchonok DA, Nosek L, Kouřil R, Fucile G, Boekema EJ, Eichacker LA. Supercomplexes of plant photosystem I with cytochrome b₆f, light-harvesting complex II and NDH. (2017) *Biochim Biophys Acta Bioenerg*. **1858**(1):12-20. doi: 10.1016/j.bbabi.2016.10.006.

Yamamoto H, Peng L, Fukao Y, Shikanai T. An Src homology 3 domain-like fold protein forms a ferredoxin binding site for the chloroplast NADH dehydrogenase-like complex in *Arabidopsis*. (2011) *Plant Cell*. **23**(4):1480-93. doi: 10.1105/tpc.110.080291.

Yang H, Liu J, Wen X, Lu C. Molecular mechanism of photosystem I assembly in oxygenic organisms. (2015) *Biochim Biophys Acta*. **1847**(9):838-48. doi: 10.1016/j.bbabi.2014.12.011.

Yano J, Yachandra V. Mn₄Ca cluster in photosynthesis: where and how water is oxidized to dioxygen. (2014) *Chem Rev*. **114**(8):4175-205. doi: 10.1021/cr4004874.

Yi X, McChargue M, Laborde S, Frankel LK, Bricker TM. The manganese-stabilizing protein is required for photosystem II assembly/stability and photoautotrophy in higher plants. (2005) *J Biol Chem*. **280**(16):16170-4. doi: 10.1074/jbc.M501550200.

Yoshioka-Nishimura M, Nanba D, Takaki T, Ohba C, Tsumura N, Morita N, Sakamoto H, Murata K, Yamamoto Y. Quality control of photosystem II: direct imaging of the changes in the thylakoid structure and distribution of FtsH proteases in spinach chloroplasts under light stress. (2014) *Plant Cell Physiol.* **55**(7):1255-65. doi: 10.1093/pcp/pcu079.

Yu Q, Feilke K, Krieger-Liszak A, Beyer P. Functional and molecular characterization of plastid terminal oxidase from rice (*Oryza sativa*). (2014) *Biochim Biophys Acta.* **1837**(8):1284-92. doi: 10.1016/j.bbabi.2014.04.007.

Zabret J, Bohn S, Schuller SK, Arnolds O, Möller M, Meier-Credo J, Liauw P, Chan A, Tajkhorshid E, Langer JD, Stoll R, Krieger-Liszak A, Engel BD, Rudack T, Schuller JM, Nowaczyk MM. Structural insights into photosystem II assembly. (2021) *Nat Plants.* **7**(4):524-538. doi: 10.1038/s41477-021-00895-0.

Zaitsev SY, Volchenkova TA, Kalabina NA, Schaefer C, Zubrov P. Purification and monolayer study of the thylakoid lipids of moss *Marchantia polymorpha*. (2011) *Macromol Symp.* **136**:119-129. doi: 10.1002/masy.19981360117

Zhang H, Whitelegge JP, Cramer WA. Ferredoxin:NADP⁺ oxidoreductase is a subunit of the chloroplast cytochrome b6/f complex. (2001) *J Biol Chem.* **276**(41):38159-65. doi: 10.1074/jbc.M105454200.

Zhang M, Bommer M, Chatterjee R, Hussein R, Yano J, Dau H, Kern J, Dobbek H, Zouni A. Structural insights into the light-driven auto-assembly process of the water-oxidizing Mn₄CaO₅-cluster in photosystem II. (2017) *Elife.* **6**:e26933. doi: 10.7554/eLife.26933.